

**ANALYSIS OF HUNTINGTIN PROTEIN
AGGREGATION MECHANISMS AND THE
DEVELOPMENT OF A CLINICALLY-DERIVED
HUMAN CELL MODEL OF HUNTINGTON'S DISEASE**

**ANALYSIS OF HUNTINGTIN PROTEIN
AGGREGATION MECHANISMS AND THE
DEVELOPMENT OF A CLINICALLY-DERIVED
HUMAN CELL MODEL OF HUNTINGTON'S DISEASE**

BY: CLAUDIA HUNG, B.Sc.

**A Thesis Submitted to the School of Graduate Studies in Partial Fulfilment of the
Requirements for the Degree Doctor of Philosophy**

McMaster University © Copyright by Claudia Hung September 2018

Doctor of Philosophy – Biochemistry & Biomedical Sciences (2018)
McMaster University Hamilton, Ontario

**Title : Analysis of Huntingtin Protein Aggregation Mechanisms and the
Development of a Clinically-Derived Human Cell Model of Huntington's
Disease**

Author : Claudia L.K. Hung, Honours B.Sc.

Supervisor : Dr. Ray Truant

Number of Pages : ix, 205

ABSTRACT

Neurodegenerative diseases are characterized by selective neuronal vulnerability and subsequent degeneration in specific areas of the brain. Huntington's Disease (HD) is inherited as an autosomal dominant mutation that primarily affects the cells of the striatum and the cerebral cortex, leading to a triad of symptoms that include the progressive loss of motor function, defects in cognitive ability and psychiatric manifestations. HD is caused by a CAG repeat expansion that exceeds 37 repeats in Exon1 of the *HTT* gene, manifesting as a pathogenic polyglutamine (polyQ) amino acid tract expansion in the huntingtin protein. HD is a late onset disorder, with disease onset around 40-50 years of age and symptoms that worsen over 10-20 years. Only a few symptomatic treatments are available and there is currently no cure for the disease. Therapeutics to target the huntingtin gene itself have only been in clinical trial in the past 2 years.

The length of the expansion has an inverse relationship with the age of disease onset. Most patients that have repeats between 40-45 CAG, however, have varying age of disease onset. Recent genome-wide association studies (GWAS) have implicated DNA handling and repair pathways as modifiers of age of disease onset up to 6 years. Therapeutic approaches to modify and delay onset indefinitely through other genetic targets will require identification of pathological mechanisms that precede disease onset.

Several hallmark phenotypes have been identified in cell and animal models, including pathogenic aggregate formation. These models are not reflective of human biology, using excessively large CAG repeats (>100) associated with the more aggressive, juvenile HD, overlooking the importance of GWAS results and the progression of disease with lower pathogenic CAG repeats (40-50 CAG). We have therefore generated novel, clinically-relevant human patient fibroblast cell lines and have characterized several disease phenotypes. My thesis presents a culmination of several projects that focus on disease modelling, primarily outlining phenotypic differences between wildtype and HD cells that will benefit our understanding of disease pathogenesis.

ACKNOWLEDGEMENTS

I would first like to thank my supervisor, Dr. Ray Truant, for his support and guidance throughout my undergraduate thesis and graduate studies. I would also like to thank our lab technicians, Jianrun Xia, for his support and assistance over the past few years, and Mina Falcone, for her unwavering support and encouragement. Also, my committee members, Dr. Karun Singh and Dr. Brad Doble, for their guidance and support over the years.

Thank you to current and past students in the Truant lab, especially Dr. Nicholas Caron, who mentored me when I first started, Laura Bowie, whose support, counsel, and friendship I have shared throughout my graduate student experience, and Dr. Tamara Maiuri, for all of the wise advice and project insight. I would also like to thank Tanya Woloshansky, Jenny Williamson, Shreya Patel, Susie Son, Andrew Mocle, Laura Digiovanni, Glenn Walpole, Sid Nath and Celeste Suart, who have all been important members of the lab during my time there, and I could not have gotten through all these years without them!!

Last but not least, I would also like to thank my family and friends, who have also supported me throughout my studies, especially all of my friends who were also completing graduate studies during this time. I definitely could not have done it without all of your support, advice, patience, kindness, motivation and encouragement.

LIST OF ABBREVIATIONS

3-NP: 3-nitropropionic acid
A: adenine
AAV: adeno-associated virus
A β : amyloid beta
AD: Alzheimer's disease
APRT:
ASO: anti-sense oligonucleotide
ATP: adenosine triphosphate
BAC: bacterial artificial chromosome
BDNF: brain-derived neurotrophic factor
C: cytosine
CAG: cytosine-adenine-guanine
CBP: CREB-binding protein
Cdc6: cell division cycle 6
Cdt1: chromosome licensing and DNA replication factor 1
Cep164: centrosomal protein of 164kDa
CFP: cyan fluorescent protein
CoQ10: coenzyme Q10
CNS: central nervous system
CREB: cAMP response element binding protein 1
CRM-1: chromosome-region maintenance 1
DMSO: dimethyl sulfoxide
DNA: deoxyribonucleic acids
DRPLA: dentatorubral-pallidoluyisian atrophy
ER: endoplasmic reticulum
Exon1 Q17: exon 1 with 17Q residues
Exon Q138: exon 1 with 138Q residues
Exon 1 Q142S13AS16A: exon1 with 142Q, serines 13 and 16 are substituted with alanine
Exon1 Q142S13ES16E: exon1 with 142Q, serines 13 and 16 are substituted with glutamic acid
FEN1: flap endonuclease 1
FLIM: fluorescence lifetime imaging microscopy
FRAP: fluorescence recovery after photobleaching
FRET: Förster resonance energy transfer
G: guanine
GFP: green fluorescent protein
GWAS: genome-wide association study
HAP: huntingtin-associated protein
HD: Huntington's Disease
HDAC: histone deactylase

HEAT: huntingtin, elongation factor 3, protein phosphatase 2A, target of rapamycin (TOR)
hTERT: human telomerase reverse transcriptase
Htt: huntingtin protein
HTT: huntingtin gene
iPSCs: induced pluripotent stem cells
mCer: monomeric Cerulean fluorescent protein
M8: methionine 8
MSN: medium spiny neuron
mTOR: mammalian target of rapamycin
N17: first 17 amino acids of the amino-terminal region of huntingtin
N17-phospho: phosphorylation huntingtin at serines 13 and 16 in N17
NAD⁺: nicotinamide adenine dinucleotide
NES: nuclear export signal
NLS: nuclear localization signal
NMDA: N-methyl-D-aspartate
P53: tumour protein 53
PCNA: proliferating cell nuclear antigen
PD: Parkinson's disease
PDE10A: phosphodiesterase 10A
PET: positron emission tomography
polyP: polyproline tract
polyQ: polyglutamine tract
pRb: retinoblastoma protein
REST/NRSF: RE1-Silencing Transcription factor also known as Neuron-Restrictive silencing factor
RNA: ribonucleic acids
ROS: reactive oxygen species
SBMA: spinobulbar muscular atrophy
SCA: spinocerebellar ataxia
SDS: sodium dodecyl sulfate
seFRET: sensitized emission Förster resonance energy transfer
SR-SIM: super resolution structured illumination microscopy
STHdb: striatal-derived mouse neuronal cells
SUMO: small ubiquitin-like modifier
SV40: simian virus 40
TruHD: hTERT-immortalized patient fibroblasts
XRCC1: X-ray repair cross-complementing protein 1
YAC: yeast artificial chromosome
YFP: yellow fluorescent protein

LIST OF FIGURES

- Figure 1.1** Huntingtin protein structure
- Figure 1.2** Subcellular distribution of huntingtin
- Figure 2.1** Huntingtin fragments can form two morphologically unique inclusion types
- Figure 2.2** Fibrillar inclusions are detectable by thioflavin-T staining assay
- Figure 2.3** Comparing the fluorescence lifetime (τ) changes in globular versus fibrillar inclusion types
- Figure 2.4** Comparing the dynamics of globular versus fibrillar inclusions
- Figure 2.5** Active recruitment of mutant huntingtin into globular inclusions is microtubule dependent
- Figure 2.6** Comparing the formation of fibrillar versus globular inclusions using temporal seFRET
- Figure 2.7** Full-length, endogenous huntingtin is actively recruited and sequestered within fibrillar inclusions
- Figure 2.8** Phosphorylation state of N17 S13 and S16 can influence the fate of the inclusion type
- Figure 2.9** Model of the dynamics of two distinct inclusion types formed from mutant huntingtin protein
- Figure S2.1** HA-tagged mutant huntingtin exon1 forms two inclusion types
- Figure S2.2** Fibrillar and globular inclusions are not differentially ubiquitinated
- Figure S2.3** FLIM-FRET controls
- Figure S2.4** Endogenous huntingtin is detectable within fibrillar inclusions with methanol fixation
- Figure 3.1** Inclusion formation is similar in primary cortical neurons
- Figure 3.2** Inclusion populations in wildtype versus mutant cells by live cell imaging
- Figure 3.3** Inclusion populations in wildtype versus mutant cells by flow cytometry

Figure 3.4 Formation of fibrillar inclusions is preferable in *STHdb*^{Q7/Q7} and with phosphomimetic mutation

Figure 3.5 Visualizing toxicity of inclusion formation in *STHdb* cells by live cell imaging

Figure 3.6 Measuring toxicity of inclusion formation in *STHdb* cells by flow cytometry

Figure 3.7 Dependence of microtubules in inclusion formation mechanism

Figure 4.1 Generation of TruHD immortalized cell lines

Figure 4.2 TruHD cell properties

Figure 4.3 Huntingtin protein levels in TruHD cells

Figure 4.4 Huntingtin localizes to nuclear speckles in response to stress

Figure S4.1 TruHD cell line senescence

Figure S4.2 TruHD cell properties

Figure S4.3 N17-phospho antibody validation

Figure S4.4 Full huntingtin immunoblots from Figure 3

Figure 5.1 Direct conversion of TruHD patient fibroblasts to post-mitotic neurons

Figure 5.2 Huntingtin knockout HEK cells show minimal huntingtin protein levels compared to control

Figure 5.3 Dose-dependent knockdown of huntingtin using PTC Therapeutics compounds

Figure 5.4 Stages of the cell cycle in TruHD cells

Figure 5.5 N17-phospho is upregulated during mitosis by flow cytometry

Figure 5.6 Quantification of primary cilia formation in TruHD cells

TABLE OF CONTENTS

TABLE OF CONTENTS	1
CHAPTER 1: THESIS INTRODUCTION	6
1.1 Overview of Huntington's Disease	6
1.2 History of HD	7
1.2.1 Chorea	7
1.2.2 Collaborative Efforts to Understand HD	8
1.2.3 Discovery of the Huntingtin Gene	9
1.3 Genetic Cause of HD	10
1.3.1 CAG Repeat Disorders	10
1.3.2 CAG Expansion in HD	11
1.3.3 Somatic Expansion of CAG Repeat	12
1.3.4 Genome-Wide Association Studies (GWAS)	13
1.4 Neuropathology and Symptoms of HD	14
1.4.1 Neuropathology in HD Brains	14
1.4.2 Huntington's Disease Symptoms	15
1.5 Gene and Protein Structure of Huntingtin	16
1.5.1 Huntingtin Gene	16
1.5.2 Huntingtin Sequence Conservation and Evolution	16
1.5.3 Huntingtin Protein Sequence	17
1.5.4 Post-Translational Modification of Huntingtin	17
1.5.5 Huntingtin Protein Secondary and Tertiary Structure	18
1.6 Localization of the Huntingtin Protein	19
1.6.1 Cellular and Tissue Distribution of the Huntingtin Protein	19
1.6.2 Regulation of Subcellular Localization of the Huntingtin Protein	20
1.7 Huntingtin Protein Function	21
1.7.1 Embryonic Development	21
1.7.2 Transcriptional Regulation	22
1.7.3 Vesicular Trafficking, Axonal Transport and Endocytosis	22
1.7.6 Huntingtin in Response to Cellular Stress	23
1.7.7 The Expanding Role of Huntingtin in DNA Damage Repair	24
1.8 Pathogenic Mechanisms of HD	25
1.8.1 Transcriptional Dysregulation	25
1.8.2 Mitochondrial Dysfunction	26
1.8.3 Proteolytic Cleavage of Huntingtin	27

1.8.4 Protein Misfolding and Aggregation	27
1.8.4.1 Autophagy	28
1.9 Modelling HD in Animals	29
1.9.1 Use of Animal Models to Study Huntington's Disease	29
1.9.2 Mouse Models	29
1.9.2.1 Huntingtin Fragment Mouse Models	29
1.9.2.2 Full-Length Huntingtin Mouse Models	30
1.9.2.3 Huntingtin Knock-In Mouse Models	30
1.9.3 Non-Human Primate Models	30
1.10 Modelling HD in Cells	31
1.10.1 Using Huntingtin Fragments to Model HD	31
1.10.2 Use of Cell Models to Study Huntington's Disease	31
1.11 Clinical Therapeutic Efforts	33
1.11.1 Overview of Clinical Efforts	33
1.11.1 Huntingtin Lowering	34
1.12 Thesis Outline and Rationale	36
CHAPTER 2: DEFINING TWO TYPES OF MUTANT HUNTINGTIN PROTEIN INCLUSIONS	38
2.1 Contributions to Publication	38
2.2 Implications of Work	39
2.3 Abstract	41
2.4 Introduction	42
2.5 Results	46
2.5.1 Huntingtin Fragments Can Form Morphologically Unique Inclusion Types	46
2.5.2 Fluorescence Lifetime Imaging Microscopy-FRET Reveals Two Conformationally Distinct Inclusion Types Formed by Mutant Huntingtin Fragments	47
2.5.3 FRAP Demonstrates that the Fibrillar and Globular Inclusion Types have Distinct Exchange Dynamics	49
2.5.4 Mutant Huntingtin is Actively Recruited to Globular Inclusions by Microtubules	50
2.5.5 Temporal FRET Reveals Distinct Formation and Maturation Dynamics of Fibrillar and Globular Inclusions	51
2.5.6 Full-length, Endogenous Huntingtin is Actively Recruited to Globular Inclusions and Sequestered within Fibrillar Inclusions	52
2.5.7 N17 Phospho-Mutants Influence Huntingtin Inclusion Morphology	53

2.5.8 Kinase Inhibitors Influence Huntingtin Inclusion Morphology	54
2.6 Discussion	55
2.7 Materials and Methods	59
2.8 Figures	63
CHAPTER 3: DEFINING RELEVANCE OF HUNTINGTIN PROTEIN INCLUSIONS IN CELLULAR TOXICITY	89
3.1 Introduction and Rationale	89
3.2 Exon1 Huntingtin Inclusions Form in Primary Mouse Cortical Neurons	90
3.3 Huntingtin Inclusion Formation in HD <i>STHdb</i> ^{Q111/Q111} Cells	90
3.3.1 Live Cell Counting	90
3.3.2 FRET-based Observations to Examine Huntingtin Inclusion Formation by flow cytometry	91
3.4 Exploring the Role of Phosphorylation in Inclusion Formation	92
3.5 Addressing Toxicity of Inclusions	94
3.6 Mechanism of Inclusion Formation	95
3.6 Materials and Methods	96
3.7 Discussion and Conclusion	97
3.8 Figures	99
CHAPTER 4: DEVELOPMENT OF NOVEL PATIENT FIBROBLAST CELL LINES FOR STUDYING HD BIOLOGY	113
4.1 Contributions to Manuscript in Submission	113
4.2 Implications of Work	114
4.3 Abstract	116
4.4 Introduction	117
4.5 Results	119
4.5.1 Immortalization of Primary Fibroblasts with hTERT	119
4.5.2 Validation of CAG Repeats in TruHD Cell Lines	120
4.3.3 Defining Senescence in TruHD Cell Lines	120
4.5.4 Cell Morphology, Size, Growth and Viability	121
4.5.5 Total Huntingtin and Phosphorylated Huntingtin Protein Levels	123
4.5.6 Huntingtin Stress Response in Human Patient Fibroblasts	124
4.6 Discussion	125
4.7 Materials and Methods	127
4.7.1 Cell Culture and Generation of hTERT-Immortalized Fibroblasts	127
4.7.2 Quantitative PCR to Measure hTERT mRNA Levels	127

4.7.3	Telomeric Repeat Amplification Protocol	128
4.7.4	Cryogenic Storage of TruHD Cells	128
4.7.5	Sizing of CAG Repeat	128
4.7.6	Karyotyping	129
4.7.7	Senescence-Associated Beta-Galactosidase Activity Assay	129
4.7.8	Phenoripper and Cell Surface Area Measurement	129
4.7.9	Cell Counting	130
4.7.10	ADP/ATP Ratio Assay	130
4.7.11	Cell Viability Assay	130
4.7.12	Immunoblotting	131
4.7.13	Flow Cytometry	132
4.7.14	3NP Treatment and Nuclear Speckle Count	132
4.7.15	Dot Blot Assay for Antibody Validation	133
4.7.16	Immunofluorescence Peptide Competition Assay for Antibody Validation	133
4.7.17	Huntingtin siRNA Knockdown for Antibody Validation	133
4.7.18	Statistics	133
4.7.19	Data Availability	134
4.8	Figures	135
4.9	Tables	151
	Table 4.9.1: TruHD Patient Fibroblast Information	151
	Table 4.9.2: G-band Karyotyping	151
	Table 4.9.3: Sizing of CAG Repeats in TruHD Fibroblasts	151
CHAPTER 5: FURTHER EXPLORATION OF HUNTINGTIN FUNCTION IN TRUHD CELLS		152
5.1	Introduction	152
5.2	Direct Re-Programming of TruHD Fibroblasts to Post-Mitotic Neurons	153
5.3	Observing the Effects of Huntingtin Knockdown in TruHD Cells Using Small Molecule Compounds	154
5.4	The Role of Huntingtin in Cell Cycle Regulation	156
	5.4.1 Evidence from Previous Work in the Lab	156
	5.4.2 Cell Cycle Re-Entry of Post-Mitotic Neurons Leads to Apoptosis	157
	5.4.3 Aberrant Cell Cycle Checkpoints in HD Cells	157
	5.4.4 Increased Huntingtin Phosphorylation at Serines 13 and 16 During Mitosis	159
	5.4.5 Hyperciliation in HD Cells	159
5.5	Discussion and Future Directions	161

5.5.1 Discussion	161
5.5.2 Future Directions	161
5.8 Figures	163
CHAPTER 6: DISCUSSION	175
6.1 Context of Work in HD Cell Biology Research	175
6.2 Energy Deficit: A Consistent Thread in HD Biology	177
6.3 Expanding the Role of DNA Damage Repair in HD Progression	178
6.4 Future Avenues of HD Research with TruHD Cells	180
6.5 Conclusions	180
REFERENCES	182

CHAPTER 1: THESIS INTRODUCTION

1.1 Overview of Huntington's Disease

Neurodegenerative diseases are characterized by selective neuronal vulnerability and subsequent degeneration in specific areas of the brain. Huntington's Disease (HD) is a genetic disorder that affects approximately 1 in 10000 individuals¹ and is inherited as an autosomal dominant mutation that primarily affects the cells of the striatum and the cerebral cortex²⁻⁵. Disease symptoms include the progressive loss of motor function, defects in cognitive ability, and potential psychiatric manifestations, such as depression and irritability, that typically begin between 40-50 years of age and worsen over 10-20 years⁶.

HD is one of nine CAG trinucleotide-repeat expansion diseases, along with various types of spinocerebellar ataxias (SCA), spinobulbar muscular atrophy (SBMA) and dentatorubral pallidoluysian atrophy (DRPLA)^{6,7}. HD is characterized by a cytosine-adenine-guanine (CAG) trinucleotide expansion in Exon1 of the *HTT* gene on chromosome 4, leading to the expression of a polyglutamine (polyQ) amino acid tract expansion in the huntingtin protein⁸. Individuals with polyQ lengths between 4 and 36 repeats express normal length, wild-type huntingtin, while repeats greater than 36 are associated with disease⁹⁻¹¹. The length of the expansion has an inverse correlation with the age of disease onset^{10,11}. The longer the CAG repeat, the earlier the disease onset. HD patients are mostly heterozygous carriers of the expanded gene, with a pathogenic repeat of ~40-50 CAG. At lower expansion repeats (~40-45 CAG repeats), there is a large variability in disease onset age between individuals with the same CAG repeat length¹¹. At larger repeats (greater than 50), the variability in disease onset is reduced correlating with a lower disease onset age (closer to 40 years of age).

HD is a monogenic disorder, meaning the CAG expansion alone is sufficient and necessary for disease, however, genome wide association studies (GWAS) have identified other genetic factors that can modify disease onset age, mainly those involved in DNA handling and repair¹¹. Affected individuals usually succumb to the disease 10-20 years after onset, with a

median of 18 years¹¹, as there is currently no cure. Since the discovery of the huntingtin gene in 1993⁶, only treatments that alleviate some of the symptoms exist, but none target the root of the problem: mutant, expanded huntingtin.

Current therapeutic approaches are focused on using antisense oligonucleotides (ASOs) to lower huntingtin levels at the RNA level, indiscriminately lowering wild-type and mutant huntingtin levels. The stage of disease that patients are treated in is now of importance. With the average worldwide life expectancy ranging from 70-80 years of age¹², managing disease symptoms by delaying or preventing onset indefinitely seems like an appropriate approach. Therapeutic approaches that are meant to delay age onset or prevent disease onset would therefore require treatment prior to disease manifestation. Biomarkers to track disease progression are therefore critical for future development of therapies. Additionally, longitudinal observational studies of HD patients, such as in Enroll-HD, reveal trends in HD pathogenesis that may be important when conducting future clinical trials.

1.2 History of HD

1.2.1 Chorea

The primary symptoms of Huntington's chorea and patterns of disease manifestation have been described in various capacities as early as the 15th century. "Chorea" is derived from the Ancient greek word "chorea" which means dance. The first descriptions of a hysterical "dancing mania" described individuals who would dance wildly in circles for hours until they fell from exhaustion¹³. In the early 16th century, the physician Paracelsus coined the term "chorea Sancti Viti", associating the dancing mania with Saint Vitus, as affected individuals reported being cured if they touched churches storing his relics^{4,14,15}.

Later in the 17th century, physician Thomas Sydenham^{16,17} provided a clinical description of involuntary, rapid, purposeless chorea, where "there is a kind of convulsion...it first shows itself by limping or unsteadiness in one of the legs, which the patient drags. The hand cannot be steady for a moment"¹⁸ which was then termed Sydenham's chorea (SC). Further accounts of chorea and rheumatism in children under the age of 15 showed confusion

between 18th century physicians. Later, it became clear that SC would likely be a disorder distinct from those who were afflicted with the syndrome that would later be described as HD¹⁴.

In the mid to late 19th century, several physicians contributed to the refinement of the definition of chorea, and its regard as a syndrome, including Jean-Martin Charcot, Silas Weir Mitchell Osler, William Gowers and Charles Waters¹⁴. This syndrome was later described by George Huntington in 1872 in his seminal paper "On Chorea"¹⁹. He described a neurological disorder, which was later named after him, to have three major characteristics; (1) a hereditary nature, (2) a tendency to insanity and suicide, and (3) its manifestation as a grave disease only in adult life^{20,21}. Huntington regarded chorea as a spectrum, which extended from childhood manifestations (SC) to adulthood (HD). By the late 19th century, studies of patients grew tremendously to further define the types of chorea, describing the adult, hereditary form of HD to be an unrelenting progression of disability, frequent suicide, dementia, inappropriate and uninhibited behaviour, lack of response to treatment and early death^{22,23}. Neuropathology was further described for the disease noting that the caudate nucleus was the central target of brain death^{22,24,25}.

1.2.2 Collaborative Efforts to Understand HD

Prior to the discovery of the gene, it was unclear as to how the disease was passed on, but it was clear that there was a hereditary nature to the disease. In 1955, a physician in Venezuela named Dr. Americo Negrette observed an unusually large population of individuals with chorea living in the village of San Luis near Lake Maracaibo^{4,15,21,26}. Currently, over 18000 individuals are descendants of a family of 11 generations that date back to the 1800s, confirming the autosomal dominant pattern of disease transmission. Many of these individuals are currently affected by HD or at risk. This is the largest single population of individuals with HD in the world. Studies show that they are all descendants of Maria Concepcion Soto, an inhabitant in the early 18th century who inherited from her European father. Others believe

that the population is descended from a Spanish sailor from Germany, named Antonio Justo Doria, who lived in the area in the 1860s^{15,26}.

Interest into the nature of the disease became an important factor into how the gene of interest was founded. The well-known American folk singer and songwriter, Woody Guthrie, was diagnosed with HD in the early 1950s. In the late 1940s, Woody's health rapidly deteriorated and his behaviour became erratic, leading to his initial diagnosis of alcoholism and schizophrenia. After he was eventually diagnosed, his wife, Marjorie Guthrie, founded the Committee to Combat Huntington's Disease (CCHD) which later became the Huntington's Disease Society of America (HDSA)²⁷.

Another notable member of an HD family and a prominent member of the HD community is Dr. Nancy Wexler. Her father, Dr. Milton Wexler, was a psychoanalyst who turned his attention to HD when his wife and Nancy's mother, Leonore, was diagnosed with HD in 1968. Leonore's father, Abraham Sabin, and her three brothers were also previously diagnosed with HD. The same year of her diagnosis, Dr. Milton Wexler founded the Hereditary Disease Foundation (HDF) which was dedicated towards HD research. Nancy, a geneticist herself, organized a trip to Lake Maracaibo in 1979, forming the Venezuelan Collaborative Huntington's Disease Society. With the help of neurologists, geneticists, anthropologists and historians, they conducted a 20-year-long survey, documenting over 18000 individuals to generate a pedigree which led to the discovery of the *HTT* gene.

1.2.3 Discovery of the Huntingtin Gene

The development of recombinant DNA technology for detecting specific regions of DNA made it possible to identify genetic mutations to predict disease²⁸. The rise of advocacy by HD families in the 1960s pushed the eventual turning point in HD history, when the gene was discovered in 1993²⁹. Since 1985, presymptomatic and prenatal testing for HD has been available³⁰. Linkage analysis was used to identify the genetic locus responsible for the disease was in the short arm of chromosome 4³¹. In 1993, the Huntington's Disease Collaborative Research Group precisely identified the gene on chromosome 4 (4p 16.3), naming the gene

interesting transcript 15 (IT15), later referred to as “huntingtin”²⁹. After discovery of the gene, mouse models containing the CAG repeat expansion were generated, such as the R6/2 transgenic line in 1996, and exhibited clinical features of HD³². This marked a turning point in the pursuit to understand one of the most devastating neurological disorders.

1.3 Genetic Cause of HD

1.3.1 CAG Repeat Disorders

Repetitive DNA sequences make up almost 50% of the human genome³³⁻³⁵. These repeats are found in non-coding or coding regions and can be involved in a range of functions. Changes in these repeats can introduce diversity, as alterations in repeat lengths change during evolution. Several human diseases are a result of these repeat lengths exceeding critical thresholds.

HD is a hereditary, autosomal-dominant disorder. HD is one of nine CAG repeat disorders, which include various types of spinocerebellar ataxias (SCA), spinobulbar muscular atrophy (SBMA) and dentatorubral-pallidoluysian atrophy (DRPLA)^{7,36,37}. SBMA was the first disease shown to be caused by the CAG repeat³⁸. Each disease is associated with a CAG expansion in a different gene, with slightly different disease thresholds³⁹ for the CAG repeat (Table 1.1). Even though these diseases share a common mutation type, each mutation occurs in different genes, affecting different proteins and ultimately different clinical symptoms.

Expanded CAG repeats can variably cause ataxia (SCAs), chorea (HD or DRPLA), or neither (SBMA), in association with a variety of other symptoms³⁹⁻⁴¹.

Table 1.1 CAG Repeat Disorders

Disorder	Affected Gene	Affected Protein	Wild-type CAG Length	Pathogenic CAG Expansion Length
HD	<i>HTT</i>	Huntingtin	9-26	>37
SCA1	<i>ATXN1</i>	Ataxin 1	6-35	>38
SCA2	<i>ATXN2</i>	Ataxin 2	13-31	>32
SCA3	<i>ATXN3</i>	Ataxin 3	11-44	>60
SCA6	<i>CACNA1A</i>	Alpha-1 subunit of calcium channel CaV2.1	4-18	>18
SCA7	<i>ATXN7</i>	Ataxin 7	4-19	>33
SCA17	TBP	TATA-binding protein	25-40	>40
DRPLA	ATN1	Atrophin 1	6-35	>47
SBMA	AR	Androgen receptor	9-34	>37

1.3.2 CAG Expansion in HD

The clinical threshold for CAG repeat expansion number in HD is 37. Children of HD carriers have a 50% chance of developing the disease. Normal individuals have CAG repeats between 6 and 26, with an average of 17 CAG repeats. Studies regarding genetic anticipation, where affected children have disease onset earlier than their affected parents did, show that the CAG repeat expands through paternal transmission due to an epigenetic methylation event that is specific to the allele inherited from the father⁴². Therefore, individuals who inherited HD from their father were more likely to have earlier disease onset than if inherited from their mother⁴². Therefore, individuals with 27 to 35 do not develop HD, but the repeat may expand through paternal transmission to children, possibly expanding beyond the threshold for HD. Individuals with repeats between 36 and 39 repeats have reduced penetrance, where they may or may not develop HD. Individuals with over 40 repeats

will have complete penetrance and will develop HD, with an average of 43 repeats. Individuals with repeats greater than 60 have a variant of HD known as juvenile HD. Most HD patients are heterozygous carriers of an expanded allele, but there are rare cases of homozygous carriers of two expanded alleles⁴³⁻⁴⁵. The presence of a second expanded allele does not influence age of onset of motor manifestations, such that the longest, expanded allele exerts dominant action in HD pathology⁴⁵.

1.3.3 Somatic Expansion of CAG Repeat

CAG expansions in coding and non-coding regions can occur, but those in coding regions are usually selected against, while those in untranslated regions are better tolerated. The largest expansions in trinucleotide repeats actually occur in somatic cells under non-dividing conditions^{46,47}. Post-mortem HD striatum samples show CAG expansions up to thousands of repeats that increased with age, consistent with striatal cell vulnerability in HD^{48,49}. Cells with the longest repeats were most vulnerable, showing a potential mechanism in disease pathogenesis.

CAG repeat expansion in somatic cells occurs in conjunction with the accumulation of oxidized bases⁵⁰. Oxidative DNA damage has long been associated with aging and neurological disorders, but the effect of oxidation on these mechanisms is still unclear. Age-dependent somatic CAG expansion mutations can occur in HD during the process of removing oxidized base lesions, dependent on the base excision repair (BER) enzyme, 7-8-dihydro-8-oxoguanine-DNA glycosylase (OGG1)^{50,51}. OGG1 initiates an escalating oxidation-excision cycle that leads to progressive age-dependent expansion, providing a link between oxidative damage and toxicity in post-mitotic neurons through DNA damage responses and erroneous repair of single-stranded breaks.

For expansion to occur, single-stranded loops must be formed in order to provide the “extra” DNA, and then this DNA must be incorporated into double-stranded DNA⁵². When DNA bases are damaged, single-stranded breaks are formed by base excision repair (BER) mechanisms and can result in these looped intermediates⁵³. After removal of damaged bases,

DNA synthesis mechanisms restore the missing base and ligates the DNA. However, during this, displaced single-strand flaps can be generated by long patch mechanisms of repair that can result in hairpin loop formation^{50,53}. Flap endonuclease 1 (FEN1) normally cleaves and removes any displaced strands, but expanded CAG tracts can interfere with FEN1-mediated cleavage and contribute to further loop formation and expansion⁵⁴⁻⁵⁶.

1.3.4 Genome-Wide Association Studies (GWAS)

The length of the CAG repeat expansion in HD patients is inversely correlated with the age of onset, however this correlation is only about 50%^{11,57-59}, showing variability in disease onset in patients with similar repeat lengths, especially close to the pathogenic threshold (around 40-45 repeats). These individuals will inevitably develop HD, but a long-standing question in HD research is how individuals that have the same number of inherited CAG repeats can have disease onset that can differ by over 20 years. Analysis of single nucleotide polymorphisms (SNPs) in genome-wide association studies (GWAS) with ~4000 HD patients revealed that there are other genetic factors, besides the CAG expansion itself, that are modifiers of disease onset¹¹. These modifiers were primarily involved in DNA handling and repair pathways, showing a potential therapeutic approach to delaying HD disease onset. Loci on chromosome 15 show two independent effects that either accelerate or delay onset by 6.1 years and 1.4 years, respectively. Another locus on chromosome 8 can also accelerate onset by 1.6 years¹¹. The most notable delay in psychiatric symptom onset was found on chromosome 3, *MLH1*, the human homolog of DNA mismatch repair gene *mutL* in *E. coli* and *Mlh1*, the mouse homolog that has been implicated in modifying somatic instability of the CAG repeat⁶⁰. *MLH1* association and pathway analysis therefore implicated DNA handling in disease modification, providing new approaches for research targets and therapeutic avenues. This publication marked a turning point in HD research, as the identified targets were validated in humans and are currently the most promising genetic targets, besides the huntingtin gene itself, to modify disease onset.

1.4 Neuropathology and Symptoms of HD

1.4.1 Neuropathology in HD Brains

HD is caused by a selective loss of neurons in the striatum and cerebral cortex in the brain. The striatum is a subcortical region of the forebrain that is classified into the dorsal and ventral striatal regions. Atrophy is mostly seen in the dorsal striatal regions, the putamen and caudate⁶¹. The striatum is composed of dopaminergic and glutamatergic neurons, serving as the primary input to the basal ganglia. There are two main populations of neurons, medium spiny neurons (MSNs), projection neurons that signal to other regions of the brain, and interneurons which signal locally within the striatum^{62,63}. The most vulnerable cells in the striatum to degeneration are the GABAergic MSNs, which are the main targets of striatal input. Pyramidal projection neurons in the cerebral cortex are also vulnerable as HD progresses⁶⁴. The pattern and extent of striatal degeneration in HD patients is classified by five Vonsattel grades⁶⁴, correlating closely to the degree of clinical disability⁶¹.

Table 1.2 Vonsattel Grading of HD Striatal Degeneration

Grade	Striatal Volume	Gross Examination	Microscopic Examination
0	30-40% caudate neuronal loss	Indistinguishable from normal brains, presymptomatic	Neuronal nuclear huntingtin aggregates
1	50% caudate neuronal loss	Minimal to no atrophy detected	Neuron loss in portions of the caudate, in the tail of the caudate, and in the dorsal part of the putamen
2	>50% caudate neuronal loss	Atrophy detected	Ventricular profile of the caudate remains convex, but less so than in normal brain
3	>50% caudate neuronal loss	Atrophy detected, more severe	Striatal atrophy is more severe, and the ventricular profile of the caudate is flat
4	Up to 95% striatal atrophy	Atrophy detected, severe	Ventricular surface of the caudate is concave

This grading system is widely used in neuropathological studies of HD describe changes in disease progression. Other regions, including globus pallidus, hippocampus,

amygdala, thalamus, subthalamic nucleus, substantia nigra, and cerebellum, can also show varying degrees of neuronal loss, depending on disease stage⁶⁵.

Neuronal dysfunction likely occurs before any selective loss of neurons in the brain. Neuroimaging in pre-symptomatic patients shows changes in brain activity before disease onset and neuronal loss⁶⁶⁻⁷⁰, highlighting the importance of monitoring and treatment of HD patients prior to symptom and disease onset.

1.4.2 Huntington's Disease Symptoms

HD is a slow, progressive disorder that has a large range of clinical symptoms that present psychiatric, cognitive and motor impairment. Symptoms usually manifest in adulthood, between 40-50 years of age. Symptoms usually begin with a variety of cognitive and psychiatric impairment, such as personality changes, behavioural abnormalities, depression, restlessness, irritability, disinhibition and anxiety. These usually precede motor symptoms or can accompany small, subtle uncharacteristic motor symptoms like clumsiness, tremors, trouble balancing and jerkiness. These involuntary movements are the most well-known motor symptoms of HD known as chorea. Disease symptoms will progress considerably as the movements become more severe, affecting voluntary movements and activities of everyday life. Further motor impairments include rigidity, bradykinesia, ataxia, dystonia, postural instability, impaired fine motor skills, sensory dysfunction and oculomotor dysfunction. As the disease progresses, the complex spectrum of HD symptoms becomes complicated in the late stages of HD by severe muscle wasting and weight loss and cachexia. Psychiatric, cognitive and neuropsychological symptoms usually worsen throughout the course of the disease as well. By the end of the disease course, patients are completely dependent and bed-ridden, and frequently die from complications such as heart failure and aspiration pneumonia.

1.5 Gene and Protein Structure of Huntingtin

1.5.1 *Huntingtin Gene*

The huntingtin gene (*HTT*) contains 67 exons and is found on the short arm of chromosome 4 at position 16.3 (4p 16.3). Differential polyadenylation of the 3' end results in generation of two mRNA transcripts of 10 366 bp and 13 711 bp. The second transcript has an additional 3' UTR sequence of 3360 bp and is enriched in the brain. Alternative splicing has been reported that generates huntingtin protein that lacks exons 10, 12, 29 and 46, retain a 57 bp portion of intron 28, or have an additional exon (41b).

1.5.2 *Huntingtin Sequence Conservation and Evolution*

Huntingtin has no sequence similarity to other proteins. The elevated expression of huntingtin in human brains and testes shows that the function of huntingtin during mammalian development reflects the evolutionary steps of huntingtin. Acquisition of the polyQ tract traces back to the protostome-deuterostome tree, where the earliest ancestors have either a single Q or no Q. A hydrophilic NHQQ group was more recently found in sea urchins, more similar to a string of QQQQ⁷¹. Huntingtin in species with no or poorly organized nervous systems have less polyQ compared to humans. Huntingtin in higher vertebrate species is required for newly formed nervous systems and post-mitotic neurons and contains a relatively long polyQ tract of variable length.

The most amino terminal region, N17, is highly conserved across most vertebrate species^{1,41,72}, consistent with the importance of N17 on huntingtin localization, toxicity and function⁷³⁻⁷⁶. Additionally, tandem repeat structures known as HEAT repeats (protein-protein interaction domains found in huntingtin, elongation factor 3, protein phosphatase 2A and TOR1) are conserved, but are specific to the deuterostome or vertebrate groups, which may indicate selective pressure for specific protein-protein interactions^{41,71,77}.

1.5.3 Huntingtin Protein Sequence

The huntingtin protein does not possess a catalytic domain^{1,41}, but contains several regions, including HEAT repeats, a nuclear localization signal (NLS) and a nuclear export signal (NES) (Figure 1.1)⁷⁸⁻⁸¹. Much of the huntingtin sequence is conserved between species. Exon1 of the protein (amino acids 1-81) is made up of the polymorphic polyglutamine (polyQ) tract that is flanked upstream at the amino terminal by 17 highly conserved amino acids known as the N17 region and downstream by a polyproline (polyP) rich region. The amino terminal of the protein is the most extensively studied region due to the interest in the pathogenic polyQ tract. Proteins that are rich in HEAT repeats are typically scaffolding proteins that ensure proper protein-protein interactions^{71,77,81}.

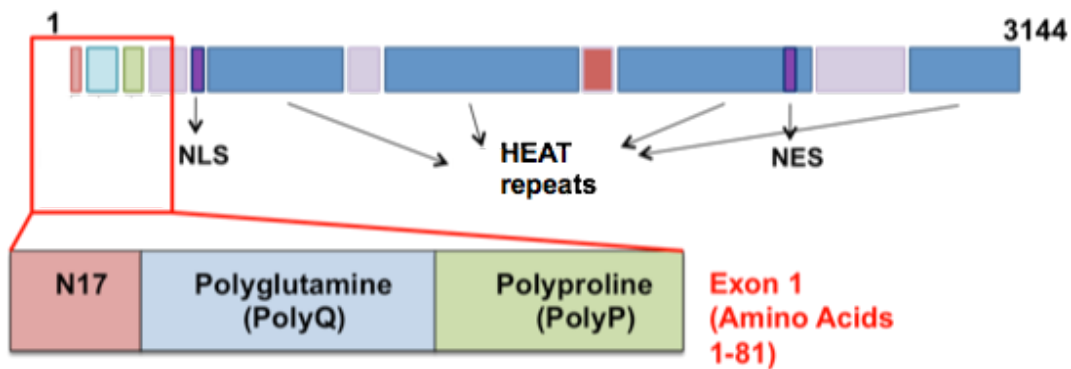


Figure 1.1 Huntingtin Protein Structure. Exon1 region is the most well-characterized as it contains the pathogenic polyQ repeat. The amino terminal domain, N17, is critical to huntingtin function. Not to scale.

1.5.4 Post-Translational Modification of Huntingtin

Post-translational control of the huntingtin protein has mostly been studied on the amino terminal region, close to the polyQ expansion. Huntingtin is subject to a wide variety of modifications, including phosphorylation, acetylation, palmitoylation, ubiquitination and SUMOylation^{74,82-90}, regulating its clearance, trafficking, structure and overall function. Two

critical phosphorylated serine residues (S13 and S16) have been identified in the most amino terminal region, N17. These residues have been shown to be critical for regulation of huntingtin function, localization, stress response^{73,74,76,82,83} and are hypophosphorylated in mutant huntingtin. N17 is the most well-characterized region of the protein, and understanding and restoring aberrant phosphorylation is a major therapeutic target^{72-74,76,78,82,83,91}. Kinases known to affect N17 phosphorylation include casein kinase 2 (CK2) and inhibitor of nuclear factor kappa B kinase subunit beta (IKK- β)^{74,90,92}.

Another serine residue that is phosphorylated is serine 421 (S421)^{93,94}. S421 phosphorylation regulates huntingtin cleavage, aggregate formation and vesicular transport and can be affected by protein phosphatase 2A (PP2A) activity⁹⁵. Acetylation of lysine 444 (L444) regulates trafficking of huntingtin to the autophagosome⁸⁵. Palmitoylation of cysteine 214 (C214) regulates vesicular trafficking^{41,86}. Ubiquitination and SUMOylation of lysine residues in N17 maintains huntingtin homeostasis, localization, activity and stability^{89,96-98}. PolyQ-expanded huntingtin is aberrantly modified, resulting in defective protein degradation, activity, aggregation, localization, vesicular trafficking and overall cellular toxicity.

1.5.5 Huntingtin Protein Secondary and Tertiary Structure

N17 is an amphipathic helix that modulates huntingtin localization⁷³, is involved in various interactions of the huntingtin protein, and is a chromosome-region maintenance 1 (CRM-1)-dependent nuclear export signal (NES)⁷⁸. The N17 region is a highly conserved amphipathic helix that modulates huntingtin localization. Normal polyQ tracts allow for flexibility, such that the N17 region can fold back towards the polyP region and other distal regions⁹⁹. The polyQ tract forms beta-sheet structures which disrupt protein conformation. At pathogenic threshold of 37 glutamine repeats, there is a loss in flexibility, resulting in a “rusty hinge”.

Through various biophysical methods such as circular dichroism and electron microscopy, huntingtin is shown to adopt a solenoid structure¹⁰⁰. Limited structural information is known about huntingtin because of the large size of the protein. Huntingtin is

regarded as a scaffolding hub for protein-protein interactions. Purified human, huntingtin protein exhibits predominantly alpha helical secondary structure circular dichroism (CD) analysis of human huntingtin with polyQ tracts Q2, Q23, Q46, Q67 and Q78¹⁰⁰. Similar to other proteins with HEAT repeats, huntingtin is likely a HEAT domain solenoid that functions as a mechanical scaffold for multi-member complexes^{77,101}. The structures of smaller HEAT repeat protein or HEAT-like solenoid scaffold proteins, such as PR65/A and importin beta, have been solved with high resolution showing stacking characteristics of the HEAT/HEAT-like repeats¹⁰¹. Huntingtin solenoid maintains this stacking characteristic and 3D electron microscopy analysis reveals a spherical shape with a central cavity. The huntingtin solenoid comprises of a major hinge that separates two large, nearly equal-sized domains that folds together so that there is an internal cavity. This is consistent with other HEAT repeat proteins, such as importin beta, which have critical protein-protein binding interfaces located of the inner face of the solenoid structure. Huntingtin is a much larger protein, and has functional domains inside the cavity, allowing internal and external binding to proteins and nucleic acids, supporting its role as a mechanical HEAT/HEAT-like repeat interaction scaffold. There is a subtle, but detectable change in structure as the polyQ tract increases, changing the interaction patterns of carboxy terminal and amino terminal regions. Recently, cryo-electron microscopy was used to determine the structure of full-length, human huntingtin bound to huntingtin associated protein 40 (HAP40) at a resolution of 4 angstroms¹⁰².

1.6 Localization of the Huntingtin Protein

1.6.1 Cellular and Tissue Distribution of the Huntingtin Protein

Huntingtin is ubiquitously expressed in all cells, but has elevated expression in the brain and testis^{103,104}. Even though huntingtin expression is widespread, cell loss in HD is limited to the striatum and cerebral cortex. In neurons, huntingtin is localized to the cytoplasm, nucleus, axonal processes, synapses, microtubules, vesicles and various cell organelles such as the endoplasmic reticulum (ER), Golgi complex and mitochondria^{73,105-109}.

It is a scaffolding protein that is known to interact with many proteins, with normal functions ranging from vesicular transport, stress response, mitochondrial function, and transcriptional regulation^{1,41,73-75,81,91,110-114}, and is therefore found in all cells.

1.6.2 Regulation of Subcellular Localization of the Huntingtin Protein

Huntingtin N17 is a membrane-binding domain that can reversibly target huntingtin to vesicles and the ER⁷³. Huntingtin vesicular interaction mediated by N17 is specific to late endosomes and autophagic vesicles. The association of huntingtin to the ER is affected by cellular stress, as huntingtin lifts off the ER and shuttles into the nucleus upon stress. Nuclear localization is regulated by chromosomal region maintenance 1 (CRM1), a nuclear export factor that binds the hydrophobic face of N17 and is dependent on the RanGTP/GDP gradient. N17 phosphorylation results in increased nuclear entry by preventing CRM1 binding and nuclear export. Increased nuclear entry of mutant huntingtin due to loss of ER-targeting is associated with increased toxicity¹¹⁵⁻¹¹⁸. Additional regulation of huntingtin nucleocytoplasmic localization occurs through the proline-tyrosine nuclear localization signal (PY-NLS) found between amino acids 174-207 which is regulated by the importin/karyopherin $\beta 1/\beta 2$ pathway⁷⁹.

Huntingtin can also interact directly with cytoskeletal components such as actin and microtubules. Huntingtin is also found at centrosomes, the mitotic spindle, the cleavage furrow, and cofilin-actin stress rods. Huntingtin can also associate with deoxyribonucleic acids (DNA) and ribonucleic acids (RNA), as well as lipids, resulting in huntingtin binding to membranes and vesicles. Because of this large network of interactions, huntingtin is involved in many cellular functions. Huntingtin is also made up of several domains that interact with various proteins from different pathways. Huntingtin is therefore regarded as a scaffolding protein for various protein interactors, with normal functions ranging from vesicular transport, stress response, mitochondrial function, and transcriptional regulation^{1,41,73-75,81,91,110-114}, and is therefore localized to several different regions in the cell (Figure 1.2).

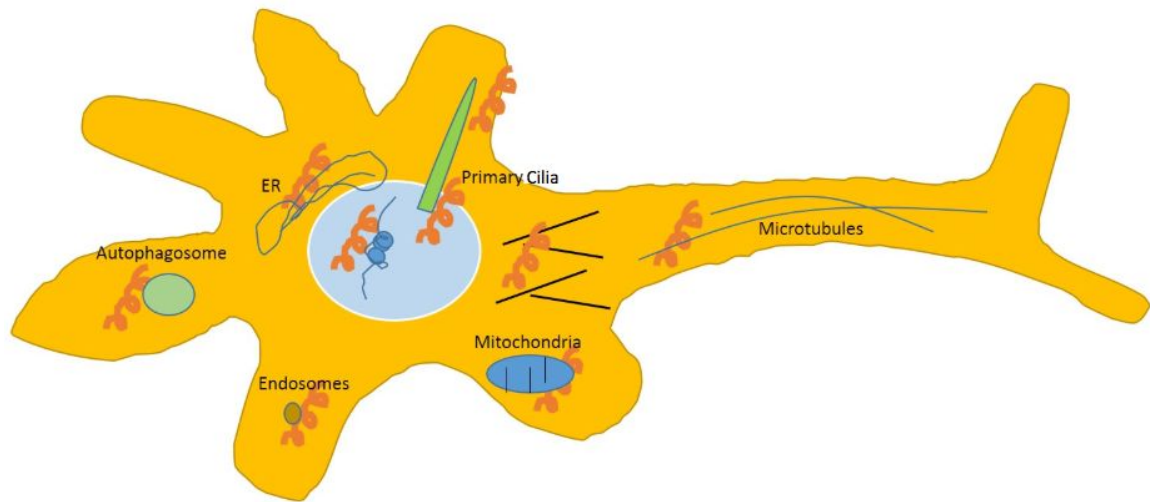


Figure 1.2 Subcellular distribution of huntingtin. Huntingtin is represented by orange helix. Not to scale.

1.7 Huntingtin Protein Function

1.7.1 Embryonic Development

Normal, wildtype huntingtin has been implicated in several cellular mechanisms that are critical to physiological function. Complete inactivation of huntingtin (mouse homolog *Hdh*) in knockout mice (*Hdh*^{-/-}) results in embryonic lethality before gastrulation and formation of the nervous system¹¹⁹⁻¹²¹. Defects in embryonic development are a result of increased apoptosis and defects in the organization of extraembryonic tissue^{119,121,122}.

Reduction of huntingtin levels below 50% results can result in defective epiblast formation, disrupting formation the neural tube and central nervous system (CNS)¹²². Having just a single copy of the *Hdh* gene (+/-) is sufficient to prevent embryonic lethality^{119,121}. Additionally, having a single copy of either wild-type or mutant, CAG-expanded *Hdh* is sufficient for normal development¹²². Huntingtin is therefore expressed early in development,

and a certain amount of it is necessary for normal embryonic development, wild-type or mutant.

1.7.2 Transcriptional Regulation

PolyQ motifs are often found in transcription factors and can mediate binding of transcription factors with transcriptional regulators^{1,41,122-125}. Wild-type huntingtin binds several transcription factors, including cAMP-response element binding (CREB)-binding protein (CBP)¹²⁶, NeuroD¹²⁷, specificity protein-1 (SP1)^{118,128}, nuclear factor kB (NF-kB)⁷⁷ and p53⁷⁷. Huntingtin can also bind transcriptional activators and repressors, such as the co-activator TAFII130¹²⁸ and the repressor element-1 transcription factor/neuron restrictive¹²⁸ silencer factor (REST/NRSF)^{41,125}. Huntingtin therefore promotes and represses gene transcription in several cellular responses.

The exact mechanisms of transcriptional regulation by wild-type huntingtin are unclear for each potential pathway, but it is likely that huntingtin acts a scaffold for transcriptional complexes, similar to its role as a scaffold for other protein-protein interactions. Huntingtin may bind transcription factors and mediate their transport to the nucleus.

1.7.3 Vesicular Trafficking, Axonal Transport and Endocytosis

Huntingtin is found primarily in the cytoplasm and is enriched in compartments that contain vesicle-associated proteins¹²⁹. Wild-type huntingtin regulates axonal transport by contributing to assembly of motor complexes on microtubules¹¹⁴. Huntingtin can associate with motor proteins via huntingtin associated protein 1 (HAP1), which can also interact with the p150 subunit of dynactin, enabling retrograde and anterograde transport¹³⁰⁻¹³². Wild-type huntingtin is also involved in fast axonal trafficking of mitochondria in mammalian neurons¹¹⁴, contributing to assembly of motor complexes on microtubules.

Huntingtin interacts with several proteins that are involved in endocytosis, such as huntingtin interacting protein 1 (HIP1) and dynamin 1. These proteins are involved in clathrin-mediated endocytosis, participating in membrane invagination, assembly of the

clathrin membrane coating and severing the membrane¹³³⁻¹³⁵. Huntingtin also interacts with GTPase Rab11 which participates in vesicle recycling during endocytosis¹³⁶. Huntingtin also regulates endosomal trafficking via huntingtin associated protein 40 (HAP40), which can also interact with Rab5 and form a complex that is recruited onto early endosomes¹³⁷. In this complex, huntingtin can mediate transition of endosomes between actin filaments and microtubules.

1.7.5 Synaptic Transmission

Several proteins are required to regulated communication between neurons at the synapse. Excessive activation of receptors by excitatory neurotransmitters results in excitotoxicity. MSNs receive extensive glutamatergic input from the cortex and thalamus¹³⁸. Activation of N-methyl-D-aspartate (NMDA) receptors results in an influx of Ca²⁺ ions, activating downstream pathways required for gene transcription, neuronal survival and synaptic plasticity¹³⁹.

Huntingtin is highly expressed in presynaptic terminals of nerve cells and is important in synaptic activity by scaffolding components of the cytoskeleton and synaptic vesicles¹³⁸. In HD, overactivation and hypersensitization of NMDA receptors results from the increased release of glutamate from the cortex, causing excitotoxicity and neurodegeneration. Increased Ca²⁺ from excessive activation of NMDA receptors can activate downstream pathways that lead to neuronal death^{140,141}, including generation of reactive oxygen species (ROS), the activation of caspases, mitochondrial dysfunction and impaired cellular calcium homeostasis^{19,138,142}.

1.7.6 Huntingtin in Response to Cellular Stress

Huntingtin has been shown to be a critical component of cellular stress responses in a number of studies^{73-75,143-145}. In steady state conditions, huntingtin is mostly targeted to the ER membrane^{73,98}. Upon stress conditions, such as heat shock or unfolded protein response (UPR)-inducing stresses, N17 is phosphorylated at serine residues 13 and 16, causing

huntingtin to dissociate from the ER and translocate to the nucleus^{73,74}. More recently, we published that oxidative stress, from increased ROS, oxidizes methionine 8 of N17, facilitating huntingtin translocation off of the ER membrane and subsequent phosphorylation and nuclear translocation^{72-74,78}.

In the nucleus, huntingtin can then participate in transcriptional regulation or localize to stress-dependent cofilin-actin rods. Cofilin is an actin-binding protein that is involved in the disassembly of actin filaments necessary for actin treadmilling. This is a very energy-consuming process, and upon cellular stress, treadmilling is halted when cofilin saturates actin filaments to free up ATP levels for other cellular processes¹⁴⁶. In wild-type cells, several short rods are formed and will clear after the cellular insult is removed. However, in HD cells, these rods are elongated and persist, resulting in cell death^{143,144}. Similarly, huntingtin can also translocate from the ER to huntingtin stress bodies (HSBs) under stress conditions in order to conserve ATP levels, by transiently arresting early to late endosome maturation¹⁴⁵.

1.7.7 The Expanding Role of Huntingtin in DNA Damage Repair

DNA damage repair pathways are important processes in the cell that exist to prevent sporadic mutations in the cell from occurring during cell division. Mismatch repair pathways have been implicated in modifying disease onset and progression of CAG disorders by affecting the repeat lengths themselves^{39,147}. In addition, many CAG-repeat containing proteins have roles in DNA damage response, such as in base excision repair (BER) and the pathogenic expansion results in aberrant function.

ROS-induced oxidative stress is associated with aging and selective neuronal loss in neurodegeneration^{148,149}. DNA strand breaks and damaged bases have been reported in HD patient samples and mouse models¹⁵⁰⁻¹⁵², supporting GWAS, which showed that DNA damage repair pathways were implicated as the predominant modifiers of HD pathogenesis¹¹. There is also increased DNA damage seen in HD cells⁹¹. Huntingtin (specifically methionine 8 of N17) can sense oxidative stress and cause its translocation from the cytoplasm to the nucleus⁷². When in the nucleus, huntingtin can be recruited to sites of DNA damage and act as a

scaffolding protein for ataxia telangiectasia mutated (ATM)-mediated oxidative DNA damage repair, interacting with DNA repair proteins such as XRCC1, FEN1 and APE1^{91,153}.

Moreover, ATM has been shown to contribute to disease progression in the BACHD mouse model^{91,153}, highlighting a role for huntingtin in DNA damage repair.

1.8 Pathogenic Mechanisms of HD

1.8.1 Transcriptional Dysregulation

Changes in gene expression profiles are pronounced in HD striatal neurons. Different groups of genes are altered at different stages of HD^{112,118,124,125,128}. Transcription factors can aberrantly interact with mutant huntingtin, resulting in transcriptional arrest and downregulation of several genes.

Brain-derived neurotrophic factor (BDNF) is a neurotrophin that is produced in the cerebral cortex. Cortical BDNF levels are reduced to ~50% in HD, as BDNF mRNA and protein levels are reduced in postmortem HD brain tissues and mouse models^{124,154}. BDNF is particularly important for the survival of striatal neurons and activity of cortico-striatal synapses. Huntingtin is part of a cytoplasmic complex that includes the repressor REST/NRSF^{124,125}. Mutant huntingtin disrupts the repressive REST/NRSF complex, increasing activity of the RE1/NRSE silencer on the BDNF promoter. Other transcriptional factors that regulate the activity of BDNF promoters are also affected by mutant huntingtin such as cAMP response element-binding protein (CREB), CREB binding protein (CBP), specificity protein 1 (Sp1) and TBP associated factors 130 (TAF130)^{41,123,154}.

Mutant huntingtin can also change the balance of histone acetylation, resulting in chromatin structure changes and transcriptional repression of several genes¹⁵⁵. Histone acetylation at specific lysine residues are regulated by histone acetyltransferases (HAT) and histone deacetylases (HDAC) and is critical for establishing conformational structure of DNA-chromatin complexes, regulating gene expression.

1.8.2 Mitochondrial Dysfunction

Mitochondrial dysfunction results in reduced energy production and calcium handling which contributes to HD pathogenesis, as many of the defects precede clinical onset of symptoms. It was first predicted that there was a bioenergetic defect linked with HD pathogenesis because of profound weight loss in patients despite maintained caloric intake¹⁵⁶⁻¹⁵⁹. In addition to defects in mitochondrial structure detected in post-mortem brain tissue¹⁶⁰, reductions in glucose utilization were also reported in striatum of HD patients by positron electron tomography (PET). These studies also reveal that energy dysfunction preceded onset of clinical symptoms, suggesting that the energy impairment played a primary role in HD disease pathogenesis.

Several critical enzymes involved in mitochondrial function and energy metabolism are also defective, such as succinate dehydrogenase, a component of both the Krebs cycle and complex II of the electron transport chain in the caudate¹⁶¹. Decreased activity of complex II in the caudate, complex III in the caudate and putamen and complex IV in the putamen have also been noted^{158,162,163}. Prior to the discovery of the huntingtin gene, early cell and animal models of HD actually utilized 3-nitropropionic acid (3-NP), an irreversible inhibitor of succinate dehydrogenase that inhibits both the Krebs cycle and complex II activity, achieve selective atrophy of the striatum to mimic pathology and symptoms characteristic of HD.

Striatal mitochondria are more sensitive to mitochondrial permeability transition (mPT), which occurs in response to calcium and oxidative stress¹⁶⁴. mPT leads to a loss of mitochondrial membrane potential, which may result in cytochrome c release, signalling apoptosis and loss of ATP production.

There is also evidence that the presence of mutant huntingtin can cause neuronal cell death by interfering with trafficking and distribution of mitochondria, which is necessary for maintaining ATP levels for energy-dependent processes, such as at synapses¹⁶⁵. Firstly, aggregation of mutant huntingtin can result in sequestration of important mitochondrial trafficking components, which results in defective anterograde and retrograde mitochondrial transport and impaired motility along microtubules¹¹⁴. Mutant huntingtin also binds the

mitochondrial fission GTPase dynamin-related protein-1 (DRP1)¹⁶⁶, disrupting the balance of mitochondrial fission and fusion cycles which are necessary for neuronal function^{167,168}. This imbalance triggers mitochondrial fragmentation in mouse and rat neurons and HD patient fibroblasts. These mitochondria possess a shorter and rounder morphology¹⁶⁶.

1.8.3 Proteolytic Cleavage of Huntingtin

Huntingtin cleavage has been implicated in HD pathogenesis by several groups¹⁶⁹⁻¹⁷⁴. Huntingtin is targeted for cleavage by cysteine-aspartic proteases; caspase 3, caspase 6 and caspase 7 at amino acids 513, 586 and 552 respectively^{165,171-173,175-179} to produce small huntingtin fragments. Cells expressing fragments of huntingtin had increased toxicity, suggesting a role of proteolysis in HD pathogenesis referred to as the toxic fragment hypothesis. Additionally, mouse models that overexpress a small amino terminal fragment, R6/2 mouse, provide evidence that a small portion of huntingtin (Exon1 containing the expanded polyQ tract) is sufficient to cause disease symptoms³². Preventing huntingtin proteolysis was shown to be beneficial in HD mice. Caspase-cleaved fragments of huntingtin have been detected in post-mortem HD brains^{169,171}.

YAC128 mice expressing full-length mutant huntingtin resistant to caspase 3 showed similar pathology as regular YAC128 mice. Conversely, mice that were expressing full-length mutant huntingtin that were resistant to caspase 6 cleavage showed no neurodegeneration or HD pathology¹⁷⁸, suggesting caspase 6 cleavage as a critical step in neuronal dysfunction.

1.8.4 Protein Misfolding and Aggregation

Abnormal accumulation of intra/extracellular proteins in affected brain regions is a hallmark of neurodegenerative diseases such as Alzheimer's disease (AD), Parkinson's disease (PD), as well as other polyQ disorders¹⁸⁰⁻¹⁸⁴. A hallmark characteristic of HD brains is the formation of intracellular huntingtin aggregates^{2,96}. Neurodegeneration in AD has been described by the amyloid hypothesis, which suggests that the mechanism for pathogenesis is related to the formation of insoluble plaques in the brain consisting of misfolded amyloid-beta

(A β) protein^{180,185}. This hypothesis has been adopted to describe pathogenic mechanisms in other neurodegenerative disorders; in HD this is called the toxic fragment hypothesis^{117,186}. Toxic amino-terminal fragments are created from the proteolytic cleavage of mutant huntingtin^{170,175,176} and mutant huntingtin with more than 37 glutamine repeats favour a rigid β -sheet conformation. Anti-parallel β -sheets form hydrogen bonds between glutamines resulting in the accumulation of insoluble mutant huntingtin protein, which form insoluble aggregates known as inclusions^{187,188}. Mutant huntingtin inclusions have shown differential effects on cell toxicity¹⁸⁹ and could possibly be protective entities^{76,190-192}. These studies propose that the formation of inclusions is a cellular stress response to sequester the mutant huntingtin protein into an insoluble form to prevent it from interfering with cellular functions, suggesting that the soluble mutant huntingtin is the toxic species. The mechanism of inclusion formation is generally described by a nucleation event where a few monomers of the polyQ tract combine to form oligomers. Once these oligomers form, polyQ monomers rapidly join the growing aggregate to form β -sheet rich fibrils, exhibiting features that are characteristic of amyloid fibrils such as thioflavin-T binding¹⁹¹. Alternative explanations have been described, where the N17 region is involved in nucleating the aggregate in solution, and that the polyQ tract promotes amyloid fibril formation¹⁸⁸. The precise mechanism behind inclusion formation in cells is not currently known. This is discussed in detail in Thesis Chapters 2 and 3.

1.8.4.1 Autophagy

Autophagy is a critical biological process that is essential for the removal of damaged organelles and aggregated proteins by delivering them to the lysosome for degradation. Several defects in autophagy have been reported in HD cells¹⁹³⁻¹⁹⁵. PolyQ-expanded huntingtin abnormally activates the autophagy pathway in various HD models through inactivation of mammalian target of rapamycin (mTOR) kinase^{196,197}. Formation of autophagosomes is abnormally high in HD^{196,198,199}, and a defect in loading of the autophagosomes is observed, leading to a reduced capacity of cells to degrade aggregated proteins¹⁷⁴.

1.9 Modelling HD in Animals

1.9.1 Use of Animal Models to Study Huntington's Disease

Successful alleviation of disease symptoms in animal models is a well established pre-requisite for clinical trials of drugs. Symptoms of HD are regularly corrected in several different animal models, but since the discovery of the gene, there have been no effective treatments that have translated to human disease. This may have been a result of the model system. Since HD is caused by a single genetic mutation, genetically engineered animal models that present HD symptoms are feasible to generate.

1.9.2 Mouse Models

Several mouse models exist with either truncated human huntingtin, full-length human huntingtin or full length mouse huntingtin. Each model therefore shows slight differences in their phenotypes. Mouse models are regularly used to test potential drugs for all diseases, but there are limitations for studying a late-onset neurodegenerative disorder. In order to mimic a late-onset human disease within the lifespan of a mouse, large, unrealistic CAG repeats are used (well over 100 repeats). Repeats that long are associated with juvenile HD in humans or even exceed the threshold seen in juvenile HD. Human huntingtin protein is 3144 amino acids, while mouse huntingtin protein is only 3120 amino acids. The proteins are 91% identical, excluding the polymorphic polyQ and polyP regions²⁰⁰.

1.9.2.1 Huntingtin Fragment Mouse Models

The R6/2²⁰¹ and N-171¹¹⁶ mouse models express truncated exon1 or the first 171 amino acids, respectively, with polyQ-expanded human huntingtin. These mice were among the first to be generated in the HD field. The fragments result in neuronal toxicity in the mice, similar to the expected pathology for HD. However, the context of that expansion within the rest of the protein is lost, and the function of the huntingtin protein is no longer representative

of what actually happens in disease²⁰⁰. Pathogenic mechanisms and progression of disease therefore cannot be studied as easily in these mice.

1.9.2.2 Full-Length Huntingtin Mouse Models

Transgenic mouse models expressing full-length mutant, human huntingtin have also been generated using yeast artificial chromosomes (YAC)^{115,202} and bacterial artificial chromosomes (BAC)²⁰³. These mice show earlier behavioural abnormalities more suitable for studying therapeutic intervention. These mice also show a progressive, age-dependent motor and cognitive impairment combined with late-onset selective neurodegeneration in the striatum and cortex consistent with human disease.

1.9.2.3 Huntingtin Knock-In Mouse Models

In contrast to fragment models and transgenic models, knock-in models utilized homologous recombination to introduce expanded CAG repeats directly into the mouse huntingtin gene. The advantages of these systems are that variability in transgene copy number expression levels. Additionally, like most HD patients, the knock-in (KI) mice are heterozygous for one wild-type allele and one CAG-expanded allele. Current models either knock-in the CAG expansion directly into the mouse huntingtin gene (such as the CAG140^{204,205} and zQ175²⁰⁶⁻²⁰⁸), or into a humanized exon1 gene, creating a mouse-human chimeric mouse (*HdbQ111*)^{209,210}. KI mice express huntingtin in the most accurate genomic and protein context, but inherent differences in human and mouse huntingtin gene regulation could be a limitation.

1.9.3 Non-Human Primate Models

HD mouse models do not accurately reflect neurological and behavioural changes seen in humans. Non-human primates, monkeys, are more closely related to humans^{211,212} and are useful for modelling clinical features of HD. Transgenic monkeys expressing mutant

huntingtin showed dystonia and chorea, important clinical features of HD²¹³⁻²¹⁵. Currently, therapeutics trials in non-human primates is expensive and labour-intensive.

1.10 Modelling HD in Cells

1.10.1 Using Huntingtin Fragments to Model HD

Most of the previously published work in our lab and in the HD cell biology research field has utilized overexpression of fluorophore-tagged huntingtin fragments^{72-74,76,78,99,145} as it is technically challenging to overexpress full length huntingtin due to its large size. These fragments were generally amino-terminal fragments to encompass the polyQ repeat expansion. In order to mimic disease transiently in the cells, large polyQ repeats are necessary (70+ repeats).

There is evidence showing that HD pathology can be related to the formation of amino-terminal mutant huntingtin fragments, but their overexpression in cells is not a proper reflection of endogenous huntingtin biology. These systems have several limitations, and over the past few years it has become evident that repeats that are closer to clinically reported lengths are more important to study.

1.10.2 Use of Cell Models to Study Huntington's Disease

Studying HD cell biology in relevant cell models has faced many challenges. Cell models range from primary striatal neurons to immortalized cell lines, derived from mice and human tumour cells. Several types of cell lines have been used to model HD, such as human cervical HeLa cells, human embryonic kidney HEK293T cells, mouse neuroblastoma Neuro2a cells, rat embryonic striatal ST14A cells and neuron-like rat PC12 cells^{216,217}. Similar to the limitations with HD animal models, long CAG repeats that are well beyond the threshold in human disease are used. Additionally, these cell lines are either tumourigenic to begin with, or are expressing SV40 large T-antigen to induce malignant transformation of the cells, resulting in binding and perturbation of retinoblastoma (pRb) and p53 tumour-suppressor

proteins^{218,219}. SV40 large T-antigen is an oncogenic hexamer protein that is derived from polyomavirus SV40, so once the cells are virally infected, they will essentially be immortalized and are capable of continued proliferation and can survive in a wide range of environmental conditions that they usually would not be able to. However, cells that have been transformed with SV40 T-antigen have defective karyotypes^{220,221}. *In vitro* studies transformed cell lines has been critical to understanding several cellular mechanisms for various pathways and diseases. However, a large caveat is that p53, widely regarded as the master regulator of cell biology, controlling cellular stress responses and apoptosis, is perturbed and inactivated in these cells. Several functions of p53 that overlap with those that huntingtin is implicated in, such as cellular stress response and DNA damage repair, enforce the need to stray away from transformed cell lines. Additionally, the huntingtin gene has a p53 responsive element upstream of the promoter²²². Since GWAS, it is evident that p53 is important to HD cellular biology, so primary neuronal cells from animal models can be used, but are once again subject to the limitations from the animal model from which they are taken from. These cells have been an excellent resource that has been used extensively in the field since they were generated, but efforts to use more relevant cell lines have been prominent in recent years.

The most relevant cell lines would be neurons from human patients. Unfortunately, obtaining neurons from HD patients is not currently feasible. However, clinicians can obtain fibroblasts from a skin biopsy, which can then be cultured^{32,223}. These cells are valuable tools because they are taken from actual HD patients and their CAG lengths are clinically relevant. For most of the HD patients, there is usually a corresponding control patient (i.e spouse, sibling, offspring). Further, skin fibroblasts can be differentiated into neurons through induced pluripotent stem cells (iPSCs)²²⁴ or by direct reprogramming strategies²²⁵⁻²²⁸. This makes patient skin fibroblasts the most attractive cellular model for HD cell biology research.

1.11 Clinical Therapeutic Efforts

1.11.1 Overview of Clinical Efforts

Unlike other neurodegenerative disorders like AD and PD, HD is caused by a single genetic mutation in the huntingtin gene, so predictive genetic testing can be done to diagnose HD prior to disease onset, allowing for early intervention. Reliable biomarkers are necessary in order to track disease progression in order to isolate an ideal window for intervention. Detection of several biomarkers in cerebrospinal fluid (CSF) including neurotransmitters, transglutaminase activity, kynurenine pathway metabolites, oxidative stress markers, inflammatory markers, neuroendocrine markers, protein markers of neuronal death, proteomic approaches and mutant huntingtin protein itself can track disease progression and these assays are currently used in ongoing clinical trials^{229,230}.

Several avenues have been attempted to treat HD, based on pathological mechanisms detected in vitro and in vivo (summarized in Table 1.3)

Table 1.3: Summary of Therapeutic Attempts

Compounds	Targeted Effect Based on Pre-Clinical Results	Clinical Trial Results
Memantine	NMDA receptor antagonist, prevent excitotoxicity ^{231,232}	No significant effect
HDAC inhibitors (ex. Resveratrol)	Relax chromatin to increase transcription of pro-survival genes ²³³	No significant effect
Minocycline	Inhibit caspase 1 and 3 ²³⁴	No significant effect
Riluzole	Inhibit aggregation of mutant huntingtin ^{234,235}	No significant effect
PDE10 inhibitor	Improved corticostriatal input caused by increases in cAMP and cGMP ^{229,236}	No significant effect
Creatine	Increased intracellular ATP to address energy deficit ^{237,238}	No significant effect
Coenzyme Q10	Increased intracellular ATP to address energy deficit ²³⁹⁻²⁴¹	No significant effect

Pre-clinical results from mouse studies, therefore, do not always translate to clinical trials in humans, as evidenced by lack of significant effects in clinical trials in Table 1.3.

1.11.1 Huntingtin Lowering

The huntingtin protein itself is the most validated target for therapeutic invention of HD. Because mutant huntingtin exerts toxicity in a dominant fashion, most patients are heterozygous, meaning they have one copy of a wild-type allele and one copy of the mutant, CAG-expanded allele. Silencing expression of the mutant, CAG-expanded allele would theoretically ameliorate HD phenotypes, allowing wild-type huntingtin to still be expressed.

RNA interference (RNAi) and anti-sense oligonucleotide (ASO) approaches are currently being tested for gene silencing. RNAi approaches, using short hairpin RNA (shRNA) inhibit gene expression post-transcriptionally by targeting specific mRNAs for destruction²⁴². These shRNA are delivered by adeno-associated virus (AAV) directly to the striatum, and can ameliorate disease manifestations in YAC128 mice²⁴³. ASOs are small, single stranded oligonucleotides that share the same fundamental principle as RNAi, but since ASOs are delivered as a single strand, through Watson-Crick base pairing, can bind directly to the RNA target^{242,244}. An advantage of using ASOs is that it can be delivered by injection and infusion without the need for viral delivery. ASOs can have a high degree of specificity for its target and can be adapted for various single nucleotide polymorphisms (SNPs). Since the polyQ tract itself is repetitive and not specific enough to huntingtin, SNPs that distinguish the mutant gene from the wild-type gene can be exploited²⁴⁵⁻²⁴⁷ to selectively target the mutant copy.

The effect of the mutation on huntingtin function is often debated as being referred to as a loss of function or a gain of function. Therapeutic approaches that target huntingtin are focused on lowering huntingtin levels, suggesting a pathogenic gain of function is at fault, so toxicity can therefore be reduced along with lowering of huntingtin levels. This would imply that indiscriminately lowering both wild-type and CAG-expanded huntingtin would be beneficial to reduce toxicity to compensate for the gain of function. which is basis for the

IONIS-HTT Rx (RG6042) ASO trial started in 2017, with the first results of Phase I/II reported in December 2017²⁴⁸. The Phase I/II study was a randomized, placebo-controlled dose escalation in 46 participants with early stage HD. Participants were treated for 13 weeks with four intrathecal injections of 10mg, 30mg, 60mg, 90mg or 120mg of ASO, administered monthly. The drug passed safety tests and no serious adverse effects were reported. Significant dose-dependent reduction in mutant huntingtin were observed in CSF up to 60%, the first ever human trial of a drug for HD that can suppress huntingtin protein. The ASO is, however, not specific for mutant huntingtin and indiscriminately lowers both wild-type and mutant huntingtin. As described earlier, huntingtin plays a critical role in several cellular functions, and the CAG expansion results in a disruption, or loss of these functions. Therefore, the effect of lowering wild-type huntingtin cannot be overlooked. The drug can lower huntingtin levels, but longitudinal observation and reliable biomarkers is needed to confirm if there is any effect of disease symptoms.

In order to address the potential problem with indiscriminately lowering both wild-type and mutant huntingtin, Wave Life Sciences are currently in Phase I/II clinical trials of two, stereopure, allele-specific ASOs, WVE-120101 and WVE-120102 (trials referred to as PRECISION-HD1 and PRECISION-HD2 respectively). These trials are multi-centre, randomized, double-blind, placebo-controlled studies that will primarily evaluate the safety and tolerability of the drug. This approach utilizes SNPs present in the huntingtin gene in early manifest HD patients, rs362307 (SNP1) or rs362331 (SNP2), corresponding with PRECISION-HD1 and PRECISION-HD2 respectively. Approximately two-thirds of all HD patients carry either or both SNPs in associated with the HD gene^{248,249}. This trial is currently ongoing, and results from Phase I/II have not yet been reported, except for safety and tolerability.

1.12 Thesis Outline and Rationale

A hallmark feature of HD brains is the formation of inclusions, composed of accumulated mutant huntingtin protein. Uncontrolled accumulation is classically viewed as toxic, however, there is growing debate about whether these entities are toxic in HD, or if they are protective. A possible explanation for this could be that there are two types of inclusions. We published a study describing two distinct types of inclusions: fibrillar and globular. The fibrillar type is tightly packed and irreversibly collects the mutant huntingtin from the rest of the cell. In contrast, the globular type allows huntingtin to exchange in and out. Formation of fibrillar inclusions may be protective, by quickly removing toxic mutant htt from the rest of the cell. We were working towards uncovering a new model for huntingtin aggregation, hopefully revealing an avenue with therapeutic potential to favour formation of fibrillar inclusions, or inhibit globular inclusions to treat the disease. However, these studies were performed in mouse cells with overexpressed proteins, so research for therapeutic potential for human disease was inconclusive.

In the pursuit of studying HD cellular biology, several methods have been designed to model classic HD phenotypes seen at the level of animal models, post-mortem human brain tissue and human disease characteristics. Cellular modelling of HD has relied on several manipulations to standard models, such that the research is made more feasible. The study of HD cell biology has unfortunately been limited to models that are not reflective of human disease (such as mouse cells and disease-exaggerated cell lines). Obtaining brain cells from a living patient is not feasible, but skin cells can be obtained and studied, and even converted into brain cells. These cells, however, have a limited lifespan and lack consistency between trials and long-term experiments. We sought to overcome this by immortalizing the cells by preventing processes that are involved in cell senescence. We have therefore generated patient-specific, human cell lines that are clinically relevant and will provide an improved tool for the HD research community.

The contents of this thesis therefore describe two major projects:

1. Investigating the properties and role of cellular mutant huntingtin protein inclusions
2. Developing and characterizing novel patient fibroblast cell lines to define HD cellular phenotypes in clinically relevant cells

Both projects revolved around a central theme, which was to model cellular phenotypes that are characteristic in HD, and investigating critical phenotypes in distinguishing wild-type and HD cells to investigate how reversing those phenotypes in HD cells could have therapeutic potential. Overall, many of these phenotypes are a result of an inability of the huntingtin protein to function properly when the polyQ tract is expanded, a concept that is explored in this thesis by analyzing mechanisms and readouts of these functions in wildtype and HD cells.

CHAPTER 2: DEFINING TWO TYPES OF MUTANT HUNTINGTIN PROTEIN INCLUSIONS

The material presented in this chapter is a representation of the following publication:

*Caron, N.S., *Hung, C.L.K., Atwal, R.S. and Truant, R. (2014) Live cell imaging and biophotonic methods reveal two distinct types of mutant huntingtin inclusions. *Hum. Mol. Gen.* 23(9):2324-38. doi: 10.1093/hmg/ddt625

*Co-first authorship

Permission was given for re-publication by Oxford Academic University Press through Copyright Clearance Center.

Changes were made in the following publication for thesis continuity and formatting.

2.1 Contributions to Publication

This publication was co-first authored with a former graduate in the lab, Dr. Nicholas Caron (N.S.C.). The project and experiments were initially designed by N.S.C., R.S.A. and R.T.. Experiments were performed by N.S.C or C.L.H. C.L.H. contributions include: SR-SIM imaging, temporal FRET imaging using sensitized-emission (se-FRET), amyloid beta staining and beta-tubulin immunofluorescence. These contributions are further clarified and annotated in the figure captions. N.S.C. wrote the manuscript and C.L.H. helped with editing and revisions.

2.2 Implications of Work

In this publication, we explored the formation of huntingtin protein aggregates, a hallmark of HD brain pathology. The importance of these inclusions have been debated, presenting as either toxic or protective. To address this, we modelled aggregation in mouse striatal-derived neurons (*STHdb^{Q7Q7}*) by overexpressing a small fragment of huntingtin, Exon1, with a pathogenic, expanded polyglutamine tract tagged with a fluorescent fluorophore (Exon1 Q138-YFP). Using several biophotonic methods such as environmentally controlled live cell imaging, fluorescence recovery after photobleaching (FRAP), temporal FRET imaging, FRET detection by fluorescence-lifetime imaging microscopy (FLIM) and super-resolution structured illumination microscopy (SR-SIM), we were able to define two distinct types of mutant huntingtin protein inclusions, named globular and fibrillar. The globular type is round, amorphous and formation is microtubule-dependent. In contrast, the fibrillar type is tightly packed, astral shaped and formation is microtubule-independent. We hypothesized that the presence of two distinct types of inclusions could help explain the discrepancy between inclusions being toxic or protective.

The work in this manuscript defined the characteristics that makes these inclusions different and described methods for distinguishing the in this model system. These characteristics were exploited to follow up on the hypothesis regarding toxicity (Thesis Chapter 3). Learning more about huntingtin aggregates and their method of formation is important if they are relevant to disease progression. If one type of inclusion is protective, we can find a mechanism to favour formation of that type.

Live Cell Imaging and Biophotonic Methods Reveal Two Distinct Types of Mutant Huntingtin Inclusions

*Caron, Nicholas, S.¹, *Hung, Claudia L.K.¹, Atwal, Randy, S.¹ and Truant, Ray¹.

*Co-first authorship

¹Department of Biochemistry and Biomedical Sciences, McMaster University, Hamilton, Ontario, Canada, L8N3Z5.

Address correspondence to: Ray Truant, HSC 4N54, 1200 Main Street West, Hamilton, Ontario, Canada L8N3Z5; Fax: 905-522-9033; Email: truantr@mcmaster.ca

FUNDING

This work was supported with operating grants to R.T. from the Huntington Society of Canada, the Canadian Institutes of Health Research (CIHR MOP-119391) and the Krembil Family foundation.

2.3 Abstract

Huntington's disease (HD) is an autosomal dominant, neurodegenerative disorder that can be characterized by the presence of protein inclusions containing mutant huntingtin within a subset of neurons in the brain. Since their discovery, the relevance of inclusions to disease pathology has been controversial. We show using super-resolution fluorescence imaging and Förster resonance energy transfer (FRET) in live cells, that mutant huntingtin fragments can form two morphologically and conformationally distinct inclusion types. Using fluorescence recovery after photobleaching (FRAP), we demonstrate that the two huntingtin inclusion types have unique dynamic properties. The ability to form one or the other type of inclusion can be influenced by the phosphorylation state of serine residues at amino acid positions 13 and 16 within the huntingtin protein. We can define two types of inclusions: fibrillar, which are tightly packed, do not exchange protein with the soluble phase, and result from phospho-modification at serines 13 and 16 of the N17 domain, and globular, which are loosely packed, can readily exchange with the soluble phase, and are not phosphorylated in N17. We hypothesize that the protective effect of N17 phosphorylation or phospho-mimicry seen in animal models, at the level of protein inclusions with elevated huntingtin levels, is to induce a conformation of the huntingtin amino-terminus that causes fragments to form tightly packed inclusions that do not exit the insoluble phase, and hence exert less toxicity. The identification of these sub-types of huntingtin inclusions could allow for drug discovery to promote protective inclusions of mutant huntingtin protein in HD.

2.4 Introduction

Huntington's disease (HD) is a progressive, neurodegenerative disease caused by a CAG trinucleotide expansion within the *Htt* gene that codes for a polymorphic polyglutamine tract near the amino-terminus of the 350 kDa huntingtin protein⁶. Individuals having polyglutamine tracts with 4–36 repeats do not develop disease, whereas those with tracts exceeding the critical threshold of 37 glutamines develop HD pathology with an inverse correlation between age-onset and CAG expansion length^{250,251}. The huntingtin protein is ubiquitously expressed in every human cell, yet neurodegeneration in early HD is selectively restricted to the basal ganglia and cerebral cortex of the brain. Huntingtin is a highly conserved protein across vertebrates and is involved in a variety of cellular functions including roles in vesicular transport^{130,252,253}, transcriptional regulation^{118,124,125,254} and cytoskeletal dynamics^{143,255}. The diverse functions of huntingtin likely stem from its ability to promote molecular interactions by behaving as a scaffold protein²⁵⁶. The polyglutamine expanded mutant huntingtin protein disrupts many of these critical cellular functions. Notably, mutant huntingtin can aggregate to form inclusion bodies, where a cellular hallmark of HD is the presence of mutant huntingtin containing inclusions within neurons and glia of human patient brains⁹⁶.

The ability of mutant huntingtin fragments to form cytoplasmic and nuclear inclusions was initially described in the R6/2 transgenic HD mouse model, which expresses human huntingtin exon1 with a CAG expansion^{32,198}. Brain slices from the R6/2 mice revealed the presence of numerous inclusion bodies composed of mutant huntingtin fragments that stained positive for ubiquitin¹⁹⁸. Similar inclusions reported in human HD patient brains also contained amino-terminal fragments of huntingtin and stained positive for ubiquitin⁹⁶.

Many studies have demonstrated that full-length huntingtin can be proteolytically cleaved to produce several prominent amino-terminal fragments, the smallest being exon1 (huntingtin 1–81)^{169–171,175,176,257}. Furthermore, aberrant splicing of the huntingtin mRNA transcript can lead to the translation of the pathogenic exon1 huntingtin protein in HD mouse

models and HD human fibroblasts²⁵⁸. Therefore, it is hypothesized that small fragments of mutant huntingtin occur naturally in HD brains where they self-associate to form inclusions.

Protein aggregation occurs in most neurodegenerative disorders including Alzheimer's disease (AD), Parkinson's disease, amyotrophic lateral sclerosis and the polyglutamine disorders. In these diseases, aggregated protein commonly forms either amyloid or amorphous aggregates. Amyloid aggregates are highly insoluble and have a rigid β -sheet structure, whereas amorphous aggregates are unstructured. The classic amyloid hypothesis defines the deposition of misfolded amyloid- β protein into insoluble plaques within the brain as one of the primary pathogenic causes of neurodegeneration in AD^{180,185}. The amyloid hypothesis has since been revised and adapted to describe a common pathogenic mechanism for most neurodegenerative diseases²⁵⁹. In HD, this hypothesis is often referred to as the toxic fragment hypothesis^{117,175,186}. It postulates that the proteolytic cleavage of mutant huntingtin generates toxic amino-terminal fragments that can misfold and accumulate in neuronal inclusions, leading to the neurodegeneration associated with HD. For the sake of nomenclature consistency, this manuscript will refer to aggregated mutant huntingtin in concentrated puncta as inclusion bodies.

Several pathogenic mechanisms have been proposed to describe the toxicity of mutant huntingtin inclusions in HD. Inclusions have been implicated in neuronal death by sequestering critical cellular proteins leading to their functional loss²⁶⁰, physically occluding active vesicle trafficking between the nucleus and neuronal extremities²⁶¹, and by impairing ubiquitin-dependent proteolysis of misfolded proteins by the proteasome⁹⁷. Alternative hypotheses view inclusion formation as being either benign or even neuroprotective²⁶². Live cell imaging in neurons reveals that the presence of huntingtin exon1 fragment inclusions correlates with enhanced survival, relative to neurons expressing exon1 without inclusions^{190,262}. It has been proposed that the response to mutant huntingtin-induced cell stress is the formation of these inclusions, which accumulate and sequester mutant protein. These studies identify the soluble monomeric or oligomeric forms of mutant huntingtin as being the cytotoxic species. This is observed by the protective effect of the

polyglutamine-binding peptide (QBP1) in cultured cells, which preferentially binds soluble mutant huntingtin²⁶³. Using high-throughput screens, compounds have been identified that can paradoxically reduce cellular toxicity by either inhibiting²⁶⁴ or promoting²⁶⁵ the formation of mutant huntingtin inclusions. Studies like these have necessitated the need to revisit the toxic fragment hypothesis for HD¹⁸⁹.

HD is one of nine CAG trinucleotide repeat disorders that are all caused by expanded polyglutamine tract lengths within different cellular proteins⁴⁰. Despite the commonality between the polyglutamine disorders, each of these diseases typically affect only a specific subset of neurons within the brain⁴⁰. Furthermore, the polyglutamine thresholds for disease pathology in most of the CAG trinucleotide diseases differ from the 37 repeats required for HD, which suggests that the context of polyglutamine within the pathogenic protein is important. Thus, some studies have focused on the importance of the sequences flanking the polyglutamine tract in mediating the toxicity of mutant huntingtin as well as its ability to form inclusions^{99,266}. The N17 domain of huntingtin comprises the first 17 residues of the protein prior to the polyglutamine tract. N17 adopts an amphipathic alpha-helical structure that allows it to interact with various proteins in the cytoskeleton and to associate with membranes^{73,98}. Recent studies performed by our group and others have shown that introducing serine 13 and 16 mutations within N17 can influence the ability of mutant huntingtin to form inclusions, the rate of inclusion formation, and also the morphology of the huntingtin inclusions^{74,83}. Additionally, promoting phosphorylation at residues 13 and 16 of the N17 domain has been shown to alleviate mutant huntingtin toxicity in an animal model of HD⁸². Flanking the polyglutamine tract on the carboxyl-terminus is a region with two pure proline tracts separated by a proline-rich region. This domain has also been shown to interact with a variety of proteins that directly impact the toxicity of mutant huntingtin and its ability to form inclusions^{267,268}. Therefore, these studies strongly implicate the importance of flanking sequences to the polyglutamine tract in modulating toxicity and inclusion formation.

Previously, our group developed a Förster resonance energy transfer (FRET) sensor to demonstrate that the polyglutamine tract of huntingtin can behave as a hinge, allowing the

N17 domain to fold back onto the distal polyproline region of huntingtin⁹⁹. FRET involves the non-radiative transfer of energy between a donor and an acceptor molecule, which allows for the high spatial resolution of dynamic molecular interactions and conformational changes in live cells^{143,269,270}. The exon1 FRET sensor was used to measure the intramolecular interactions between N17 and the polyproline domain as an indication of the conformation of soluble huntingtin in live cells. Here, we have applied the mutant huntingtin exon1 FRET sensor to observe the organization of polyglutamine expanded huntingtin within protein inclusions, measuring the intermolecular interaction between individual huntingtin fragments. We demonstrate using FRET, fluorescence recovery after photobleaching (FRAP) and super-resolution fluorescence imaging that mutant huntingtin fragments can form two morphologically and dynamically distinct inclusion types. We also show that the morphology of inclusions can be influenced by altering the phosphorylation state of serines 13 and 16 of N17. The definition of two distinct inclusion types, and the ability to identify them could lead to new insights into the controversy of the role of protein inclusions in HD and other polyglutamine diseases.

2.5 Results

2.5.1 *Huntingtin Fragments Can Form Morphologically Unique Inclusion Types*

Using fluorescence microscopy imaging, three dimensional (3D) deconvolution and iso-surface rendering, we were able to identify two morphologically distinct types of inclusions formed by the overexpression of mutant huntingtin fragments in striatal neuron derived *STHdb^{Q7/Q7}* cells (Figure 1.1). Image deconvolution involves capturing multiple images in the *z* plane and using algorithms to restore the out-of focus light to one focal point in a quantitative manner, increasing the signal-to-noise ratio and resolution. Two different mutant huntingtin (Q138) fragments were generated by fusing a fluoro-phore at the carboxyl-terminus to generate huntingtin exon1 Q138-YFP (Ex1 Q138-YFP) and huntingtin amino acids 1–171 Q138-YFP (1–171 Q138-YFP). The first type of inclusion, which we termed fibrillar, appears to lack a defined shape and is composed of mutant huntingtin fibres organized in an astral morphology (Figure 1.1A). The second type, which we termed globular, tends to be spherically shaped with discrete and well-defined edges (Figure 1.1B). To further distinguish the morphologies of these inclusions, super-resolution structured illumination microscopy (SR-SIM) was used, a method that improves lateral resolution to ~100 nm by illuminating the sample with a series of excitation light patterns²⁷¹. Imaging revealed very distinct morphologies between the globular inclusions (Figure 1.1C) and fibrillar inclusions (Figure 1.1D), highlighting a cytoskeletal element in the globular inclusion.

To confirm that these different inclusion types were not just an artifact of the fluorescent protein fusion, we also generated huntingtin constructs with a small hemagglutinin (HA) tag and expressed them in *STHdb^{Q7/Q7}* cells. Immunofluorescence (IF) with additional antigen retrieval revealed that both huntingtin exon1 Q138-HA (Ex1 Q138-HA) and 1–171 Q138-HA fragments can form both fibrillar and globular inclusion types (Supplemental Figure S2.1). Thus, these morphologies were validated as fluorescent protein fusions, allowing further observations in live cells.

In addition to characterizing the inclusions by their morphology, the fibrillar type of inclusion can be distinguished from the globular type using a thioflavin-T staining assay.

Thioflavin-T is commonly used to stain amyloid fibrils with a detectable β -sheet structure²⁷². Fibrillar inclusions were thioflavin-T positive (Figure 2.2A), while globular inclusions did not show thioflavin-T specific staining (Figure 2.2B). As a positive control, *STHdb*^{Q7/Q7} cells were transfected with amyloid-beta 1–42-mRFP ($A\beta$ 1–42-mRFP), the amyloid fibril-forming cleavage product of the amyloid precursor protein in AD. Inclusions formed from the overexpression of the amyloid- β construct stained positive for thioflavin-T (Figure 2.2C).

Immunofluorescence against ubiquitin was performed to test whether one or both types of inclusions consisted of misfolded protein. Both types of inclusions formed in *STHdb*^{Q7/Q7} cells transfected with Ex1 Q138-HA revealed ubiquitinated protein; however, no difference in ubiquitination between types was detected (Supplemental Figure S2.2).

2.5.2 Fluorescence Lifetime Imaging Microscopy-FRET Reveals Two Conformationally Distinct Inclusion Types Formed by Mutant Huntingtin Fragments

Despite their unique phenotypes, visually distinguishing between the two types of inclusions was challenging due to the high intensity and diffraction-limited spatial resolution of these inclusions using standard microscopy. To overcome these limitations, we implemented FRET-based techniques to study these two types of inclusions at nanometer resolution in live cells. FRET is a well-established technique used to measure molecular interactions and conformational changes in live cells²⁷⁰. As donor and acceptor probes for FRET, we chose a well-established FRET pair consisting of a cyan fluorescent protein variant, mCerulean (mCer), and an enhanced yellow fluorescent protein (eYFP)^{273,274}. The most accurate method of measuring FRET is using fluorescence lifetime imaging microscopy (FLIM), where fluorescence lifetime refers to the amount of time a valence electron remains in the excited state prior to returning to ground state and emitting a photon^{275,276}. The lifetime of a fluorophore can be directly affected by the biochemical and biophysical properties of the surrounding microenvironment; notably, FRET between two molecules causes a decrease in the donor fluorophore lifetime²⁷⁵. All controls for FLIM were performed to validate the use of mCer and eYFP as a FRET pair in our live cell system (Supplemental Figure S2.3).

To determine if we could detect FRET changes when huntingtin fragments were organized into higher-order inclusion structures within live *STHdb^{Q7/Q7}* cells, we tested the huntingtin exon1 Q138 sensor tagged at the amino-terminus with mCer and at the carboxyl-terminus with eYFP (mCer-Ex1 Q138-eYFP). Using FLIM to measure FRET, we were able to accurately measure intra- and intermolecular interactions between individual huntingtin molecules during the nucleation and maturation of inclusions, allowing us to differentiate between the two inclusion types based on overall structure. The fibrillar type of inclusion consistently had significantly higher percent FRET efficiency values relative to the globular type of inclusion (Figure 2.3A, B and D). This suggested a higher degree of interaction within or between huntingtin molecules in the fibrillar inclusions compared with the globular type. To determine whether the FRET we measured was a result of intra- or intermolecular FRET, we co-expressed mCer-Ex1 Q138 and Ex1 Q138-eYFP constructs on separate plasmids and measured fluorescence lifetime at both fibrillar (Figure 2.3C) and globular (data not shown) inclusions. Since the lifetimes at fibrillar and globular inclusions were similar to those found using the FRET sensor, we concluded that the majority of the FRET measured at each type of inclusion was a result of intermolecular FRET between huntingtin fragments.

In order to acquire higher spatial resolution of FRET values within each inclusion type, we collected z-stacks and performed deconvolution on both fibrillar and globular inclusions formed by the huntingtin exon1 FRET sensor. FRET efficiency was calculated using sensitized emission FRET (seFRET) as an alternative to FLIM-FRET. seFRET is a technique in which the excitation of the donor leads to the non-radiative transfer of energy between the probes, causing an increase in fluorescence intensity of the acceptor (sensitized emission) that can be quantified to generate ratiometric FRET images²⁷⁷. Consistent with the data collected using FLIM, we observed that the FRET within fibrillar inclusions was dramatically higher than that in the globular type of inclusions (Figure 2.3E and F). Additionally, we noted a heterogeneous distribution of FRET efficiency values within the fibrillar inclusions; ranging from high FRET in the centre to progressively lower FRET towards the edges of the inclusion (Figure 2.3F). This suggested tighter, more densely packed

huntingtin molecules at the core of fibrillar inclusions relative to the edges, and overall more loosely packed protein in globular inclusions (Figure 2.3E), throughout the entire volume of the inclusion.

2.5.3 FRAP Demonstrates that the Fibrillar and Globular Inclusion Types have Distinct Exchange Dynamics

Next, we used FRAP to gain insight into the recruitment dynamics of mutant huntingtin entering both fibrillar and globular inclusions within live *STHdh*^{Q7/Q7} cells. FRAP uses photolysis to permanently destroy the fluorophore of a fluorescent protein with high-intensity light. Any signal seen in a region of interest (ROI) over time is the result of unbleached molecules entering this space, thus giving a read-out of protein dynamics^{278,279}. We precisely photobleached both types of inclusions and measured the recovery of fluorescence to these ROI over time. The fluorescence recovery to the ROI in this assay represented the recruitment of soluble polyglutamine expanded huntingtin into inclusions. We observed that the fluorescence recovery within the globular type of inclusion occurred rapidly relative to the fibrillar inclusion type (Figure 2.4A and B). The recovery of fluorescence to each inclusion type was temporally quantified for both Ex1 Q138-YFP and 1-171 Q138-YFP. The globular inclusions recovered significantly faster than the fibrillar types for both constructs (Figure 2.4C and D).

To test whether inclusion formation could recruit and sequester soluble huntingtin protein, we monitored inclusion formation temporally within *STHdh*^{Q7/Q7} cells over 24 h periods using an environmentally controlled microscope system (33°C, 5% CO₂). We observed that the formation of the globular inclusions did not affect the fluorescence of the soluble mutant huntingtin within the cells (Figure 2.4E). Conversely, the formation of fibrillar inclusions progressively caused all the soluble mutant huntingtin in the cell to be absorbed and sequestered to the inclusion (Figure 2.4F). We quantified the recruitment of soluble huntingtin into inclusions by temporally measuring the loss of fluorescence from a specific ROI in the cytoplasm of cells forming inclusions following expression of either Ex1 Q138-YFP

(Figure 2.4G) or 1–171 Q138-YFP (Figure 2.4H). We measured significantly more fluorescence loss in cells forming fibrillar compared with globular inclusions at multiple time points (Figure 2.4G and 2.4H).

2.5.4 Mutant Huntingtin is Actively Recruited to Globular Inclusions by Microtubules

In order to investigate whether mutant huntingtin inclusions localized to components of the cytoskeleton, IF was performed against β -tubulin, actin and vimentin. Globular inclusions were found to localize along microtubule filaments (Figure 2.5A) whereas fibrillar inclusions did not (Figure 2.5B). To test if mutant huntingtin was being actively recruited to either inclusion type along cytoskeletal structures, we treated cells expressing the mutant exon1 fragment with compounds that would inhibit microtubule or actin polymerization. We noted that live cells expressing mutant exon1 for ~10 h treated with low concentrations of nocodazole, a potent inhibitor of microtubule polymerization, greatly reduced the formation of large globular inclusions and caused many smaller inclusions to be dispersed throughout the cytoplasm after ~3 h of treatment (Figure 2.5C). These results complement our FRAP data which demonstrated that fluorescence within the globular inclusions recovered rapidly as if recruitment of mutant huntingtin was driven via an active process. This was further demonstrated by temporal observation of the effect of nocodazole on fully formed globular inclusions (Figure 2.5E). Cells expressing mutant exon1 for 24 h revealed that large globular inclusions could break up into smaller inclusions due to the disruption of the active recruitment of mutant huntingtin. Notably, treatment with the highest concentrations of nocodazole had no effect on the formation of fibrillar inclusions within the cell (Figure 2.5D). Treatment of live cells with phalloidin, a potent inhibitor of actin polymerization, had no effect on the formation or size of either fibrillar or globular inclusion types (data not shown). Therefore, these data support the hypothesis that mutant huntingtin is being shuttled into globular inclusions via molecular motors on microtubules, whereas mutant huntingtin is being recruited to fibrillar inclusions by passive diffusion.

2.5.5 Temporal FRET Reveals Distinct Formation and Maturation Dynamics of Fibrillar and Globular Inclusions

To gain further insight into the structure of both inclusion types during their formation and maturation in live cells, we used the huntingtin exon1 sensor to generate temporal FRET videos using the seFRET technique. For these temporal experiments, we substituted mCerulean for mTurquoise2 (mTq2) due to its increased brightness and photostability over other cyan fluorescent protein variants²⁸⁰. seFRET is an appropriate method in this context because the donor and acceptor fluorophores have approximately the same quantum yield, and expression levels are identical due to the fixed 1:1 ratio of the sensor. This method allows rapid and continuous temporal measurements of FRET. The FRET images were pseudocoloured with a lookup table (LUT) where FRET efficiency values correspond to the color ramp presented below the images. Following expression of mTq2-Ex1 Q138-eYFP in *STHdh*^{Q7/Q7} cells for ~24 h, we measured the changes in FRET efficiency at 2 min intervals for 60 min. The formation of fibrillar inclusions caused a dramatic increase in relative FRET efficiency over the period of observation (Figure 2.6A and B). These high FRET values measured in fibrillar inclusions using seFRET were consistent with the relative values measured using FLIM, and thus validated the use of seFRET in our system with the huntingtin sensor. Conversely, the formation and maturation of globular inclusions did not cause any significant increase in FRET efficiency over time, despite having comparable fluorescence intensities to the fibrillar inclusions (Figure 2.6C and D). As a control to normalize FRET values between inclusion types, we captured a cell that formed both fibrillar and globular inclusions (Figure 2.6E and F, white arrows F, G). As seen in cells forming only one type inclusion, fibrillar formation caused a drastic increase in FRET efficiency whereas globular formation caused little to no FRET changes above background values (Figure 2.6E and F).

2.5.6 Full-length, Endogenous Huntingtin is Actively Recruited to Globular Inclusions and Sequestered within Fibrillar Inclusions

In order to validate the physiological relevance of studying huntingtin exon1 inclusions, we wanted to test whether endogenous huntingtin could be recruited and sequestered to sites of mutant huntingtin aggregation. Most standard methods of cell fixation for IF fall within two categories: the crosslinking (aldehydes) and the denaturing (alcohol) fixatives. Therefore, we tried both fixation methods with a variety of permeabilization techniques to determine which would be optimal to assay the presence of endogenous huntingtin within exon1 inclusions. To label endogenous huntingtin, we chose validated huntingtin monoclonal antibodies 1HU4C8 (MAB2166) which recognizes an epitope between amino acids 181–810 of huntingtin and HDC8A4 which recognizes amino acids 2703–2911. These antibodies were generated to huntingtin epitopes downstream of exon1 (amino acids 1–81) and therefore do not recognize the overexpressed Ex1 Q138-YFP. To control for spectral bleed through between channels due to the high fluorescence intensity of the inclusions, all primary antibodies were indirectly labelled with a Cy5 conjugated secondary antibody that is spectrally distinct from YFP. Fixation with paraformaldehyde (PFA) followed by antigen retrieval using formic acid and permeabilization with a detergent allowed us to detect full length, endogenous huntingtin at fibrillar (Figure 2.7A and C) but not globular (Figure 2.7B and D) inclusions using both 1HU4C8 (Figure 2.7A and B) and HDC8A4 (Figure 2.7C and D) antibodies. Alternatively, fixation and permeabilization with methanol, which denatures cellular proteins by disrupting hydrophobic interactions, caused loss of the fluorescence at the globular but not the fibrillar type of inclusion (Supplemental Figure S2.4A). Notably, 1HU4C8 (Supplemental Figure S2.4B), MAB2168 (Supplemental Figure S2.4C) and HDC8A4 (Supplemental Figure S2.4D) antibodies detected full-length huntingtin within the fibrillar inclusions under these conditions. Despite attempting every permutation of fixative and permeabilization agents to perform IF, we were never able to identify increased endogenous huntingtin at globular inclusions. This result was consistent with the fragment

FRET and FRAP data, where soluble huntingtin had a low residence time in globular inclusions.

2.5.7 N17 Phospho-Mutants Influence Huntingtin Inclusion Morphology

Phospho-modifications of serine residues 13 and 16 within N17 have been shown to affect the localization and toxicity of huntingtin within the cell^{73,74,83}. Previous work by others with synthetic huntingtin 1–50 peptides have shown that phospho-mimicry at serines 13 and 16 alters inclusion morphology *in vitro*⁸³. In order to assay the effects of phospho-mutations on the type of inclusions formed in live cells, we generated mutant huntingtin Ex1 Q142-YFP constructs with serines 13 and 16 mutated to glutamic acids (S13ES16E) to mimic phosphorylation or to alanines (S13AS16A) to render N17 resistant to phosphorylation. A polyglutamine repeat length of 142 was considered to be similar to the 138 polyglutamine length, so Ex1 Q138-YFP without serine mutations was used as a control. When overexpressed in *STHdbQ7/Q7* cells, the huntingtin phospho-mimetic (S13ES16E) mutant predominantly formed the fibrillar type of inclusion (Figure 2.8A). Conversely, the alanine mutation skewed the inclusion population towards the globular type of inclusion (Figure 2.8A). As expected, the polyglutamine expanded N17 wild type constructs produced a mixed phenotype of both fibrillar and globular types of inclusions, as residues S13 and S16 can exist in both phospho-states (Figure 2.8A). We also observed the effect on inclusion morphology of fusing YFP to the amino-terminus of the exon1 mutants (Figure 2.8B). Consistent with the carboxyl-terminus tagged constructs, phospho-mimetic mutants formed more fibrillar and phospho-resistant mutants formed more globular inclusions (Figure 2.8B). This suggested that the location of the fluorescent tag on huntingtin fragments can alter inclusion formation properties, but does not affect the type of inclusion formed by altering the phosphorylation status.

2.5.8 Kinase Inhibitors Influence Huntingtin Inclusion Morphology

In order to study the effects of true phospho-modulation on the type of inclusion formed by amino-terminal huntingtin fragments, we used kinase inhibitors known to either inhibit or promote phosphorylation of huntingtin at serine residues 13 and 16 of N17. Phosphorylation at N17 can be inhibited by casein kinase 2 (CK2) inhibitors DMA^T and quinalizarin⁷⁴. Conversely, N17 phosphorylation can be promoted by treatments with IKK inhibitors, the ATP analog Bay 11-7082, and the allosteric inhibitors BMS-345541 and IMD-0354⁷⁴. *STHdb*^{Q7/Q7} cells overexpressing Ex1 Q138-YFP treated with CK2 inhibitors had little effect on the type of inclusion formed in the cell, whereas the IKK inhibitors skewed the cellular inclusion population towards the fibrillar type (Figure 2.8C). These results suggest that the fate of inclusions that form in the cell can be influenced by kinase inhibitors or other small molecules that alter the phosphorylation state of serines 13 and 16 of N17.

To further validate the effect of small molecules on inclusion type, we treated *STHdb*^{Q7/Q7} cells expressing Ex1 Q138-YFP with either CK2 or IKK beta inhibitors and looked at the inclusion migration under non-denaturing conditions using polyacrylamide gel electrophoresis (PAGE). Native PAGE maintains the folded structure/conformation and the hydrodynamic size of proteins, thus mobility varies with changes in the biophysical properties of the huntingtin inclusions. Consistent with data that IKK inhibitors skew the cellular inclusion population towards the fibrillar type of inclusions, we noted that these inclusions migrated further since they are more tightly packed (Figure 2.8D). Conversely, CK2 inhibitor treatment of cells had little effect on inclusion type (Figure 2.8C) and also did not alter the migration of inclusions relative to untreated using native PAGE (Figure 2.8D).

2.6 Discussion

The concept that mutant huntingtin can form multiple types of inclusions has previously been proposed by others, based on observations with small huntingtin fragments in cell culture and synthetic protein *in vitro* at super-physiological concentrations^{83,177,266}. Fibrillar and heterogeneous morphology inclusions have also been noted in HD brains⁹⁶. The formation of amorphous or amyloid aggregates is initiated by the presence of abnormally folded protein. Past studies have described a pathway for the formation of amyloid aggregates where abnormally folded monomers initiate the formation of oligomeric intermediates. These intermediates have been described to be globular in shape and lead to the formation of fibrillar aggregates²⁸¹. The globular inclusions described in this study were not the same as the intermediates since we never observed the direct conversion of globular to fibrillar inclusions. These two types of inclusions were therefore identified as two distinct terminal forms of aggregated mutant huntingtin. We also concluded that these inclusions were not aggresomes, a type of cytoplasmic aggregate that forms at the centrosome, since neither inclusion type was found to localize to the centrosome or cause the characteristic redistribution of vimentin to the periphery of the inclusions²⁸².

This manuscript characterizes different inclusion types based on a number of biophysical properties in live cells. A thioflavin-T fluorescent staining assay shows that the fibrillar type of inclusion has a detectable amyloid fibril structure and that the globular type does not. Notably, both types of inclusions were positive for ubiquitin, a characteristic of misfolded protein. Using biophotonic techniques including FLIM-FRET, seFRET, FRAP, deconvolution and temporal imaging, we observed that the fibrillar and globular inclusion types formed by polyglutamine expanded huntingtin have distinct morphological, structural and dynamic properties in live cells. We consistently measured increased FRET efficiency of the huntingtin sensor in fibrillar inclusions relative to the globular type, regardless of the intensity and size of the inclusion formed. Notably, intermolecular FRET between multiple huntingtin molecules represented the majority of the FRET measured at both inclusion types, with a small contribution of intramolecular FRET between the N17 and polyproline domains.

Therefore, the higher FRET values we observed within fibrillar inclusions represented a tighter, more compact and structured organization of huntingtin fragments, as compared with the globular inclusions.

Using FRAP, we demonstrated that globular and fibrillar inclusions formed by mutant huntingtin fragments have very distinct recruitment dynamics. FRAP studies have been performed on multiple polyglutamine protein inclusions to show heterogeneity in the dynamics of inclusions from different diseases. This implies that the context of polyglutamine is important and regions flanking the polyglutamine tracts may contribute to different dynamic properties in different polyglutamine disease proteins²⁸³. Here, we describe that inclusion heterogeneity can exist within one polyglutamine disease protein, mediated by post-translational modifications of a flanking region. We noted that following photobleaching of inclusions, the soluble huntingtin in the cell was recruited back into globular inclusions significantly more rapidly relative to the fibrillar type of inclusions. We demonstrated that soluble huntingtin was actively being shuttled into globular inclusions along microtubules. Treatment of cells expressing mutant exon1 fragments with low concentrations of nocodazole prevented the formation of large globular inclusions and caused a redistribution of smaller inclusions throughout the cell. These results are consistent with previous research that has shown that huntingtin plays a critical role in cytoskeletal dynamics and interacts directly with microtubules¹⁰⁶.

Temporal experiments done with an incubated microscope showed that fibrillar inclusion formation caused all the soluble mutant huntingtin in the cell to be progressively recruited and sequestered within the inclusion. These data suggested that the huntingtin within fibrillar inclusions remained relatively static and was not being dynamically exchanged between the soluble and insoluble phases. Conversely, when the globular type formed, these inclusions quickly grew and maintained their size without affecting the fluorescence of the soluble huntingtin within the cells. This suggested that there was a constant dynamic exchange between the soluble and insoluble phases in these inclusions.

Using site directed mutagenesis, we demonstrated that S13E/S16E or S13A/S16A mutants in the context of polyglutamine-expanded exon1 were enough to push the cellular population of inclusions towards the fibrillar or globular type, respectively. This observation is consistent with work done by others using purified synthetic huntingtin 1–56 Q37 constructs with either phospho-mimetic or alanine mutations at serine residues 13 and 16 expressed *in vitro*⁸³. Using electron microscopy, they discovered that huntingtin peptides with S13 and S16 mutations can associate to form morphologically different inclusion types⁸³. Despite this, our data showed that constitutive phospho-mimicry or alanine mutations at these sites did not skew the population of inclusions entirely to one form or the other, suggesting that other factors can influence inclusion fate within the cell. We hypothesize that these auxiliary factors could be other post-translational modifications or molecular interactions with either N17 or the polyproline domain. A recent study by our group has shown that N17 phosphorylation can affect soluble huntingtin conformation⁹⁹, and we hypothesize that these conformational differences can influence the nucleation and properties of an inclusion when high levels of protein are present.

Previous work has shown that mutant huntingtin is hypo-phosphorylated at serines 13 and 16 of N17 and that increasing phosphorylation at these sites can reduce the toxicity of the mutant protein⁷⁴. Others have demonstrated that promoting phosphorylation at these residues can dramatically improve motor function in an HD mouse model⁸². In this study, we show that the type of inclusion formed by mutant huntingtin can be affected by small molecule kinase inhibitors that modulate the phospho-state of serine residues 13 and 16 of N17, described by us previously⁷⁴.

The distinct properties of these huntingtin inclusions suggest that one type may represent a toxic form, whereas the other may be benign or even protective to the cell. The globular inclusions were shown to have a looser packing of mutant huntingtin, which allowed for the rapid recruitment and continuous exchange of mutant protein with the soluble phase. Additionally, S13A/S16A mutations skewed the population of inclusions toward the globular type. Conversely, fibrillar inclusions were shown to be densely packed and soluble mutant

huntingtin was slowly recruited and sequestered within these inclusions (see model, Figure 2.9). This sequestration of the mutant protein within the fibrillar inclusions could represent a cellular stress response to cope with mutant huntingtin load.

Many groups have shown that transgenic mice expressing exon1 of huntingtin rapidly develop motor and cognitive symptoms comparable to HD³². Despite the striking phenotypes in these transgenic animals, the question of whether this small fragment occurs naturally in the brains of HD patients has been controversial. However, recent work has elegantly shown that aberrant splicing of the huntingtin pre-mRNA leads to the translation of an exon1 fragment in a variety of HD models and human HD fibroblasts²⁵⁸. This work supports the hypothesis that exon1 fragments can occur naturally in abundance within neurons and other cells. However, a caveat of our studies, and those of others using small fragment over-expression, is that the protein concentrations are either super-physiological, or only relevant to neurons in late-stage HD with a massive accumulation of mutant protein. Regardless, the characterization of inclusions in late or severe HD could provide insight into huntingtin properties in early HD or even premanifest HD, which is likely the therapeutic window in this disease.

Using FRET techniques in live cells to visualize inclusions provides a valuable tool to accurately measure the unique conformational/structural differences for each type of inclusion within a cell. Additionally, FRET offers an added level of information by providing high spatial resolution, beyond even that of super-resolution microscopy. This assay is amenable to high-content screening since it provides a reliable and robust phenotypic read-out of inclusion type. This would allow for the screening of compounds that could skew the cellular population of inclusions towards one type or the other. Furthermore, since inclusion formation is a characteristic of most neurodegenerative disorders, a FRET sensor to quantify different inclusion types could be adapted to other neurodegenerative disease proteins.

2.7 Materials and Methods

2.1 Tissue Culture

Immortalized mouse striatal *STHdb*^{Q7/Q7} cells were grown as previously described (42).

2.7.2 Plasmid construct

The huntingtin exon1 Q138 sensor was generated from cDNA using forward primer GATCTCCGGAATGGCGACCCTG with a *Bsp*EI restriction site and reverse primer GATCGGTACCGGGTCGGTGCAGCGGCTC with an *Acc*65I site. The PCR insert was then cloned into either a YFP-N1 plasmid (Clontech) or a modified mCerulean-C1 plasmid (Clontech) with an eYFP insert cloned into *Bam*HI and *Xba*I sites at the opposing end of the multiple cloning site. The HA-tagged constructs were generated using synthetic oligos (MOBIX) GATCCTACCCATACGATGTTCCAGATTACGCTT with a *Bam*HI restriction site overhang and CTAGAAGCGTAATCTGGAACATCGTATGGGTAG with an *Xba*I restriction site overhang. The insert was then cloned into a huntingtin exon1 Q138 or huntingtin 1–171 Q138 vector.

2.7.3 Transfection

Transfection of *STHdb*Q7/Q7 cells was done using TurboFect *in vitro* reagent (Fermentas, R0531) as previously described⁹⁹.

2.7.4 Primary antibodies

The huntingtin specific mouse monoclonal 1HU 4C8 (Millipore International, MAB2166) and HDC8A4 (Pierce Antibodies, MA1-82100) antibodies were used to perform IF of endogenous huntingtin in *STHdb*^{Q7/Q7} cells.

2.7.5 Immunofluorescence

Immunofluorescence on *STHdb*^{Q7/Q7} cells to visualize endogenous huntingtin was done either using the antigen retrieval or the methanol method. For the antigen retrieval method, cells were

fixed with 4% PFA for 20 min at 4°C. Cells were then washed 2× with PBS and treated with 10% formic acid for 20 min at room temperature. Cells were then washed again 2× with PBS and subsequently permeabilized with Triton X-100 detergent (BioShop, TRX777.100) for 10 min at room temperature. Using the methanol method, cells were fixed and permeabilized using ice-cold methanol for 12 min at -20°C. Consistent between both methods, cells were then blocked 3× with 2% FBS in PBS blocking solution. Primary antibodies were added to cells at a concentration of 1:100 in a solution of 2% FBS in PBS with 0.02% Tween 20 (Sigma, P9416). Antibodies were then labelled with the far-red Cy5 (Molecular Probes, A10524) (ex 650 nm/em 670 nm) dye at a concentration of 1:500.

To visualize overexpressed huntingtin HA-tagged constructs, IF was done using the antigen retrieval method described above. Primary antibody to the HA tag (Abcam, AB16918) was added to the cells at a concentration of 1:250 in a solution of 2% FBS in PBS with 0.02% TWEEN20. Antibody was then labeled with the AlexaFluor 488 (Molecular Probes, A21206) (ex 499 nm/em 519 nm) dye at a concentration of 1:500.

For visualization of ubiquitin, IF was done using antigen retrieval method with an anti-ubiquitin antibody (Sigma, SAB4503053) added to the cells at a concentration of 1:100 in a solution of 2% FBS in PBS with 0.02% Tween 20. For visualization of β -tubulin, IF was done with 4% PFA fixation without antigen retrieval with an anti β -tubulin antibody (University of Iowa Hybridoma Bank, E7-S) at a concentration of 1:250 in 2% FBS in PBS with 0.02% Tween 20. Both anti-ubiquitin and anti β -tubulin primary antibodies were labelled with Cy5 dye at a concentration of 1:500.

2.7.6 Imaging

Live cell temporal videos of inclusion formation were acquired with a 40× air objective using a Lumascope 500 inverted widefield epifluorescent microscope (Etaluma Inc., Carlsbad, CA, USA) housed in an incubator regulated at 33°C with 5% CO₂.

Inclusion imaging was done with a 60× oil immersion objective (PlanApo NA = 1.4) on a Nikon Eclipse Ti2000 inverted widefield epifluorescent microscope using the Orca-Flash4.0 CMOS camera (Hamamatsu, Japan). Image acquisition was done using the NIS-Elements Advanced Research version 4.10.01 64-bit acquisition software from Nikon (USA). z-Stacks of inclusions were acquired using a motorized stage (Prior Scientific, USA) with step sizes of 0.3–0.5 μm . Deconvolution was done on z-stacks using the AutoQuant blind deconvolution module as part of the NIS-Elements version 4.10.01 software package (Nikon). Iso-surface rendering on inclusions was applied using the Imaris software from Bitplane (AG).

2.7.7 Thioflavin-T Amyloid Fibril Staining

After 24 h of expression of Ex1 Q138-mRFP, transfected *STHdb*Q7/Q7 cells were fixed with 4% PFA for 30 min and stained with 0.05% thioflavin-T (Sigma, T3516) for 8 min. Cells were washed 3× with PBS and imaged. Positive control for the assay was *STHdb*Q7/Q7 cells transfected with A β 1–42-mRFP with 24 h of expression. Cells were fixed and stained as described above.

2.7.8 Native Polyacrylamide Gel Electrophoresis

Cell samples were lysed using an NP-40 lysis buffer on ice for 15 min. Supernatants were collected and the remaining pellet was resuspended in NP-40 lysis buffer and sonicated. Protein concentrations for soluble and insoluble fractions were calculated using a Bradford assay. Samples were prepared with a non-reducing loading buffer without boiling. The 7% acrylamide gels and running buffers were prepared without SDS or any other reducing agents.

2.7.9 Small Molecule Treatments

Transfected *STHdb*^{Q7/Q7} cells were treated with compounds at concentrations optimized previously⁷⁴. Cells were treated with compounds for ~16 h prior to experiments.

2.5.10 Time-Domain FLIM and Analysis

Time-domain FLIM and analysis of FLIM data were performed as previously described^{99,269}.

2.7.11 Sensitized Emission FRET

seFRET was performed using the FRET module as part of NIS-Elements version 4.10.01. All controls were performed as required by the FRET module. Percent FRET efficiency values were calculated by the module using equations derived from the Gordon method. A rainbow look-up table was applied to the ratiometric FRET image to show the range of FRET efficiency values.

2.7.12 Statistical Analysis

All statistical analyses were done using the SigmaPlot software 11.0 (Systat Software Inc.). For comparisons between two groups, Student's *t*-tests were performed if data passed the normality assumptions. If data did not pass the normality test, it was analyzed by the Mann–Whitney method. For multiple pairwise comparisons, one-way analysis of variance (ANOVA) using the Student–Newman–Keuls method was performed if the data passed the normality test of distribution. If the data did not pass the normality assumptions, then we performed a one-way ANOVA on ranks using the Tukey test. For FLIM quantifications, every cell was represented as its own N and the box-whisker plot graph was generated using cumulative data from three-independent trials.

2.8 Figures

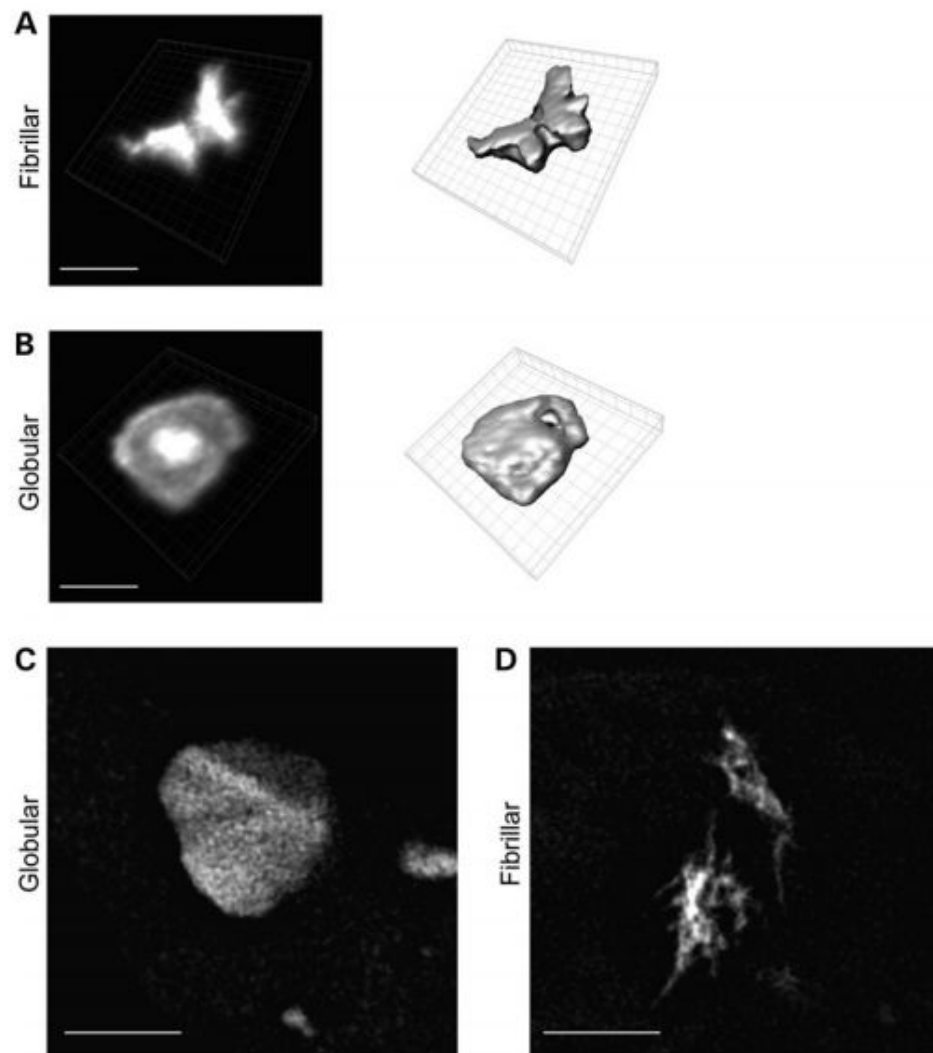


Figure 2.1 Huntingtin fragments can form two morphologically unique inclusion types. Maximum intensity projections of deconvolved z-stacks followed by iso-surface rendering of (A) fibrillar and (B) globular inclusion types formed in *STHdb^{Q7/Q7}* cells using Ex1 Q138-YFP. (C) SR-SIM images of a globular inclusion with a cytoskeletal structure present in the inclusion. (D) SR-SIM image of a fibrillar inclusion. Scale bar = 1 μm .

Contributions: N.C. performed (A) and (B), C.H. performed (C) and (D)

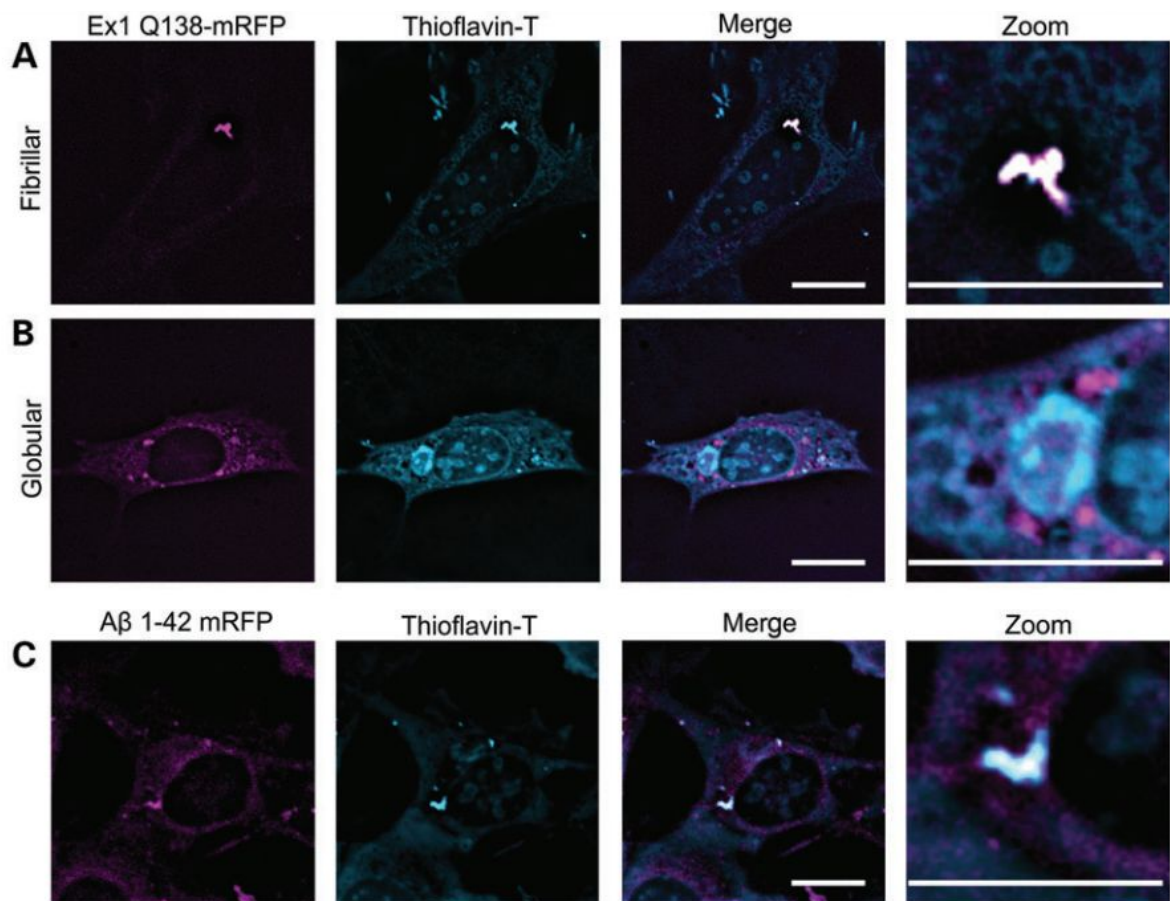


Figure 2.2 Fibrillar inclusions are detectable by thioflavin-T staining assay.

Thioflavin-T staining of *STHdb*^{Q7/Q7} cells that formed either (A) fibrillar or (B) globular inclusions following 24 h expression of Ex1 Q138-mRFP. (C) Positive control for thioflavin-T assay showing staining of *STHdb*^{Q7/Q7} cells expressing A β 1-42-mRFP for 24 h that have formed amyloid fibril aggregates. Inclusions of interest are denoted with an arrow, where G refers to a globular inclusion, and F refers to a fibrillar inclusion. Scale bar = 10 μ m.

Contributions: C.H. performed all experiments

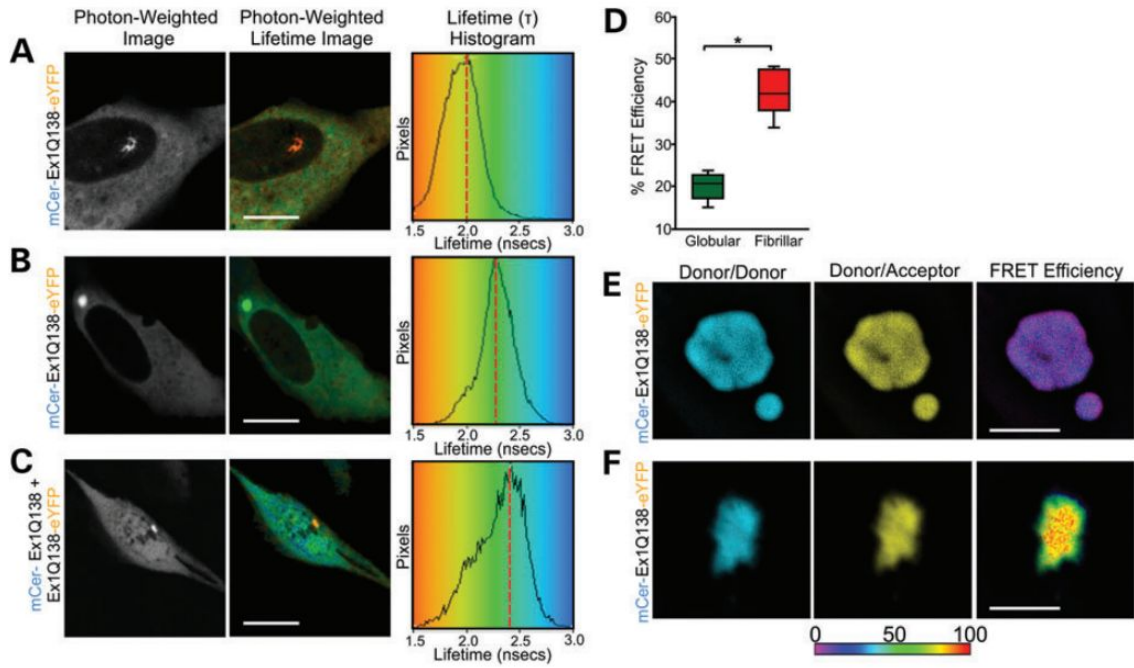


Figure 2.3 Comparing the fluorescence lifetime (τ) changes in globular versus fibrillar inclusion types. Sample FLIM images of (A) fibrillar and (B) globular inclusions formed using the mCer-Ex1 Q138-eYFP FRET sensor. (C) Co-expression of mCer-Ex1 Q138 and Ex1 Q138-eYFP as a control to show contribution of intermolecular versus intramolecular FRET. Photon-weighted images, photon-weighted lifetime images and lifetime histograms of each image are presented. Lifetimes shown in the photon-weighted lifetime images are pseudo-colored using the rainbow scale lookup table (LUT) and correspond to lifetime values represented in the histogram. The dashed red lines within each histogram represents the approximate lifetime with the most representative pixels (mode). Scale bar = 10 μm . (D) Quantification of FRET efficiency using the huntingtin FRET sensor comparing globular versus fibrillar inclusion types under steady state conditions in live cells ($n = 30$, $N = 3$, $*P < 0.001$). All imaging was done in Hank's balanced salt solution (HBSS) (pH 7.3). Sample deconvolved z-stacks of (E) globular and (F) fibrillar inclusions using seFRET. The donor/donor image represents excitation and emission of mCerulean. Donor/acceptor image represents excitation of mCerulean and emission of eYFP. FRET efficiency images have been pseudocolored using a rainbow LUT that corresponds to the corrected FRET efficiency values represented on the scale below the panels. Scale bar = 1 μm .

Contributions: N.C. performed all experiments

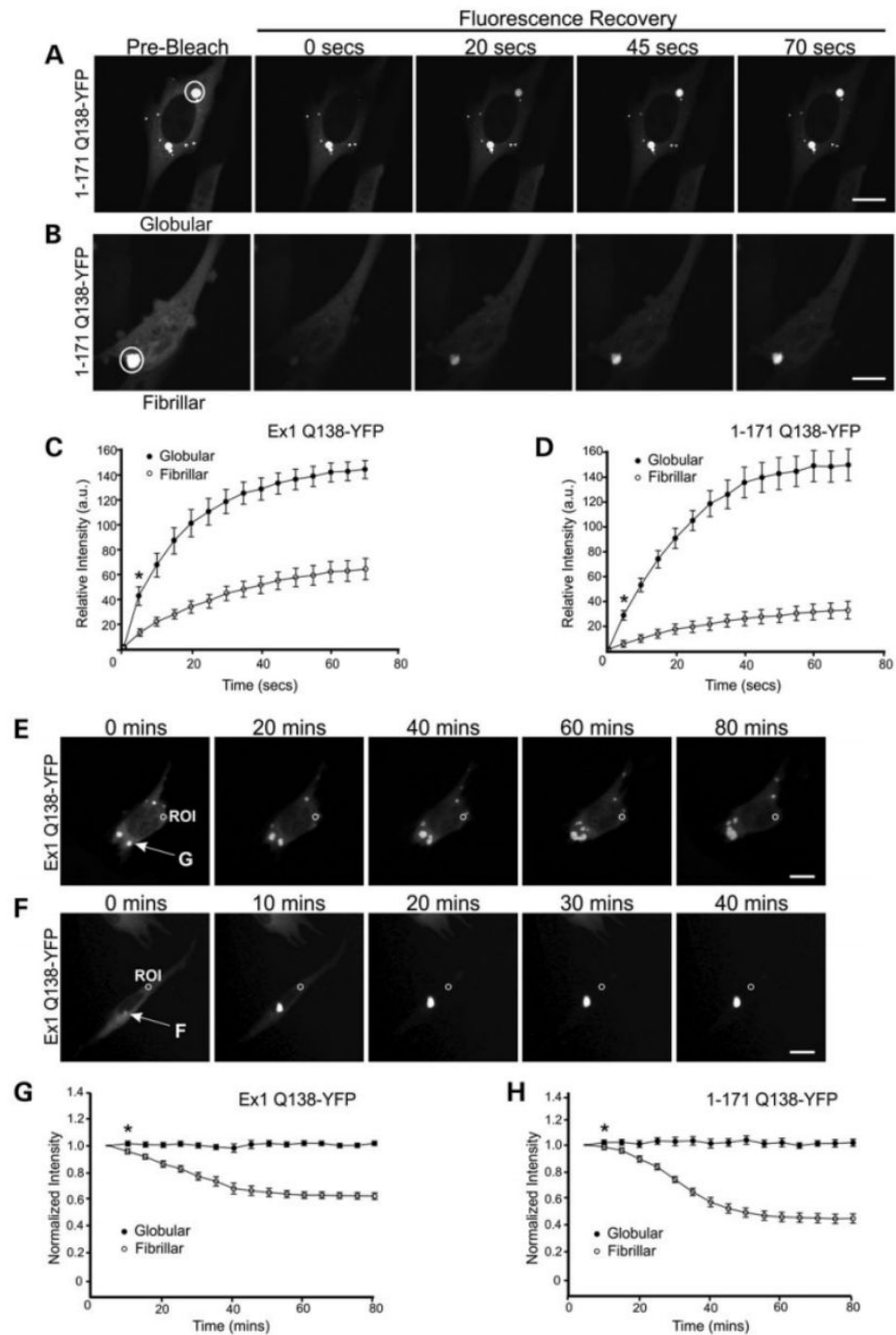


Figure 2.4 Comparing the dynamics of globular versus fibrillar inclusions. Live cell assay showing the recovery of fluorescence following bleaching of either (A) globular or (B) fibrillar inclusion using a high-intensity 488 nm laser in *STHdb^{Q7/Q7}* cells overexpressing 1–171 Q138-YFP. Pre-bleach acquisition shows the cell prior to ROI (circle) photobleaching. Quantifications of relative fluorescence recovery to either fibrillar or globular inclusions (over a 75 s time period) following expression of either (C) Ex1 Q138-YFP or (D) 1–171 Q138-YFP huntingtin fragments in *STHdb^{Q7/Q7}* cells for 24 h. Plotted values represent arbitrary units (AU) of fluorescence intensity and error bars represent standard error. The asterisk represents time point and forward where $P < 0.001$ ($N = 3$, $n = 10$). Temporal movies of live cells expressing Ex1 Q138-YFP constructs forming either (E) globular or (F) fibrillar inclusions. Movies were made with an environmentally controlled microscope at 33°C, 5% CO₂ using a 40× objective where images were taken every 5 min for 24 h. Quantification of temporal fluorescence loss at a specific ROI for both fibrillar and globular inclusions following expression of either (G) Ex1 Q138-YFP or (H) 1–171 Q138-YFP in *STHdb^{Q7/Q7}* cells for 24 h. Plotted values represent normalized intensity, and error bars represent standard error ($n = 5$, $N = 10$ for Ex1 and $n = 9$, $N = 8$ for 1–171, $*P < 0.001$).

Contributions: N.C. performed all experiments. C.H. contributed experimental trials for (E), (F) and (G)

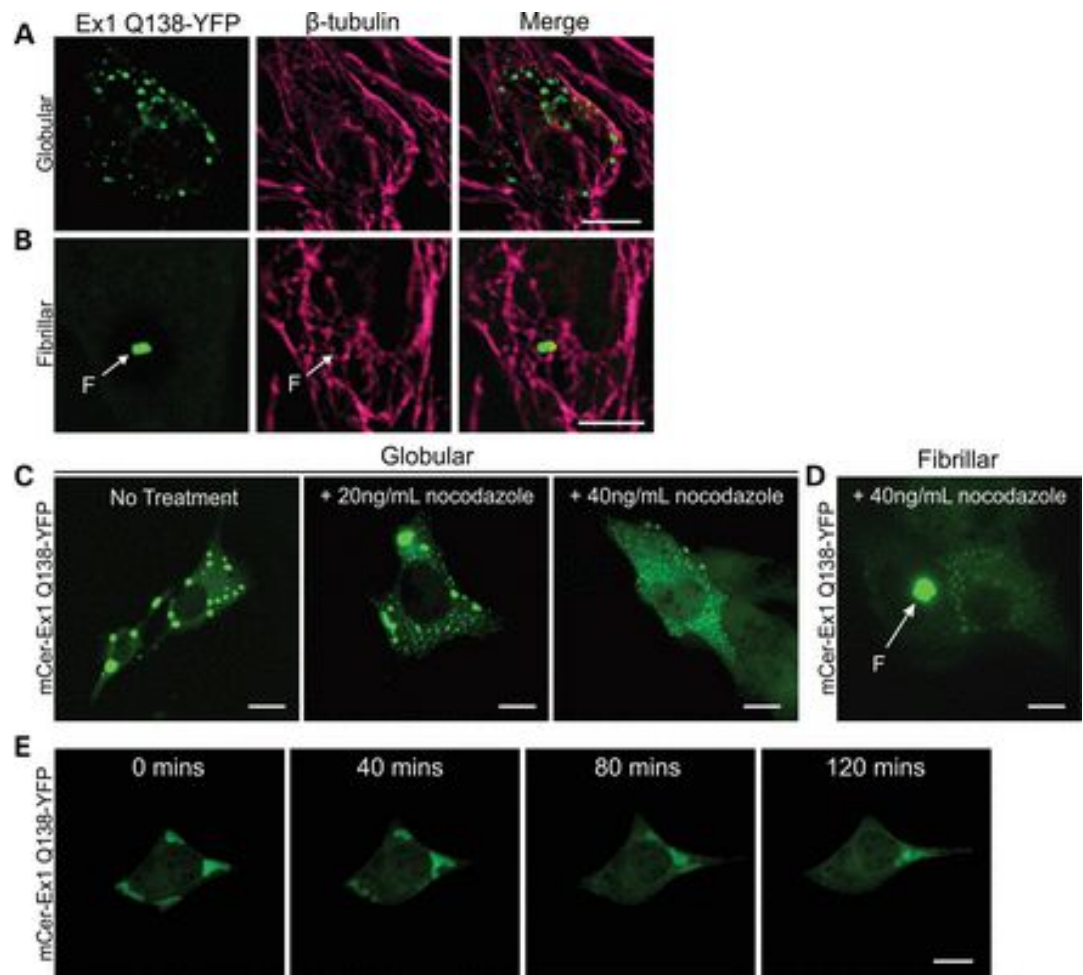


Figure 2.5 Active recruitment of mutant huntingtin into globular inclusions is microtubule dependent. Immunofluorescence (IF) β -tubulin performed on *STHdb*^{Q7/Q7} cells that formed either (A) globular or (B) fibrillar inclusions following 24 h expression of Ex1 Q138-YFP. Effect of ~3 h nocodazole treatment on *STHdb*^{Q7/Q7} cells expressing mCer-Ex1 Q138-YFP for ~10 h forming either (C) globular or (D) fibrillar inclusions. (E) Temporal movie of a live cell with fully formed globular inclusions after expression of mCer-Ex1 Q138-YFP for 24 h treated with 40 ng/mL nocodazole over 2 h. Inclusions of interest are denoted with an arrow, where F refers to a fibrillar inclusion. Scale bar = 10 μ m.

Contributions: C.H. performed (A) and (B). N.C. performed (C) and (D)

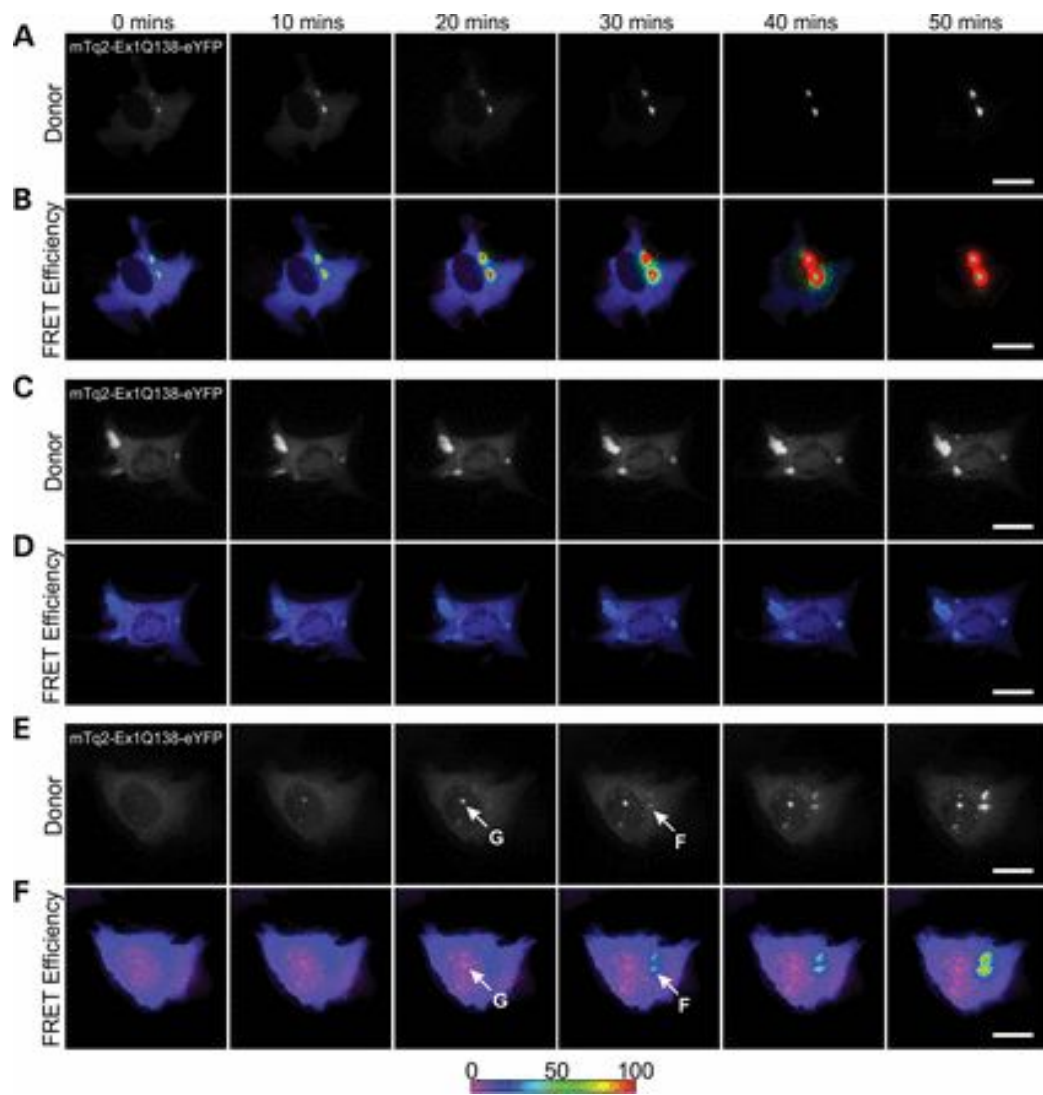


Figure 2.6 Comparing the formation of fibrillar versus globular inclusions using temporal seFRET. (A, C and E) Temporal fluorescence intensity images of *STHdb^{Q7/Q7}* cells expressing mTq2-Ex1 Q138-eYFP FRET sensor during the formation of (A and E) fibrillar and (C and E) globular inclusions. (B, D and F) Corresponding temporal corrected FRET efficiency images generated using seFRET module showing the formation of (B and F) fibrillar and (D and F) globular inclusions. FRET images have been pseudocoloured using a rainbow LUT that corresponds to corrected FRET efficiency values represented on the scale below the panels. Inclusions of interest are denoted with an arrow, where G refers to a globular inclusion, and F refers to a fibrillar inclusion. Scale bar = 10 μm .

Contributions: C.H. performed all experiments

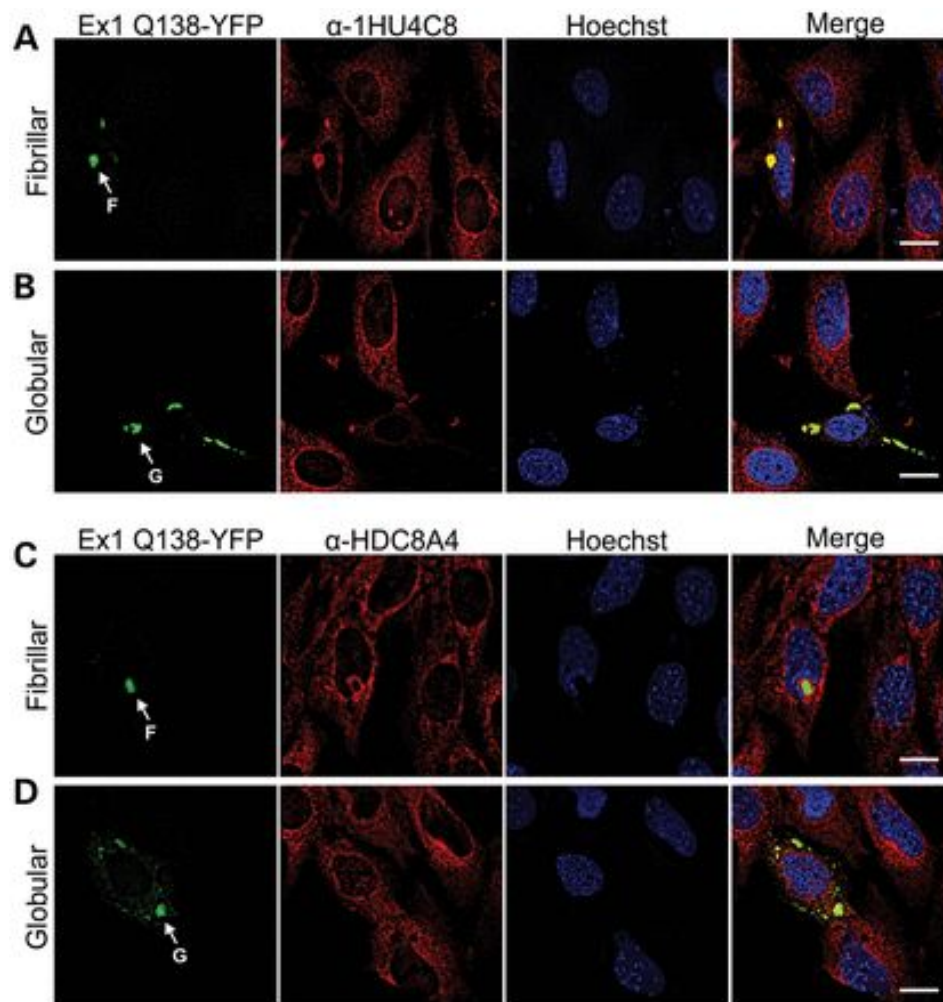


Figure 2.7 Full-length, endogenous huntingtin is actively recruited and sequestered within fibrillar inclusions. Representative IF images of *STHdb^{Q7/Q7}* cells expressing Ex1 Q138-YFP followed by fixation with 4% PFA, antigen retrieval using 10% formic acid and permeabilization using Triton X-100 detergent. IF was performed using both (A and B) 1HU4C8 and (C and D) HDC8A4 monoclonal antibodies on either (A and C) fibrillar or (B and D) globular huntingtin inclusions. Primary antibodies were indirectly labelled with secondary antibodies conjugated with Cy5 to prevent spectral bleedthrough due to the high fluorescence intensity of the inclusions. Inclusions of interest are denoted with an arrow, where G refers to a globular inclusion, and F refers to a fibrillar inclusion. Scale bar = 10 μ m.

Contributions: N.C. performed all experiments

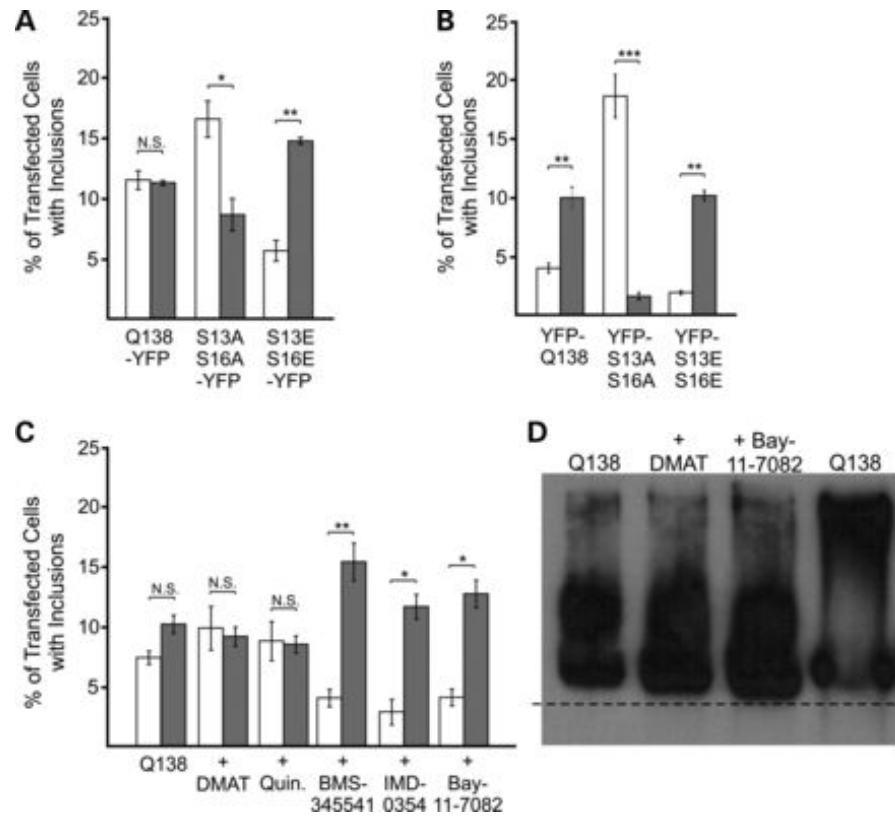


Figure 2.8 Phosphorylation state of N17 S13 and S16 can influence the fate of the inclusion type. Quantification of percent transfected cells with globular (white bars) or fibrillar (grey bars) inclusions following expression in *STHdb^{Q7/Q7}* of (A) Ex1 Q138-YFP or (B) YFP-Ex1 Q138 constructs with serines 13 and 16 mutated to either alanines (S13A16A) or glutamic acids (S13E16E). NS, not significant, * $P = 0.029$, ** $P = 0.009$ and *** $P < 0.001$. $N = 4$, $n = 150$. (C) Quantification of percent transfected cells with either fibrillar or globular inclusions for Ex1 Q138-YFP following either no treatment or treatment with CK2 and IKK inhibitors (2 μM DMAT, 1 μM quinalizarin, 4 μM BMS-345541, 2 μM IMD-0354 and 5 μM Bay 11-7082). NS, not significant, * $P = 0.029$, ** $P = 0.009$. $n = 150$, $N = 3$. (D) Differential migration of mCer-Ex1 Q138-YFP inclusions following treatment with CK2 or IKK inhibitors (1 μM DMAT and 5 μM Bay 11-7082) under native non-denaturing conditions. All bands migrate at ~ 440 kDa.

Contributions: N.C. performed all experiments

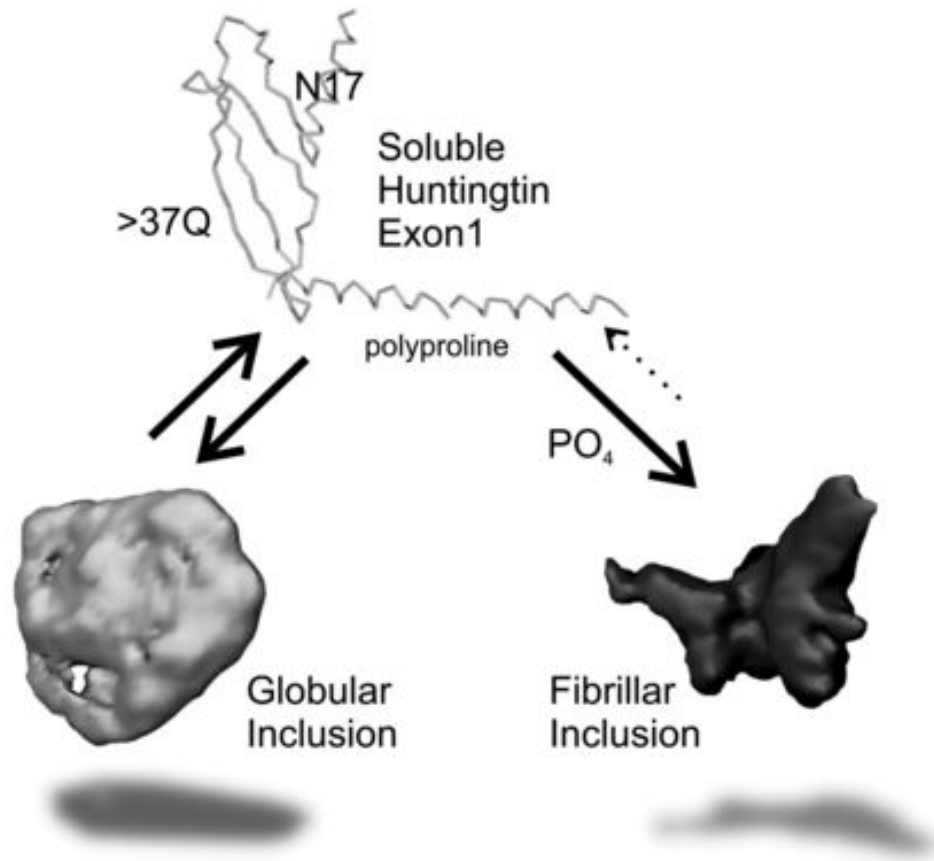


Figure 2.9 Model of the dynamics of two distinct inclusion types formed from mutant huntingtin protein. Soluble huntingtin exon1 with a CAG expansion beyond 37 repeats adopts an open conformation, pushing N17 and polyproline out of alignment. Globular inclusions can form, and readily exchange protein with the soluble phase, likely allowing mutant huntingtin to interact functionally in pathways required by normal huntingtin. Fibrillar inclusions can also form, especially if N17 is phosphorylated, causing tightly-packed protein deposits that do not exchange with the soluble phase, thus are protective in HD. We did not observe one inclusion type directly converting to another.

Contributions: R.T. generated model figure

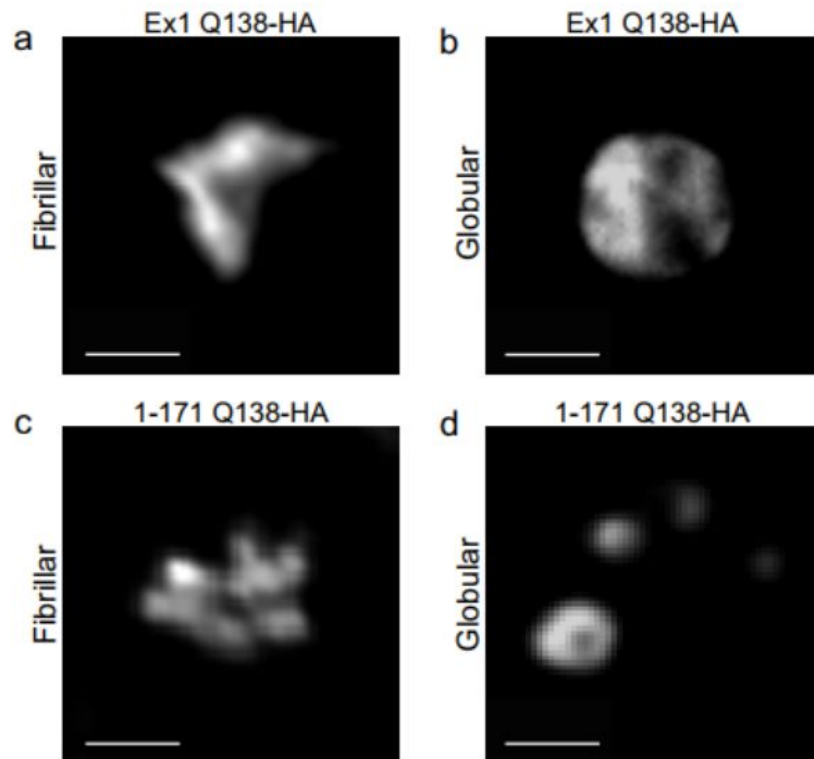


Figure S2.1 HA-Tagged mutant huntingtin exon1 forms two inclusion types.

Representative images of the two inclusion types as HA-tagged constructs in fixed cells. Both (A and C) fibrillar and (B and D) globular inclusions were observed with both Ex1 Q138-HA and 1-171 Q138-HA contexts. Scale bar = 1 μ m.

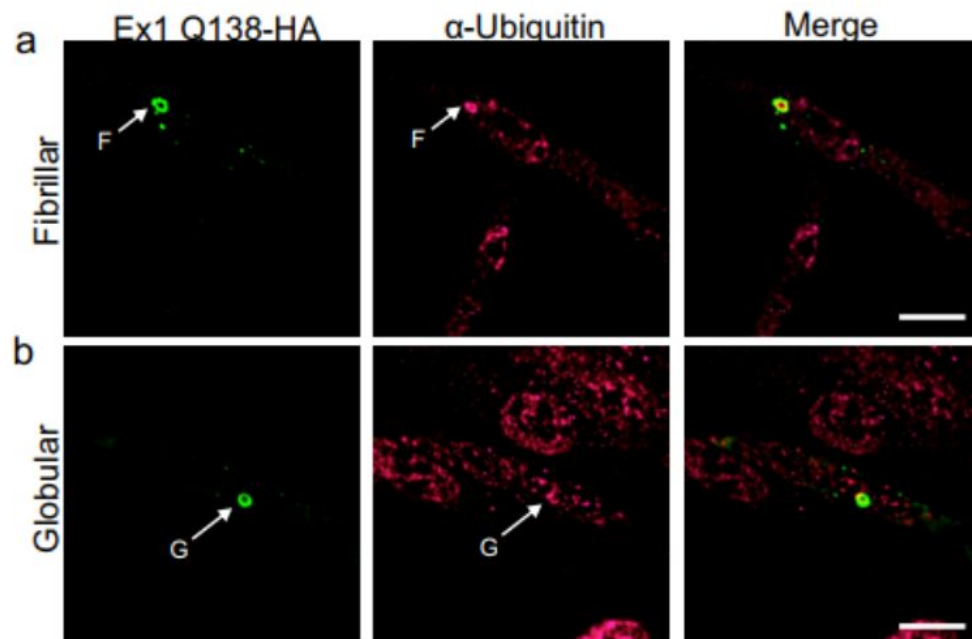


Figure S2.2 Fibrillar and globular inclusions are not differentially ubiquitinated.

Immunofluorescence for ubiquitin performed on *STHdb^{Q7/Q7}* cells that formed either (A) fibrillar or (B) globular inclusions following 24 hours expression of Ex1 Q138-HA. Primary antibodies for HA-tag and ubiquitin were indirectly labelled with secondary antibodies conjugated with AlexaFluor488 and Cy5 respectively. Scale bar = 10 μ m.

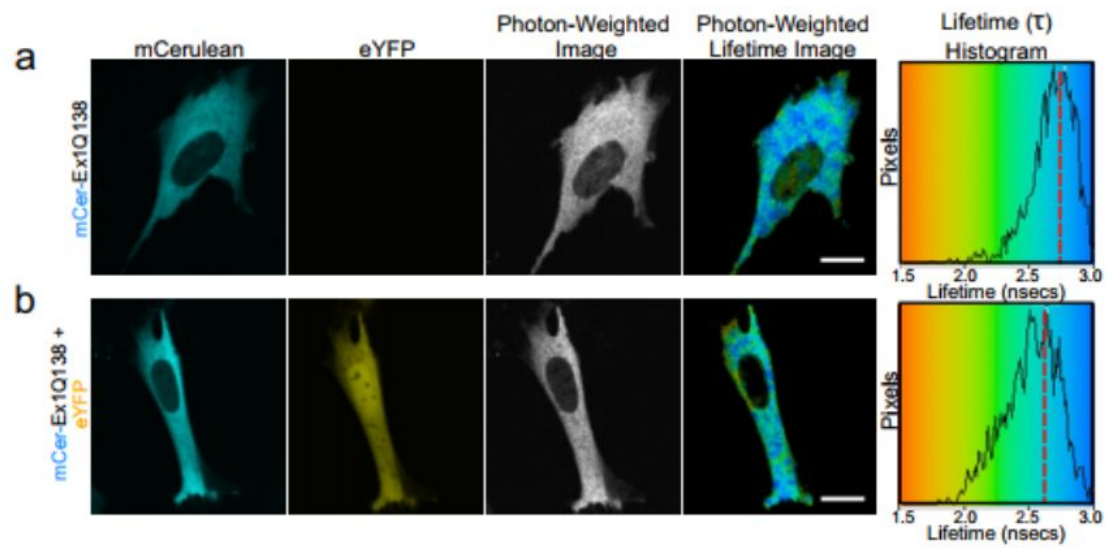


Figure S2.3 FLIM-FRET controls. Sample negative control FLIM images for mCer-Ex1 Q138 in the (A) absence and in the (B) presence of an eYFP acceptor co-expressed in *STHdb^{Q7/Q7}* cells for ~36 hours. Photon-weighted images, photon-weighted lifetime images and lifetime histograms of each image are presented. Lifetimes shown in the photon-weighted lifetime images are pseudo-coloured using the rainbow scale lookup table (LUT) and correspond to lifetime values represented in the histogram. The dashed red lines within each histogram represent the approximate lifetime with the most representative pixels (mode). Scale bar = 10 μ m.

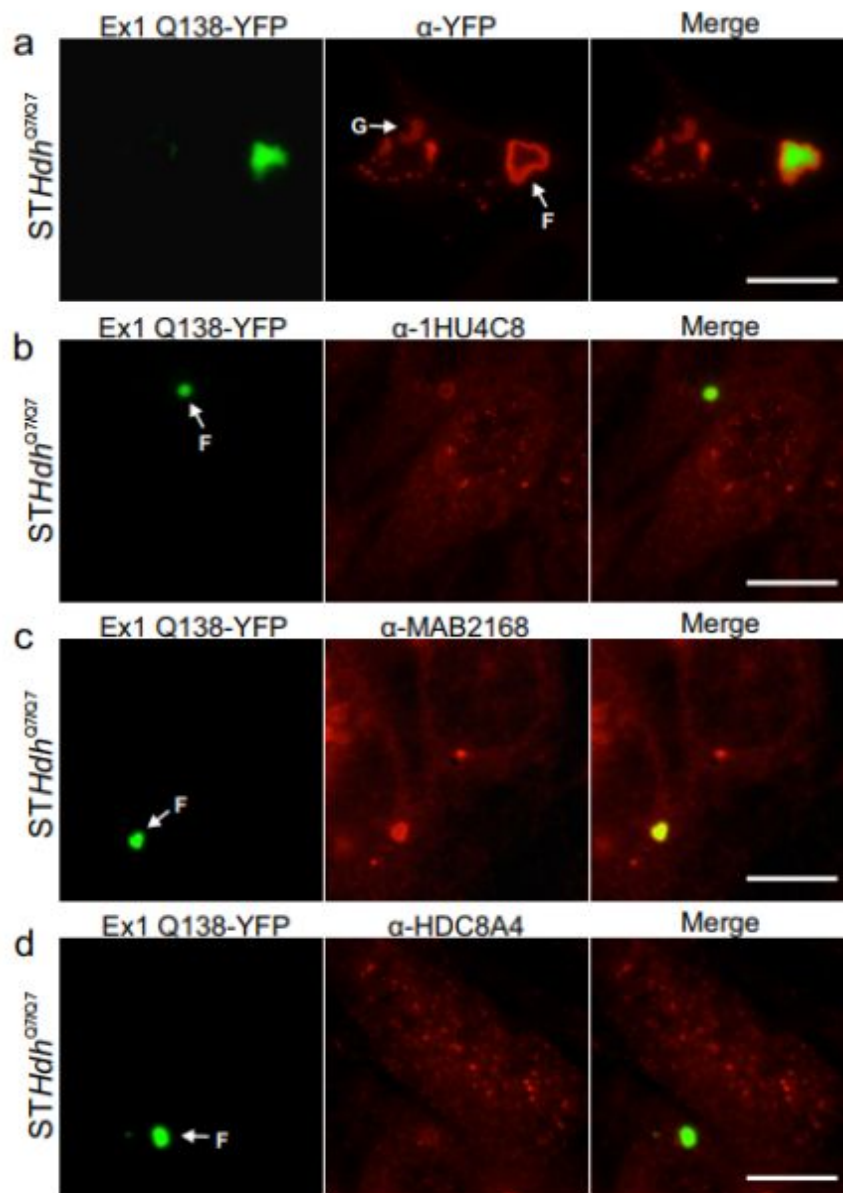


Figure S2.4 Endogenous huntingtin is detectable within fibrillar inclusions with**methanol fixation.** (A) Representative images showing that methanol

fixation/permeabilization causes a loss of fluorescence at globular but not fibrillar inclusions following expression of Ex1 Q138-YFP and immunofluorescence with an anti-YFP antibody

and an AlexaFluor488 secondary. Representative images of *STHdb^{Q7/Q7}* cells fixed and

permeabilized using methanol followed by immunofluorescence using (B) 1HU4C8, (C)

MAB2168 and (D) HDC8A4 monoclonal antibodies showing that fibrillar inclusions formed

by huntingtin exon1 Q138 constructs can recruit endogenous full-length huntingtin.

Antibodies were labelled with secondary antibodies conjugated with Cy5 to prevent spectral

bleed through due to the high fluorescence intensity of the inclusions. Inclusions of interest are

denoted with an arrow, where G refers to a globular inclusion, and F refers to a fibrillar

inclusion. Scale bar = 10 μ m.

CHAPTER 3: DEFINING RELEVANCE OF HUNTINGTIN PROTEIN INCLUSIONS IN CELLULAR TOXICITY

3.1 Introduction and Rationale

The presence of insoluble, polyQ-expanded mutant huntingtin inclusions is debated to be either toxic or protective. As described in Thesis Chapter 2, we observed formation of two distinct types of mutant huntingtin inclusions in a wild-type mouse striatal cell line (*STHdb*^{Q7/Q7}) by overexpressing a fluorophore-tagged fragment of polyQ-expanded huntingtin. Globular inclusions allow the free exchange of mutant huntingtin in and out of the inclusion. In contrast, fibrillar inclusions irreversibly sequester mutant huntingtin in densely packed aggregates. We hypothesized that the presence of these two types of inclusions (globular and fibrillar) could explain the discrepancy of inclusions regarded as toxic or protective in cell and mouse models^{115,116,189,190,192,202,209,258,260,283}, but we did not directly address cellular toxicity in that publication.

Inclusion formation was further investigated after description of these two distinct types, described in this chapter. Since inclusion formation was only tested in wild-type *STHdb*^{Q7/Q7}, I wanted to investigate if one type was possibly protective compared to the other by observing inclusion formation in mutant, HD cells (*STHdb*^{Q111/Q111}). There were a few gaps in our experiments described in Chapter 2 to make conclusions about the importance of inclusion mechanism to disease pathogenesis. A series of experiments are presented in this chapter to either address (1) a difference in inclusion type in wildtype vs HD cells, (2) if globular inclusions were more toxic than fibrillar or (3) the mechanism of inclusion formation using what we know about N17 phosphorylation in fibrillar inclusion formation and globular inclusion dependence on microtubules.

Hypothesis: If the formation of fibrillar inclusions is a protective cellular stress response that prevents mutant huntingtin from disrupting cellular functions, understanding the conditions that favour the formation of fibrillar over globular inclusions could be beneficial and provide therapeutic leads for the treatment of HD.

3.2 Exon1 Huntingtin Inclusions Form in Primary Mouse Cortical Neurons

The relevance of these huntingtin inclusions to cellular biology were questionable due to our model system. We wanted to see if these two types of inclusions could be formed in non-transformed, post-mitotic primary mouse neurons, a more clinically relevant cell type for experiments involving cellular toxicity and cellular death. In collaboration with Vickie Kwan in Dr. Karun Singh's lab, primary mouse cortical neurons were transfected with mCer-Exon1Q138-YFP and imaged live in an incubated microscope. Both globular and fibrillar inclusions formed and live cell observation showed that they formed similarly to those in *STHdb* cells (i.e. once fibrillar inclusion formed, all fluorescence signal was sequestered into the inclusion) (Figure 3.1). There were no conclusive benefits of using primary neurons over the *STHdb* cells, which are much easier to work with technically, so *STHdb* cells were continued to be used for future experiments.

3.3 Huntingtin Inclusion Formation in HD *STHdb*^{Q111/Q111} Cells

3.3.1 Live Cell Counting

So far, we had only characterized globular and fibrillar inclusion formation in wild-type *STHdb*^{Q7/Q7} cells. Overexpression of the same fragment of huntingtin, Exon1-Q138 YFP, polyQ-expanded HD cells, *STHdb*^{Q111/Q111}, showed minimal formation of fibrillar inclusions but many globular inclusions. However, quantification of inclusion number at a static point (usually around 20-24 hours) varies inconsistently depending on time post-transfection and transfection efficiency. Fibrillar inclusions form very rapidly (within 20 minutes) and can form in cells that already have globular inclusions, nucleating from a different cellular location. In order to account for these factors for a more accurate reflection of inclusion population, live cells were incubated microscope and images were captured every 5 minutes after 16-18 hours of transfection as the cells underwent the process of inclusion formation and then numbers were quantified. After 6 hours of observation, in wild-type *STHdb*^{Q7/Q7} cells, most cells that form an inclusion will form a fibrillar inclusion (Figure 3.2).

Conversely, in HD *STHdb*^{Q111/Q111} cells, globular inclusions are generally formed (Figure 3.2). Cells with globular inclusions were quantified if they maintained them during the span of observation and did not form fibrillar inclusions.

3.3.2 FRET-based Observations to Examine Huntingtin Inclusion Formation by flow cytometry

We showed that sensitized emission FRET (seFRET) could be used to detect relative FRET efficiency changes at subcellular locations temporally in live cells. This method relies on two different fluorophores with spectral overlap attached to one protein, and when the donor is excited, the subsequent emission can lead to energy transfer that excites the acceptor fluorophore. Experiments were performed on the Nikon TEclipse widefield microscope using the seFRET module²⁸⁴ with a three-filter CFP/YFP FRET cube. This filter set allows for the excitation of the donor while looking at two channels:

FRET DD = excitation of the donor and detection of the emission in the donor channel

FRET DA = excitation of the donor and detection of the emission in the acceptor channel

From using the FRET sensor, we know that the two inclusion types can be distinguished by their FRET efficiency levels, measured using a series of corrected signals detected in the FRET DD and FRET DA channels that account for crosstalk (detection of donor fluorescence in acceptor channel²⁸⁴). Globular inclusions having moderate efficiency, and fibrillar inclusions having a very high FRET efficiency (Thesis Chapter 2 and Caron/Hung et al.)⁷⁶. As an alternative to counting inclusion populations by eye, a less biased method of counting populations of cells would be to measure seFRET detection with flow cytometry using a similar setup of filters^{285,286} (schematic in Figure 3.3A, B). The main advantages of using flow cytometry are that we can identify large populations of inclusion-forming cells (can analyze hundreds of thousands of cells in minutes instead of a few hundred cells by eye over a few hours) and distinguish populations of cells with high FRET and lower FRET populations to

observe fibrillar and globular inclusion formation respectively. Gating and correction procedures are performed per trial with the same series of controls as with microscopy (Thesis Chapter 2, Caron/Hung et al.)⁷⁶ to identify cells with “positive FRET” (Figure 3.3C) and “negative FRET” (Figure 3.3D). The FRET sensor (mCer-Exon1Q138-YFP) was overexpressed for 24 hours in *STHdb*^{Q7/Q7} and *STHdb*^{Q111/Q111} prior to fixation with 4% paraformaldehyde (PFA). Results were consistent with quantifications with microscopic detection (Figure 3.2), showing that *STHdb*^{Q7/Q7} were more likely to form fibrillars, demonstrated by population of cells with high FRET) (Figure 3.3E) and *STHdb*^{Q111/Q111} were more likely to form globulars (Figure 3.3F). Even though the cells were harvested at a single time point, this provides more robust, quantitative method of determining inclusion type formation compared with counting inclusion types by microscopy.

3.4 Exploring the Role of Phosphorylation in Inclusion Formation

3.4.1 Filter Trap Aggregate Assays to Distinguish Fibrillar and Globular Inclusions

We showed in Chapter 2 that N17 phosphorylation promoted formation of fibrillar inclusions. Protein aggregates are commonly analyzed using filter trap assays and could be used to determine populations of fibrillar and globular inclusions by probing for N17-phospho.

Fibril-type aggregates are so tightly packed that they are resistant to protein denaturation by sodium dodecyl sulfate (SDS)²⁸⁷. Filter trap aggregation assays have been used to quantify products of protein aggregation. Cell lysates are filtered through nitrocellulose membrane that traps and retains large protein aggregates while smaller species (such as protein monomers and non-aggregated huntingtin) pass through the membrane.

STHdb^{Q7/Q7} cells were transfected with wild-type Exon1 expressing 17Q, mCer-Exon1Q17-YFP, for 32 hours or mutant mCer-Exon1Q138-YFP for either 16 or 32 hours. Inclusion formation begins around 16 hours, so most of the cells have no inclusions. By 24-30 hours, most of the cells will have fibrillar inclusions. Cells were lysed with sonication and 200µg of protein was filtered through a 0.2µm pore nitrocellulose membrane. We have shown that fibrillar inclusions favourably form with phosphorylated N17, so immunoblotting was

performed on the membrane detect N17 in the filtered aggregates using our validated N17-phospho antibody⁷⁴.

We expected increased signal corresponding to increased fibrillar inclusion formation. mCer-Exon1Q17-YFP should not aggregate, so there should be little to no signal on the blot. However, there was a strong signal on the blot, meaning the membrane did not filter the aggregate, but the soluble protein just bound the nitrocellulose membrane.

Unexpectedly, there was a steady decrease in N17-phospho signal with longer expression (Figure 3.4A). Visual observation of *STHdb*^{Q7/Q7} expressing mCer-Exon1Q138-YFP showed primarily fibrillar formation by 32 hours, so it was expected that increasing fibrillar inclusions would result in increasing N17-phospho levels. Technical challenges have been reported for filter trap aggregate assays and could explain this result²⁸⁸. There is evidence that the N17 region is buried in the centre of aggregates^{41,188,289}. Antigen retrieval protocols are often commonly used for improved immunocytochemistry detection^{182,290,291}. The combined effect could result in restricted access to the N17 epitope, explaining the detectable signal with overexpression of Exon1 Q17 (no restriction) and decreasing signal with Exon1 Q138. Additionally, if the lysate is not properly filtered through, the soluble protein could bind to the membrane instead, with the aggregated protein being washed off during the process, resulting in the same observation. Even though the assays was inconclusive for detecting phosphorylated N17, suggesting the N17 epitope was buried and involved in seeding of the aggregate and that the phosphorylation status was important.

3.4.2 Further Exploration of N17 Importance in Inclusion Formation by Microscopy

We have previously shown that overexpression of phosphomimetic Exon1Q138 favours the formation of fibrillar inclusions (Thesis Chapter 2 and Caron/Hung et al.)⁷⁶, but we wanted to explore if there was phosphorylated huntingtin (endogenous or overexpressed) in the inclusion itself.

STHdb^{Q7/Q7} were transfected with mCer-Exon1Q138-YFP for 24 hours.

Immunofluorescence was performed with an unphosphorylated N17 antibody and our

N17-phospho antibody (both validated in Atwal et al.)⁷⁴. Fibrillar inclusions are so tightly packed that antigen retrieval is necessary to reveal epitopes for antibody binding⁷⁶. After fixation with 4% paraformaldehyde, heated citrate buffer at 90°C was added to the cells for 20 minutes. Even after antigen retrieval, there was no observable signal where the inclusion was (Figure 3.4B), suggesting that the types of inclusions we are observing may be consistent with those described by Thakur et al.¹⁸⁸, where N17 is buried in the inclusion and is involved in forming inclusions in the context of expanded polyglutamine.

To further explore this, *STHdb*^{Q7/Q7} cells were transfected with both Exon1Q138-YFP and Exon1-mCherry bearing phosphomimetic amino acids (ExonQ142S13ES16E)(Figure 3.4C). Expression of Exon1Q138-YFP was necessary to show both types of inclusions forming independent of the phosphomutant species. Fibrillar inclusions are primarily made up of phosphomimetic Exon1, evident by the greater signal intensity of Exon1Q142S13ES16E-mCherry compared to Exon1Q138-YFP. Since huntingtin can move in and out of globular inclusions, it is not surprising that phosphomimetic Exon1Q142S13ES16E-mCherry is detected. These results suggested that the fibrillar inclusions were primarily formed by the phosphomimetic mutant.

3.5 Addressing Toxicity of Inclusions

3.5.1 Live Cell Observation of Inclusion Toxicity

STHdb^{Q7/Q7} and *STHdb*^{Q111/Q111} cells were transfected with mCer-Exon1 Q138-YFP and imaged live on an incubated microscope. Cells that formed fibrillar inclusions are usually less prone to die. Healthier cells (wild-type or healthier HD cells) can form fibrillar inclusions and will survive for up to 72 hours. However, cells with globular inclusions will either find a way to form fibrillar inclusions or will die within 12 hours of observation (Figure 3.5A). Live cell imaging showed that cells with fibrillar inclusions survived at least 48 hours after transfection, while cells with globular inclusions were not as viable. Therefore, globular inclusions are associated with increased cellular toxicity, either causing cellular death directly or

reflective of a more unhealthy cell that cannot form a fibrillar inclusion (modelled in Figure 3.5B).

3.5.2 Observing Cellular Toxicity Trends with Flow Cytometry

To confirm that globular or fibrillar inclusions affect cellular toxicity, phosphomimetic or phosphoresistant Exon1 mutants (mCer-Exon1 Q142S13ES16E-YFP or mCer-Exon1 Q142S13AS16A-YFP respectively) were overexpressed to enrich each type of inclusion and then stained with a far-red LIVE/DEAD cell viability dye (ThermoFisher Scientific) for flow cytometry analysis. Live and dead cells can be distinguished by the amount of intracellular staining, as dead cells will have decreased cell membrane permeability and increased staining (schematic in Figure 3.6A). Untransfected cells that were either untreated (healthiest) or subject to multiple rounds of freeze/thaw (to kill as many cells as possible) were analyzed to establish our range of live to dead cells (Figure 3.6B). Other constructs were also transfected to establish minimal toxicity from our transfection protocol (Figure 3.6C-E). The phosphoresistant mutant (which would favour globular formation) had a smaller population of live cells (albeit a small difference) compared to the phosphomimetic mutant, consistent with the hypothesis that globular inclusions are associated with increased cellular toxicity. Optimization of this method could allow for robust observation of the effects of small molecule compounds on inclusion formation to possibly reveal other mechanisms.

3.6 Mechanism of Inclusion Formation

3.6.1 Direct Interaction of N17 and Microtubules

We previously showed that globular inclusions were dependent on microtubules for formation and that fibrillars were not. In line with our theories on N17 importance on inclusion formation, we wanted to see if a direct interaction between N17 and tubulin was involved. Regions of full-length huntingtin can interact with microtubules^{292,293}, but the interaction with N17 in the context of serine phosphomutants is unknown. A microtubule-binding assay was performed, exploiting the property that microtubules can be

pelleted when centrifuged at $>100\ 000g$. Pure tubulin polymers were formed and incubated with N17 or N17-phospho (at S13 and S16) peptides. Supernatant fractions were separated from the pellet fraction and were run separately on a 12% native gel (Figure 3.7A). Native gels were used to prevent dissociation of microtubule-peptide complex for detection. Using our antibody against any form of N17 (recognizes amino acids 1-8, prior to residues that are phosphorylated), binding of peptides to microtubules in the pellet fraction were analyzed, with no obvious differences in microtubule binding.

3.6.2 Skewing Inclusion Formation Using Small Molecule Compounds

We have previously shown disruption of globular inclusions using a microtubule polymerization inhibitor, nocodazole. We also showed that increasing phosphorylation by treating cells with BMS 345541 promotes formation of fibrillar inclusions. Observation of live *STHdb*^{Q7/Q7} cells transfected with mCer-Exon1 Q138-YFP showed disruption of globular inclusions and subsequent formation of fibrillar inclusions (Figure 3.7B). As mentioned previously, it is not rare that a wild-type cell will switch from having globular inclusions to fibrillar inclusions, so the effect of BMS-345541 is inconclusive. However, the disruption of globular inclusions in conjunction with small molecule compounds that restore hypophosphorylation of N17 in *STHdb*^{Q111/Q111} cells could skew formation towards fibrillar.

3.6 Materials and Methods

Materials and methods specific to each experiments can be found in more detail in the figure captions. Inclusion types can be distinguished primarily by morphology. Unless otherwise stated, striatal cells (*STHdb*^{Q7/Q7} or *STHdb*^{Q111/Q111}) were transfected with 1-3 μ g mCer-Exon1-YFP constructs with Turbofect (ThermoScientific) for 16-24 hours. Cells were imaged live at 33°C in an incubated chamber with a Nikon TiEclipse epifluorescent widefield microscope.

3.7 Discussion and Conclusion

Further experimentation beyond what was presented in this Chapter was halted because these phenotypes could not be observed with endogenous huntingtin protein and their significance to human disease was questionable. Another major limitation of the project was that a small fragment of huntingtin was overexpressed with extremely large CAG repeats. However, there was some interesting data that was consistent with other researchers in the HD field regarding huntingtin aggregation and structure^{83,188–190,192,257,263,265,289,294}. It became evident that the inclusions were likely to be a readout, rather than reflective of inclusion formation by endogenous huntingtin. Cells that appeared healthier (wild-type cells or healthier HD cells) were able to form fibrillar inclusions, and cells that formed globular inclusions were more likely to die. A likely explanation for this is consistent with phenotypes seen in HD cells. Phosphorylation of S13 and S16 is critical for huntingtin function, stress-response mechanisms and cellular survival^{72,74,82,83}. Mutant huntingtin is hypophosphorylated at these sites. Our lab published that N17 folds back onto the polyP region downstream of the polyQ tract, and that this flexibility is disrupted when the polyQ exceeds the pathogenic threshold of 37Q⁹⁹. Therefore, kinases that are necessary for phosphorylation may be sterically hindered, resulting in hypophosphorylation. Aberrant energy metabolism is also observed in HD models^{216,295–298}, contributing to hypophosphorylation of N17. As fibrillar inclusions are associated with increased N17-phospho, it is likely that their formation is simply a readout of how the protein is phosphorylated. This research could therefore be used for compound screening or for high content screening to observe the effects of small molecule compounds on Exon1 conformation.

In 2016, we published that N17 can act as a ROS sensor, where oxidation of methionine 8 (M8) of N17 promoted phosphorylation at S13 and S16⁷². N17 is normally tethered to the ER membrane in steady state⁷³. The proposed mechanism was that M8 was oxidized in response to oxidative stress, and N17 could be released into the soluble phase, where it is more accessible to kinases for phosphorylation. However, the experiments were performed with N17 only, and was not in the context of polyQ-expanded huntingtin.

Analyzing inclusion formation could support this research as increased solubility and phosphorylation could be quantified by increased fibrillar inclusion formation.

3.8 Figures

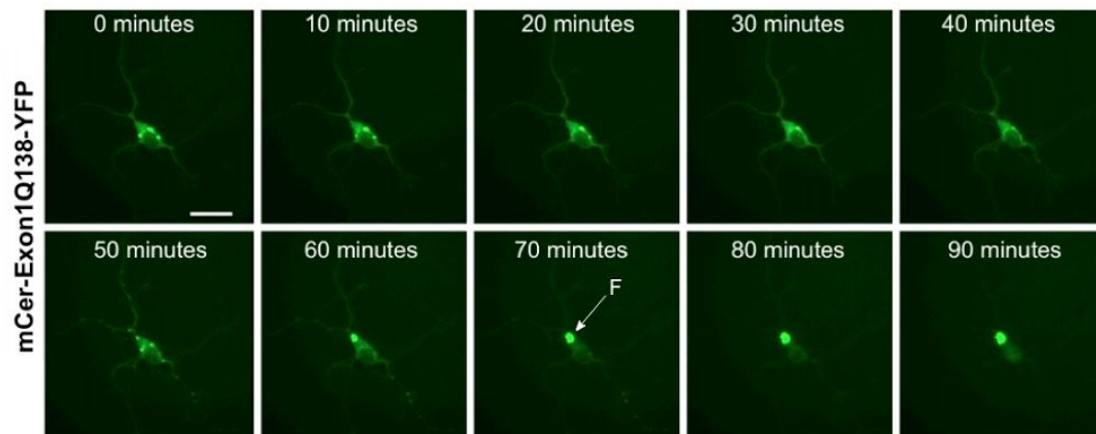


Figure 3.1 Inclusion formation is similar in primary cortical neurons. Live cell imaging using Nikon TiEclipse widefield microscope of a wildtype primary cortical mouse neuron with globular inclusions after overexpressing 3 μ g of mCer-Exon1Q138-YFP for 24 hours, followed by sequestration of all fluorescence into a fibrillar inclusion. Globular inclusions remain at similar fluorescence intensity (0-30 minutes) while fibrillar inclusions rapidly sequester huntingtin with an increase in intensity within the inclusions (60-90 minutes). Cells left in incubated chamber at 37°C. Scale bar = 10 μ m. Representative of 50 cells from 2 trials.

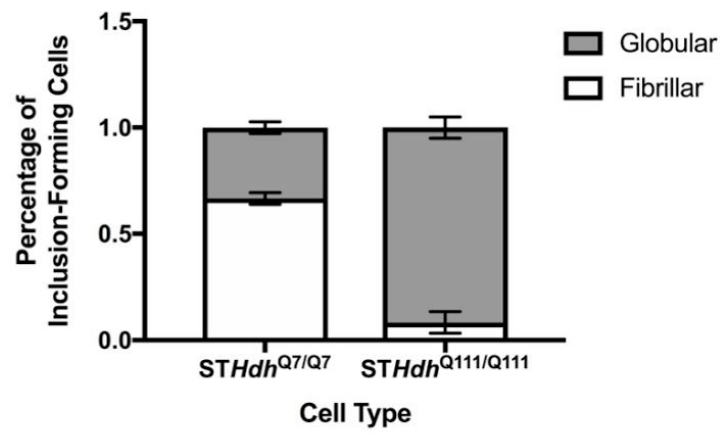


Figure 3.2 Inclusion populations in wildtype versus mutant cells by live cell imaging.

Cells were overexpressing mCer-Exon1Q138-YFP for 16-18 hours. Cells were then imaged live for the following 6 hours at 33°C and 5% CO₂. Counts of inclusions per type were based on observation of inclusion formation during the 6 hours. *STHdb*^{Q7/Q7} form fibrillar inclusions (white) more than globular inclusions (grey) (N=70, n=3) and *STHdb*^{Q111/Q111} form globular inclusions (grey) more than fibrillar inclusions (white) (N=40, n=3). Error bars represent standard deviation. ***p= <0.001.

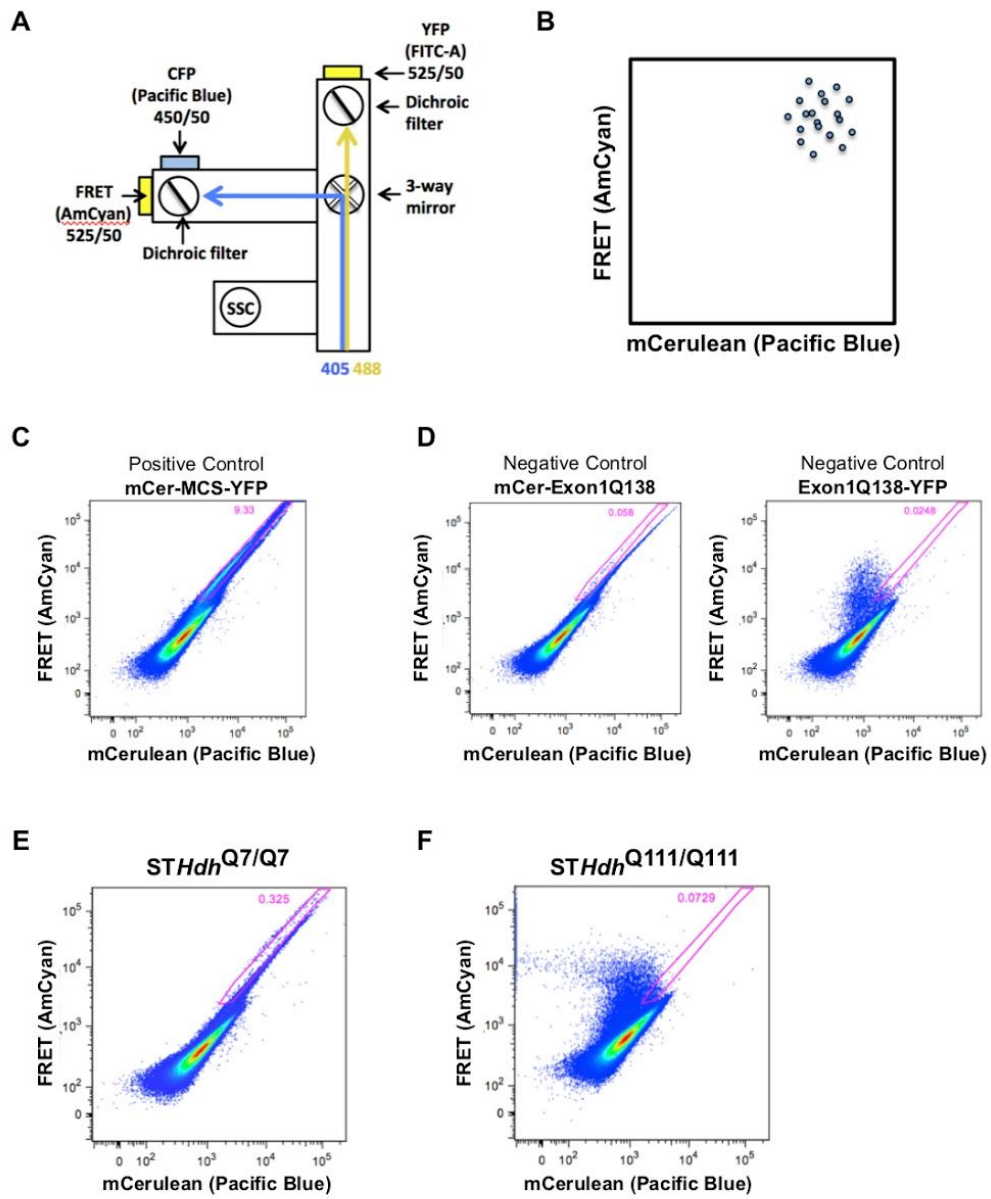
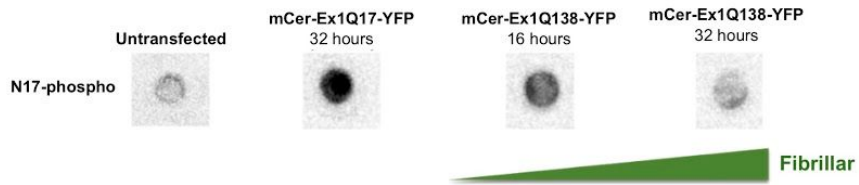


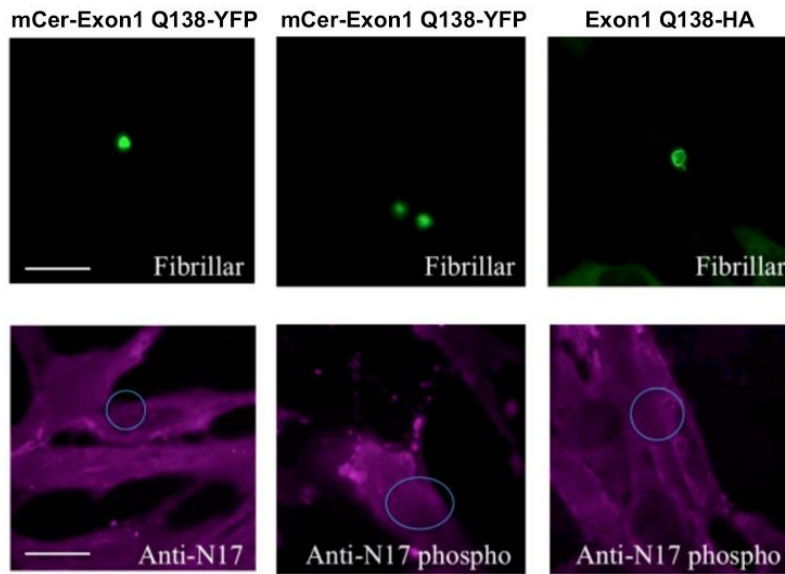
Figure 3.3 Inclusion populations in wildtype versus mutant cells by flow cytometry.

Using flow cytometry as another method to detect FRET, various fluorophore-tagged Exon1Q138 constructs were overexpressed for 24 hours. (A) Schematic of filter setup for flow cytometer. Pacific Blue filter detects mCerulean (excite donor, detect donor emission) signal and AmCyan filter detects FRET signal (excited donor, detect acceptor emission). (B) Theoretical gated region of cells with positive FRET, showing high signal in both channels. (C) Positive controls to establish gate. mCer-MCS-YFP is the FRET sensor with a multiple cloning site (MCS) as a linker so that FRET can occur. (D) Negative controls should show little to no FRET. Donor alone (mCer-Exon1 Q138) and acceptor alone (Exon1 Q138-YFP). Pink gate represents region of positive FRET as determined by positive and negative controls. (E) Overexpression of the FRET sensor reveals cells with high positive FRET in the *STHdb*^{Q7/Q7} but not in the *STHdb*^{Q111/Q111} cells. Each graph plots ~500 000 cells. Representative of n=2.

A



B



C

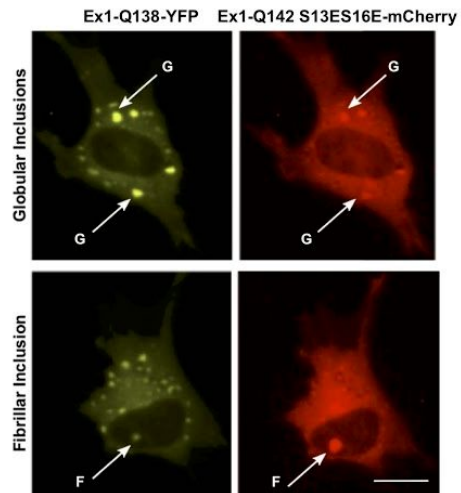


Figure 3.4 Formation of fibrillar inclusions is preferable in *STHdb*^{Q7/Q7} and with

phosphomimetic mutation. (A) Filter trap aggregate assay. Cells were transfected with either mCer-Exon1Q17-YFP or mCer-Exon1Q138-YFP. Plates were observed under a microscope prior to lysis to estimate population of fibrillar inclusions. As fibrillar inclusion formation increased (longer expression time in *STHdb*^{Q7/Q7} always results in more fibrillar inclusions), N17-phospho signal decreased. n=2. (B) Immunofluorescence cannot be performed with anti-N17 antibodies to detect N17 in inclusions formed by overexpressed mCer-Exon1 Q138. Cells were transfected and fixed after 24 hours. Antigen retrieval was performed after fixation prior to antibody incubation. Immunofluorescence was performed with N17 pan antibody (first 8 amino acids of N17, can detect unphosphorylated and phosphorylated N17) and N17-phospho antibody. In the location where the inclusion is, there is no detectable N17 signal. To check if the two fluorophores played a role in blocking the antibody-epitope interaction, HA-tagged Exon1 was also transfected. Scale bar = 10µm. n=2. Representative of >50 cells. (C) Cells were transfected with Exon1Q138-YFP and Exon1Q142 S13ES16E-mCherry. There is more Exon1Q142 S13ES16E-mCherry than Exon1Q138-YFP in fibrillar inclusions. n=2. Representative of >50 cells. Scale bar = 10µm.

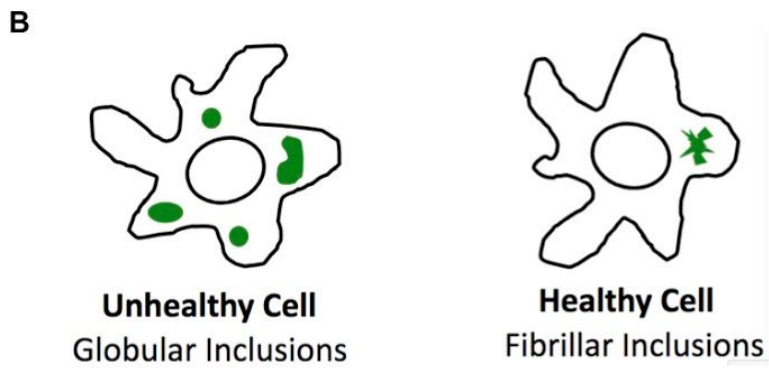
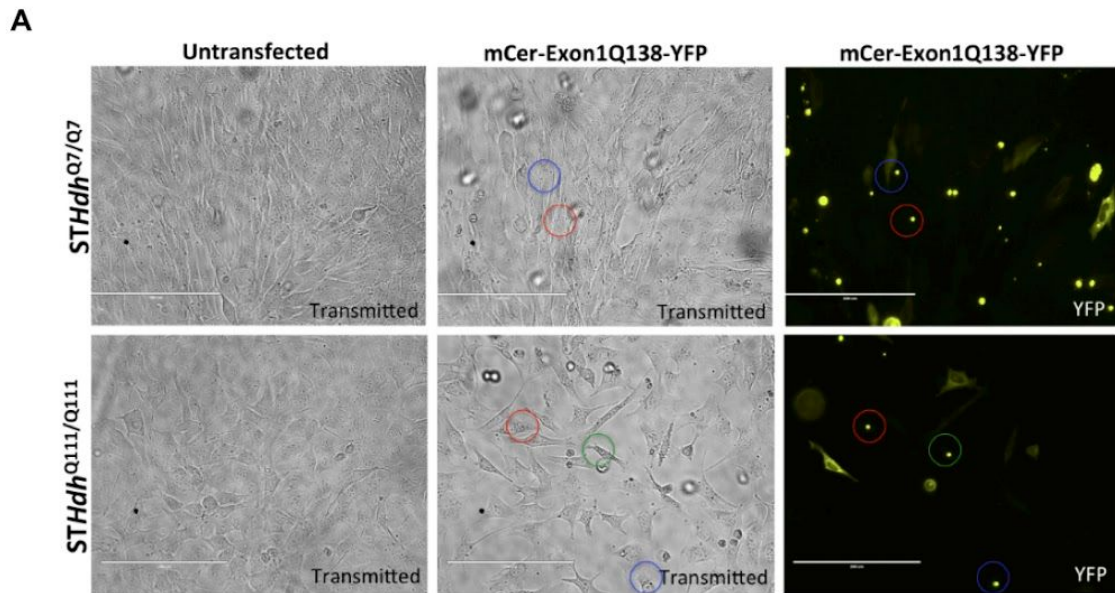


Figure 3.5 Toxicity of inclusion formation in *STHdb* cells by live cell imaging. (A)

STHdb^{Q7/Q7} and *STHdb*^{Q111/Q111} cells were transfected with mCer-Exon1Q138-YFP. Images of cells after 48 hours, showing that there is a lot of cell death but a population of fibrillar-forming cells have survived (red, green and blue circles). Throughout the time course, *STHdb*^{Q7/Q7} cells had primarily formed fibrillar inclusions and cell density is not that different than untransfected cells. (B) Model of cell toxicity. Although huntingtin aggregates are not necessarily the disease causing aspect of HD, there may be a cell toxicity-related role of the inclusions where they can be either toxic or protective. This discrepancy between the two theories could possibly be explained by the fact that there are two types of mutant huntingtin inclusions. Healthier cells may be able to deal with mutant huntingtin load by sequestration to remove the toxic species from the cell. Unhealthy cells (diseased) are unable to do that, so the type of inclusion may be regarded as non-protective because cells that form these inclusions usually do not survive. Representative of n=4. Scale bar = 200µm.

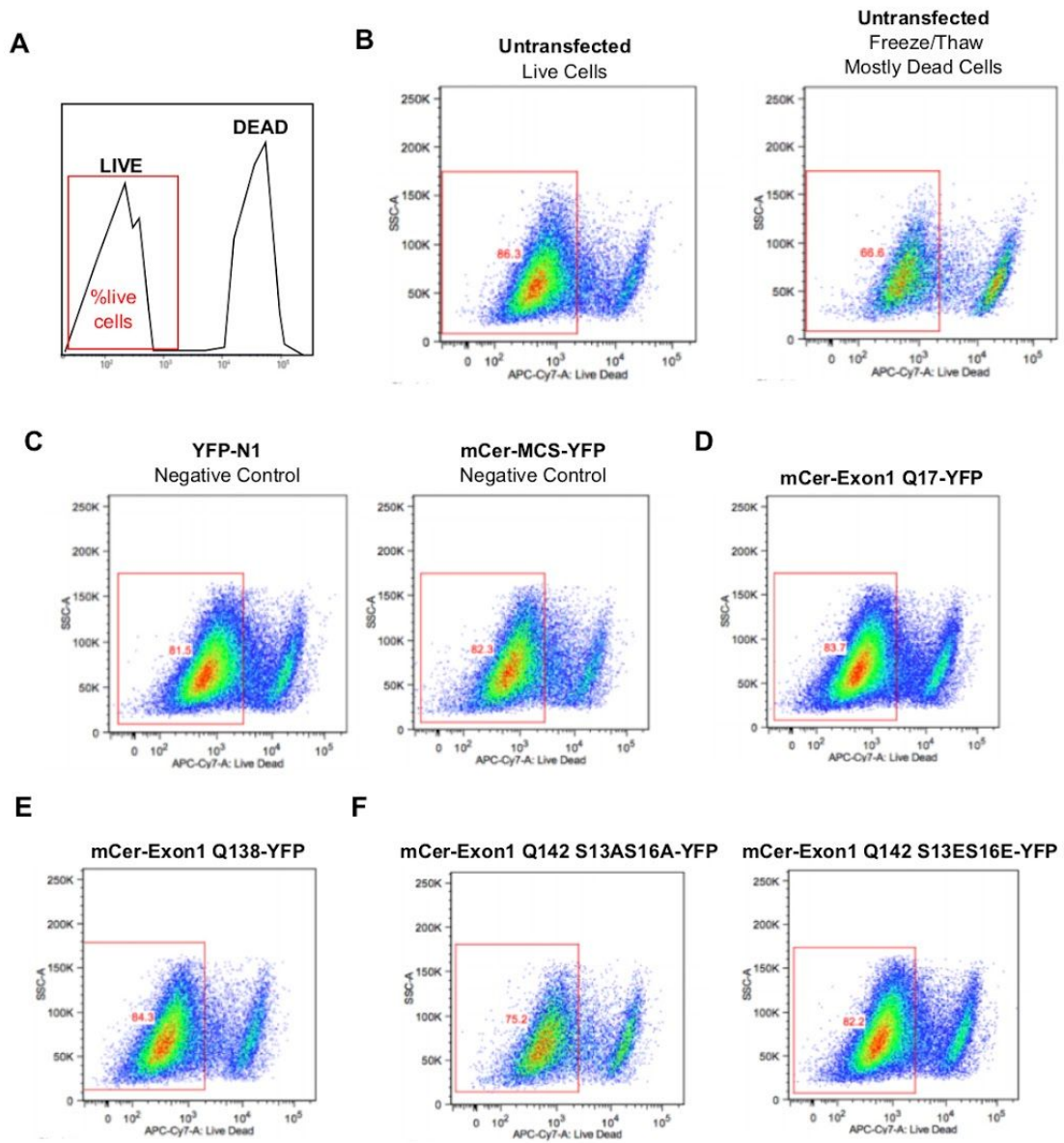
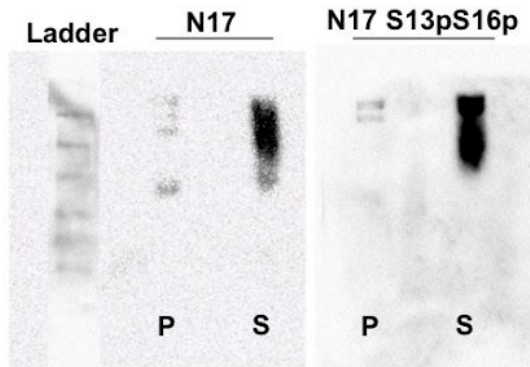


Figure 3.6 Measuring toxicity of inclusion formation in *STHdb* cells by flow

cytometry. (A) Schematic of LIVE/DEAD staining by flow cytometry analysis. Cells that are live will only bind the dye on the membrane of the cell. Cells that are dead will internalize the dye, and signal will be much stronger. (B) Live cell percentage was determined in untransfected cells and is gated with red box. (C) Negative controls to confirm that transfection of constructs did not result in toxicity. (D) Huntingtin Exon1 controls to confirm that transfection did not result in toxicity. (E) There is a small difference between the phosphoresistant (Exon1 Q142-S13QS16A) or phosphomimetic (Exon1 Q142-S13ES16E) mutant. Representative of >100 000 cells, n=2.

A



B

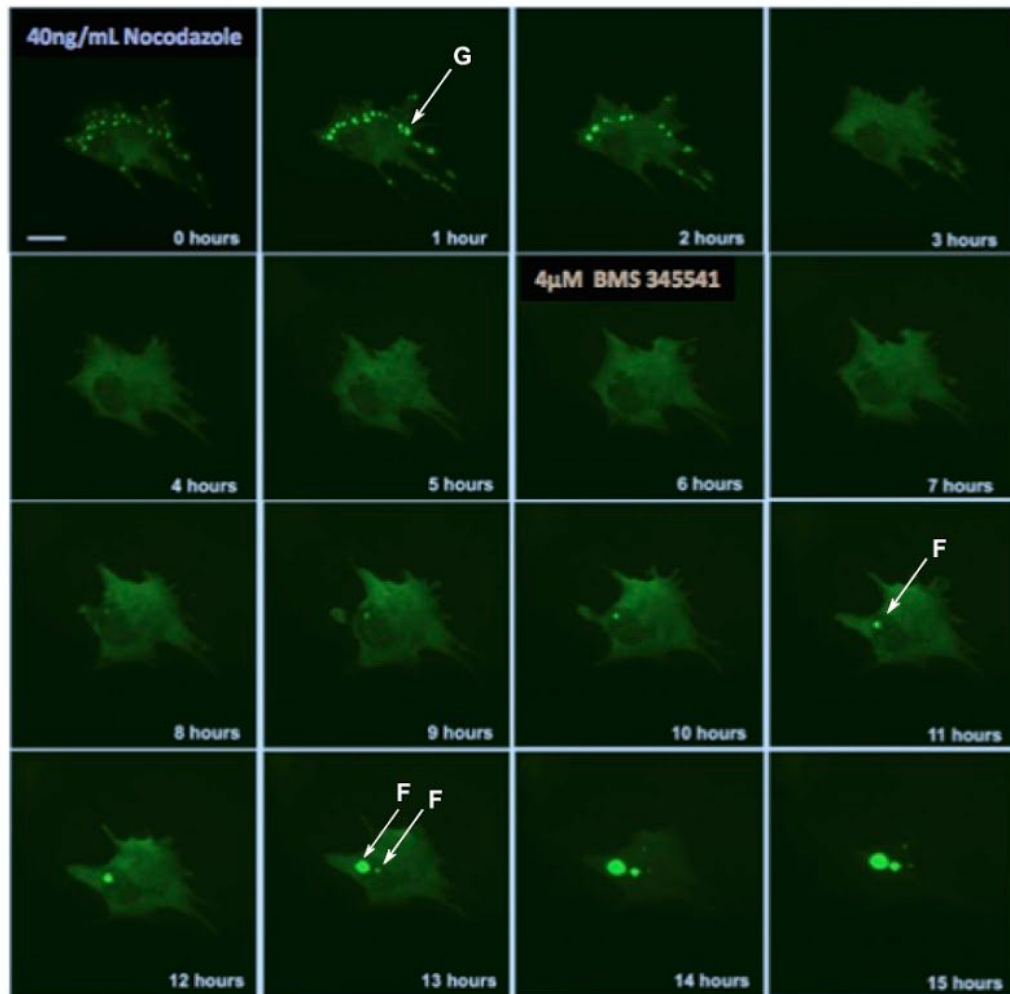


Figure 3.7 Dependence of microtubules in inclusion formation mechanism. (A)

Microtubule binding assay. Peptides were ordered from Genscript. Pure peptide was resuspended in HEPES buffer. Microtubules were polymerized from tubulin monomers and incubated with peptides and centrifuged at 100,000g. Fractions were separated and loaded on a 12% native gel. L denotes protein ladder. P denotes pellet fraction (where microtubules are found). S denotes supernatant (peptide not bound to microtubules). Anti-N17 pan antibody was used to see all variations of N17. n=2. (B) After 10 hours overexpression of Exon1 Q138-YFP, *STHdb^{Q7/Q7}* cells were treated with 40ng/mL nocodazole (first panel) for 6 hours, followed by 4 μ M BMS 345541 treatment. Live cell imaging of cell that formed globular inclusions was observed in an incubated microscope at 33°C with 5% CO₂. Scale bar = 10 μ m.

CHAPTER 4: DEVELOPMENT OF NOVEL PATIENT FIBROBLAST CELL LINES FOR STUDYING HD BIOLOGY

The material presented in this chapter is a representation of the following manuscript which has been submitted for publication:

Hung, C.L.K., Maiuri, T., Bowie, L.E., Gotesman, R.G., Son, S., Falcone, M., Giordano, J.V., Gillis, T., Mattis, V., Lau, T., Kwan, V., Wheeler, V., Schertzer, J., Singh, K. and Truant R. “A Patient-Derived Cellular Model for Huntington’s Disease Reveals Phenotypes at Clinically Relevant CAG Lengths”

Manuscript submission history:

BioRxiv pre-print server: <https://doi.org/10.1101/291575>

Scientific Reports: SREP-18-11906. Received April 17th, 2018

Revisions received July 19th, 2018

Molecular Biology of the Cell: E18-09-0590.

Revisions transferred and re-submitted Sept 19th, 2018

Changes were made in the following publication for thesis continuity and formatting.

4.1 Contributions to Manuscript in Submission

C.L.H. and R.T. created experiments. C.L.H. wrote manuscript and generated figures. T.M. and R.T. helped with editing. M.F. provided technical assistance. C.L.H. performed all experiments except for the following: V.M., V.K. and K.S. transduced patient cell lines for immortalization. J.V.G., T.G. and V.W. performed CAG repeat sizing. T.L. and J.S. performed qPCR. L.E.B performed antibody validation experiments. R.G. performed cell viability experiments. S.S. performed nuclear speckle count. T.M. performed super-resolution imaging of nuclear speckles. These contributions are further clarified and annotated in the figure captions.

4.2 Implications of Work

Some of the roadblocks to HD cell biology research are a result of disease model systems. Most cell and mouse models are generated with irrelevantly long CAG repeats that overlook the importance of researching why some patients with the same CAG mutation length develop disease much sooner than other patients. Cellular biology approaches to understand functional disruptions in HD have primarily focused on cell lines with synthetically long CAG length alleles that clinically represent outliers in this disease and a more severe form of HD that lacks age-onset.

Patient-derived fibroblasts are limited to a finite number of passages before succumbing to cellular senescence. Immortalization through transformation requires disruption of p53 function, which is necessary for cellular stress responses. Instead, we used human telomerase reverse transcriptase (hTERT) to immortalize fibroblasts taken from individuals of varying age, sex, disease onset and CAG repeat length, which we have termed TruHD cells. Phenotypes were consistent with those previously reported in HD cells, even at clinically relevant CAG repeats. These cells are now the standard cell line used in our lab, and we have since distributed them for use in other labs. Some of the challenges with patient fibroblasts is the lack of characterization and identification of cellular readouts, such as ADP/ATP ratio and cell proliferation. Here, we presented several established phenotypes that could be distinguished between wild-type and HD cells which can be followed-up on, providing a basis for Thesis Chapter 5.

A Patient-Derived Cellular Model for Huntington's Disease Reveals Phenotypes at Clinically Relevant CAG Lengths

Claudia Lin-Kar Hung¹, Tamara Maiuri¹, Laura Erin Bowie¹, Ryan Gotesman¹, Susie Son¹, Mina Falcone¹, James Victor Giordano^{2,3}, Virginia Mattis⁴, Trevor Lau¹, Vickie Kwan^{1,5}, Vanessa Wheeler^{2,3}, Jonathan Schertzer¹, Karun Singh¹, *Ray Truant¹

¹Department of Biochemistry and Biomedical Sciences, Faculty of Health Sciences, McMaster University

²Center for Genomic Medicine, Massachusetts General Hospital, Harvard Medical School, Boston, MA

³Department of Neurology, Massachusetts General Hospital, Harvard Medical School, Boston, MA

⁴Cedars-Sinai Medical Center, Board of Governors Regenerative Medicine Institute, Los Angeles, CA

⁵Stem Cell and Cancer Research Institute, Faculty of Health Sciences, McMaster University

FUNDING

This work was supported by the Canadian Institutes of Health Research, grant MOP-119391, the Krembil Foundation and the Huntington Society of Canada.

4.3 Abstract

The huntingtin protein participates in several cellular processes that are disrupted when the polyglutamine tract is expanded beyond a threshold of 37 CAG DNA repeats in Huntington's disease (HD). Cellular biology approaches to understand these functional disruptions in HD have primarily focused on cell lines with synthetically long CAG length alleles that clinically represent outliers in this disease and a more severe form of HD that lacks age-onset. Patient-derived fibroblasts are limited to a finite number of passages before succumbing to cellular senescence. We used human telomerase reverse transcriptase (hTERT) to immortalize fibroblasts taken from individuals of varying age, sex, disease onset and CAG repeat length, which we have termed TruHD cells. TruHD cells display classic HD phenotypes of altered morphology, size and growth rate, increased sensitivity to oxidative stress, aberrant ADP/ATP ratios and hypophosphorylated huntingtin protein. We additionally observed dysregulated ROS-dependent huntingtin localization to nuclear speckles in HD cells. We report the generation and characterization of a human, clinically relevant cellular model for investigating disease mechanisms in HD at the single cell level, which, unlike transformed cell lines, maintains TP53 function critical for huntingtin transcriptional regulation and genomic integrity.

4.4 Introduction

Huntington's disease (HD) is a late-onset, autosomal-dominant neurodegenerative disorder characterized by a triad of motor, cognitive and psychiatric symptoms. The disease is caused by a CAG trinucleotide expansion of >37 repeats in the huntingtin gene, manifesting as polyglutamine-expanded huntingtin protein⁶. The functional implications of this expanded, mutant huntingtin are not fully understood. Much of the existing research on HD cell biology in relevant neuronal cell types has been limited to primary post-mitotic neurons from murine brain tissue or transformed cell lines, which have several limitations, including the use of synthetically long CAG lengths in order to mimic human disease in mice^{32,112,115,116,202,203,206,208,216,299–303}. These alleles actually genetically model juvenile or Westphal variant HD, which are not age-onset diseases. The mean clinical CAG allele length is 43 repeats, with even >50 repeats representing statistical outliers³⁰⁴. Disease models in Neuro-2A cells, HEK293 or HeLa cells rely on cell transformation to maintain line longevity, but transformation typically involves initiating genomic instability and “shattering” of genomes^{305,306}, affecting intra- and inter-laboratory reproducibility.

The pursuit of investigating human cells has driven researchers to culture patient fibroblast cells that can be extracted from a skin biopsy^{307–309}. Primary fibroblasts from HD patients possess clinically relevant polyglutamine expansion lengths, making them an attractive model for studying HD human cell biology. Further, they can be reprogrammed into induced pluripotent stem cells (iPSCs)²²⁴, which can be differentiated into various neuronal cell lineages^{310–312} or directly reprogrammed to medium spiny neurons^{226,228,313,314}. However, primary fibroblasts are subject to telomere-controlled senescence, which limits the number of passages as telomeres shorten with each cell division^{315,316}. Senescent cells display altered gene expression, decreased proliferation and resistance to apoptotic mechanisms^{317,318}, hindering long-term use and consistency between trials.

We sought to overcome these limitations by immortalizing patient fibroblasts with human telomerase reverse transcriptase (hTERT). hTERT has been extensively used to immortalize human cell types to study cell biology in a number of diseases^{319–324}. Like primary

cells, hTERT-immortalized cells mimic *in vivo* tissue phenotypes³²⁵, with the added benefits of proliferative capacity, karyotypic stability, and inter-experimental reproducibility³²⁵.

We sought to generate a panel of human cell lines with polyglutamine expansions in the 40-50 CAG range, reflective of those seen in the clinic. We immortalized fibroblasts from 3 individuals and termed the cell lines TruHD cells: control female (TruHD-Q21Q18F), heterozygous male (TruHD-Q43Q17M), and homozygous female (TruHD-Q50Q40F) (Table 1). To validate these cells as HD models, we examined known model and patient phenotypes. Consistent with previous reports, we found that HD cells could be distinguished from wild type based on morphology^{216,303}, size³⁰³, growth rate^{308,326,327}, sensitivity to stress^{73,91,202,295}, aberrant ADP/ATP ratios^{113,216,328}, hypophosphorylated huntingtin protein^{74,82,83} and altered ROS-dependent localization to nuclear speckles⁷². We have therefore generated and characterized a panel of clinically relevant cellular models for investigating disease mechanisms in HD.

Genome-wide association studies (GWAS) in the HD research field revealed DNA damage and oxidative stress mechanisms as critical modifiers of the age of disease onset in patients¹¹. One of the most important regulators of DNA repair, cell stress, and cell death responses is the TP53 protein³²⁹⁻³³¹, which also directly regulates huntingtin transcription via a response element in the *HTT* promoter region^{222,332}. To date, the most widely used HD cell lines are SV40 large T-antigen-transformed mouse striatal cell lines (*STHdb*)²¹⁶, which have become an invaluable tool for studying HD cell biology. However, conditional cell immortalization by transformation requires inhibited TP53 function. Investigation of the role of huntingtin in DNA damage and cell stress pathways may therefore be confounded by TP53 inactivation. In contrast, hTERT immortalization does not alter TP53 function^{320,333,334}, making TruHD cells an attractive model for these disease mechanisms in particular. Immortalized fibroblasts provide the added benefits of inter-experimental and inter-laboratory reproducibility, and long-term applications such as generation of stable cell lines and direct conversion to patient-specific human neurons. These cell models are readily available to the HD research community and will be freely distributed by our group.

4.5 Results

4.5.1 *Immortalization of Primary Fibroblasts with hTERT*

Primary fibroblasts from various patients were obtained from the Coriell Institute for Medical Research and transduced with TERT Human Lentifect™ Purified Lentiviral Particles as described in methods. Three immortalized cell lines were generated from patients with varying CAG repeat lengths and disease onset age (Table 1) as representatives of control (TruHD-Q21Q18F), heterozygous HD (TruHD-Q43Q17M) and homozygous HD (TruHD-Q50Q40F). We standardized the line naming to a format compatible with digital file annotation, defining the CAG length of each *HTT* allele and the sex of the donor.

To verify that cells were successfully overexpressing hTERT, RNA levels in primary cells and TruHD cells were compared by quantitative PCR (qPCR), showing detectable hTERT mRNA levels in TruHD cells compared to primary cells normalized to commercially available hTERT-immortalized retinal pigment epithelial (RPE1) cells (Figure 1A). To ensure that the increased hTERT expression was associated with increased hTERT catalytic activity, telomerase activity was tested in TruHD-Q21Q18F and TruHD-Q43Q17M cells using a telomeric repeat amplification protocol (TRAP) assay. As shown in Figure 1B, multiple amplification products resulting from active hTERT were observed in TruHD cells, but not primary cells, indicating that the transduced hTERT is catalytically active in TruHD cells.

Unlike immortalization by transformation, hTERT immortalization maintains karyotypic stability in normal, human diploid cells^{320,323,333}. Chromosomal instability leading to polyploidy and aneuploidy can affect gene expression and cell viability, which is a hallmark of transformed cancer cells^{335,336}. To confirm karyotypic stability in TruHD cells after 25+ passages, we compared the karyotypes of *STHdb* cells and TruHD cells. Large chromosomal abnormalities were detected in transformed HD mouse striatal derived cells (*STHdb*^{Q111/Q111}) cells (Supplemental Figure 1A, Table 2), consistent with a recently published study³⁰³. No chromosomal changes were recorded for control TruHD-Q21Q18F, and minor chromosomal changes were recorded in TruHD-Q43Q17M and TruHD-Q50Q40F cell lines (Figure 1C, Table 2). In TruHD-Q43Q17M cells, the majority of the analyzed cells were missing one

chromosome 16, and in TruHD-Q50Q40F cells, most of the cells had an abnormal banding pattern on chromosome 4. These changes should be considered when interpreting results of phenotypic analysis.

4.5.2 Validation of CAG Repeats in TruHD Cell Lines

To verify that the CAG repeats of the fibroblasts matched the clinical information reported after successful immortalization, the CAG repeats were sized using a standardized *HTT* CAG repeat sizing assay^{59,337}. The length of each CAG tract was as expected (Table 3). The human *HTT* gene typically bears an additional CAACAG sequence beyond the pure CAG DNA tract sequence⁶. These two additional codons encoding glutamine residues were not considered in the annotation by the Coriell Institute. Therefore, TruHD-Q21Q18F, for example, only refers to the polyglutamine tract that corresponds to the pure CAG tract, but the full polyglutamine tract lengths are actually Q23Q20. The true polyglutamine lengths corresponding to each TruHD cell line are listed in Table 3.

4.3.3 Defining Senescence in TruHD Cell Lines

Primary fibroblasts are typically cultured for approximately 15 passages from the initial skin biopsy before reaching senescence, while the successfully immortalized cells reported here can be passaged beyond 80 passages without reaching senescence (data not shown). Senescent cells show changes in cell growth, morphology and gene expression, which can be detected by an associated beta-galactosidase activity^{338,339}. Senescence was not detectable in TruHD immortalized cell lines (Supplemental Figure 1B) under normal culture conditions. We did note, however, that control TruHD-Q21Q18F fibroblasts seeded too sparsely exhibited senescence-associated beta-galactosidase activity (Supplemental Figure 1C) and stopped dividing. Normal, adherent cells in culture undergo contact inhibition, or post-confluence inhibition of cell mitosis^{338,340,341}. Essentially, once the cells become too confluent and make contact with nearby cells, they stop dividing and do not grow because of contact inhibition,

unlike transformed cell lines. Cells that are left in this state for too long can become senescent and do not recover in culture³⁴². Specific protocols for freeze/thaw were therefore considered and explained in detail in the methods section. After 7 days of confluence without media changes, control cells were more susceptible to senescence compared to the HD cell line (Supplemental Figure 1D). Upon karyotypic analysis of TruHD-Q21Q18F cells cultured under these conditions, a small percentage of control cells displayed tetraploidy (Supplemental Figure 1E), a phenomenon which has been reported to be a result of cellular senescence^{338,343}. In contrast, tetraploidy did not occur for either of the HD cell lines. Overall, we observed that cells did not senesce after extended passaging (over 80 passages), but control cells did senesce if cultured too sparsely or at high confluence, unlike HD cells which have a more senescence-resistant phenotype. This aspect of these cell lines could provide utility to study huntingtin biology in senescent cells, or cells in transition from mitotic to senescent. As with any cell lines though, it is important to note that prolonged culturing of cells (beyond 100 passages), even if immortalized, can result in abnormal behaviour^{344,345}, especially if cell confluence and senescence are not monitored regularly.

4.5.4 Cell Morphology, Size, Growth and Viability

Mutant *STHdh* cells exhibit altered morphology^{216,295,303}. To probe whether TruHD cells could be distinguished by their morphology, nuclei were stained with Hoechst and immunofluorescence was performed with antibodies against phosphorylated huntingtin at serines 13 and 16 (N17-phospho) and beta-tubulin (Figure 2A). Images were analyzed with Phenoripper open software (www.phenoripper.org), which defines textures of the images in a non-supervised manner, and plots vectors of the three most variant textures in unitless 3D space using principal component analysis (PCA). This allows for identification of similarity between the images based on those defined features. Merged images of TruHD-Q21Q18F, TruHD-Q43Q17M and TruHD-Q50Q40F, considering the three parameters Hoechst, N17-phospho, and beta-tubulin, clustered apart from each other on a PCA plot (Figure 2B). The clustering pattern from each individual channel is shown in Supplemental Figure 2A,

where beta-tubulin alone showed the greatest separation in the clusters compared to Hoechst and N17-phospho. This unbiased detection of a morphology phenotype between control and HD cells may be attributed to differences in cell size. We therefore compared cell size in control and mutant TruHD cells. Quantification of cell surface area shows that HD cells are smaller than control cells (Figure 2C). Therefore, consistent with numerous independent previous reports, huntingtin may be involved in cytoskeletal regulation^{303,346-348}.

Re-entry of post-mitotic neuronal cells into the cell cycle is a potential mechanism in the neurodegenerative process (see review³⁴⁹). A consistent observation when culturing TruHD fibroblasts is that the mutant fibroblasts divide more rapidly, as seen with primary HD fibroblasts³⁰⁸. Monitoring proliferation of TruHD cells over 72 hours showed that TruHD-Q43Q17M cells double after ~20 hours, TruHD-Q50Q40F cells double after ~24 hours, while TruHD-Q21Q18F double after ~72 hours (Figure 2D). These observations are consistent with reports implicating huntingtin in cell cycle regulation and DNA damage repair mechanisms^{91,348,350} and that these functions are aberrant in HD cells.

Susceptibility to various types of cell stress is a well documented phenomenon in HD cellular models^{73,74,346,351}. We have previously shown that huntingtin responds to oxidizing agents by becoming phosphorylated, translocating from the ER to the nucleus and interacting with chromatin^{72,91}. We therefore tested TruHD cell viability upon oxidative stress with potassium bromate (KBrO₃) treatment over 24 hours. As shown in Figure 2E, both HD cell lines were most susceptible to cell death compared to the control line. Dose-dependent response of treatments in each individual TruHD cell line can be found in Supplemental Figure 2B.

Besides response to cell stress, another well documented HD phenotype is an energy deficit as measured by ADP/ATP ratio^{113,216,295}. The detection of ADP/ATP ratio in TruHD cells demonstrated an energy deficit in HD cell lines compared to the wild type cell line (Figure 2F) similar to the trend in *STHdb* cells (Supplemental Figure 2C), which is consistent with previously reported studies in HD models and synthetic allele lengths^{216,328}.

These phenotypes described in TruHD cells such as cell morphology, size, growth rate, susceptibility to oxidative stress and energy levels, demonstrate their utility as a cellular model with clinically relevant CAG allele lengths as phenotypes in mutant TruHD cells were all consistent with previous HD cellular models.

4.5.5 Total Huntingtin and Phosphorylated Huntingtin Protein Levels

Since the cells were taken from various patients and are not isogenic, the amount of total huntingtin was quantified. Validated antibodies to different epitopes of full-length huntingtin were used (EPR5526 and mAb2166), showing a minor decrease in total huntingtin levels in TruHD-Q50Q40F compared to TruHD-Q21Q18F and TruHD-Q43Q17M (Figure 3A, B; full immunoblots Supplemental Figure 4A, B).

Phosphorylation is a protective post-translational modification in HD cells^{74,82,83}. Restoration of N17 phosphorylation is a therapeutic target in HD that has been explored by our lab and others because mutant, polyglutamine-expanded huntingtin is hypophosphorylated at serines 13 and 16 (S13p and S16p respectively)^{74,82,83}. Immunoblotting performed with a validated antibody against both serines (α -N17-phospho) (Supplemental Figure 3) showed decreased levels of N17 phosphorylation in mutant TruHD fibroblast cell lines compared to wild type (Figure 3C; full immunoblot Supplemental Figure 4C). Two distinct molecular weight bands are seen with the antibody, at ~350kDa and ~220kDa. Degradation products are often reported with other huntingtin antibodies as well, due to the large size of the protein and the rigorous processing steps of immunoblotting^{352,353}. Both bands were considered in quantifications, and this confirms hypophosphorylation of mutant huntingtin in a human HD. These results were verified by measuring whole-cell mean fluorescence intensity by flow cytometry (Figure 3D). Therefore, N17-phospho levels vary, but total huntingtin levels are invariant. This phenotype is consistent with previous reports^{74,82,83} and further validates N17-phosphorylation restoration as a target for HD therapeutic development.

4.5.6 *Huntingtin Stress Response in Human Patient Fibroblasts*

Huntingtin is a stress response protein and is involved in the unfolded protein response (UPR), DNA damage repair, oxidative stress and endoplasmic reticulum (ER) stress pathways^{72,73,91,354,355}. Previous studies from our lab show that huntingtin is bound to the ER membrane in steady state conditions and is released under conditions of stress, particularly ROS stress^{73,74}. Once soluble, huntingtin is phosphorylated at serines 13 and 16 (S13,S16), translocates to the nucleus and localizes to nuclear puncta^{72,74,78}. Using super-resolution structured-illumination microscopy (SR-SIM), we have now identified that these previously reported nuclear puncta are SC35 positive nuclear speckles: dynamic RNA/protein structures that are rich in mRNA splice factors that are important in cell stress responses³⁵⁶⁻³⁵⁸ (Figure 4A).

We previously reported that stress-dependent phosphorylation of S13 and S16 promotes huntingtin localization to nuclear speckles in hTERT-immortalized human retinal pigment epithelial cells (RPE1)⁷². We therefore tested this phenomenon in TruHD cells. Cells were treated with 0.1mM 3-nitropropionic acid (3NP), a mitochondrial complex II inhibitor, for 1 hour to induce oxidative stress. We observed a significant increase in the number of nuclear speckles in TruHD-Q21Q18F cells (Figure 4B, C). However, in both the mutant TruHD-Q43Q17M and TruHD-Q50Q40F lines, there was no significant difference in the number of nuclear speckles between treated and untreated conditions. The number of nuclear speckles in both heterozygote and homozygote HD cells were similar to that of TruHD-Q21Q18F in the presence of 3NP (N.S., $p=0.8475$), suggesting that in HD cells are under a chronic stress load.

Characterization of several HD phenotypes, combined with the establishment of methods to easily detect these disease-relevant phenotypes, in TruHD cells demonstrate their utility as a cellular model and will hopefully facilitate further investigation into pathological mechanisms.

4.6 Discussion

Patient fibroblasts have been used previously by us and others^{91,307,326,327} to study HD cell biology, but currently there are no defined cell lines that are used consistently between projects. After generation of hTERT-immortalized TruHD cells, we focused on defining characteristics of these cells in order to facilitate their use. Our wild type line (TruHD-Q21Q18F), heterozygous HD line (TruHD-Q43Q17M) and homozygous HD line (TruHD-Q50Q40F) were chosen for this study as their CAG repeat lengths were most representative of annotated lengths, but also because they cultured well and the observed phenotypes were consistent throughout the study. A homozygote TruHD-Q50Q40F was chosen, because although a rare clinical example, this line could have utility as both alleles of huntingtin are mutant expanded, and thus can help resolve data in heterozygote lines, where mutant huntingtin phenotypes could be confounded by the presence of the normal allele.

We observed HD phenotypes in both heterozygous TruHD-Q43Q17M and homozygous TruHD-Q50Q40F cells, at clinically relevant CAG repeat lengths. Typical HD cell phenotypes include reduced cell size³⁰³, decreased cell viability upon cellular stress^{73,74,359}, altered cell proliferation³⁰³, decreased ADP/ATP ratio²¹⁶ and hypophosphorylation of huntingtin N17 at serines 13 and 16^{74,82,83}. Here, we have also demonstrated that HD cells showed altered susceptibility to cellular senescence and deficient response to oxidative stress as seen by SC35 nuclear speckle counts. Additionally, TruHD cells can be distinguished in an unbiased manner using non-supervised image texture analysis and principal component analysis via software such as Phenoripper. Phenoripper can be used as a readout for future high-content drug screening assays.

Improvement in inter-experimental and inter-laboratory reproducibility have also been observed and may be beneficial for long-term applications such as generation of stable cell lines and cellular reprogramming to generate patient-specific neurons that maintain age-associated signatures^{226,228,313}. However, as with all cell lines, strict culturing practices are needed to maintain proper cellular function and genomic stability, as critical cellular pathways involving

TP53 should be monitored as they can change over a prolonged period of time, even in immortalized cells, especially over 100 passages^{344,345}.

Recent developments in understanding cell biology throughout the course of HD progression highlight the need for improved methods for disease modelling. DNA damage repair pathways have been implicated as the predominant modifiers of HD pathogenesis¹¹. Previous observations in our lab show that huntingtin can sense oxidative stress and that huntingtin is involved in the DNA damage response⁹¹. These processes require TP53 which an important transcription factor that integrates various cellular stress signals and is widely considered the master regulator of genomic integrity due to its roles in DNA damage sensing, cell cycle checkpoint control and apoptotic regulation (see reviews³⁶⁰⁻³⁶²).

The choice of model system for studying certain aspects of cell biology is therefore critical. Historically, synthetically long CAG repeat alleles of *HTT* have been used in cell models because of the apparent lack of obvious phenotypes of clinical HD alleles in animal models. Cell biology research in HD has been primarily focused on neurons from HD mouse models and easily accessible cell lines, each with their own restrictions and limitations. The main limitation of cells taken from mouse models are the synthetically long polyglutamine tracts used in order to mimic a late-onset human disease within the lifespan of a mouse. In these models, it can be overlooked that the majority of patients have CAG repeats between 40-50, and that these patients have varying age onset that is not attributed to just the number of repeats. Additionally, some models are transgenic, and thus do not have an accurate gene dosage, while others express huntingtin at super-physiological levels, confounding data with incorrect protein stoichiometry, which can be a concern for a scaffolding protein. This is the first characterized human HD immortalized cell line model and can therefore be used to test therapeutic reagents that are designed specifically for human cells and will be a tool for the HD research community.

4.7 Materials and Methods

4.7.1 Cell Culture and Generation of *hTERT*-Immortalized Fibroblasts

Patient fibroblasts were purchased from the Coriell Institute from the NINDS repository. HD patient fibroblasts (ND30013, GM04857) and control patient fibroblasts (ND30014) were obtained. Cells were cultured in Minimum Essential Media (MEM, Gibco #10370) with 15% fetal bovine serum (FBS, Gibco) and 1X GlutaMAX (Gibco #35050). Cells were infected with 1×10^6 TERT Human Lentifect™ Purified Lentiviral Particles (GeneCopoeia, LPP-Q0450-Lv05-200-S). To aid in infection, 10 $\mu\text{g}/\text{mL}$ polybrene was added. After 8 hours, cells were infected again and left for 24 hours. Media was changed and cells were left for an additional 48 hours. Successfully transduced cells were selected in media with 1 $\mu\text{g}/\text{mL}$ puromycin. Cells were grown at 37°C with 5% CO₂.

STHdh cells (a kind gift from Dr. Marcy Macdonald) were cultured in Dulbecco's Modified Eagle Medium (DMEM, Gibco #11995) with 10% FBS. Cells were grown at 33°C with 5% CO₂. RPE1 cells (ATCC) were cultured in 1:1 Dulbecco's Modified Eagle Medium/Nutrient Mixture F-12 (DMEM/F12, Gibco #11330) with 10% FBS and 0.01% hygromycin. Cells were grown at 37°C with 5% CO₂.

4.7.2 Quantitative PCR to Measure *hTERT* mRNA Levels

Primary, TruHD and RPE1 cells were grown to ~85% confluence. Total RNA was obtained from frozen cell pellets lysed in 1 mL of Trizol (Thermo Fisher Scientific) per $\sim 1 \times 10^6$ cells, followed by phenol-chloroform extraction. RNA was treated with DNase I (Thermo Fisher Scientific) and cDNA was prepared using 1000 ng total RNA and SuperScript III Reverse Transcriptase (Thermo Fisher Scientific). Transcript expression was measured using TaqMan Assays with AmpliTaq Gold DNA polymerase (Thermo Fisher Scientific), and *hTERT* (Hs00972650_m1) was compared to *ACTB* (Hs01060665_g1) housekeeping gene using the $\Delta\Delta C_T$ method.

4.7.3 Telomeric Repeat Amplification Protocol

Primary fibroblasts and corresponding TruHD cells were grown to ~85% confluence. A two-step PCR method (TRAPeze® Telomerase Detection Kit S7700, Millipore) was used to evaluate hTERT catalytic activity. Briefly, in the first step, telomerases from lysed cells add telomeric repeats (AG followed by repetitive GGTAG sequences) on the 3' end of a substrate oligonucleotide (TS). In the second step, the extended products are amplified by PCR using a primer specific for the beginning of TS, and a reverse primer specific for the end of the repeats. The lowest amplification product should be 50 bp, and increases by 6 bp-long repeat increments are visualized, on a 10% TBE polyacrylamide gel.

4.7.4 Cryogenic Storage of TruHD Cells

For freezing one vial of TruHD cells, a plate was grown to 90% confluence (~1 x 10⁵/mL) on a 10 cm dish and was split in half. The next day, two ~60% confluent plates, that were still in growth phase, were trypsinized and combined. Cells were centrifuged at 1500 rpm and pellets were resuspended in culture media with 1 mL of 5% DMSO. Vials were put into a slow-freeze unit in the -80°C to ensure optimal cell preservation. After 24-48 hours, vials were moved to a -150°C for long-term storage.

Vials were thawed slowly at 37°C for around 2-5 minutes. Using a 10 mL pipette, the 1 mL of cells were moved directly into a 10 cm plate already pre-incubated with media. After 24 hours, media was changed to remove residual DMSO.

4.7.5 Sizing of CAG Repeat

TruHD cells were grown to ~90% confluence in a 10 cm plate. Cells were scraped and centrifuged at 4°C at 1500 rpm. Genomic DNA was extracted using the PureLink® Genomic DNA kit (ThermoFisher). A fluorescence-based assay was used to size the CAG repeats, based on the originally described assay by Warner et al.³³⁷ and further described in Keum et al.⁵⁹

4.7.6 Karyotyping

Karyotyping was performed by The Centre for Applied Genomics, The Hospital for Sick Children, Toronto, Canada. Karyotype analysis via G-banding was performed on cells from two T25 flasks per cell line. When cells reached 80-90% confluence, Karyomax Colcemid[®] was added to each flask to a final concentration of 0.1 µg/mL (Gibco #15212-012) and incubated in 37°C CO₂ incubator for 1.5-2 hours (for TruHD-Q43Q17M and TruHD-Q50Q40F) and 3-4 hours for TruHD-Q21Q18F. Cells were then collected and suspended in 6 mL of 0.075 M KCl, and incubated at 37°C for 20 minutes. Eight drops of Carnoy's Fixative (methanol/acetic acid, 3:1) was added and mixed together. The cells were centrifuged at 1000 rpm for 10 minutes at room temperature and cell pellets were collected. After three rounds of fixations (add 8 mL fixative and centrifuge at 1000 rpm for 10 minutes), cells were resuspended in 0.5-1 mL of fixative and cells from each suspension were dispensed onto glass slides and baked at 90°C for 1.5 hours. Routine G-banding analysis was then carried out. Approximately 15-20 metaphases per cell line were examined.

4.7.7 Senescence-Associated Beta-Galactosidase Activity Assay

TruHD and primary fibroblasts were seeded into a 6 well plate. Primary fibroblasts reached ~20 passages before analysis and TruHD cells reached ~50 passages. When cells reached ~90% confluency, media was aspirated and cells were washed 1X with PBS and experiments were carried out using Senescence Detection Kit (Abcam, ab65351) manufacturer instructions.

4.7.8 Phenoripper and Cell Surface Area Measurement

Immunofluorescence was performed with Hoechst 33342 (ThermoFisher), beta-tubulin antibody (E7, DSHB, 1:250 dilution in 2% FBS in PBS with 0.02% Tween) and N17-phospho antibody (NEP, see section on antibody validation) were analyzed using Phenoripper. Five images per trial of TruHD fibroblasts acquired on a Nikon TiEclipse

inverted epifluorescent widefield using a 20X objective (NA=0.75) and Spectra X LED lamp (Lumencor) capture using an Orca-Flash 4.0 CMOS camera (Hamamatsu). Cell surface area was calculated with ImageJ. Cells were thresholded to remove background to identify whole-cell region of interest and area of each cell was measured and plotted.

4.7.9 Cell Counting

Cells were seeded into a 24 well plate (10^5 /mL). After 24 hours, nuclei were stained for 15 minutes with NucBlue Live ReadyProbes Reagent (1 drop/mL of media) (ThermoFisher). Cells were imaged using the Nikon TiEclipse inverted widefield epifluorescent microscope, and using an automated round object detector in NIS Elements Advanced Research 4.30.02v software (Nikon), cell nuclei were counted. This was repeated repeat plates that were left for 48 and 72 hours for all cell lines.

4.7.10 ADP/ATP Ratio Assay

ADP/ATP Ratio Assay Kit (Sigma MAK135) was used according to the protocol, except the first step to seed TruHD cells directly into a 96 well plate which the rest of the assay is performed on. If seeded directly into a 96 well plate, there is not enough room to grow the suggested 10^4 fibroblast cells because of their large size. Therefore, TruHD cells were seeded into a 24 well plate, for no more than 48 hours, to ~80% confluency. After reaching confluency, the cells are lysed with the working reagent (provided in the kit). After lysing, cells from the 24 well plate were moved directly into a 96 well plate to continue the rest of the assay according to the protocol. For *STHdb* cells, assay was performed according to the protocol with no changes.

4.7.11 Cell Viability Assay

Cells were seeded into a 96 well plate. After 24 hours, cells were stained for 15 minutes with NucBlue Live ReadyProbes Reagent (1 drop/mL of media) (ThermoFisher) in Hank's

Balanced Salt Solution (HBSS) (Gibco). Cells were washed with once with HBSS and treated with 100 μ L of potassium Bromate (KBrO₃) (Millipore) at concentrations of 0, 1, 10, 100 and 200 mM in HBSS with NucGreen Dead 488 ReadyProbes Reagent (1 drop/mL of media) (ThermoFisher).

The 96 well plate was imaged immediately over the course of 24 hours every 20 minutes at 37°C using a Nikon TiEclipse inverted A1 confocal microscope equipped with a 20X objective (NA= 0.75) and driven by NIS Elements AR 4.30.02v 64-bit acquisition software (Nikon). Cells were imaged simultaneously in the FITC (NucGreen) and DAPI (NucBlue) channels. A cell was defined as undergoing cell death when 50% or more of the nucleus, as defined by NucBlue-positive pixels, was overlapped by NucGreen-positive pixels. Cell death was multiplied by 100% and subtracted from 100 to calculate % Viability. Images were analyzed using Python.

4.7.12 Immunoblotting

TruHD cells were grown to ~90% confluence. Cells were scraped and centrifuged at 4°C at 1500 rpm. Cell pellets were lysed in radioimmunoprecipitation assay (RIPA) buffer with 10% phosphatase (Roche) and 10% protease inhibitors (Roche) for 12 minutes on ice and centrifuged at 10 000 x g at 4°C for 12 minutes. Supernatant was collected and 40 μ g of protein was loaded into a pre-cast 4-20% polyacrylamide gradient gel (Biorad). Proteins were separated by SDS-PAGE and electroblotted onto 0.45 μ m poly-vinyl difluoride (PVDF) membrane (EMD Millipore).

Blots were blocked with 5% non-fat dry milk in TBS-T (50 mM Tris-HCl, pH 7.5, 150 mM NaCl, 0.1% Tween-20) for 1 hour at room temperature. Blots were cut horizontally at 75kDa marker to probe for huntingtin (~350kDa) or GAPDH (loading control, ~37kDa) separately. Blots were then incubated with primary N17-phospho antibody (1:1250), EPR5526 (1:2500, Abcam ab106115), mAb2166 (1:2500, Millipore) or GAPDH (1:10 000, Abcam ab8425) overnight at 4°C. Blots were washed 3 times for 10 minutes with TBS-T and then incubated with anti-rabbit or anti-mouse HRP secondary (1:50 000, Abcam) for 45

minutes at room temperature. Finally, blots were washed 3 times for 10 minutes with TBS-T and visualized with enhanced chemiluminescent HRP substrate (EMD Millipore) on a MicroChemi system (DNR Bio-imaging Systems). Huntingtin bands were quantified using NIH ImageJ and normalized to the GAPDH loading control.

4.7.13 Flow Cytometry

TruHD cells were grown to ~90% confluence. Cells were scraped and centrifuged at 4°C at 1500 rpm. Cells (~10⁶) were resuspended and fixed in ice-cold methanol for 12 minutes, inverting every 4 minutes. Cells were centrifuged at 4°C at 10 000 x g for 5 minutes followed by 2 washes in flow buffer (PBS with 2.5 mM EDTA and 0.5% BSA), and blocked in flow buffer with 2% FBS for 1 hour at room temperature. Cells were incubated overnight in AlexaFluor488-conjugated N17-phospho antibody, diluted 1:15 in flow buffer with 0.02% Tween-20, rotating at 4°C. Cells were washed twice and resuspended in flow buffer.

4.7.14 3NP Treatment and Nuclear Speckle Count

TruHD cells were treated with 0.1 mM 3-nitropropionic acid (3NP) for 1 hour at 37°C, then fixed and permeabilized with ice-cold methanol for 12 min. Cells were washed in PBS and blocked in antibody solution (2% FBS, 0.1% (v/v) Triton X-100 in 1X TBS) at room temperature for 10 minutes. AlexaFluor488-conjugated N17-phospho antibody was diluted 1:15 in antibody solution and incubated overnight at 4°C. Cells were washed in PBS and stained with Hoechst 33342 dye for 12 minutes at room temperature and left in PBS prior to imaging.

Cells were imaged using Nikon TiEclipse inverted widefield epifluorescent microscope using a Plan Apo 60X (NA=1.4) oil objective and Spectra X LED lamp (Lumencor) captured on an Orca-Flash 4.0 CMOS camera (Hamamatsu). A z-stack was obtained for each image and displayed as a maximum projection prior to image analysis. Image acquisition was completed using the NIS-Elements Advanced Research 4.30.02v 64-bit acquisition software (Nikon).

Nuclear speckles were quantified in over 200 cells over 3 trials using an open source speckle counting pipeline in CellProfiler (www.cellprofiler.org).

4.7.15 Dot Blot Assay for Antibody Validation

Varying concentrations (from 25-1000 ng) of different synthetic N17 peptides (N17, N17S13p, N17S16p, and N17S13pS16p) were spotted onto a nitrocellulose membrane (Pall Life Sciences) and allowed to dry at room temperature for 45 minutes. Immunoblotting was carried out as described earlier.

4.7.16 Immunofluorescence Peptide Competition Assay for Antibody Validation

The N17-phospho antibody (1:250) was incubated, with rotation, with 1000 ng of synthetic N17 peptides (N17, N17S13p, N17S16p, N17S13pS16p, and a control peptide – p53 (371-393); New England Peptides) at room temperature for 1 hour prior to overnight incubation with RPE1 cells fixed with methanol. Cells were washed 3 times with 2% FBS in PBS and then incubated in anti-rabbit AlexaFluor488 secondary antibody (1:500, Molecular Probes) for 45 minutes at room temperature and then washed and left in PBS before imaging using a Nikon TiEclipse inverted epifluorescent microscope.

4.7.17 Huntingtin siRNA Knockdown for Antibody Validation

Endogenous huntingtin knockdown was established with huntingtin siRNA (Santa Cruz, sc35617) in RPE1 cells. siRNA was transfected using Lipofectamine RNAiMax (Invitrogen) according to manufacturer instructions. Control dishes were transfected with scrambled siRNA. Protein was extracted using as described earlier, and 60 µg protein was loaded. Immunoblotting was carried out as described earlier.

4.7.18 Statistics

Data with a normal distribution were analyzed by unpaired t-test unless otherwise stated. Error bars represent standard error of the mean (S.E.M.).

4.7.19 Data Availability

The raw datasets generated and analyzed for this study are available from the corresponding author on reasonable request.

4.8 Figures

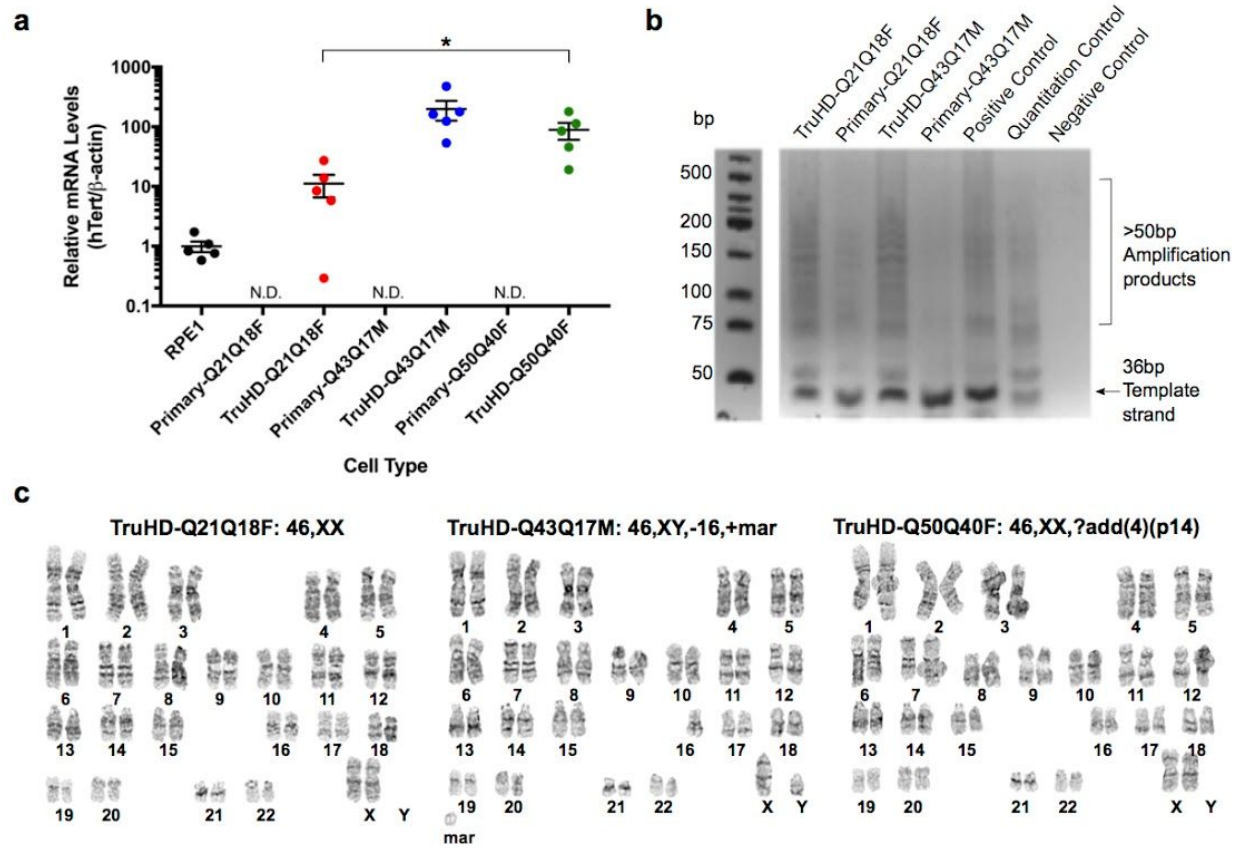


Figure 4.1 Generation of TruHD immortalized cell lines. (A) hTERT mRNA levels normalized to beta-actin (β -actin) mRNA levels in RPE1 cells (positive control), primary cells and TruHD cells. hTERT levels in primary cells were not detectable (N.D.). n=5. Error bars represent S.E.M. *p=0.0369 comparing TruHD-Q21Q18F, TruHD-Q43Q17M and TruHD-Q50Q40F by one-way ANOVA. (B) Telomeric repeat amplification product (TRAP) assay. Amplification products run on 10% TBE gel after telomere extension reaction, showing telomeric repeats >50 bp in increments of 6 bp. Template strand is 36 bp. Negative control contains no Taq polymerase or template strand. (C) Representative karyotypes of TruHD-Q21Q18F, TruHD-Q43Q17M and TruHD-Q50Q40F cells. “mar” denotes marker chromosomes, “+” are additional chromosomes and “?add(4)(p14)” denotes additional patterns observed on chromosome 4 at band p14. Results from full karyotype shown in Table 2.

Contributions: (A) C.H. collected cell lysates and T.L. performed qPCR. C.H. performed (B). (C) C.H. cultured cells and karyotypic analysis was performed at the TCAG Facility by Raymond Wong at SickKids

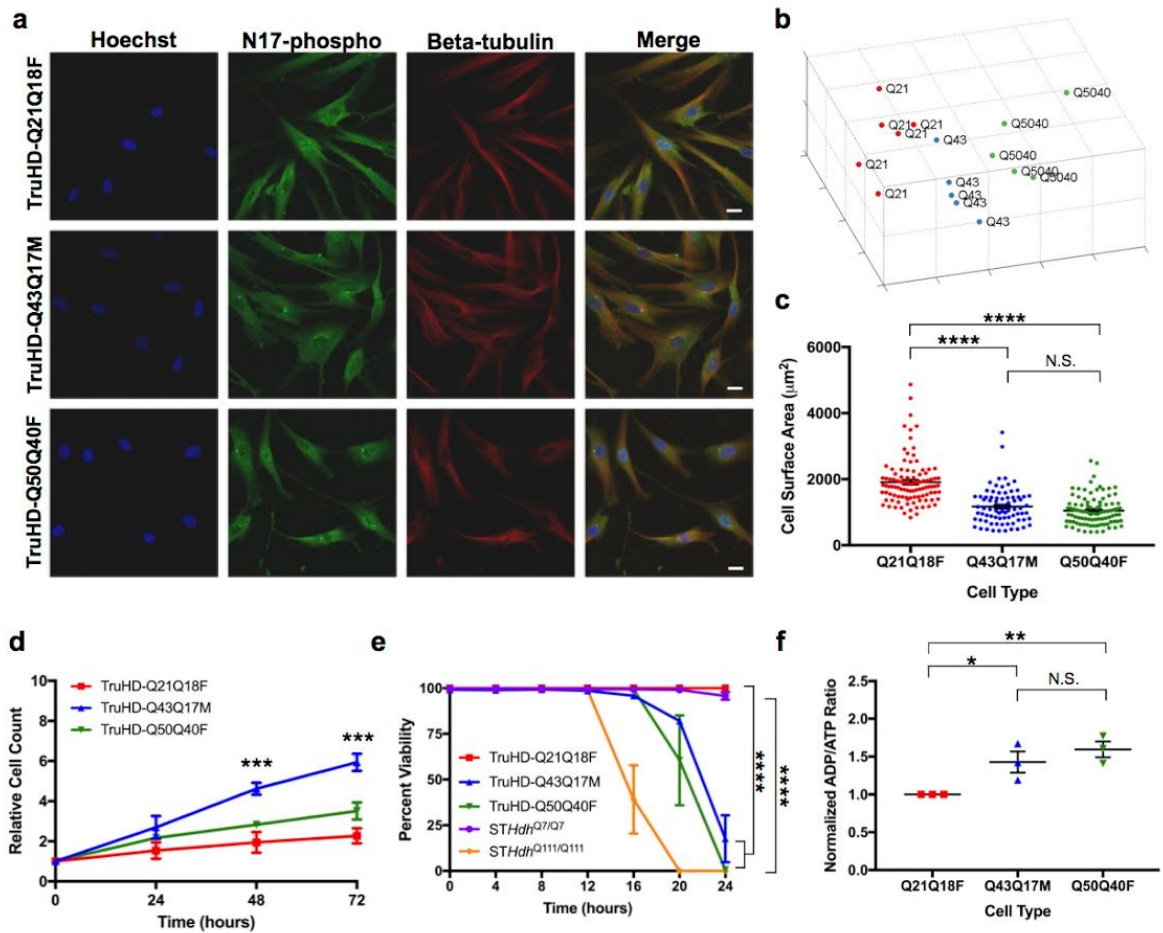


Figure 4.2 TruHD cell properties. (A) Immunofluorescence images of TruHD-Q21Q18F, TruHD-Q43Q17M and TruHD-Q50Q40F. Scale bar = 10 μ m. (B) PCA plot of images sorted with Phenoripper. (C) Cell surface area comparison in TruHD cells. n=3, N>200. Error bars represent S.E.M. *p <0.0001. (D) Relative cell count measured every 24 hours. n=3, N>200. Error bars represent S.E.M. ***p=0.0003 at 48 hours, ***p=0.0001 at 72 hours by one-way ANOVA. (E) Percent cell viability of TruHD cells compared to *STHdb* cells. n=3, N>200. Error bars represent S.E.M. At 24 hours, ****p<0.0001 for *STHdb*^{Q7/Q7} vs *STHdb*^{Q111/Q111} by two-ANOVA and ****p<0.0001 for TruHD-Q21Q18F vs TruHD-Q43Q17M and TruHD-Q50Q40F by two-way ANOVA. (F) Normalized ADP/ATP ratio in TruHD cells at ~75% confluency 24 hours after seeding. n=3, N>200. Error bars represent S.E.M. *p=0.0371 and **p=0.0048.

Contributions: C.H. performed (A), (B),(C) and (F). R.G. performed (D) and (E)

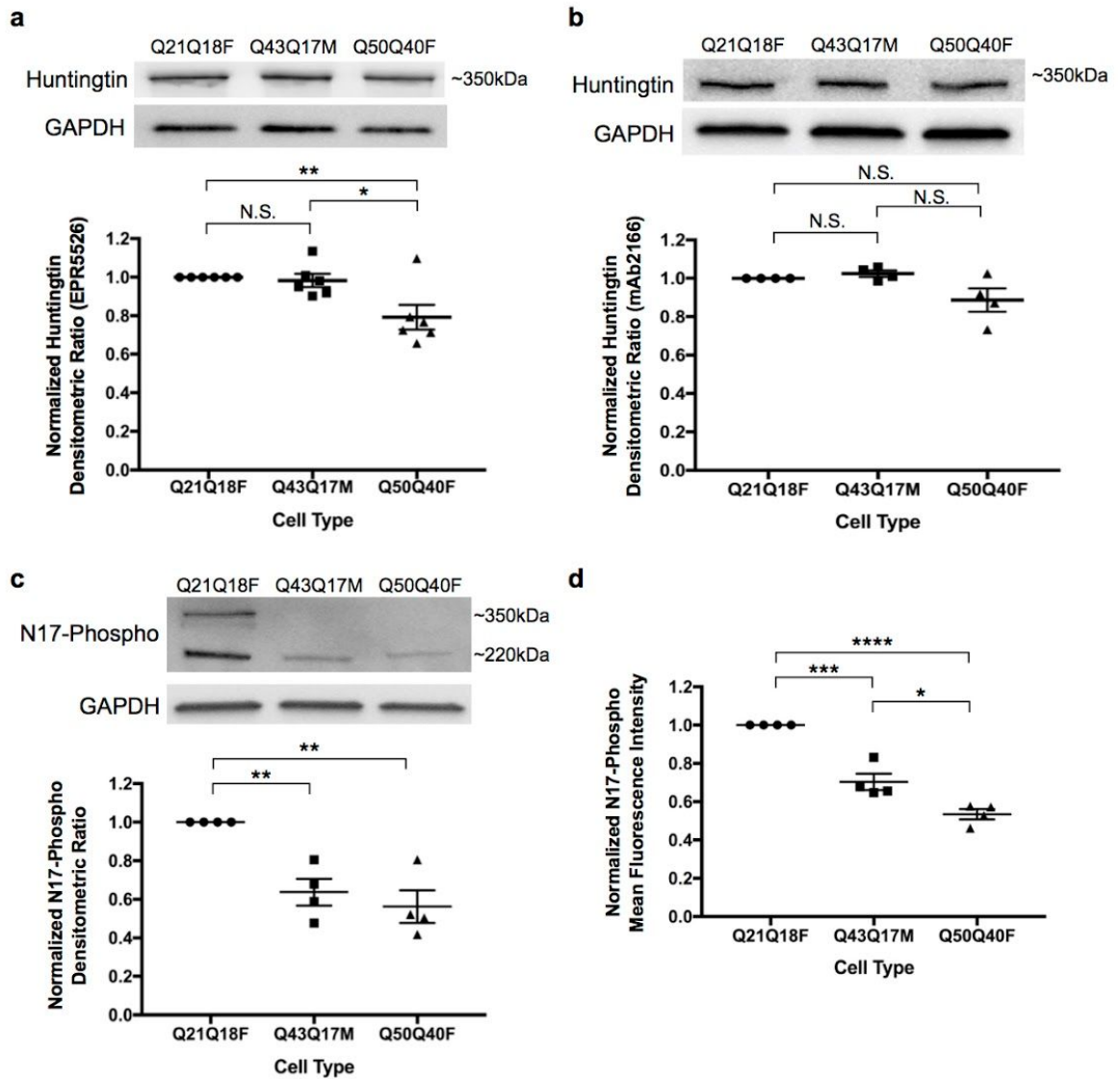


Figure 4.3 Huntingtin protein levels in TruHD cells. (A) Densitometric analysis of total huntingtin levels using western blot with EPR5526 antibody. Normalized to control TruHD-Q21Q18F cells. n=6. Error bars represent S.E.M. **p=0.0087 and *p=0.0254 by unpaired t-test. (B) Densitometric analysis of total huntingtin levels using western blot with mAb2166 antibody. Normalized to control TruHD-Q21Q18F cells. n=4. Error bars represent S.E.M. (C) Densitometric analysis of N17-phospho levels using western blot. Normalized to control TruHD-Q21Q18F cells. n=4. Error bars represent S.E.M. **p=0.0020 by unpaired t-test. (D) Mean fluorescence intensity analysis of N17-phospho using flow cytometry. Normalized to control TruHD-Q21Q18F. n=4. Error bars represent S.E.M. ***p=0.0005, *p=0.0159 and ****p<0.0001 by unpaired t-test.

Contributions: C.H. performed all experiments

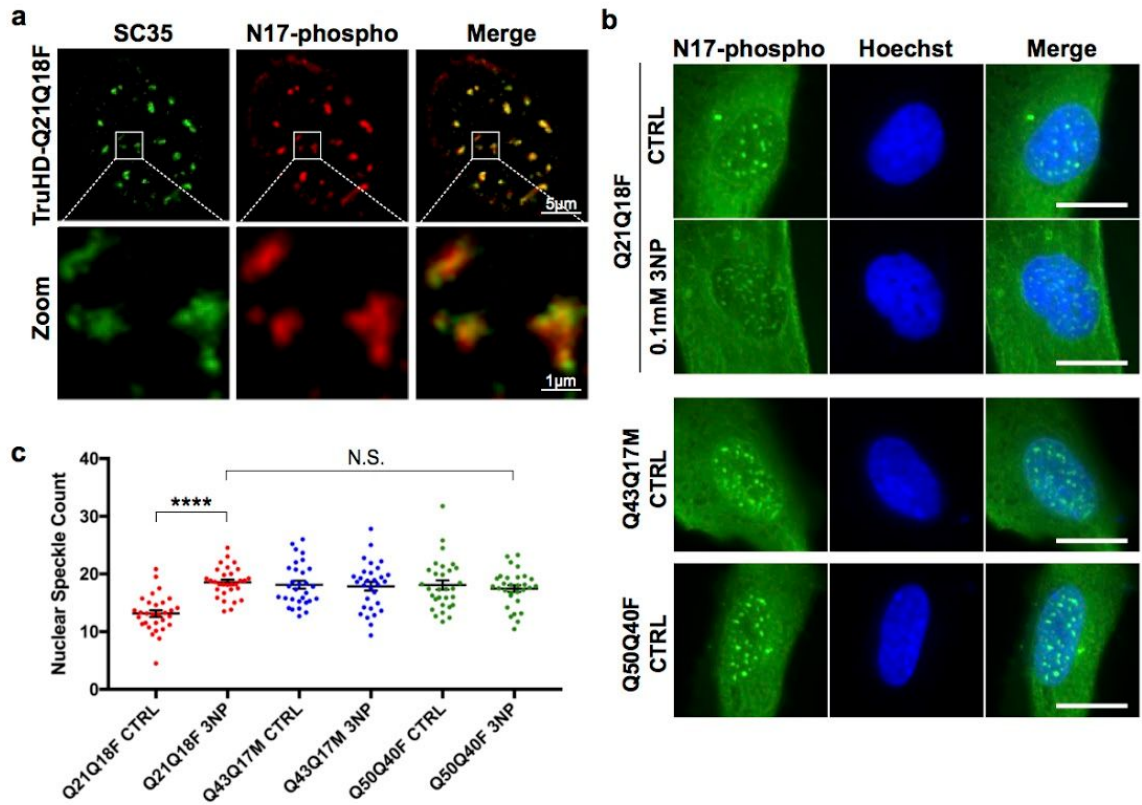


Figure 4.4 Huntingtin localizes to nuclear speckles in response to stress. (A)

N17-phospho localizes to SC35+ nuclear speckles. (B) Nuclear speckles are increased in

TruHD-Q21Q18F control cells upon treatment with 0.1mM 3NP, but not for

TruHD-Q43Q17M or TruHD-Q50Q40F. Scale bar = 10 μ m. (C) Quantification of nuclear

speckles. n=3, N=180. Error bars represent S.E.M. ****p<0.0001 by unpaired t-test.

Comparison of TruHD-Q21Q18F 3NP, TruHD-Q43Q17M CTRL, TruHD-Q43Q17M 3NP, TruHD-Q50Q40F CTRL and TruHD-Q50Q40F 3NP by one-way ANOVA shows no significant difference (p=0.8475).

Contributions: T.M. performed (A). S.S. performed (B) and (C)

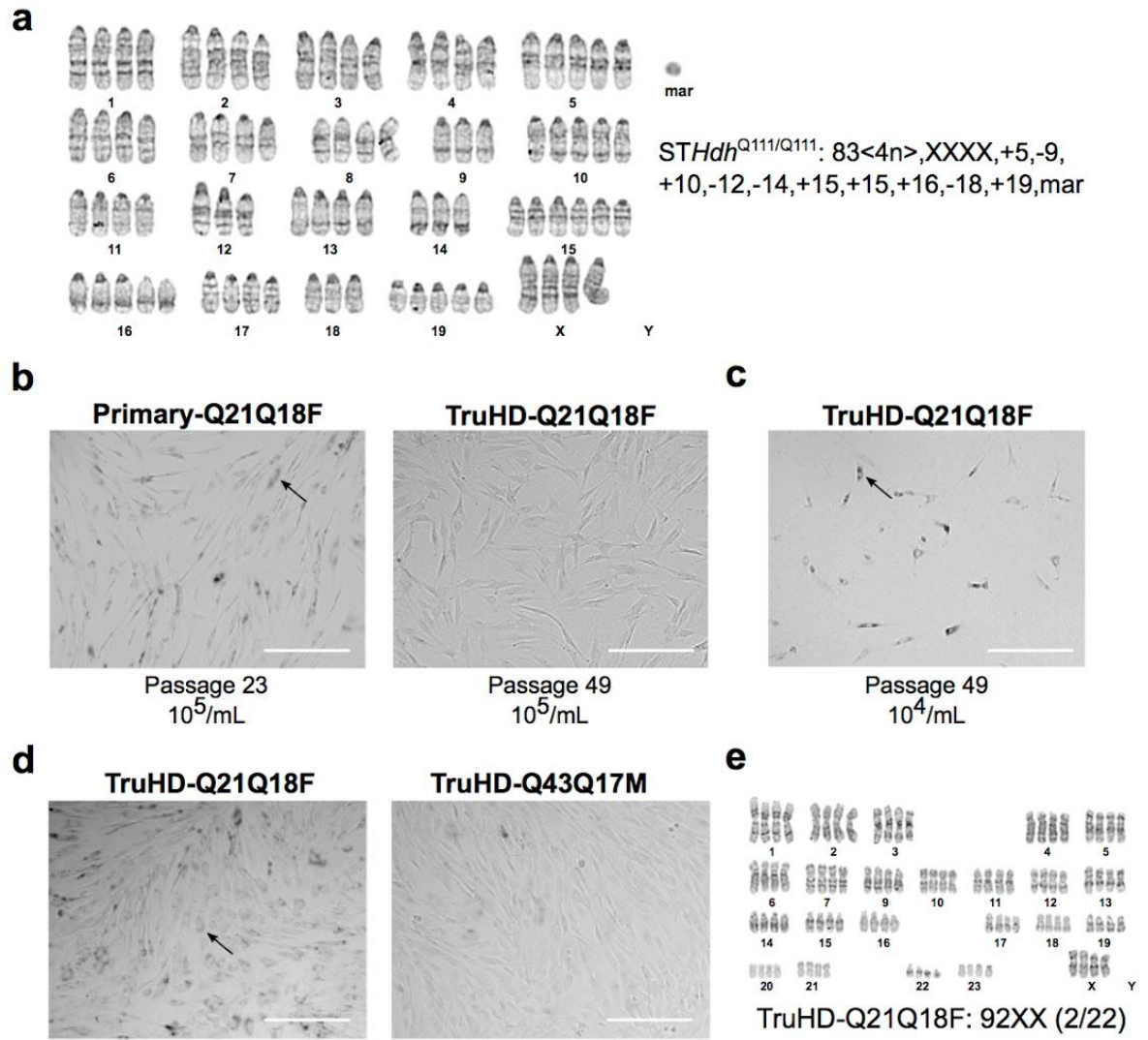


Figure S4.1 TruHD cell line senescence. (A) *STHdb*^{Q111/Q111} example karyotype. “mar” denotes marker chromosomes, “+” are additional chromosomes and “-” are missing chromosomes. (B) Senescence-activated beta-galactosidase assay comparing primary-Q21Q18F and TruHD-Q21Q18F cells at ~80% confluency. Senescent cells present blue colour pseudocoloured in greyscale and indicated by black arrow. Scale bar =250µm. (C) TruHD-Q21Q18F plated at lower density (<40% confluency) showed presence of blue colour pseudocoloured in greyscale and indicated by black arrow. Scale bar =250µm. (D) TruHD-Q21Q18F cells at high density that were left to overgrow (100% confluency) showed presence of blue colour pseudocoloured in greyscale and indicated by black arrow, but not as much in TruHD-Q43Q17M. Scale bar =250µm. (E) TruHD-Q21Q18F karyotype of senescent cells showing tetraploidy in 2 of 22 cells analyzed.

Contributions: C.H. performed all experiments, but (A) and (E) were analyzed at the TCAG Facility by Raymond Wong at SickKids

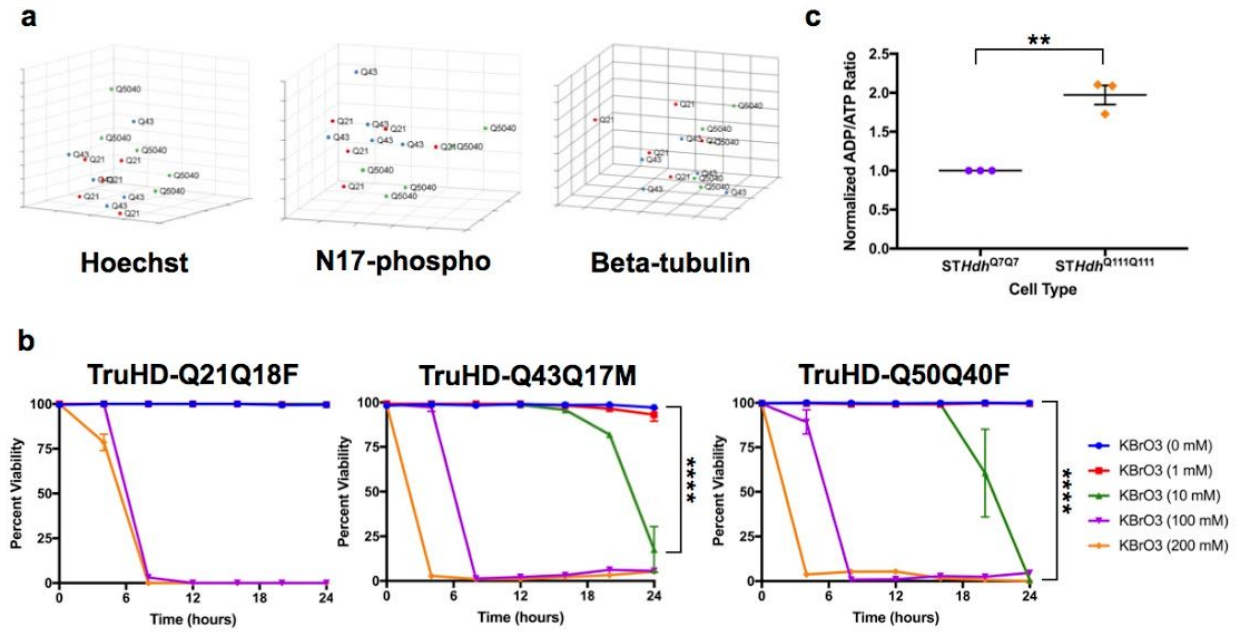


Figure S4.2 TruHD cell properties. (A) Individual PCA plots from Phenoripper comparing images of TruHD cell lines using only Hoechst (405nm), N17-phospho (488nm) and beta-tubulin (640nm) channels. (B) Dose response curves of TruHD cell lines to KBrO_3 . $n=3$, $N>200$. Error bars represent S.E.M. At 24 hours, $***p<0.0001$ between 0mM and 10mM treatments in TruHD-Q43Q17M and TruHD-Q50Q40F cells by two-way ANOVA. (C) Normalized ADP/ATP ratio in *STHdb* cells at ~75 percent confluency 24 hours after seeding. $n=3$. Error bars represent S.E.M. $**p=0.0014$.

Contributions: C.H. performed (A) and (C). R.G. performed (B)

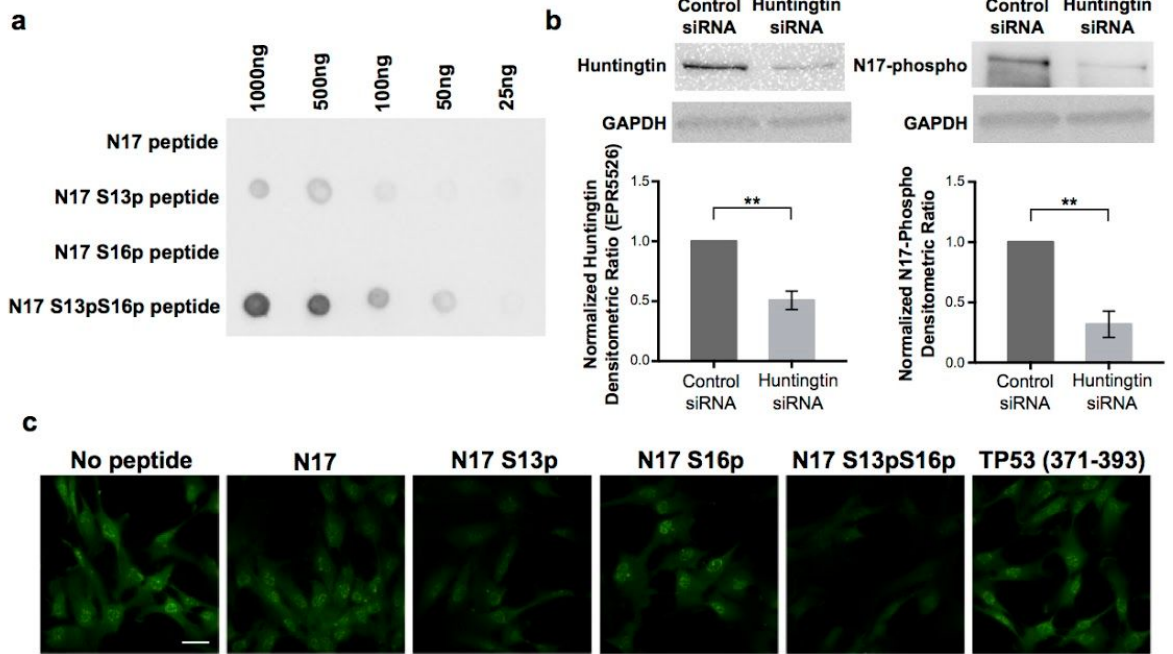


Figure S4.3 N17-phospho antibody validation. (A) Dot blot with N17 peptides. Unphosphorylated (N17), phosphorylated on serine 13 only (N17 S13p), phosphorylated on serine 16 only (N17 S16p) and phosphorylated on both serines 13 and 16 (N17 S13pS16p). (B) Huntingtin knock-down showing N17-phospho antibody specificity compared to the commercially available total huntingtin antibody EPR5526. ** $p=0.0035$ for N17-phospho and ** $p=0.0031$ for EPR5526. (C) Peptide competition assay with N17 peptides and non-specific TP53 peptide. Scale bar = $20\mu\text{m}$.

Contributions: L.B.. performed all experiments

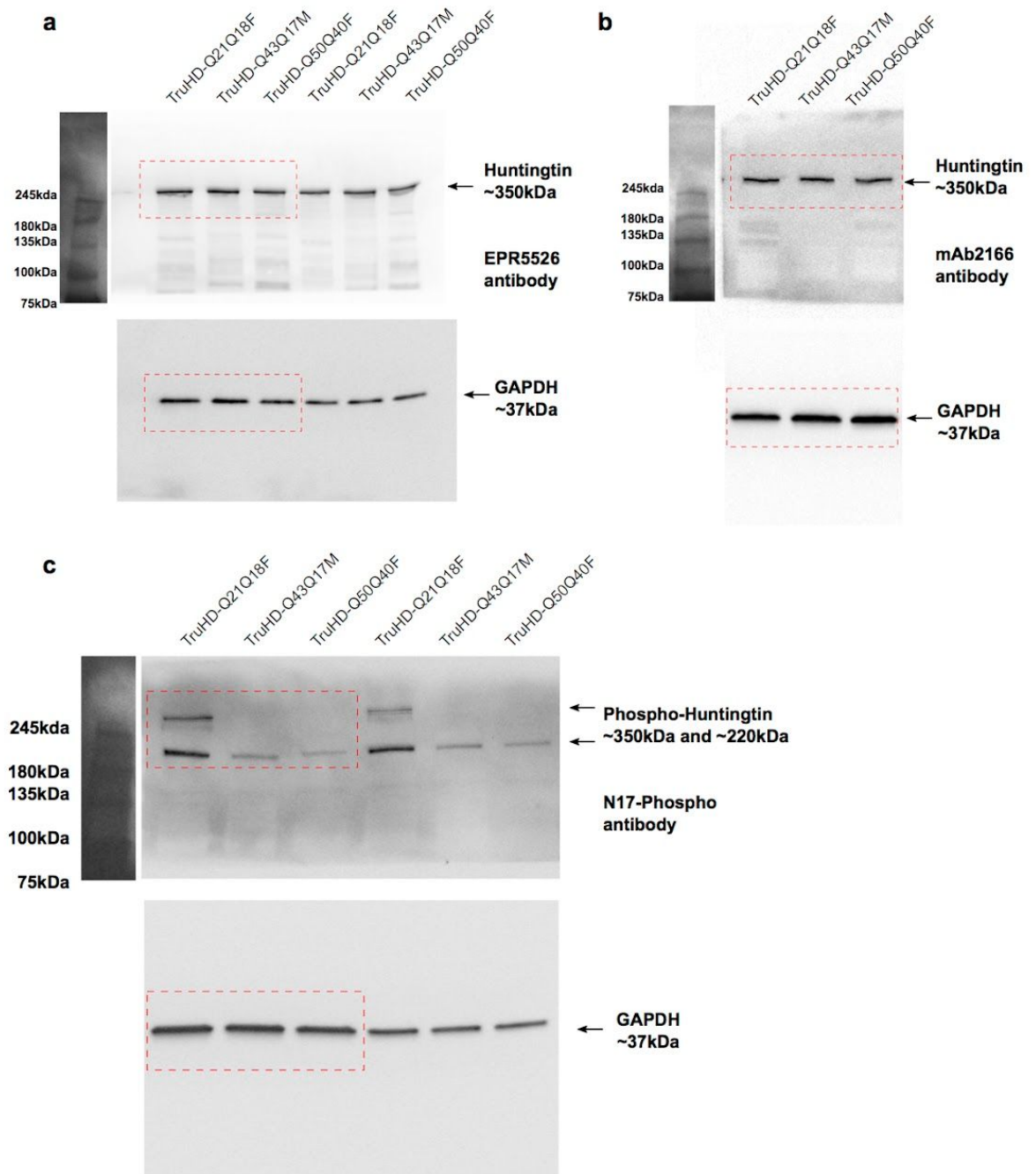


Figure S4.4 Full huntingtin immunoblots from Figure 3. (A) Huntingtin immunoblot with EPR5526 antibody. Samples were loaded in duplicate. Gel was cut horizontally at 75 kDa marker and blots were probed with EPR5526 or GAPDH antibody. Red, dashed-boxes denotes cropped region used for main figure. (B) Huntingtin immunoblot with mAb2166 antibody. Gel was cut horizontally at 75 kDa marker and blots were probed with mAb2166 or GAPDH antibody. Red, dashed-boxes denotes cropped region used for main figure. (C) Phospho-huntingtin immunoblot with N17-Phospho antibody. Samples were loaded in duplicate. Gel was cut horizontally at 75 kDa marker and blots were probed with EPR5526 or GAPDH antibody. Two main bands were visible (at ~350 kDa and ~220 kDa). Red, dashed-box denotes cropped region used for main figure.

Contributions: C.H. performed all experiments

4.9 Tables

Table 4.9.1: *TruHD Patient Fibroblast Information*

Primary Cell Name	Cell Line Name	Allele 1	Allele 2	Sex	Age at Sampling	Disease Onset Age
ND30013	TruHD-Q43Q17M	43 CAG	17 CAG	Male	54	50
ND30014	TruHD-Q21Q18F	21 CAG	18 CAG	Female	52	-
GM04857	TruHD-Q50Q40F	50 CAG	40 CAG	Female	23	28

Table 4.9.2: *G-band Karyotyping*

[] = number of analyzed cells with specified karyotype

Cell Line	Karyotype (bold = representative result)
TruHD-Q21Q18F	46,XX[13] , 92,XXXX[2]
TruHD-Q43Q17M	46,XY,-16,+mar[9] , 47,XY,+7[3], 46,XY[3]
TruHD-Q50Q40F	46,XX,?add(4)(p14)[9]
<i>STHdb</i> ^{Q111/Q111}	70-82<4n>, XX or XXX or XXXX, -X[12], -X[4],add(X)(F1)[2],-1[9],add(1)(F)[3],del(1)(?G)[3],+2[2],-2[7],-4[7],?add(4)(C4)[3],dic(4;?)(?D;?)[2],+5[3],-6[8],-7[19],-7[5],+8[4],-8[4],rob(8;8)(A1;A1)[2],-9[12]+11[4],-11[3],-12[19],-12[6],-13[6],-14[15],-14[6],+15[18],+15[15],+15[4],-17[11],-17[3],-18[15],-18[3],+19[17],+1-15mar[20][cp20]

Table 4.9.3: *Sizing of CAG Repeats in TruHD Fibroblasts*

Cell Line Name	CAGn Repeats	Q lengths (= CAG +2, based on genetic structure of CAGnCAACAG in humans)
TruHD-Q21Q18F	21 CAG/18 CAG	23Q/20Q
TruHD-Q43Q17M	43 CAG/17 CAG	45Q/19Q
TruHD-Q50Q40F	50 CAG/40 CAG	52Q/42Q

CHAPTER 5: FURTHER EXPLORATION OF HUNTINGTIN FUNCTION IN TRUHD CELLS

5.1 Introduction

There are various mechanisms that are involved in neurodegeneration in HD, such as excitotoxicity, mitochondrial dysfunction, oxidative stress, metabolic dysfunction and altered apoptosis and autophagy. The likely cause of striatal degeneration in late stages of life is the accumulative effects of these pathogenic mechanisms. The effect of expanded huntingtin has been studied outside of the brain. These pathogenic mechanisms are generally still observed in dividing cells, however, except for those specific to neurons, such as excitotoxicity. After generation of these cells, we wanted to explore some of new phenotypes we identified, as well as analyzing how these fit into pathways we already know that huntingtin is involved in.

An interesting phenotype observed in the TruHD cell lines was the resistance to senescence seen in HD cells described in Thesis Chapter 4, Figure S4.1. Cellular senescence is regulated by cell cycle checkpoints^{338,342,363} and results in cell cycle exit. Aberrant checkpoint regulation in HD cells could explain resistance to senescence. This observation is consistent with the observations in Figure 4.2 regarding differences in cell proliferation, since HD cells proliferate much faster than wild-type cells. DNA damage is checked for at the G1/S checkpoint, where repair mechanisms will correct the damage prior to re-entry. Defects in DNA damage repair seen in HD could therefore be a consequence of faulty checkpoint regulation, consistent with observations showing a role of huntingtin in the DNA damage response⁹¹. These observations are also consistent with proteomic studies showing huntingtin interaction with several cell cycle proteins^{364,365}. The final chapter of my thesis will be to explore those observations and focus on using TruHD cells to look at phenotypes that would be ideally modelled in non-transformed cells. The major caveat of the current unpublished data in the lab is that the majority of the experiments were performed in *STHdb*^{Q7/Q7}, *STHdb*^{Q111/Q111} or HeLa cells.

5.2 Direct Re-Programming of TruHD Fibroblasts to Post-Mitotic Neurons

There has always been a question of why we are using dividing cells when HD primarily affects neurons. The most relevant cell lines to studying HD cell biology would be neurons from human patients. Unfortunately, obtaining neurons from HD patients is not currently feasible. After generation and characterization of the TruHD cell lines, we wanted to explore the ability to differentiate human neurons from the patient fibroblasts. Efforts have been made to generate neurons from patient fibroblasts through induced pluripotent stem cells²²⁴. The process of culturing iPSCs are not as trivial as culturing cell lines are³⁶⁶, so their use in the HD community is not as common. There has also been evidence that upon generation of iPSCs, the epigenome is reset which is not ideal for a late-onset disease³⁶⁷. Methods have been published to directly convert fibroblasts to neurons^{225,227,314,368}. One group published direct conversion of Alzheimer's patient fibroblasts to neurons using a cocktail of small molecule compounds²²⁵ (Figure 5.1A).

Neurons are positive for microtubule-associated protein 2 (MAP2), a protein important in stabilizing the neuronal cytoskeleton. Immunofluorescence was performed and a few MAP2 positive cells were visible for TruHD-Q43Q17M (Figure 5.1B). However, they did not look too healthy. The cells tend to die somewhere in the maturation stage (Figure 5.1C). If they survived to the neuron maintenance stage, they did not look healthy. I performed the same immunofluorescence experiment with non-converted fibroblasts and there was little to no MAP2 signal noticed (data not shown).

An alternative method was published that used microRNAs, directly converting primary fibroblasts from HD patients to medium spiny neurons, the primary type of neuron that is affected in HD^{226,228}. In collaboration with Dr. Andrew Yoo, we tried the protocol with the TruHD cells. One caveat that Dr. Yoo's group encountered was that primary fibroblasts sometimes senesce prematurely during the conversion process, so the immortalized TruHD cell lines could be beneficial to the process. However, the conversion efficiency was very low and the cells were not healthy.

Reprogramming was attempted in TruHD-Q21Q18F, TruHD-Q43Q17M and TruHD-Q57Q17 cells, as well as their control, wild-type hTERT-immortalized line (WT-hTERT). TruHD-Q57Q17 cells were later removed from our studies because they were difficult to culture, but provided additional information for this experiment. There were live cells for TruHD-Q43Q17M and TruHD-Q57Q17 as reported with calcein staining (Figure 5.1D), but there were fewer healthy cells than their WT-hTERT line and they did not survive further neuronal maintenance culturing conditions. In their protocol, they preferred to use cells that were extracted after disease onset in order to generate cells that were most reflective of diseased neurons. Considering our wildtype line (TruHD-Q21Q18F) was unable to be reprogrammed, it is possible that cells from different patients may be better or worse for reprogramming. We intend to repeat the workflow for generation of TruHD cell lines with cells from patients that we have the full clinical information for, potentially finding cells that are more amenable to the reprogramming process as disease manifestation age may be important.

5.3 Observing the Effects of Huntingtin Knockdown in TruHD Cells Using Small Molecule Compounds

Cells that do not have any huntingtin are not viable^{121,369,370}. Huntingtin protein levels can be lowered using RNA interference (i.e. siRNA), but the effects are transient and not very efficient. Knockout lines have been generated, but still have low levels of detectable huntingtin. Immunoblot, PCR, and immunofluorescence analysis of HEK 293 KO lines were inconclusive in determining full knockout of huntingtin (Figure 5.2). There was no obvious difference in cell morphology (Figure 5.2A). By PCR, there was no detectable huntingtin present (Figure 5.2B). By western blot, huntingtin protein could be slightly detected with the EPR5526 anti-huntingtin antibody, but not our validated anti-N17 antibodies (Figure 5.2C). By primary and secondary immunofluorescence, HEK and HEK KO lines did not look any

different (Figure 5.2D). HEK 293 cells are known to have abnormal karyotypes³³⁵, possibly contributing to a low level expression if there are many copies of each chromosome.

Besides using anti-sense oligonucleotides (ASO) for lowering huntingtin levels, PTC Therapeutics have developed small molecule compounds to also indiscriminately lower huntingtin levels, which we can use in the lab to confirm several hypotheses about huntingtin function, as opposed to RNAi approaches which are very inconsistent. We were blinded to the identities and effects of 6 compounds (labelled as #38-#43). Experiments were performed with the intention to identify one of the compounds that were able to knockdown huntingtin and then perform future experiments with this compound, therefore some of the experiments were n=1.

I initially wanted to see if mutant protein and wild-type protein levels were different in heterozygous TruHD-Q43Q17M cells by immunoblotting with EPR5526 (Figure 5.3A). There was a small, but significantly higher amount of normal huntingtin (Q17) compared to the mutant (Q43). I chose to perform the rest of the experiments in TruHD-Q50Q40F, as I did not want the extra variable of having both mutant and wild-type protein.

TruHD-Q50Q40F were treated with each compound at 50nM for 48 hours (Figure 5.4C,D). Immunoblotting with EPR5526 huntingtin antibody showed that compounds #39 and #42 were able to knockdown huntingtin. Further experiments was performed with compound #39, showing dose-dependent knockdown of huntingtin after 48 hours (Figure 5.4F,G). There were not obvious differences in cellular morphology or confluency in cells treated with 50nM or 1000nM at 20 hours or 45 hours (Figure 5.4E). To address if constant dosing could result in knockdown lower than 25%, the cells were treated with the compound every 24 hours, but huntingtin levels seemed to increase (Figure 5.4H, I). Since the timepoint used for the other experiments was 48 hours, changing the media every 24 hours with new compound could possibly be affecting the compound's effect on huntingtin. As the compound identities were hidden from us, further experimentation is required in order to draw any conclusions.

5.4 The Role of Huntingtin in Cell Cycle Regulation

5.4.1 Evidence from Previous Work in the Lab

Immunofluorescence performed with various huntingtin antibodies shows that phosphorylated huntingtin at serines 13 and 16 (N17-phospho) is differentially localized from that of unphosphorylated huntingtin. This has been demonstrated by several previous members of the lab, including Dr. Randy Atwal⁷⁴, Dr. Nicholas Caron³⁷¹, Dr. Tam Maiuri⁷⁸, Tanya Woloshansky^{78,372}, Shreya Patel³⁷³ and Glenn Walpole (unpublished undergraduate senior thesis). N17-phospho has been observed at centrosomes, mitotic spindles, mid-bodies, primary cilia and other cytoskeletal elements in *STHdh* cells, HeLa cells, RPE1 cells, and primary fibroblasts. Additionally, increased N17-phospho levels correlate with the onset of mitosis (Patel, unpublished)³⁷³, suggesting the involvement of huntingtin in regulation of the cell cycle. One of the major problems during Shreya's thesis was the inability to properly synchronize the cell cycle in the *STHdh* cells, especially in the HD *STHdh*^{Q111/Q111} cells, leading to the hypothesis that HD cells have aberrant cell cycle checkpoints. Since huntingtin interacts (directly or indirectly) with several proteins that are involved in cell cycle regulation¹¹⁰, it was hypothesized that mutant, polyglutamine expanded huntingtin had altered functions compared to wild-type huntingtin. This hypothesis is corroborated by observations that HD cells always proliferate faster and have deficient oxidative DNA damage repair compared to normal cells, both potentially due to aberrant cell cycle checkpoint regulation³⁷⁴. The detection of damaged DNA and subsequent repair are coordinated with cell cycle regulators at different checkpoints. Primary cilia, microtubule-based organelles that can sense mechanical and chemical environmental cues, can facilitate transduction of external signals into the cell, which can also regulate cell differentiation and division³⁷⁵⁻³⁷⁷. Hyperciliation and altered ciliary morphologies were seen in HD cells compared to control (Woloshansky, unpublished)³⁷².

Additionally, when I was looking at cell senescence in the TruHD cells, it was evident that the HD cells had an aberrant senescence phenotype. Entry into cellular senescence is also dependent on cell cycle checkpoint regulation³⁷⁸. Normal, adherent cells in culture have been described to become senescent in culture when seeded too thin or too dense because of

“contact inhibition”^{340,341,379}. Essentially, once the cells become too confluent and make contact with nearby cells, they stop dividing and do not grow on top of each other (unlike transformed cell lines). The heterozygote and homozygote HD cells, TruHD-Q43Q17M and TruHD-Q50Q40F respectively, were more resistant to contact inhibition, demonstrated in Figure S4.1 in Thesis Chapter 4.

5.4.2 Cell Cycle Re-Entry of Post-Mitotic Neurons Leads to Apoptosis

But what exactly is the importance of looking at the cell cycle in a brain disease? In addition to neurological symptoms, HD also affects peripheral areas of the body, and the huntingtin protein is necessary for development³⁷⁰. Neurons in the brain are post-mitotic, and are kept in this state by cell cycle regulators that are also critical to dividing cells^{349,380}. However, some neurons are able to exit quiescent state and begin cycling again³⁸¹. Activation of cell machinery is linked to death of terminally differentiated neurons³⁸²⁻³⁸⁵. Neuronal maintenance regularly requires cell cycle activation for DNA-damage-induced neuronal apoptosis. The re-entry of post-mitotic neurons targets the cell for apoptosis, a potential mechanism described for neurodegeneration^{380,386}. In situations where there is DNA damage in post-mitotic neurons, repair may require the cells to re-enter the cell cycle but will return once the damage is repaired. Therefore, huntingtin may be involved in the cell cycle regulation that keeps neurons in a post-mitotic state, and is disrupted in HD cells, leading to abnormal re-entry into the cell cycle and apoptosis.

5.4.3 Aberrant Cell Cycle Checkpoints in HD Cells

In Thesis Chapter 4, cell proliferation was quantified in TruHD cells. We know that HD cells grow faster, but the mechanism is unclear. A previous Masters student, Shreya Patel, suggested that HD cells may have aberrant cell cycle checkpoints because she was unable to synchronize *STHdb*^{Q111Q111} cells in G1/S using a double thymidine block³⁷³. A possible defect in cell cycle checkpoint regulation was also corroborated by data in Thesis Chapter 4 (Figure S4.1) showing a senescence-resistance phenotype in HD fibroblasts, a process highly regulated

by the G1/S checkpoint. We hypothesize that defective cell cycle checkpoint regulation contributes to increase cellular proliferation.

In order to dissect how defective checkpoints can contribute to increased cellular proliferation, live cell imaging of TruHD cell lines was performed using a derivative of the fluorescence ubiquitination cell cycle indicator (FUCCI) system (Premo™ FUCCI Cells, Life Technologies) that exploits the specific presence of two cell cycle-regulated proteins, geminin and Cdt1, during specific phases of the cell cycle. Between the phases, these proteins are targeted for ubiquitination and degradation. Cell cycle progression can therefore be visualized by alternating increases in expression of geminin-GFP (green channel) during S, G2 and M phases, and Cdt1-RFP (red channel) in G1. Both are expressed during G1/S phase transition (merged as yellow)(Figure 5.4A, taken from Premo™ FUCCI reagent manual³⁸⁷). Cells were imaged in an environmentally controlled chamber and images were taken every 10 minutes for 48 hours, analyzing the timing cell cycle progression between wildtype TruHD-Q21Q18F, heterozygous TruHD-Q43Q17M and homozygous TruHD-Q50Q40F cells. Unfortunately, FUCCI systems lack the ability to resolve differences between S, G2 and M, and most of the cells were expressing both geminin-GFP and Cdt1-RFP, presumably transitioning between G1 and S phase (Figure 5.4B).

Variations on the FUCCI system have been used, exploiting proteins that are selectively regulated during cell cycle progression. Temporal resolution can be improved using proliferating cell nuclear antigen (PCNA) fused to a fluorescent protein³⁸⁸. PCNA, in contrast, is not degraded during the cell cycle, but changes its uniform nuclear distribution from uniform to nuclear foci upon entry into S phase. In conjunction with Cdc6, which is nuclear in late G1, cytoplasmic during S and G2, and degraded in mitosis and early G1, more phases of the cell cycle can be distinguished compared to FUCCI systems. Several different phases of the cell cycle were identified in TruHD-Q21Q18F (Figure 5.3C) and TruHD-Q43Q17M cells (Figure 5.4D), but cells will need to be synchronized and then released back into the cell cycle in order to have a more consistent analysis of cell cycle progression in future attempts.

5.4.4 Increased Huntingtin Phosphorylation at Serines 13 and 16 During Mitosis

There is differential localization of phosphorylated huntingtin at serines 13 and 16 (N17-phospho) during cell division to various mitotic structures, such as the centrosome, microtubule spindles and the cleavage furrow in *STHdb* and primary fibroblasts^{74,371}. Additional immunofluorescence was performed in HeLa cells by a previous undergraduate thesis student, Glenn Walpole, that showed that huntingtin localizes to the midbody, a transient structure that appears at the end of cytokinesis right before the cells divide (unpublished data). Immunofluorescence conducted by Dr. Nicholas Caron on *STHdb* cells also showed an increased in N17-phospho intensity during mitosis³⁷¹, corroborated by immunoblotting performed by a previous Masters student, Shreya Patel, showing increased N17-phospho in mitosis.

With a fellow Ph.D candidate in the lab, Laura Bowie, we used flow cytometry to quantify N17-phospho levels in TruHD fibroblasts. We modified the protocol and used the validated N17-phospho antibody from Thesis Chapter 4 by adding a marker for mitotic cells by probing for mitotic phosphoproteins which are upregulated during mitosis^{389,390} (Abcam, ab14581). We isolated populations of relatively low, medium and high levels of mitotic phosphoproteins, since we did not synchronize the cells, and then measured N17-phospho intensity (Figure 5.5A). We saw the highest N17-phospho intensity in the cells with high levels of mitotic phosphoproteins (Figure 5.5B), consistent with Dr. Nicholas Caron and Shreya Patel. A control with an antibody specific for unphosphorylated huntingtin would need to be included to ensure that the increase in intensity was specific to N17-phospho.

5.4.5 Hyperciliation in HD Cells

Huntingtin localizes to diverse types of cilia that are involved in homeostasis, including motile cilia in the trachea and ependymal cells, as well as non-motile sensory cilia in neurons. The non-motile, primary cilia are singular signalling organelles that are found on the surface of most mammalian cells. Primary cilia develop from a basal body that is attached to the plasma

membrane. The basal body is a modified centriole, composed of nine microtubule triplets arranged in a barrel with additional transitional fibres for structural integrity and intraflagellar transport (IFT). Primary cilia are sensory organelles that relay signals from the extracellular environment. These signals are responsible for initiating several pathways including cell migration, differentiation, apoptosis, division, homeostasis, intracellular calcium regulation, neurogenesis and cell polarity. Defects in primary cilia result in rare genetic disorders known as ciliopathies.

There is evidence that HD is a ciliopathy^{376,377,391-393}. Huntingtin is involved in dynactin-mediated transport of pericentriolar material 1 (PCM1) in ciliogenesis. HD mice have abnormally elongated cilia, increased incidence of ciliated cells, have hyperacetylated alpha-tubulin and show aberrant localization of intraflagellar transport proteins IFT57 and IFT88. A previous Masters student in our lab, Tanya Woloshansky, previously described several differences regarding primary cilia in wildtype and HD primary fibroblasts³⁷² as well as differential localization of phosphorylated huntingtin at serines 13 and 16 compared to unphosphorylated huntingtin⁷⁸. Hyperciliation was also quantified in TruHD cells (Figure 5.6) after 24 hours of serum starvation to arrest the cells in G1 and immunofluorescence with acetylated tubulin and ADP ribosylation factor like GTPase 13b (ARL13b) to ensure primary cilia identification.

Primary cilia are post-mitotic structures, assembled in the G0 or G1 phases of the cell cycle and resorbed upon re-entry into the cell cycle³⁹⁴⁻³⁹⁶. There is increasing evidence of crosstalk between the DNA damage response and ciliogenesis, which are both stress response mechanisms that are tightly regulated with the cell cycle. Several proteins involved in DNA damage repair are found at the centrosome^{397,398}, and ciliogenesis-associated proteins, such as Cep164, can participate in DNA damage responses³⁹⁸⁻⁴⁰⁰. The role of primary cilia in dividing cells is likely to help maintain cellular integrity, allowing for cell cycle re-entry after the G1/S checkpoint after DNA damage responses, adding further context into the evidence showing HD as a ciliopathy.

5.5 Discussion and Future Directions

5.5.1 Discussion

Since huntingtin has a role in DNA damage repair and is implicated in ciliogenesis/cilia resorption and cell cycle regulation, there is an interesting possibility that mutant huntingtin is disrupting all of these processes and their respective pathways simultaneously, consistent with GWAS results and other phenotypes described in this Chapter, as well as those pointed out from Thesis Chapter 4.

If we can successfully knock-down huntingtin in a dose-dependent manner, and if cells are reliant on huntingtin function to survive, we can perform long-term live cell imaging to see how cells divide, as well as testing all the HD phenotypes characterized in TruHD cells (such as ADP/ATP ratio, cell proliferation etc.) at 50% huntingtin levels or 25% huntingtin levels, hopefully providing insight into current clinical trials.

5.5.2 Future Directions

The cells that were obtained from Coriell to generate the TruHD cells had limited clinical information. We hope to obtain fibroblasts from patients with a larger variety of CAG repeat length, but also disease onset age and disease progression severity to further understand the cellular mechanisms involved in HD. Protocols for characterization and critical phenotypes have been described in the manuscript presented in Thesis Chapter 4, and provide a workflow for generation of new TruHD immortalized cell lines.

Most of the phenotypes described are consistent between different HD lines, but it would be important to study how disease pathogenesis dependence on CAG tract length. It would be ideal if we could also generate an isogenic series of immortalized TruHD cell lines. We have received TALEN constructs to generate an isogenic series of cells (Q18, Q45, Q65) from Dr. Mahmoud Pouladi. We decided to generate the series with each of the characterized TruHD lines (Q21Q18F, Q43Q17M and Q50Q40F) to see if cells with the same CAG repeats are different and have patient-specific phenotypes. Mina Falcone, our senior lab technician, is

currently working on it. We do not expect allele specificity, so we expect generation of homozygous lines (Q18Q18, Q45Q45 and Q65Q65).

A major benefit to using cell lines over primary cells is the ability to generate inducible, stable cell lines. Since overexpression of fluorophore-tagged huntingtin or huntingtin fragments does not properly model HD cell biology, we have utilized a modified, fluorophore-tagged huntingtin intrabody, a chromobody, to visualize endogenous huntingtin in live cells⁹¹. The chromobody is composed of a fluorophore attached to a small fragment of an antibody that is specific for huntingtin. This can be overexpressed in live cells and can bind endogenous huntingtin, allowing for visualization of endogenous huntingtin in live cells. Unregulated overexpression of the chromobody is toxic to the cells however, so we wanted to include a doxycycline inducible promoter (Tet-ON 3G system), but attempts by our Research Associate, Dr. Tamara Maiuri, to generate inducible cell lines stably expressing the chromobody were unsuccessful. Expression of the intrabody in cells that were successfully transfected was not being properly induced. Transfection efficiency is generally low in fibroblasts, but was not the limiting factor here, therefore other plasmids will be tested for generation of inducible stable cell lines.

5.8 Figures

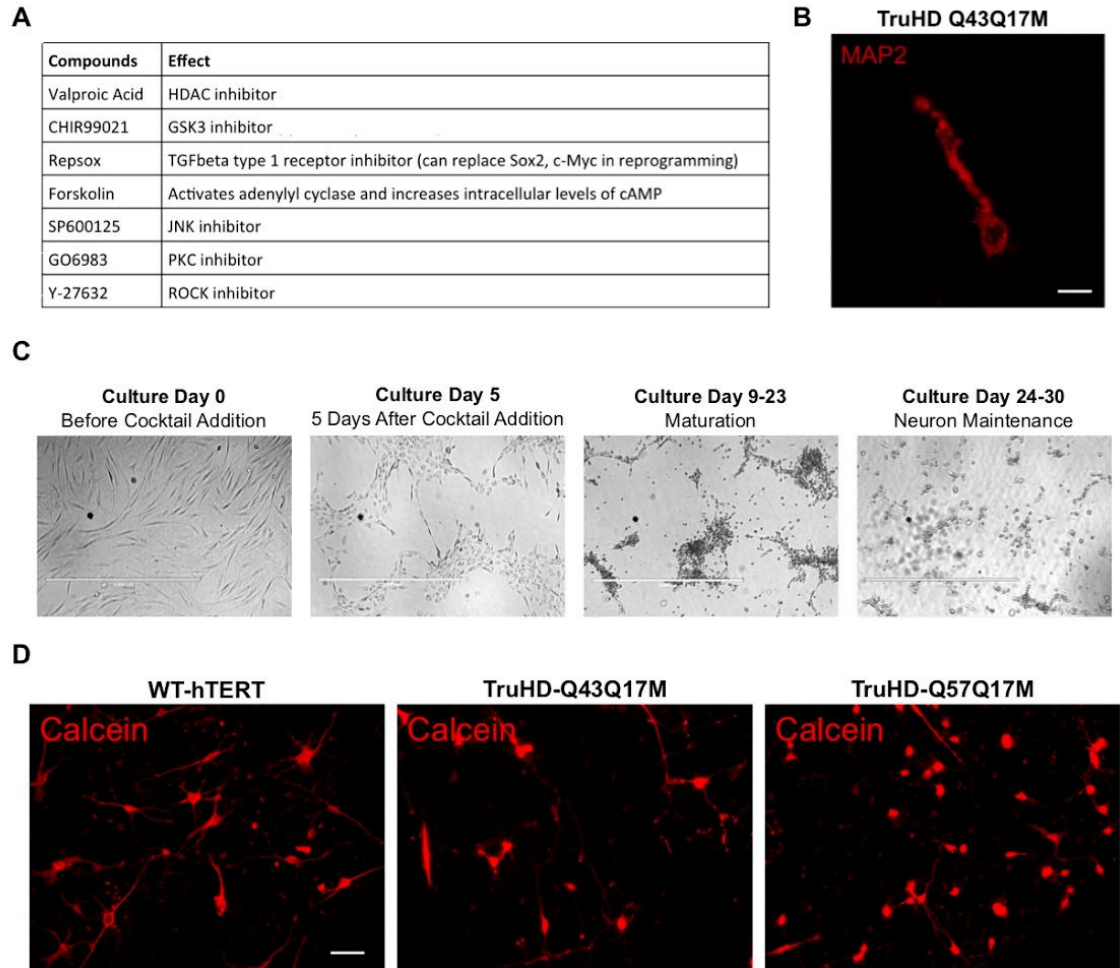


Figure 5.1 Direct conversion of TruHD patient fibroblasts to post-mitotic neurons.

(A) Small molecule compounds used in direct conversion protocol. (B) Immunofluorescent image of a TruHD-Q43Q17M cell with MAP2 antibody, showing positive staining for the neuron-specific marker, but cell looks unhealthy. Scale bar= 20 μ m. (C) Progression of cell culture through 30-day protocol, transmitted light imaging. Scale bar= (D) Calcein-stained fibroblasts (including TruHD-Q57Q17, a line that we later removed from our study because they were difficult to culture) that had undergone miRNA direct programming protocol to generate medium spiny neurons. Experiments performed by Nathan Pomper in Dr. Andrew Yoo's lab. Scale bar = 30 μ m.

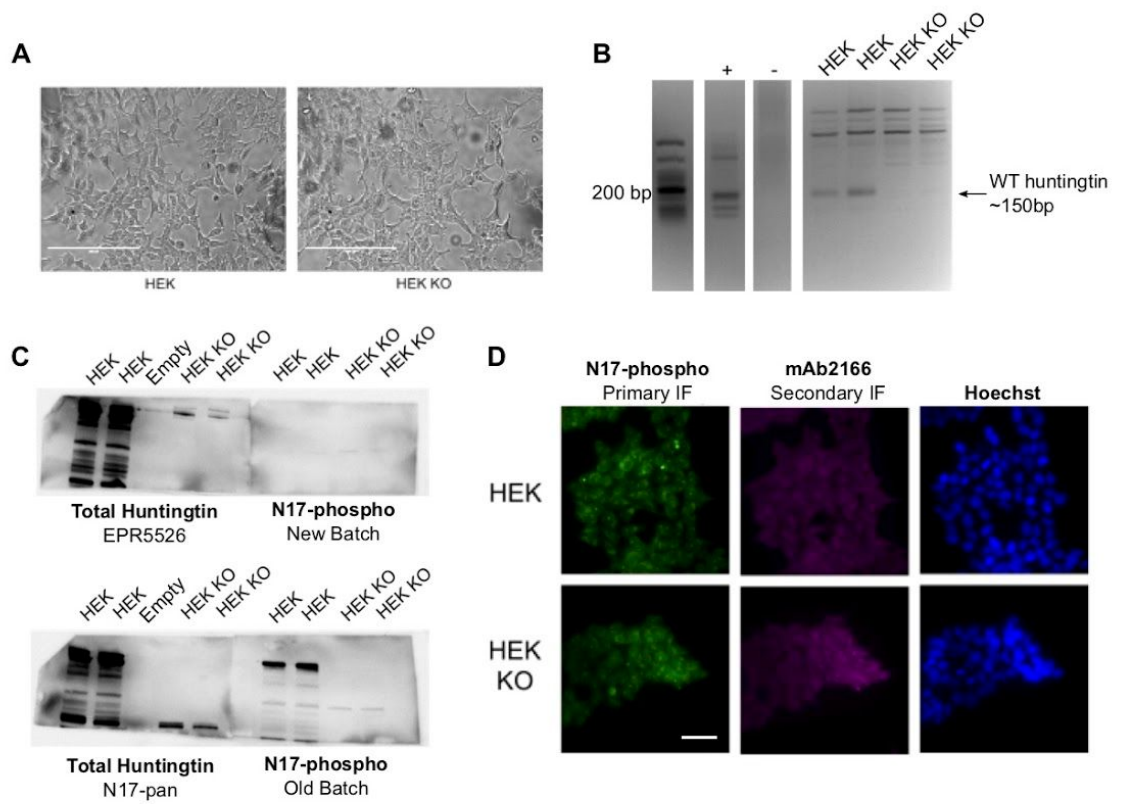


Figure 5.2 Huntingtin knockout HEK cells show minimal huntingtin protein levels compared to control.

(A) No obvious differences in cell morphology are detected in control HEK cells to knockout cells by brightfield microscopy of live cells. (B) Gel electrophoresis of PCR performed with primers that flank Exon1. Wildtype huntingtin runs at ~150bp, shown in lanes 1 and 2 (HEK control) but barely in lanes 3 and 4 (HEK knockout). (C) Immunoblotting of huntingtin with EPR5526 antibody, N17-pan antibody (recognizes first 8 amino acids of huntingtin), N17-phospho old batch (previously validated in Atwal et al.⁷⁴), and N17-phospho new batch (experimental conditions have since been optimized, validated in Hung et al. in submission). Some full length huntingtin is detected with EPR5526 (not spillover because an empty lane was left). No full length huntingtin detected with other antibodies, but possible degradation products of huntingtin are present. (D) Primary immunofluorescence with N17-phospho and secondary immunofluorescence with mAb2166 showed similar staining pattern and signal intensity. Scale bar = 30 μ m.

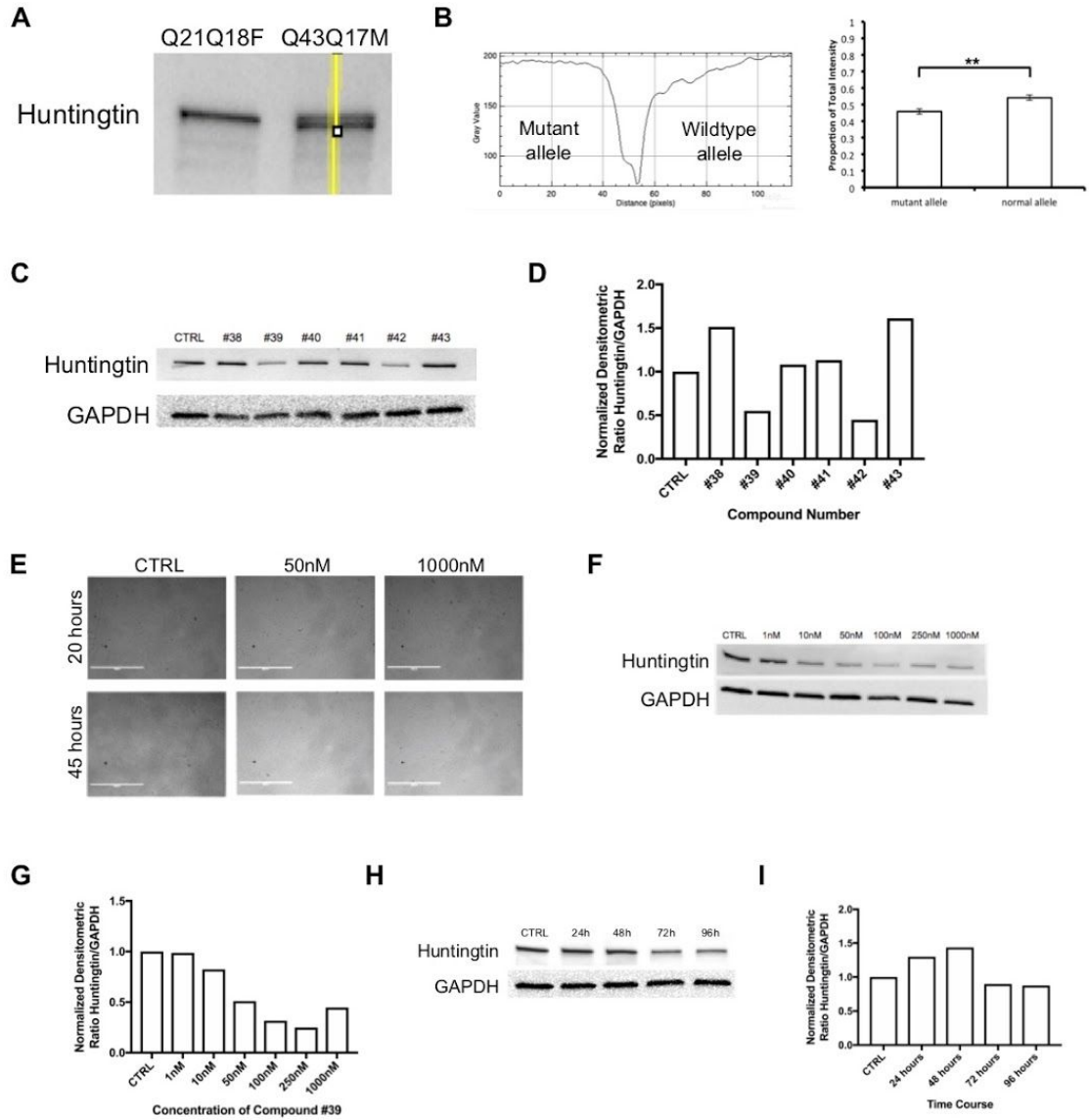


Figure 5.3 Dose-dependent knockdown of huntingtin using PTC Therapeutics

compounds. (A) Immunoblotting of both copies of huntingtin in TruHD-Q21Q18F (appears as one large band because CAG repeat difference is small) and TruHD-Q43Q17M (appears as two bands because CAG repeat is larger) with EPR5526 antibody. (B) Relative huntingtin protein quantification using a line profile measurement in ImageJ, showing the presence of two signal peaks corresponding to the mutant huntingtin band and the wild-type huntingtin band. (C) Immunoblotting with EPR5526 for huntingtin protein levels in TruHD-Q50Q40F cells after 48 hours knockdown using 50nM PTC small molecule compounds in growth media. Control is untreated TruHD-Q50Q40F cells. (D) Densitometric quantification of huntingtin protein levels. n=1. (E) Transmitted light images of TruHD-Q50Q40F cells treated with Compound #39 at 50nM and 1000nm for 20 or 45 hours. Scale bar = (F) Immunoblotting with EPR5526 for huntingtin protein levels after 48 hour dose response treatment in TruHD-Q50Q40F cells using 50nM of Compound #39. (G) Densitometric quantification of huntingtin levels after dose response. n=1. (H) Immunoblotting with EPR5526 for huntingtin protein levels after repeat treatments of TruHD-Q50Q40F cells with 50nM Compound #39 every 24 hours for 24, 48, 72 and 96 hours. (I) Densitometric quantification of huntingtin levels. n=1.

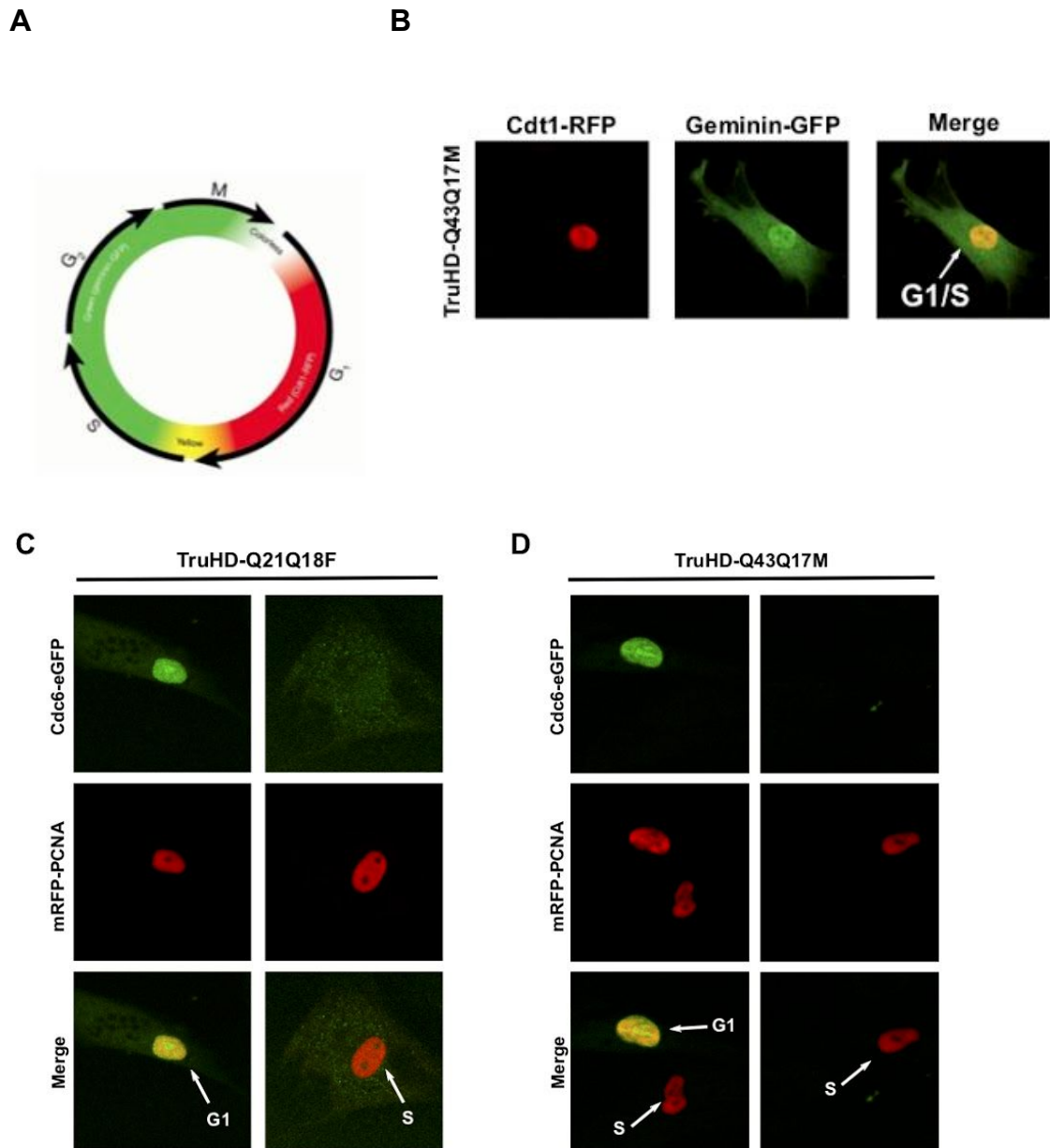
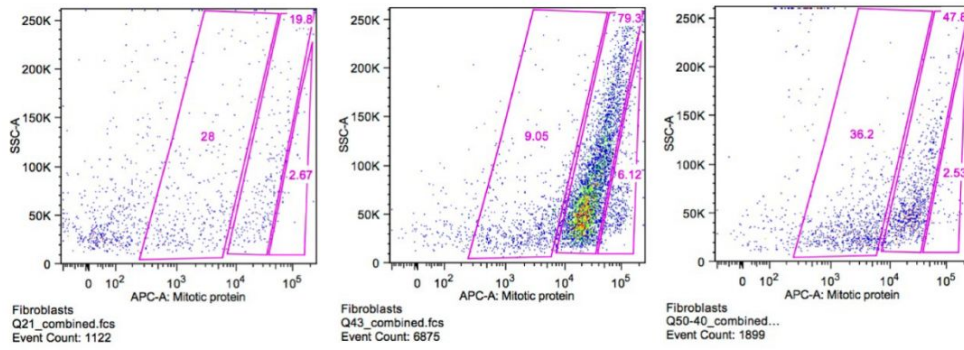


Figure 5.4 Stages of the cell cycle in TruHD cells. (A) Schematic of expected colour changes using PremoFUCCI assay (taken from ThermoFisher product manual). Merged image of channels with expression of both Cdt1-RFP and geminin-GFP are pseudocoloured yellow. (B) Live cell images of TruHD-Q43Q17M cells in G1/S phase transition. Live cell images of (C) TruHD-Q21Q18F cells and (D) TruHD-Q43Q17M cells expressing Cdc6-eGFP and mRFP-PCNA. Cells were found in S phase or G1 phases, denoted by white arrows. Merged image of channels with expression of both Cdc6-eGFP and mRFP-PCNA are pseudocoloured yellow.

A



B

Cell Type	% of cells with "High" Mitosis	MFI (N17p)	% of cells with "Medium" Mitosis	MFI (N17p)	% of cells with "Low" Mitosis	MFI (N17p)
Q21Q18F	2.67	16770	19.8	10181	28	3158
Q43Q17M	6.12	10999	79.3	6900	9.05	1899
Q50Q40F	2.53	9602	47.8	5438	36.2	1143

Figure 5.5 N17-phospho is upregulated during mitosis by flow cytometry. (A) Bottom axis shows intensity of mitotic phosphoproteins (we used an antibody specifically against mitotic phosphoproteins which is upregulated during mitosis, the same one Shreya used to see the same effect in *STHdh* cells by immunoblotting). Gate were drawn to isolate populations of “high”, “medium” and “low” mitosis based on intensity of mitotic phosphoprotein signal. (B) Percentages of total cell population that fall within each gate. To analyze whether N17 phospho is increased in cells that are mitotic, the mean fluorescence intensities (MFI) were measured. N17 phospho antibody was conjugated to AlexaFluor488 in order to accurately quantify intensity. In all three TruHD cell lines, N17-phospho intensity was higher in “high” mitosis cells.

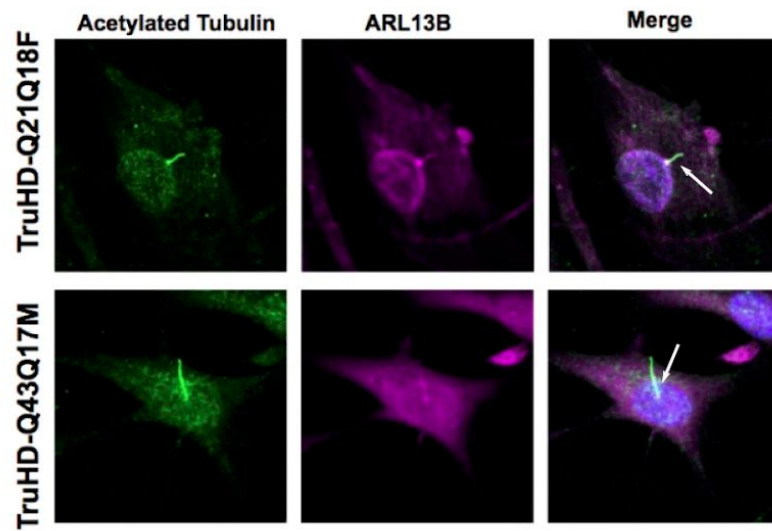
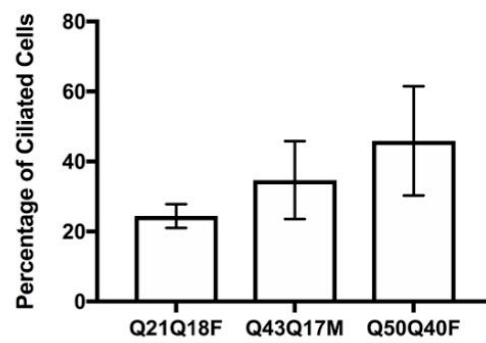
A**B**

Figure 5.6 Quantification of primary cilia formation in TruHD cells. Images of (A) TruHD-Q21Q18F and (B) TruHD-Q43Q17M cells that have formed primary cilia after 24 hours serum starvation. Immunofluorescence was performed with two ciliary markers, acetylated tubulin and ARL13b to ensure primary cilia quantification, and not of debris. (B) Percentage of ciliated cells were quantified for TruHD-Q21Q18F, TruHD-Q43Q17M and TruHD-Q50Q40F cells. n=3, N=50. Not significantly different.

CHAPTER 6: DISCUSSION

6.1 Context of Work in HD Cell Biology Research

The primary objective of the projects presented in this thesis were to explore aggregate formation in HD cells overexpressing polyQ-expanded Exon1 fragments of huntingtin (Thesis Chapters 2 and 3) and to define new cell models for HD cell biology research and to define critical phenotypes in HD cells compared to wild-type cells. In these fragment models, phenotypes like aggregate formation, were shown to be a readout of disease rather than causative. After the work performed in Thesis Chapters 2 and 3, we concluded that the inclusion type was a reflection of cell health, regarding energy levels and availability for phosphorylation. The major determining factor for inclusion type was phosphorylation state of S13 and S16, highlighting the importance of N17 phosphorylation to protein structure and localization.

The historical relevance of inclusions in HD biology research was a major driving force for the project. Because of the large size of the huntingtin protein, much of the *in vitro* work has been done with huntingtin fragments, either by structural studies or by overexpression in cell models. Much of this work therefore ignores potentially important facets of huntingtin biology. Endogenous huntingtin aggregates cannot be detected in cultured cell models. However, in tissues from animal models or post-mortem HD brains, aggregates can be detected and have been a hallmark of disease for decades. This discrepancy has therefore made it difficult to reconcile observations from *in vitro* studies to those seen in HD brains. We pursued the study of aggregates because we were able to define previously unidentified properties of aggregates formed from huntingtin fragments by using several biophotonic methods. With an increasing number of studies supporting the theory that aggregates could be toxic or protective, it made sense that since we identified two distinct types (globular and fibrillar), that one could be toxic and one could be protective. We could identify several differences between the two types of protein aggregates that supported this, but it was still difficult to reconcile what we were seeing with actual disease phenotypes seen in the brain,

even though observations continued to suggest that globular inclusions were associated with cellular toxicity, while the fibrillar inclusions were associated with a protective effect.

For the duration of the aggregate studies, transformed *STHdh* were used. Halfway through my studies, results from GWAS implicated DNA damage repair pathways in modifying disease onset. Even though there is an inverse correlation of CAG repeat length with disease onset, there is a large variation in onset between patients with the same repeat length. The average pathogenic CAG repeat length in humans is 43. In mouse models, such as that used to derive the *STHdh* cells, repeat lengths are >100. CAG repeat lengths >60 are associated with juvenile HD, which has less variation with regards to disease onset. Therefore, research into mechanisms to slow or prevent disease onset should not be done in these models, showing the necessity for better modelling in human, non-transformed cells.

We decided to generate immortalized patient fibroblast cell lines using hTERT. We had been using primary fibroblasts in the lab prior to this, but they grow slowly in culture and are prone to cellular senescence, therefore hindering reproducibility. Since fibroblasts can be easily obtained from patients in the clinic or from the Coriell Institute for Medical Research cell repository, those selected for use in studies across the HD field vary, with limited characterization prior to use. Because each fibroblast cell sample is taken from a different person, there are many more properties, besides CAG repeat length, that must be considered. After starting with 7 potential lines, I narrowed down our potential immortalized cell lines to three; one wild-type, one heterozygous and one homozygous, based on ease of culture and a wide range of phenotypes that were consistent to previously established ones in HD models. In Thesis Chapter 4, our manuscript characterizing these three lines, named TruHD cells, was presented, providing a starting point for the data presented in Thesis Chapter 5. At clinically relevant CAG lengths, we were still able to see HD phenotypes consistent with those in cell models with >100 CAG repeats.

6.2 Energy Deficit: A Consistent Thread in HD Biology

A well-established phenotype in *in vitro* models, *in vivo* models and HD patients in the clinic is an energy deficit^{297,298}. In patients, there is wasting even with increased caloric intake^{159,401}. Mitochondrial dysfunction due to the presence of mutant huntingtin is regularly noted as the culprit for reduced ATP levels^{113,156,309}, but there are likely more factors involved that regulate cellular energy levels. Energy in cells can be stored in “high-energy bonds” in nucleoside triphosphates such as ATP which is required for all cellular processes such as macromolecule synthesis, actin treadmilling and vesicular transport⁴⁰². During times of cellular stress, various response pathways trigger a high demand for ATP such as unfolded protein response (UPR), initiation of survival or cell death pathways and DNA damage repair⁴⁰³. Additionally, oxidative stress can cause DNA damage that results in an imbalance of nucleotides⁴⁰⁴. In HD cells, there is an inverted ATP/ADP ratio, and under times of stress there is an even larger energy deficit problem because of the increased need for ATP. For example, in HD cells, the presence of misfolded, polyQ expanded protein can result in persistent UPR which can contribute to lowered ATP levels⁴⁰⁵.

ATP is produced by two main processes: glycolysis and oxidative phosphorylation. Relative to other regions in the body, the brain relies heavily on glycolysis to generate ATP, even with abundant oxygen, which generates much lower levels of ATP compared to that of oxidative phosphorylation⁴⁰⁶. Nucleotide levels in both replicating and non-dividing cells are maintained by *de novo* synthesis as well as nucleotide salvaging. Nucleotide salvaging is a process where nucleotides are synthesized from intermediates that have been degraded and is particularly important in regulating ATP levels in non-dividing brain cells⁴⁰⁷, especially in conditions of stress. As described earlier, huntingtin is hypophosphorylated at serines 13 and 16 in N17. Restoring proper phosphorylation of these residues is protective in HD cell and mouse models. A screen of natural compounds performed by Laura Bowie identified kinetin, or N6-furfuryladenine (N6FFA), to increase N17 phosphorylation⁹². Kinetin/N6FFA is structurally very similar to adenine, and can therefore be synthesized to make a nucleotide triphosphate known as kinetin triphosphosphate (KTP)⁴⁰⁸. In Parkinson’s disease (PD),

reduced kinase activity of PTEN-induced kinase 1 (PINK1) results in defective mitochondrial function. Addition of KTP can increase PINK1 kinase activity, as it can use KTP as a phosphate source to regulate Bcl-xL and Parkin function. Previously in our lab, we showed that inhibition of casein kinase 2 (CK2) reduced N17 phosphorylation⁷⁴. CK2 is a promiscuous kinase and can use other nucleotide triphosphates to phosphorylate its substrates^{92,409}. *In vitro* kinase assays revealed that CK2 can use KTP to phosphorylate N17⁹². Therefore treatment of cells with kinetin/N6FFA, which can be salvaged and converted to KTP, can restore N17 phosphorylation in polyQ-expanded huntingtin by providing an alternative phosphate source to ATP, which is lower in HD cells in stress conditions. Treatment of HD cells and HD YAC128 mice showed protective effects of restoring N17 phosphorylation and reversal of HD phenotypes, which is consistent with previous studies regarding the importance of this post-translational modification, validating N17 phosphorylation as a target for therapeutic intervention to rescue the energy deficit and restore normal function in HD cells. As we learn more about the results from the current ASO clinical trials, an attractive alternative approach to therapy that still targets the only validated target for HD, the huntingtin protein itself, could be targeting restoration of N17 phosphorylation.

6.3 Expanding the Role of DNA Damage Repair in HD Progression

As other CAG repeat disorders are caused by the same expansion mutation, it is not surprising that the progression of these disorders, such as SCA1 and SCA7, have overlapping mechanisms with HD^{40,410-412}. These dominantly inherited diseases are all characterized by progressive neuronal loss over 10-20 years. The clinical manifestations of the CAG expansion depend on the genes and cell types affected by the repeat expansion, but despite the phenotypic variation between these diseases, it is likely that there are common underlying pathological mechanisms. Human genetic data suggest that DNA repair pathways are central to pathogenesis in CAG repeat diseases^{11,413}, and this hypothesis was recently reviewed by Massey and Jones in 2018³⁹. Therefore, further investigation into DNA damage repair

pathways in HD or other CAG repeat disorders can provide a better understanding into CAG repeat expansion pathology in general.

Kinetin/N6FFA is actually a naturally occurring product of oxidative DNA damage. ROS-damaged adenosine in DNA is excised during DNA repair and can be salvaged by adenine phosphoribosyltransferase (APRT) to generate KTP. This process is important in cell stress conditions when ATP levels are low, where kinetin/N6FFA acts as a signalling molecule, suggesting that HD is a metabolic disorder, and that addition of this metabolite could restore N17 phosphorylation and be protective in HD. Upstream processes may therefore be important to HD disease phenotypes and progression.

Regulation of DNA damage repair during cell division is highly connected to cell cycle checkpoint regulation. Several proteins have been implicated in both processes, such as centrosomal protein of 164kDa (Cep164) and Chk2^{375,414}. As described in Thesis Chapter 5, there may be a role of huntingtin in cell cycle checkpoint regulation which can affect downstream processes involved in DNA damage repair, consistent with reports that there is increased DNA damage in HD⁹¹. Mutant, polyQ-expanded huntingtin may be aberrantly disrupting cell cycle checkpoint regulation that is critical for proper DNA damage repair to occur. Data presented in Chapter 5 is preliminary, but supports unpublished data and hypotheses that downstream neuronal degeneration may be caused by re-entry of post-mitotic neurons into the cell cycle, due to aberrant cell cycle checkpoint regulation, and can become targeted for apoptosis^{381,415}.

Poly-ADP ribose polymerase 1 (PARP1) activity is required for initiating various DNA damage repair mechanisms⁴¹⁶. PARP1 hyperactivation is linked with various diseases that are associated with aberrant DNA damage response, such as cancer. Recently, a mutation in XRCC1, a molecular scaffold protein that assembles multi-protein complexes involved in DNA single-strand break repair, was shown to cause cerebellar ataxia. This mutation was linked to PARP1 hyperactivation. The coenzyme, nicotinamide adenine dinucleotide (NAD⁺), is critical for cellular respiration and oxidative phosphorylation to generate ATP^{417,418}. NAD⁺ is

necessary for PARP1 activity, so hyperactivation could result in depletion of NAD⁺, in turn affecting ATP levels and could be a mechanism that is present in HD cells as well.

6.4 Future Avenues of HD Research with TruHD Cells

After generation of these lines, we explored potential mechanisms that may have been inconclusive in previous, transformed models, as well as new avenues to utilize the cells, such as direct reprogramming to neurons and generation of isogenic cell lines. Performing studies in human, clinically relevant cells has opened a window of HD pathogenesis research in our lab by screening for differences at lower CAG repeats reflective of human disease, exploring DNA damage repair pathways and cell cycle regulation to understand age-dependent onset of HD. Identification of critical phenotypes in HD disease progression will drive research in the correct avenues to ensure movement towards promising therapeutic targets. We only characterized 3 lines in our study presented in Chapter 4, but the goal is to obtain more fibroblasts from patients with a wider range of disease onset age and disease progression profiles to further study factors that affect onset age. Future work should all be done in well-characterized lines with clinical information to match.

6.5 Conclusions

The work presented in this thesis has supported the need to understanding the biological mechanisms that change in HD cells. The work has focused on the importance of disease modelling, focusing on critical phenotypes that are different between human wild-type and HD cells. With current, promising therapeutic approaches focused on lowering huntingtin levels, but it is important to know how huntingtin is involved in cellular pathways in order to know how that will affect cells in the long-term. Reagents are being developed that are specific for human RNA and protein, so having a well-characterized human cell model presenting as a control, heterozygous and homozygous cases will be useful for pre-clinical therapeutic testing.

Since publication of GWAS that implicated DNA damage repair pathways as modifiers of onset age, HD research has continued to move away from studying protein aggregation as the cause of disease. Identifying mechanisms underlying how DNA damage repair pathways can modify disease onset are a promising target, particularly its connection with lowered ATP levels and the energy deficit in HD.

REFERENCES

1. Saudou, F. & Humbert, S. The Biology of Huntingtin. *Neuron* **89**, 910–926 (2016).
2. Sapp, E. *et al.* Huntingtin localization in brains of normal and Huntington's disease patients. *Ann. Neurol.* **42**, 604–612 (1997).
3. Morrison, P. J. Prevalence estimates of Huntington disease in Caucasian populations are gross underestimates. *Mov. Disord.* **27**, 1707–1708 (2012).
4. Pagan, F., Torres-Yaghi, Y. & Altshuler, M. The diagnosis and natural history of Huntington disease. in *Handbook of Clinical Neurology* 63–67 (2017).
5. Evans, S. J. W. *et al.* Prevalence of adult Huntington's disease in the UK based on diagnoses recorded in general practice records. *J. Neurol. Neurosurg. Psychiatry* **84**, 1156–1160 (2013).
6. A novel gene containing a trinucleotide repeat that is expanded and unstable on Huntington's disease chromosomes. The Huntington's Disease Collaborative Research Group. *Cell* **72**, 971–983 (1993).
7. Orr, H. T. *et al.* Expansion of an unstable trinucleotide CAG repeat in spinocerebellar ataxia type 1. *Nat. Genet.* **4**, 221–226 (1993).
8. Perutz, M. F. Glutamine repeats and inherited neurodegenerative diseases: molecular aspects. *Curr. Opin. Struct. Biol.* **6**, 848–858 (1996).
9. Snell, R. G. *et al.* Relationship between trinucleotide repeat expansion and phenotypic variation in Huntington's disease. *Nat. Genet.* **4**, 393–397 (1993).
10. Brinkman, R. R., Mezei, M. M., Theilmann, J., Almqvist, E. & Hayden, M. R. The likelihood of being affected with Huntington disease by a particular age, for a specific CAG size. *Am. J. Hum. Genet.* **60**, 1202–1210 (1997).
11. Genetic Modifiers of Huntington's Disease (GeM-HD) Consortium. Identification of Genetic Factors that Modify Clinical Onset of Huntington's Disease. *Cell* **162**, 516–526 (2015).
12. The World Factbook — Central Intelligence Agency. Available at: <https://www.cia.gov/library/publications/the-world-factbook/rankorder/2102rank.html>. (Accessed: 25th May 2018)
13. Hecker, J. F. C. & Babington, B. G. *The epidemics of the middle ages.* (Trübner & co., 1859).
14. Vale, T. C. & Cardoso, F. Chorea: A Journey through History. *Tremor Other Hyperkinet. Mov.* **5**, (2015).
15. Bhattacharyya, K. B. The story of George Huntington and his disease. *Ann. Indian Acad. Neurol.* **19**, 25–28 (2016).
16. Cardoso, F. Sydenham's Chorea. in *Chorea* 57–69 (2014).
17. Gasser, T. & Kiebertz, K. Huntington's Disease and Sydenham's Chorea. in *Neurological Disorders* 1149–1156 (2003).
18. Sydenham, T. & (m.d.), J. S. *The Entire Works of Dr Thomas Sydenham, Newly Made English from the Originals ... The Third Edition, with All the Notes Inserted in Their Proper Places. By John Swan, M.D.* (E. Cave, 1753).
19. Huntington, G. & Others. On chorea. (1872).

20. Dorsey, E. R. & Ray Dorsey, E. Natural History of Huntington Disease. *JAMA Neurol.* (2013). doi:10.1001/jamaneurol.2013.4408
21. Wexler, A. *The Woman Who Walked Into the Sea: Huntington's and the Making of a Genetic Disease.* (Yale University Press, 2014).
22. Donaldson, I., David Marsden, C., Schneider, S. & Bhatia, K. *Marsden's Book of Movement Disorders.* (OUP Oxford, 2012).
23. DeJong, R. N. *The history of Huntington's chorea in the United States of America.* (Raven Press, 1973).
24. Siemers, E. Huntington disease. *Arch. Neurol.* **58**, 308–310 (2001).
25. Lanska, D. J. George Huntington (1850-1916) and Hereditary Chorea. *J. Hist. Neurosci.* **9**, 76–89 (2000).
26. Okun, M. S. & Thommi, N. Americo Negrette (1924 to 2003): diagnosing Huntington disease in Venezuela. *Neurology* **63**, 340–343 (2004).
27. Wexler, A. Huntington's Disease - A Brief Historical Perspective. *J. Huntingtons Dis.* **1**, 3–4 (2012).
28. Hayden, M. Predictive medicine: recombinant DNA technology and adult-onset genetic disorders. *Can. Fam. Physician* **34**, 923–926 (1988).
29. MacDonald, M. E. *et al.* A novel gene containing a trinucleotide repeat that is expanded and unstable on Huntington's disease chromosomes. *Cell* **72**, 971–983 (1993).
30. Wexler, N. S., Conneally, P. M., Housman, D. & Gusella, J. F. A DNA polymorphism for Huntington's disease marks the future. *Arch. Neurol.* **42**, 20–24 (1985).
31. Gusella, J. F. *et al.* A Polymorphic DNA Marker Genetically Linked to Huntington's Disease. *Landmarks in Medical Genetics: Classic Papers with Commentaries* **306**, 153 (2004).
32. Mangiarini, L. *et al.* Exon 1 of the HD gene with an expanded CAG repeat is sufficient to cause a progressive neurological phenotype in transgenic mice. *Cell* **87**, 493–506 (1996).
33. McMurray, C. T. Mechanisms of DNA expansion. *Chromosoma* **104**, 2–13 (1995).
34. Hall, A. C., Ostrowski, L. A., Pietrobon, V. & Mekhail, K. Repetitive DNA loci and their modulation by the non-canonical nucleic acid structures R-loops and G-quadruplexes. *Nucleus* **8**, 162–181 (2017).
35. de Koning, A. P. J., Gu, W., Castoe, T. A., Batzer, M. A. & Pollock, D. D. Repetitive Elements May Comprise Over Two-Thirds of the Human Genome. *PLoS Genet.* **7**, e1002384 (2011).
36. Koide, R. *et al.* Unstable expansion of CAG repeat in hereditary dentatorubral–pallidolusian atrophy (DRPLA). *Nat. Genet.* **6**, 9–13 (1994).
37. Nagafuchi, S. *et al.* Dentatorubral and pallidolusian atrophy expansion of an unstable CAG trinucleotide on chromosome 12p. *Nat. Genet.* **6**, 14–18 (1994).
38. Spada, A. R. L. *et al.* Androgen receptor gene mutations in X-linked spinal and bulbar muscular atrophy. *Nature* **352**, 77–79 (1991).
39. Massey, T. H. & Jones, L. The central role of DNA damage and repair in CAG repeat diseases. *Dis. Model. Mech.* **11**, (2018).
40. Truant, R. *et al.* Canadian Association of Neurosciences Review: polyglutamine expansion neurodegenerative diseases. *Can. J. Neurol. Sci.* **33**, 278–291 (2006).

41. Zuccato, C., Valenza, M. & Cattaneo, E. Molecular mechanisms and potential therapeutic targets in Huntington's disease. *Physiol. Rev.* **90**, 905–981 (2010).
42. Ridley, R. M., Frith, C. D., Crow, T. J. & Conneally, P. M. Anticipation in Huntington's disease is inherited through the male line but may originate in the female. *J. Med. Genet.* **25**, 589–595 (1988).
43. Dürr, A. *et al.* Homozygosity in Huntington's disease. *J. Med. Genet.* **36**, 172–173 (1999).
44. Wexler, N. S. *et al.* Homozygotes for Huntington's disease. *Nature* **326**, 194–197 (1987).
45. Lee, J.-M. *et al.* CAG repeat expansion in Huntington disease determines age at onset in a fully dominant fashion. *Neurology* **78**, 690–695 (2012).
46. McMurray, C. T. Mechanisms of trinucleotide repeat instability during human development. *Nat. Rev. Genet.* **11**, 886 (2010).
47. Budworth, H. & McMurray, C. T. Problems and solutions for the analysis of somatic CAG repeat expansion and their relationship to Huntington's disease toxicity. *Rare Dis* **4**, e1131885 (2016).
48. Kennedy, L. *et al.* Dramatic tissue-specific mutation length increases are an early molecular event in Huntington disease pathogenesis. *Hum. Mol. Genet.* **12**, 3359–3367 (2003).
49. Shelbourne, P. F. *et al.* Triplet repeat mutation length gains correlate with cell-type specific vulnerability in Huntington disease brain. *Hum. Mol. Genet.* **16**, 1133–1142 (2007).
50. Kovtun, I. V. *et al.* OGG1 initiates age-dependent CAG trinucleotide expansion in somatic cells. *Nature* **447**, 447–452 (2007).
51. Goula, A.-V. *et al.* Stoichiometry of base excision repair proteins correlates with increased somatic CAG instability in striatum over cerebellum in Huntington's disease transgenic mice. *PLoS Genet.* **5**, e1000749 (2009).
52. McMurray, C. T. Mechanisms of trinucleotide repeat instability during human development. *Nat. Rev. Genet.* **11**, 786–799 (2010).
53. Bjelland, S. & Seeberg, E. Mutagenicity, toxicity and repair of DNA base damage induced by oxidation. *Mutat. Res.* **531**, 37–80 (2003).
54. Spiro, C. *et al.* Inhibition of FEN-1 processing by DNA secondary structure at trinucleotide repeats. *Mol. Cell* **4**, 1079–1085 (1999).
55. Liu, Y. *et al.* Coordination between Polymerase β and FEN1 Can Modulate CAG Repeat Expansion. *J. Biol. Chem.* **284**, 28352–28366 (2009).
56. Henricksen, L. A., Veeraraghavan, J., Chafin, D. R. & Bambara, R. A. DNA ligase I competes with FEN1 to expand repetitive DNA sequences in vitro. *J. Biol. Chem.* **277**, 22361–22369 (2002).
57. Orth, M. & Schwenke, C. Age-at-onset in Huntington disease. *PLoS Curr.* **3**, RRN1258 (2011).
58. Langbehn, D. R., Hayden, M. R., Paulsen, J. S. & and the PREDICT-HD Investigators of the Huntington Study Group. CAG-repeat length and the age of onset in Huntington disease (HD): a review and validation study of statistical approaches. *Am. J. Med. Genet. B Neuropsychiatr. Genet.* **153B**, 397–408 (2010).

59. Keum, J. W. *et al.* The HTT CAG-Expansion Mutation Determines Age at Death but Not Disease Duration in Huntington Disease. *Am. J. Hum. Genet.* **98**, 287–298 (2016).
60. Pinto, R. M. *et al.* Mismatch repair genes Mlh1 and Mlh3 modify CAG instability in Huntington's disease mice: genome-wide and candidate approaches. *PLoS Genet.* **9**, e1003930 (2013).
61. Reiner, A., Dragatsis, I. & Dietrich, P. Genetics and neuropathology of Huntington's disease. *Int. Rev. Neurobiol.* **98**, 325–372 (2011).
62. Reiner, A. *et al.* Differential loss of striatal projection neurons in Huntington disease. *Proc. Natl. Acad. Sci. U. S. A.* **85**, 5733–5737 (1988).
63. Cicchetti, F. & Parent, A. Striatal interneurons in Huntington's disease: selective increase in the density of calretinin-immunoreactive medium-sized neurons. *Mov. Disord.* **11**, 619–626 (1996).
64. Vonsattel, J.-P. *et al.* Neuropathological Classification of Huntington's Disease. *J. Neuropathol. Exp. Neurol.* **44**, 559–577 (1985).
65. Rosas, H. D. *et al.* Evidence for more widespread cerebral pathology in early HD: an MRI-based morphometric analysis. *Neurology* **60**, 1615–1620 (2003).
66. Rosas, H. D., Feigin, A. S. & Hersch, S. M. Using advances in neuroimaging to detect, understand, and monitor disease progression in Huntington's disease. *NeuroRx* **1**, 263–272 (2004).
67. Niccolini, F. & Politis, M. Neuroimaging in Huntington's disease. *World J. Radiol.* **6**, 301–312 (2014).
68. Paulsen, J. S. *et al.* fMRI biomarker of early neuronal dysfunction in presymptomatic Huntington's Disease. *AJNR Am. J. Neuroradiol.* **25**, 1715–1721 (2004).
69. Klöppel, S. *et al.* Automatic detection of preclinical neurodegeneration: presymptomatic Huntington disease. *Neurology* **72**, 426–431 (2009).
70. Rosas, H. D. *et al.* Diffusion tensor imaging in presymptomatic and early Huntington's disease: Selective white matter pathology and its relationship to clinical measures. *Mov. Disord.* **21**, 1317–1325 (2006).
71. Tartari, M. *et al.* Phylogenetic comparison of huntingtin homologues reveals the appearance of a primitive polyQ in sea urchin. *Mol. Biol. Evol.* **25**, 330–338 (2008).
72. DiGiovanni, L. F., Mocle, A. J., Xia, J. & Truant, R. Huntingtin N17 domain is a reactive oxygen species sensor regulating huntingtin phosphorylation and localization. *Hum. Mol. Genet.* **25**, 3937–3945 (2016).
73. Atwal, R. S. *et al.* Huntingtin has a membrane association signal that can modulate huntingtin aggregation, nuclear entry and toxicity. *Hum. Mol. Genet.* **16**, 2600–2615 (2007).
74. Atwal, R. S. *et al.* Kinase inhibitors modulate huntingtin cell localization and toxicity. *Nat. Chem. Biol.* **7**, 453–460 (2011).
75. Atwal, R. S. & Truant, R. A stress sensitive ER membrane-association domain in Huntingtin protein defines a potential role for Huntingtin in the regulation of autophagy. *Autophagy* **4**, 91–93 (2008).
76. Caron, N. S., Hung, C. L., Atwal, R. S. & Truant, R. Live cell imaging and biophotonic methods reveal two types of mutant huntingtin inclusions. *Hum. Mol. Genet.* **23**,

- 2324–2338 (2014).
77. Takano, H. & Gusella, J. F. The predominantly HEAT-like motif structure of huntingtin and its association and coincident nuclear entry with dorsal, an NF- κ B/Rel/dorsal family transcription factor. *BMC Neurosci.* **3**, 15 (2002).
 78. Maiuri, T., Woloshansky, T., Xia, J. & Truant, R. The huntingtin N17 domain is a multifunctional CRM1 and Ran-dependent nuclear and ciliary export signal. *Hum. Mol. Genet.* **22**, 1383–1394 (2013).
 79. Desmond, C. R., Atwal, R. S., Xia, J. & Truant, R. Identification of a karyopherin β 1/ β 2 proline-tyrosine nuclear localization signal in huntingtin protein. *J. Biol. Chem.* **287**, 39626–39633 (2012).
 80. Xia, J., Lee, D. H., Taylor, J., Vandelft, M. & Truant, R. Huntingtin contains a highly conserved nuclear export signal. *Hum. Mol. Genet.* **12**, 1393–1403 (2003).
 81. Andrade, M. A. & Bork, P. HEAT repeats in the Huntington's disease protein. *Nat. Genet.* **11**, 115–116 (1995).
 82. Di Pardo, A. *et al.* Ganglioside GM1 induces phosphorylation of mutant huntingtin and restores normal motor behavior in Huntington disease mice. *Proc. Natl. Acad. Sci. U. S. A.* **109**, 3528–3533 (2012).
 83. Gu, X. *et al.* Serines 13 and 16 are critical determinants of full-length human mutant huntingtin induced disease pathogenesis in HD mice. *Neuron* **64**, 828–840 (2009).
 84. Chaibva, M. *et al.* Acetylation within the First 17 Residues of Huntingtin Exon 1 Alters Aggregation and Lipid Binding. *Biophys. J.* **111**, 349–362 (2016).
 85. Jeong, H. *et al.* Acetylation targets mutant huntingtin to autophagosomes for degradation. *Cell* **137**, 60–72 (2009).
 86. Yanai, A. *et al.* Palmitoylation of huntingtin by HIP14 is essential for its trafficking and function. *Nat. Neurosci.* **9**, 824–831 (2006).
 87. Bhat, K. P., Yan, S., Wang, C.-E., Li, S. & Li, X.-J. Differential ubiquitination and degradation of huntingtin fragments modulated by ubiquitin-protein ligase E3A. *Proc. Natl. Acad. Sci. U. S. A.* **111**, 5706–5711 (2014).
 88. Kalchman, M. A. *et al.* Huntingtin is ubiquitinated and interacts with a specific ubiquitin-conjugating enzyme. *J. Biol. Chem.* **271**, 19385–19394 (1996).
 89. Steffan, J. S. *et al.* SUMO modification of Huntingtin and Huntington's disease pathology. *Science* **304**, 100–104 (2004).
 90. Thompson, L. M. *et al.* IKK phosphorylates Huntingtin and targets it for degradation by the proteasome and lysosome. *J. Cell Biol.* **187**, 1083–1099 (2009).
 91. Maiuri, T. *et al.* Huntingtin is a scaffolding protein in the ATM oxidative DNA damage response complex. *Hum. Mol. Genet.* **26**, 395–406 (2017).
 92. Bowie, L. E. *et al.* N6-Furfuryladenine is protective in Huntington's disease models by signaling huntingtin phosphorylation. *Proc. Natl. Acad. Sci. U. S. A.* **115**, E7081–E7090 (2018).
 93. Colin, E. *et al.* Huntingtin phosphorylation acts as a molecular switch for anterograde/retrograde transport in neurons. *EMBO J.* **27**, 2124–2134 (2008).
 94. Zala, D. *et al.* Phosphorylation of mutant huntingtin at S421 restores anterograde and retrograde transport in neurons. *Hum. Mol. Genet.* **17**, 3837–3846 (2008).

95. Metzler, M. *et al.* Phosphorylation of huntingtin at Ser421 in YAC128 neurons is associated with protection of YAC128 neurons from NMDA-mediated excitotoxicity and is modulated by PP1 and PP2A. *Journal of Neuroscience* **30**, 14318–14329 (2010).
96. DiFiglia, M. *et al.* Aggregation of huntingtin in neuronal intranuclear inclusions and dystrophic neurites in brain. *Science* **277**, 1990–1993 (1997).
97. Bence, N. F., Sampat, R. M. & Kopito, R. R. Impairment of the ubiquitin-proteasome system by protein aggregation. *Science* **292**, 1552–1555 (2001).
98. Rockabrand, E. *et al.* The first 17 amino acids of Huntingtin modulate its sub-cellular localization, aggregation and effects on calcium homeostasis. *Hum. Mol. Genet.* **16**, 61–77 (2007).
99. Caron, N. S., Desmond, C. R., Xia, J. & Truant, R. Polyglutamine domain flexibility mediates the proximity between flanking sequences in huntingtin. *Proc. Natl. Acad. Sci. U. S. A.* **110**, 14610–14615 (2013).
100. Vijayvargia, R. *et al.* Huntingtin's spherical solenoid structure enables polyglutamine tract-dependent modulation of its structure and function. *Elife* **5**, e11184 (2016).
101. Grinthal, A., Adamovic, I., Weiner, B., Karplus, M. & Kleckner, N. PR65, the HEAT-repeat scaffold of phosphatase PP2A, is an elastic connector that links force and catalysis. *Proc. Natl. Acad. Sci. U. S. A.* **107**, 2467–2472 (2010).
102. Guo, Q. *et al.* The cryo-electron microscopy structure of huntingtin. *Nature* **555**, 117–120 (2018).
103. Strong, T. V. *et al.* Widespread expression of the human and rat Huntington's disease gene in brain and nonneural tissues. *Nat. Genet.* **5**, 259–265 (1993).
104. Li, S.-H. *et al.* Huntington's disease gene (IT15) is widely expressed in human and rat tissues. *Neuron* **11**, 985–993 (1993).
105. Hilditch-Maguire, P. *et al.* Huntingtin: an iron-regulated protein essential for normal nuclear and perinuclear organelles. *Hum. Mol. Genet.* **9**, 2789–2797 (2000).
106. Hoffner, G., Kahlem, P. & Djian, P. Perinuclear localization of huntingtin as a consequence of its binding to microtubules through an interaction with beta-tubulin: relevance to Huntington's disease. *J. Cell Sci.* **115**, 941–948 (2002).
107. Kegel, K. B. *et al.* Huntingtin is present in the nucleus, interacts with the transcriptional corepressor C-terminal binding protein, and represses transcription. *J. Biol. Chem.* **277**, 7466–7476 (2002).
108. Panov, A. V. *et al.* Early mitochondrial calcium defects in Huntington's disease are a direct effect of polyglutamines. *Nat. Neurosci.* **5**, 731–736 (2002).
109. Strehlow, A. N. T., Li, J. Z. & Myers, R. M. Wild-type huntingtin participates in protein trafficking between the Golgi and the extracellular space. *Hum. Mol. Genet.* **16**, 391–409 (2007).
110. Ochaba, J. *et al.* Potential function for the Huntingtin protein as a scaffold for selective autophagy. *Proc. Natl. Acad. Sci. U. S. A.* **111**, 16889–16894 (2014).
111. Rui, Y.-N. *et al.* Huntingtin functions as a scaffold for selective macroautophagy. *Nat. Cell Biol.* **17**, 262–275 (2015).
112. Wyttenbach, A. *et al.* Polyglutamine expansions cause decreased CRE-mediated transcription and early gene expression changes prior to cell death in an inducible cell

- model of Huntington's disease. *Hum. Mol. Genet.* **10**, 1829–1845 (2001).
113. Milakovic, T. & Johnson, G. V. W. Mitochondrial respiration and ATP production are significantly impaired in striatal cells expressing mutant huntingtin. *J. Biol. Chem.* **280**, 30773–30782 (2005).
 114. Trushina, E. *et al.* Mutant huntingtin impairs axonal trafficking in mammalian neurons in vivo and in vitro. *Mol. Cell. Biol.* **24**, 8195–8209 (2004).
 115. Hodgson, J. G. *et al.* A YAC mouse model for Huntington's disease with full-length mutant huntingtin, cytoplasmic toxicity, and selective striatal neurodegeneration. *Neuron* **23**, 181–192 (1999).
 116. Schilling, G. *et al.* Intranuclear inclusions and neuritic aggregates in transgenic mice expressing a mutant N-terminal fragment of huntingtin. *Hum. Mol. Genet.* **8**, 397–407 (1999).
 117. Cooper, J. K. *et al.* Truncated N-terminal fragments of huntingtin with expanded glutamine repeats form nuclear and cytoplasmic aggregates in cell culture. *Hum. Mol. Genet.* **7**, 783–790 (1998).
 118. Li, S.-H. *et al.* Interaction of Huntington disease protein with transcriptional activator Sp1. *Mol. Cell. Biol.* **22**, 1277–1287 (2002).
 119. Duyao, M. P. *et al.* Inactivation of the mouse Huntington's disease gene homolog Hdh. *Science* **269**, 407–410 (1995).
 120. Nasir, J. *et al.* Targeted disruption of the Huntington's disease gene results in embryonic lethality and behavioral and morphological changes in heterozygotes. *Cell* **81**, 811–823 (1995).
 121. Zeitlin, S., Liu, J. P., Chapman, D. L., Papaioannou, V. E. & Efstratiadis, A. Increased apoptosis and early embryonic lethality in mice nullizygous for the Huntington's disease gene homologue. *Nat. Genet.* **11**, 155–163 (1995).
 122. White, J. K. *et al.* Huntingtin is required for neurogenesis and is not impaired by the Huntington's disease CAG expansion. *Nat. Genet.* **17**, 404–410 (1997).
 123. Benn, C. L. *et al.* Huntingtin Modulates Transcription, Occupies Gene Promoters In Vivo, and Binds Directly to DNA in a Polyglutamine-Dependent Manner. *Journal of Neuroscience* **28**, 10720–10733 (2008).
 124. Zuccato, C. *et al.* Loss of huntingtin-mediated BDNF gene transcription in Huntington's disease. *Science* **293**, 493–498 (2001).
 125. Zuccato, C. *et al.* Huntingtin interacts with REST/NRSF to modulate the transcription of NRSE-controlled neuronal genes. *Nat. Genet.* **35**, 76–83 (2003).
 126. Steffan, J. S. *et al.* The Huntington's disease protein interacts with p53 and CREB-binding protein and represses transcription. *Proceedings of the National Academy of Sciences* **97**, 6763–6768 (2000).
 127. Marcora, E., Gowan, K. & Lee, J. E. Stimulation of NeuroD activity by huntingtin and huntingtin-associated proteins HAP1 and MLK2. *Proc. Natl. Acad. Sci. U. S. A.* **100**, 9578–9583 (2003).
 128. Dunah, A. W. Sp1 and TAFII130 Transcriptional Activity Disrupted in Early Huntington's Disease. *Science* **296**, 2238–2243 (2002).
 129. Velier, J. *et al.* Wild-type and mutant huntingtins function in vesicle trafficking in the

- secretory and endocytic pathways. *Exp. Neurol.* **152**, 34–40 (1998).
130. Gauthier, L. R. *et al.* Huntingtin controls neurotrophic support and survival of neurons by enhancing BDNF vesicular transport along microtubules. *Cell* **118**, 127–138 (2004).
 131. Gunawardena, S. & Goldstein, L. S. B. Polyglutamine Diseases and Transport Problems. *Arch. Neurol.* **62**, 46 (2005).
 132. Gunawardena, S., Anderson, E. & White, J. Axonal transport and neurodegenerative disease: vesicle-motor complex formation and their regulation. *Degener. Neurol. Neuromuscul. Dis.* **29** (2014).
 133. Engqvist-Goldstein, Å. E. Y. *et al.* The actin-binding protein Hip1R associates with clathrin during early stages of endocytosis and promotes clathrin assembly in vitro. *J. Cell Biol.* **154**, 1209–1224 (2001).
 134. Legendre-Guillemin, V. *et al.* HIP1 and HIP12 Display Differential Binding to F-actin, AP2, and Clathrin. *J. Biol. Chem.* **277**, 19897–19904 (2002).
 135. Waelter, S. *et al.* The huntingtin interacting protein HIP1 is a clathrin and alpha-adaptin-binding protein involved in receptor-mediated endocytosis. *Hum. Mol. Genet.* **10**, 1807–1817 (2001).
 136. Li, X. *et al.* A function of huntingtin in guanine nucleotide exchange on Rab11. *Neuroreport* **19**, 1643–1647 (2008).
 137. Pal, A., Severin, F., Lommer, B., Shevchenko, A. & Zerial, M. Huntingtin–HAP40 complex is a novel Rab5 effector that regulates early endosome motility and is up-regulated in Huntington’s disease. *J. Cell Biol.* **172**, 605–618 (2006).
 138. Smith, R., Brundin, P. & Li, J.-Y. Synaptic dysfunction in Huntington’s disease: a new perspective. *Cell. Mol. Life Sci.* **62**, 1901–1912 (2005).
 139. Bliss, T. V. P. & Collingridge, G. L. A synaptic model of memory: long-term potentiation in the hippocampus. *Nature* **361**, 31–39 (1993).
 140. Arundine, M. & Tymianski, M. Molecular mechanisms of calcium-dependent neurodegeneration in excitotoxicity. *Cell Calcium* **34**, 325–337 (2003).
 141. Dong, X.-X., Wang, Y. & Qin, Z.-H. Molecular mechanisms of excitotoxicity and their relevance to pathogenesis of neurodegenerative diseases. *Acta Pharmacol. Sin.* **30**, 379–387 (2009).
 142. Li, J.-Y., Plomann, M. & Brundin, P. Huntington’s disease: a synaptopathy? *Trends Mol. Med.* **9**, 414–420 (2003).
 143. Munsie, L. *et al.* Mutant huntingtin causes defective actin remodeling during stress: defining a new role for transglutaminase 2 in neurodegenerative disease. *Hum. Mol. Genet.* **20**, 1937–1951 (2011).
 144. Munsie, L. N., Desmond, C. R. & Truant, R. Cofilin nuclear–cytoplasmic shuttling affects cofilin–actin rod formation during stress. *J. Cell Sci.* (2012).
 145. Nath, S., Munsie, L. N. & Truant, R. A huntingtin-mediated fast stress response halting endosomal trafficking is defective in Huntington’s disease. *Hum. Mol. Genet.* **24**, 450–462 (2015).
 146. Bernstein, B. W. & Bamberg, J. R. Actin-ATP hydrolysis is a major energy drain for neurons. *J. Neurosci.* **23**, 1–6 (2003).
 147. McMurray, C. T. Mechanisms of DNA expansion. *Chromosoma* **104**, 2–13 (1995).

148. Chen, X., Guo, C. & Kong, J. Oxidative stress in neurodegenerative diseases. *Neural Regeneration Res.* **7**, 376–385 (2012).
149. Ayala-Peña, S. Role of oxidative DNA damage in mitochondrial dysfunction and Huntington's disease pathogenesis. *Free Radic. Biol. Med.* **62**, 102–110 (2013).
150. Ferlazzo, M. L. *et al.* Mutations of the Huntington's Disease Protein Impact on the ATM-Dependent Signaling and Repair Pathways of the Radiation-Induced DNA Double-Strand Breaks: Corrective Effect of Statins and Bisphosphonates. *Mol. Neurobiol.* **49**, 1200–1211 (2013).
151. Illuzzi, J., Yerkes, S., Parekh-Olmedo, H. & Kmiec, E. B. DNA breakage and induction of DNA damage response proteins precede the appearance of visible mutant huntingtin aggregates. *J. Neurosci. Res.* **87**, 733–747 (2009).
152. Acevedo-Torres, K. *et al.* Mitochondrial DNA damage is a hallmark of chemically induced and the R6/2 transgenic model of Huntington's disease. *DNA Repair* **8**, 126–136 (2009).
153. Lu, X.-H. *et al.* Targeting ATM ameliorates mutant Huntingtin toxicity in cell and animal models of Huntington's disease. *Sci. Transl. Med.* **6**, 268ra178–268ra178 (2014).
154. Baquet, Z. C., Gorski, J. A. & Jones, K. R. Early striatal dendrite deficits followed by neuron loss with advanced age in the absence of anterograde cortical brain-derived neurotrophic factor. *J. Neurosci.* **24**, 4250–4258 (2004).
155. Cong, X. *et al.* Mass Spectrometric Identification of Novel Lysine Acetylation Sites in Huntingtin. *Mol. Cell. Proteomics* **10**, M111.009829 (2011).
156. Quintanilla, R. A. & Johnson, G. V. W. Role of mitochondrial dysfunction in the pathogenesis of Huntington's disease. *Brain Res. Bull.* **80**, 242–247 (2009).
157. Browne, S. E. & Beal, M. F. The energetics of Huntington's disease. *Neurochem. Res.* **29**, 531–546 (2004).
158. Browne, S. E. *et al.* Oxidative damage and metabolic dysfunction in Huntington's disease: selective vulnerability of the basal ganglia. *Ann. Neurol.* **41**, 646–653 (1997).
159. Koroshetz, W. J., Jenkins, B. G., Rosen, B. R. & Beal, M. F. Energy metabolism defects in Huntington's disease and effects of coenzyme Q10. *Ann. Neurol.* **41**, 160–165 (1997).
160. Tellez-Nagel, I., Johnson, A. B. & Terry, R. D. Studies on brain biopsies of patients with Huntington's chorea. *J. Neuropathol. Exp. Neurol.* **33**, 308–332 (1974).
161. Stahl, W. L. & Swanson, P. D. Biochemical abnormalities in Huntington's chorea brains. *Neurology* **24**, 813–819 (1974).
162. Gu, M. *et al.* Mitochondrial defect in Huntington's disease caudate nucleus. *Ann. Neurol.* **39**, 385–389 (1996).
163. Mann, V. M. *et al.* Mitochondrial function and parental sex effect in Huntington's disease. *Lancet* **336**, 749 (1990).
164. Brustovetsky, N. *et al.* Increased susceptibility of striatal mitochondria to calcium-induced permeability transition. *J. Neurosci.* **23**, 4858–4867 (2003).
165. Orr, A. L. *et al.* N-terminal mutant huntingtin associates with mitochondria and impairs mitochondrial trafficking. *J. Neurosci.* **28**, 2783–2792 (2008).
166. Song, W. *et al.* Mutant huntingtin binds the mitochondrial fission GTPase dynamin-related protein-1 and increases its enzymatic activity. *Nat. Med.* **17**, 377–382

- (2011).
167. Knott, A. B. & Bossy-Wetzel, E. Impairing the mitochondrial fission and fusion balance: a new mechanism of neurodegeneration. *Ann. N. Y. Acad. Sci.* **1147**, 283–292 (2008).
 168. Knott, A. B., Perkins, G., Schwarzenbacher, R. & Bossy-Wetzel, E. Mitochondrial fragmentation in neurodegeneration. *Nat. Rev. Neurosci.* **9**, 505–518 (2008).
 169. Kim, Y. J. *et al.* Caspase 3-cleaved N-terminal fragments of wild-type and mutant huntingtin are present in normal and Huntington's disease brains, associate with membranes, and undergo calpain-dependent proteolysis. *Proc. Natl. Acad. Sci. U. S. A.* **98**, 12784–12789 (2001).
 170. Wellington, C. L. *et al.* Caspase cleavage of gene products associated with triplet expansion disorders generates truncated fragments containing the polyglutamine tract. *J. Biol. Chem.* **273**, 9158–9167 (1998).
 171. Wellington, C. L. *et al.* Caspase cleavage of mutant huntingtin precedes neurodegeneration in Huntington's disease. *J. Neurosci.* **22**, 7862–7872 (2002).
 172. Hermel, E. *et al.* Specific caspase interactions and amplification are involved in selective neuronal vulnerability in Huntington's disease. *Cell Death Differ.* **11**, 424–438 (2004).
 173. Graham, R. K. *et al.* Cleavage at the 586 Amino Acid Caspase-6 Site in Mutant huntingtin Influences Caspase-6 Activation In Vivo. *Journal of Neuroscience* **30**, 15019–15029 (2010).
 174. Martin, D. D. O. *et al.* Identification of a post-translationally myristoylated autophagy-inducing domain released by caspase cleavage of Huntingtin. *Hum. Mol. Genet.* **23**, 3166–3179 (2014).
 175. Goldberg, Y. P. *et al.* Cleavage of huntingtin by apopain, a proapoptotic cysteine protease, is modulated by the polyglutamine tract. *Nat. Genet.* **13**, 442–449 (1996).
 176. Landles, C. *et al.* Proteolysis of mutant huntingtin produces an exon 1 fragment that accumulates as an aggregated protein in neuronal nuclei in Huntington disease. *J. Biol. Chem.* **285**, 8808–8823 (2010).
 177. Scherzinger, E. *et al.* Huntingtin-encoded polyglutamine expansions form amyloid-like protein aggregates in vitro and in vivo. *Cell* **90**, 549–558 (1997).
 178. Graham, R. K. *et al.* Cleavage at the caspase-6 site is required for neuronal dysfunction and degeneration due to mutant huntingtin. *Cell* **125**, 1179–1191 (2006).
 179. Wellington, C. L. *et al.* Inhibiting Caspase Cleavage of Huntingtin Reduces Toxicity and Aggregate Formation in Neuronal and Nonneuronal Cells. *J. Biol. Chem.* **275**, 19831–19838 (2000).
 180. Hardy, J. & Allsop, D. Amyloid deposition as the central event in the aetiology of Alzheimer's disease. *Trends Pharmacol. Sci.* **12**, 383–388 (1991).
 181. Amyloid β -protein deposition as a seminal pathogenetic event in AD: An hypothesis. *Neurobiol. Aging* **11**, 299 (1990).
 182. Deng, H.-X., Bigio, E. H. & Siddique, T. Detection of protein aggregation in neurodegenerative diseases. *Methods Mol. Biol.* **793**, 259–272 (2011).
 183. Williams, J. K. *et al.* Multi-Pronged Interactions Underlie Inhibition of α -Synuclein Aggregation by β -Synuclein. *J. Mol. Biol.* (2018). doi:10.1016/j.jmb.2018.05.024
 184. Fisher, A., Memo, M., Stocchi, F. & Hanin, I. *Advances in Alzheimer's and Parkinson's*

- Disease: Insights, Progress, and Perspectives.* (Springer Science & Business Media, 2007).
185. Hardy, J. A. & Higgins, G. A. Alzheimer's disease: the amyloid cascade hypothesis. *Science* **256**, 184–185 (1992).
 186. Hackam, A. S. *et al.* The influence of huntingtin protein size on nuclear localization and cellular toxicity. *J. Cell Biol.* **141**, 1097–1105 (1998).
 187. Perutz, M. F., Johnson, T., Suzuki, M. & Finch, J. T. Glutamine repeats as polar zippers: their possible role in inherited neurodegenerative diseases. *Proc. Natl. Acad. Sci. U. S. A.* **91**, 5355–5358 (1994).
 188. Thakur, A. K. *et al.* Polyglutamine disruption of the huntingtin exon 1 N terminus triggers a complex aggregation mechanism. *Nat. Struct. Mol. Biol.* **16**, 380–389 (2009).
 189. Truant, R., Atwal, R. S., Desmond, C., Munsie, L. & Tran, T. Huntington's disease: revisiting the aggregation hypothesis in polyglutamine neurodegenerative diseases. *FEBS J.* **275**, 4252–4262 (2008).
 190. Arrasate, M., Mitra, S., Schweitzer, E. S., Segal, M. R. & Finkbeiner, S. Inclusion body formation reduces levels of mutant huntingtin and the risk of neuronal death. *Nature* **431**, 805–810 (2004).
 191. Bates, G. Huntington aggregation and toxicity in Huntington's disease. *Lancet* **361**, 1642–1644 (2003).
 192. Ross, C. A. & Poirier, M. A. Protein aggregation and neurodegenerative disease. *Nat. Med.* **10 Suppl**, S10–7 (2004).
 193. Ehrnhoefer, D. E. *et al.* Preventing mutant huntingtin proteolysis and intermittent fasting promote autophagy in models of Huntington disease. *Acta Neuropathol Commun* **6**, 16 (2018).
 194. Martin, D. D. O., Ladha, S., Ehrnhoefer, D. E. & Hayden, M. R. Autophagy in Huntington disease and huntingtin in autophagy. *Trends Neurosci.* **38**, 26–35 (2015).
 195. Steffan, J. S. Does Huntingtin play a role in selective macroautophagy? *Cell Cycle* **9**, 3401–3413 (2010).
 196. Kegel, K. B. *et al.* Huntingtin expression stimulates endosomal-lysosomal activity, endosome tubulation, and autophagy. *J. Neurosci.* **20**, 7268–7278 (2000).
 197. Ravikumar, B. *et al.* Inhibition of mTOR induces autophagy and reduces toxicity of polyglutamine expansions in fly and mouse models of Huntington disease. *Nat. Genet.* **36**, 585–595 (2004).
 198. Davies, S. W. *et al.* Formation of neuronal intranuclear inclusions underlies the neurological dysfunction in mice transgenic for the HD mutation. *Cell* **90**, 537–548 (1997).
 199. Petersen, A. Expanded CAG repeats in exon 1 of the Huntington's disease gene stimulate dopamine-mediated striatal neuron autophagy and degeneration. *Hum. Mol. Genet.* **10**, 1243–1254 (2001).
 200. Ehrnhoefer, D. E., Butland, S. L., Pouladi, M. A. & Hayden, M. R. Mouse models of Huntington disease: variations on a theme. *Dis. Model. Mech.* **2**, 123–129 (2009).
 201. Mangiarini, L. *et al.* Exon 1 of the HD gene with an expanded CAG repeat is sufficient to cause a progressive neurological phenotype in transgenic mice. *Cell* **87**, 493–506 (1996).
 202. Slow, E. J. *et al.* Selective striatal neuronal loss in a YAC128 mouse model of Huntington

- disease. *Hum. Mol. Genet.* **12**, 1555–1567 (2003).
203. Gray, M. *et al.* Full-length human mutant huntingtin with a stable polyglutamine repeat can elicit progressive and selective neuropathogenesis in BACHD mice. *J. Neurosci.* **28**, 6182–6195 (2008).
204. Menalled, L. B. *et al.* Early motor dysfunction and striosomal distribution of huntingtin microaggregates in Huntington's disease knock-in mice. *J. Neurosci.* **22**, 8266–8276 (2002).
205. Menalled, L. B., Sison, J. D., Dragatsis, I., Zeitlin, S. & Chesselet, M.-F. Time course of early motor and neuropathological anomalies in a knock-in mouse model of Huntington's disease with 140 CAG repeats. *J. Comp. Neurol.* **465**, 11–26 (2003).
206. Menalled, L. B. *et al.* Comprehensive behavioral and molecular characterization of a new knock-in mouse model of Huntington's disease: zQ175. *PLoS One* **7**, e49838 (2012).
207. Heikkinen, T. *et al.* Characterization of neurophysiological and behavioral changes, MRI brain volumetry and 1H MRS in zQ175 knock-in mouse model of Huntington's disease. *PLoS One* **7**, e50717 (2012).
208. Southwell, A. L. *et al.* An enhanced Q175 knock-in mouse model of Huntington disease with higher mutant huntingtin levels and accelerated disease phenotypes. *Hum. Mol. Genet.* **25**, 3654–3675 (2016).
209. Wheeler, V. C. *et al.* Long glutamine tracts cause nuclear localization of a novel form of huntingtin in medium spiny striatal neurons in HdhQ92 and HdhQ111 knock-in mice. *Hum. Mol. Genet.* **9**, 503–513 (2000).
210. Lloret, A. *et al.* Genetic background modifies nuclear mutant huntingtin accumulation and HD CAG repeat instability in Huntington's disease knock-in mice. *Hum. Mol. Genet.* **15**, 2015–2024 (2006).
211. Chan, A. W. S. Transgenic nonhuman primates for neurodegenerative diseases. *Reprod. Biol. Endocrinol.* **2**, 39 (2004).
212. Chan, A. W. S. Progress and Prospects for Genetic Modification of Nonhuman Primate Models in Biomedical Research. *ILAR J.* **54**, 211–223 (2013).
213. Yang, S.-H. *et al.* Towards a transgenic model of Huntington's disease in a non-human primate. *Nature* **453**, 921 (2008).
214. Moran, S. *et al.* Germline transmission in transgenic Huntington's disease monkeys. *Theriogenology* **84**, 277–285 (2015).
215. Meng, Y., Jiang, J., Bachevalier, J., Zhang, X. & Chan, A. W. S. Developmental Whole Brain White Matter Alterations in Transgenic Huntington's Disease Monkey. *Sci. Rep.* **7**, 379 (2017).
216. Trettel, F. *et al.* Dominant phenotypes produced by the HD mutation in STHdh(Q111) striatal cells. *Hum. Mol. Genet.* **9**, 2799–2809 (2000).
217. Cattaneo, E. & Conti, L. Generation and characterization of embryonic striatal conditionally immortalized ST14A cells. *J. Neurosci. Res.* **53**, 223–234 (1998).
218. Bocchetta, M. *et al.* The SV40 Large T Antigen-p53 Complexes Bind and Activate the Insulin-like Growth Factor-I Promoter Stimulating Cell Growth. *Cancer Res.* **68**, 1022–1029 (2008).
219. Pipas, J. M. SV40: Cell transformation and tumorigenesis. *Virology* **384**, 294–303

- (2009).
220. Wolman, S. R., Hirschhorn, K. & Todaro, G. J. Early Chromosomal Changes in SV₄₀-Infected Human Fibroblast Cultures. *Cytogenet. Genome Res.* **3**, 45–61 (1964).
 221. Wolman, S. R., Steinberg, M. L. & Defendi, V. Simian virus 40-induced chromosome changes in human epidermal cultures. *Cancer Genet. Cytogenet.* **2**, 39–46 (1980).
 222. Feng, Z. *et al.* p53 tumor suppressor protein regulates the levels of huntingtin gene expression. *Oncogene* **25**, 1–7 (2006).
 223. Vangipuram, M., Ting, D., Kim, S., Diaz, R. & Schüle, B. Skin punch biopsy explant culture for derivation of primary human fibroblasts. *J. Vis. Exp.* e3779 (2013).
 224. HD iPSC Consortium. Induced pluripotent stem cells from patients with Huntington's disease show CAG-repeat-expansion-associated phenotypes. *Cell Stem Cell* **11**, 264–278 (2012).
 225. Hu, W. *et al.* Direct Conversion of Normal and Alzheimer's Disease Human Fibroblasts into Neuronal Cells by Small Molecules. *Cell Stem Cell* **17**, 204–212 (2015).
 226. Victor, M. B. *et al.* Generation of human striatal neurons by microRNA-dependent direct conversion of fibroblasts. *Neuron* **84**, 311–323 (2014).
 227. Vierbuchen, T. *et al.* Direct conversion of fibroblasts to functional neurons by defined factors. *Nature* **463**, 1035–1041 (2010).
 228. Victor, M. B. *et al.* Striatal neurons directly converted from Huntington's disease patient fibroblasts recapitulate age-associated disease phenotypes. *Nat. Neurosci.* (2018). doi:10.1038/s41593-018-0075-7
 229. Wild, E. *et al.* QUANTIFYING MUTANT HUNTINGTIN IN HUNTINGTON'S DISEASE CSF. *J. Neurol. Neurosurg. Psychiatry* **85**, e4.132–e4 (2014).
 230. Johnson, E. B. *et al.* Neurofilament light protein in blood predicts regional atrophy in Huntington disease. *Neurology* **90**, e717–e723 (2018).
 231. Pellegrini, J. W. & Lipton, S. A. Delayed administration of memantine prevents N-methyl-D-aspartate receptor-mediated neurotoxicity. *Ann. Neurol.* **33**, 403–407 (1993).
 232. Kornhuber, J., Weller, M., Schoppmeyer, K. & Riederer, P. Amantadine and memantine are NMDA receptor antagonists with neuroprotective properties. *J. Neural Transm. Suppl.* **43**, 91–104 (1994).
 233. Ho, D. J., Calingasan, N. Y., Wille, E., Dumont, M. & Flint Beal, M. Resveratrol protects against peripheral deficits in a mouse model of Huntington's disease. *Exp. Neurol.* **225**, 74–84 (2010).
 234. Chen, M. *et al.* Minocycline inhibits caspase-1 and caspase-3 expression and delays mortality in a transgenic mouse model of Huntington disease. *Nat. Med.* **6**, 797–801 (2000).
 235. Heiser, V. *et al.* Identification of benzothiazoles as potential polyglutamine aggregation inhibitors of Huntington's disease by using an automated filter retardation assay. *Proceedings of the National Academy of Sciences* **99**, 16400–16406 (2002).
 236. Beaumont, V. *et al.* Phosphodiesterase 10A Inhibition Improves Cortico-Basal Ganglia Function in Huntington's Disease Models. *Neuron* **92**, 1220–1237 (2016).
 237. Matthews, R. T. *et al.* Neuroprotective Effects of Creatine and Cyclocreatine in Animal

- Models of Huntington's Disease. *J. Neurosci.* **18**, 156–163 (1998).
238. Tabrizi, S. J. *et al.* High-dose creatine therapy for Huntington disease: a 2-year clinical and MRS study. *Neurology* **64**, 1655–1656 (2005).
239. Smith, K. M. *et al.* Dose ranging and efficacy study of high-dose coenzyme Q10 formulations in Huntington's disease mice. *Biochimica et Biophysica Acta (BBA) - Molecular Basis of Disease* **1762**, 616–626 (2006).
240. Menalled, L. B. *et al.* Comprehensive behavioral testing in the R6/2 mouse model of Huntington's disease shows no benefit from CoQ10 or minocycline. *PLoS One* **5**, e9793 (2010).
241. Deb, A., Frank, S. & Testa, C. M. New symptomatic therapies for Huntington disease. in *Handbook of Clinical Neurology* 199–207 (2017).
242. Aguiar, S., van der Gaag, B. & Cortese, F. A. B. RNAi mechanisms in Huntington's disease therapy: siRNA versus shRNA. *Transl. Neurodegener.* **6**, (2017).
243. Stanek, L. M. *et al.* Silencing mutant huntingtin by adeno-associated virus-mediated RNA interference ameliorates disease manifestations in the YAC128 mouse model of Huntington's disease. *Hum. Gene Ther.* **25**, 461–474 (2014).
244. Watts, J. K. & Corey, D. R. Silencing disease genes in the laboratory and the clinic. *J. Pathol.* **226**, 365–379 (2012).
245. Kay, C. *et al.* The targetable A1 Huntington disease haplotype has distinct Amerindian and European origins in Latin America. *Eur. J. Hum. Genet.* **25**, 332–340 (2017).
246. Kay, C. *et al.* The molecular epidemiology of Huntington disease is related to intermediate allele frequency and haplotype in the general population. *Am. J. Med. Genet. B Neuropsychiatr. Genet.* **177**, 346–357 (2018).
247. Kay, C. *et al.* Huntingtin Haplotypes Provide Prioritized Target Panels for Allele-specific Silencing in Huntington Disease Patients of European Ancestry. *Mol. Ther.* **23**, 1759–1771 (2015).
248. New Data from IONIS-HTT Rx Phase 1/2 Study Demonstrates Correlation Between Reduction of Disease-causing Protein and Improvement in Clinical Measures of Huntington's Disease | Ionis Pharmaceuticals, Inc. *Ionis Pharmaceuticals, Inc.* Available at: <http://ir.ionispharma.com/news-releases/news-release-details/new-data-ionis-htt-rx-phase-1-2-study-demonstrates-correlation>. (Accessed: 28th May 2018)
249. Iwamoto, N. *et al.* Control of phosphorothioate stereochemistry substantially increases the efficacy of antisense oligonucleotides. *Nat. Biotechnol.* **35**, 845–851 (2017).
250. Duyao, M. *et al.* Trinucleotide repeat length instability and age of onset in Huntington's disease. *Nat. Genet.* **4**, 387–392 (1993).
251. Stine, O. C. *et al.* Correlation between the onset age of Huntington's disease and length of the trinucleotide repeat in IT-15. *Hum. Mol. Genet.* **2**, 1547–1549 (1993).
252. Block-Galarza, J. *et al.* Fast transport and retrograde movement of huntingtin and HAP 1 in axons. *Neuroreport* **8**, 2247–2251 (1997).
253. Caviston, J. P., Ross, J. L., Antony, S. M., Tokito, M. & Holzbaur, E. L. F. Huntingtin facilitates dynein/dynactin-mediated vesicle transport. *Proc. Natl. Acad. Sci. U. S. A.* **104**, 10045–10050 (2007).

254. Sugars, K. L. & Rubinsztein, D. C. Transcriptional abnormalities in Huntington disease. *Trends Genet.* **19**, 233–238 (2003).
255. DiProspero, N. A. *et al.* Early changes in Huntington's disease patient brains involve alterations in cytoskeletal and synaptic elements. *J. Neurocytol.* **33**, 517–533 (2004).
256. Shirasaki, D. I. *et al.* Network organization of the huntingtin proteomic interactome in mammalian brain. *Neuron* **75**, 41–57 (2012).
257. Hoffner, G., Island, M.-L. & Djian, P. Purification of neuronal inclusions of patients with Huntington's disease reveals a broad range of N-terminal fragments of expanded huntingtin and insoluble polymers. *J. Neurochem.* **95**, 125–136 (2005).
258. Sathasivam, K. *et al.* Aberrant splicing of HTT generates the pathogenic exon 1 protein in Huntington disease. *Proc. Natl. Acad. Sci. U. S. A.* **110**, 2366–2370 (2013).
259. Glabe, C. G. Common mechanisms of amyloid oligomer pathogenesis in degenerative disease. *Neurobiol. Aging* **27**, 570–575 (2006).
260. Preisinger, E., Jordan, B. M., Kazantsev, A. & Housman, D. Evidence for a recruitment and sequestration mechanism in Huntington's disease. *Philos. Trans. R. Soc. Lond. B Biol. Sci.* **354**, 1029–1034 (1999).
261. Gunawardena, S. *et al.* Disruption of axonal transport by loss of huntingtin or expression of pathogenic polyQ proteins in *Drosophila*. *Neuron* **40**, 25–40 (2003).
262. Saudou, F., Finkbeiner, S., Devys, D. & Greenberg, M. E. Huntingtin acts in the nucleus to induce apoptosis but death does not correlate with the formation of intranuclear inclusions. *Cell* **95**, 55–66 (1998).
263. Nagai, Y. *et al.* A toxic monomeric conformer of the polyglutamine protein. *Nat. Struct. Mol. Biol.* **14**, 332–340 (2007).
264. Chopra, V. *et al.* A small-molecule therapeutic lead for Huntington's disease: preclinical pharmacology and efficacy of C2-8 in the R6/2 transgenic mouse. *Proc. Natl. Acad. Sci. U. S. A.* **104**, 16685–16689 (2007).
265. Bodner, R. A., Housman, D. E. & Kazantsev, A. G. New directions for neurodegenerative disease therapy: using chemical compounds to boost the formation of mutant protein inclusions. *Cell Cycle* **5**, 1477–1480 (2006).
266. Duennwald, M. L., Jagadish, S., Muchowski, P. J. & Lindquist, S. Flanking sequences profoundly alter polyglutamine toxicity in yeast. *Proc. Natl. Acad. Sci. U. S. A.* **103**, 11045–11050 (2006).
267. Burnett, B. G., Andrews, J., Ranganathan, S., Fischbeck, K. H. & Di Prospero, N. A. Expression of expanded polyglutamine targets profilin for degradation and alters actin dynamics. *Neurobiol. Dis.* **30**, 365–374 (2008).
268. Modregger, J., DiProspero, N. A., Charles, V., Tagle, D. A. & Plomann, M. PACSIN 1 interacts with huntingtin and is absent from synaptic varicosities in presymptomatic Huntington's disease brains. *Hum. Mol. Genet.* **11**, 2547–2558 (2002).
269. Caron, N. S., Munsie, L. N., Keillor, J. W. & Truant, R. Using FLIM-FRET to measure conformational changes of transglutaminase type 2 in live cells. *PLoS One* **7**, e44159 (2012).
270. Van Der Meer, B. W., Coker, G. & Chen, S.-Y. S. *Resonance energy transfer: theory and data.* (Wiley-VCH, 1994).

271. Gustafsson, M. G. Surpassing the lateral resolution limit by a factor of two using structured illumination microscopy. *J. Microsc.* **198**, 82–87 (2000).
272. Groenning, M. Binding mode of Thioflavin T and other molecular probes in the context of amyloid fibrils-current status. *J. Chem. Biol.* **3**, 1–18 (2010).
273. Rizzo, M. A., Springer, G. H., Granada, B. & Piston, D. W. An improved cyan fluorescent protein variant useful for FRET. *Nat. Biotechnol.* **22**, 445–449 (2004).
274. Rizzo, M. A., Springer, G., Segawa, K., Zipfel, W. R. & Piston, D. W. Optimization of pairings and detection conditions for measurement of FRET between cyan and yellow fluorescent proteins. *Microsc. Microanal.* **12**, 238–254 (2006).
275. Chen, Y., Mills, J. D. & Periasamy, A. Protein localization in living cells and tissues using FRET and FLIM. *Differentiation* **71**, 528–541 (2003).
276. Wallrabe, H. & Periasamy, A. Imaging protein molecules using FRET and FLIM microscopy. *Curr. Opin. Biotechnol.* **16**, 19–27 (2005).
277. Tsien, R. Y., Bacsikai, B. J. & Adams, S. R. FRET for studying intracellular signalling. *Trends Cell Biol.* **3**, 242–245 (1993).
278. Meyvis, T. K., De Smedt, S. C., Van Oostveldt, P. & Demeester, J. Fluorescence recovery after photobleaching: a versatile tool for mobility and interaction measurements in pharmaceutical research. *Pharm. Res.* **16**, 1153–1162 (1999).
279. Howell, J. L. & Truant, R. Live-cell nucleocytoplasmic protein shuttle assay utilizing laser confocal microscopy and FRAP. *Biotechniques* **32**, 80–2, 84, 86–7 (2002).
280. Goedhart, J. *et al.* Structure-guided evolution of cyan fluorescent proteins towards a quantum yield of 93%. *Nat. Commun.* **3**, 751 (2012).
281. Poirier, M. A. *et al.* Huntingtin spheroids and protofibrils as precursors in polyglutamine fibrilization. *J. Biol. Chem.* **277**, 41032–41037 (2002).
282. Waelter, S. *et al.* Accumulation of mutant huntingtin fragments in aggresome-like inclusion bodies as a result of insufficient protein degradation. *Mol. Biol. Cell* **12**, 1393–1407 (2001).
283. Chai, Y., Shao, J., Miller, V. M., Williams, A. & Paulson, H. L. Live-cell imaging reveals divergent intracellular dynamics of polyglutamine disease proteins and supports a sequestration model of pathogenesis. *Proc. Natl. Acad. Sci. U. S. A.* **99**, 9310–9315 (2002).
284. Gordon, G. W., Berry, G., Liang, X. H., Levine, B. & Herman, B. Quantitative fluorescence resonance energy transfer measurements using fluorescence microscopy. *Biophys. J.* **74**, 2702–2713 (1998).
285. He, L. *et al.* A flow cytometric method to detect protein-protein interaction in living cells by directly visualizing donor fluorophore quenching during CFP-YFP fluorescence resonance energy transfer (FRET). *Cytometry* **55A**, 71–85 (2003).
286. Banning, C. *et al.* A flow cytometry-based FRET assay to identify and analyse protein-protein interactions in living cells. *PLoS One* **5**, e9344 (2010).
287. Chang, E. & Kuret, J. Detection and quantification of tau aggregation using a membrane filter assay. *Anal. Biochem.* **373**, 330–336 (2008).
288. Nasir, I., Linse, S. & Cabaleiro-Lago, C. Fluorescent filter-trap assay for amyloid fibril formation kinetics in complex solutions. *ACS Chem. Neurosci.* **6**, 1436–1444 (2015).

289. Bhattacharyya, A. M., Thakur, A. K. & Wetzel, R. polyglutamine aggregation nucleation: thermodynamics of a highly unfavorable protein folding reaction. *Proc. Natl. Acad. Sci. U. S. A.* **102**, 15400–15405 (2005).
290. Emoto, K., Yamashita, S. & Okada, Y. Mechanisms of Heat-induced Antigen Retrieval: Does pH or Ionic Strength of the Solution Play a Role for Refolding Antigens? *J. Histochem. Cytochem.* **53**, 1311–1321 (2005).
291. Hayashi, T., Lewis, A., Hayashi, E., Betenbaugh, M. J. & Su, T.-P. Antigen retrieval to improve the immunocytochemistry detection of sigma-1 receptors and ER chaperones. *Histochem. Cell Biol.* **135**, 627–637 (2011).
292. Akoumianaki, T., Kardassis, D., Polioudaki, H., Georgatos, S. D. & Theodoropoulos, P. A. Nucleocytoplasmic shuttling of soluble tubulin in mammalian cells. *J. Cell Sci.* **122**, 1111–1118 (2009).
293. Franker, M. A. M. & Hoogenraad, C. C. Microtubule-based transport—basic mechanisms, traffic rules and role in neurological pathogenesis. *J. Cell Sci.* **126**, 2319–2329 (2013).
294. Muchowski, P. J., Ning, K., D’Souza-Schorey, C. & Fields, S. Requirement of an intact microtubule cytoskeleton for aggregation and inclusion body formation by a mutant huntingtin fragment. *Proc. Natl. Acad. Sci. U. S. A.* **99**, 727–732 (2002).
295. Reis, S. A. *et al.* Striatal neurons expressing full-length mutant huntingtin exhibit decreased N-cadherin and altered neuritogenesis. *Hum. Mol. Genet.* **20**, 2344–2355 (2011).
296. Seong, I. S. *et al.* HD CAG repeat implicates a dominant property of huntingtin in mitochondrial energy metabolism. *Hum. Mol. Genet.* **14**, 2871–2880 (2005).
297. Gines, S. *et al.* Specific progressive cAMP reduction implicates energy deficit in presymptomatic Huntington’s disease knock-in mice. *Hum. Mol. Genet.* **12**, 497–508 (2003).
298. Mochel, F. *et al.* Early energy deficit in Huntington disease: identification of a plasma biomarker traceable during disease progression. *PLoS One* **2**, e647 (2007).
299. Shelbourne, P. F. *et al.* A Huntington’s disease CAG expansion at the murine Hdh locus is unstable and associated with behavioural abnormalities in mice. *Hum. Mol. Genet.* **8**, 763–774 (1999).
300. Lin, C. H. *et al.* Neurological abnormalities in a knock-in mouse model of Huntington’s disease. *Hum. Mol. Genet.* **10**, 137–144 (2001).
301. Menalled, L. B., Sison, J. D., Dragatsis, I., Zeitlin, S. & Chesselet, M.-F. Time course of early motor and neuropathological anomalies in a knock-in mouse model of Huntington’s disease with 140 CAG repeats. *J. Comp. Neurol.* **465**, 11–26 (2003).
302. Ferris, C. F. *et al.* Studies on the Q175 Knock-in Model of Huntington’s Disease Using Functional Imaging in Awake Mice: Evidence of Olfactory Dysfunction. *Front. Neurol.* **5**, 94 (2014).
303. Singer, E. *et al.* Reduced cell size, chromosomal aberration and altered proliferation rates are characteristics and confounding factors in the STHdh cell model of Huntington disease. *Sci. Rep.* **7**, 16880 (2017).
304. Myers, R. H. Huntington’s disease genetics. *NeuroRx* **1**, 255–262 (2004).

305. Landry, J. J. M. *et al.* The genomic and transcriptomic landscape of a HeLa cell line. *G3* **3**, 1213–1224 (2013).
306. Mittelman, D. & Wilson, J. H. The fractured genome of HeLa cells. *Genome Biol.* **14**, 111 (2013).
307. Barkley, D. S., Hardiwidjaja, S. & Menkes, J. H. Abnormalities in growth of skin fibroblasts of patients with Huntington's disease. *Ann. Neurol.* **1**, 426–430 (1977).
308. Goetz, I. E., Roberts, E. & Warren, J. Skin fibroblasts in Huntington disease. *Am. J. Hum. Genet.* **33**, 187–196 (1981).
309. del Hoyo, P. *et al.* Oxidative stress in skin fibroblasts cultures of patients with Huntington's disease. *Neurochem. Res.* **31**, 1103–1109 (2006).
310. Juopperi, T. A. *et al.* Astrocytes generated from patient induced pluripotent stem cells recapitulate features of Huntington's disease patient cells. *Mol. Brain* **5**, 17 (2012).
311. Martinez, Y., Dubois-Dauphin, M. & Krause, K.-H. Generation and applications of human pluripotent stem cells induced into neural lineages and neural tissues. *Front. Physiol.* **3**, 47 (2012).
312. Zhang, Y. *et al.* Rapid single-step induction of functional neurons from human pluripotent stem cells. *Neuron* **78**, 785–798 (2013).
313. Yoo, A. S. *et al.* MicroRNA-mediated conversion of human fibroblasts to neurons. *Nature* **476**, 228–231 (2011).
314. Xue, Y. *et al.* Direct conversion of fibroblasts to neurons by reprogramming PTB-regulated microRNA circuits. *Cell* **152**, 82–96 (2013).
315. Hayflick, L. & Moorhead, P. S. The serial cultivation of human diploid cell strains. *Exp. Cell Res.* **25**, 585–621 (1961).
316. Hayflick, L. THE LIMITED IN VITRO LIFETIME OF HUMAN DIPLOID CELL STRAINS. *Exp. Cell Res.* **37**, 614–636 (1965).
317. Dimri, G. P. *et al.* A biomarker that identifies senescent human cells in culture and in aging skin in vivo. *Proc. Natl. Acad. Sci. U. S. A.* **92**, 9363–9367 (1995).
318. Marcotte, R., Lacelle, C. & Wang, E. Senescent fibroblasts resist apoptosis by downregulating caspase-3. *Mech. Ageing Dev.* **125**, 777–783 (2004).
319. Wood, L. D. *et al.* Characterization of ataxia telangiectasia fibroblasts with extended life-span through telomerase expression. *Oncogene* **20**, 278–288 (2001).
320. Ouellette, M. M., McDaniel, L. D., Wright, W. E., Shay, J. W. & Schultz, R. A. The establishment of telomerase-immortalized cell lines representing human chromosome instability syndromes. *Hum. Mol. Genet.* **9**, 403–411 (2000).
321. Lee, K. M., Choi, K. H. & Ouellette, M. M. Use of exogenous hTERT to immortalize primary human cells. *Cytotechnology* **45**, 33–38 (2004).
322. Morales, C. P. *et al.* Absence of cancer-associated changes in human fibroblasts immortalized with telomerase. *Nat. Genet.* **21**, 115 (1999).
323. Jiang, X. R. *et al.* Telomerase expression in human somatic cells does not induce changes associated with a transformed phenotype. *Nat. Genet.* **21**, 111–114 (1999).
324. Young, A. T. L., Lakey, J. R. T. & Moore, R. B. TRANSIENT TELOMERASE EXPRESSION IN NORMAL SOMATIC CELLS LEADS TO TELOMERE EXTENSION AND INCREASED PROLIFERATION IN THE ABSENCE OF

- MALIGNANT TRANSFORMATION. *Transplantation* **78**, 108 (2004).
325. hTERT Immortalized Cell Lines. Available at: https://www.atcc.org/Products/Cells_and_Microorganisms/hTERT_Immortalized_Cell_Lines.aspx. (Accessed: 28th January 2018)
326. Menkes, J. H. & Stein, N. Fibroblast cultures in Huntington's disease. *N. Engl. J. Med.* **288**, 856–857 (1973).
327. Kirk, D., Parrington, J. M., Corney, G. & Bolt, J. M. Anomalous cellular proliferation in vitro associated with Huntington's disease. *Hum. Genet.* **36**, 143–154 (1977).
328. Acuña, A. I. *et al.* A failure in energy metabolism and antioxidant uptake precede symptoms of Huntington's disease in mice. *Nat. Commun.* **4**, 2917 (2013).
329. Smith, M. L., Chen, I. T., Zhan, Q., O'Connor, P. M. & Fornace, A. J., Jr. Involvement of the p53 tumor suppressor in repair of u.v.-type DNA damage. *Oncogene* **10**, 1053–1059 (1995).
330. Liu, Y. & Kulesz-Martin, M. p53 protein at the hub of cellular DNA damage response pathways through sequence-specific and non-sequence-specific DNA binding. *Carcinogenesis* **22**, 851–860 (2001).
331. Fritsche, M., Haessler, C. & Brandner, G. Induction of nuclear accumulation of the tumor-suppressor protein p53 by DNA-damaging agents. *Oncogene* **8**, 307–318 (1993).
332. Bae, B.-I. *et al.* p53 mediates cellular dysfunction and behavioral abnormalities in Huntington's disease. *Neuron* **47**, 29–41 (2005).
333. Bodnar, A. G. *et al.* Extension of life-span by introduction of telomerase into normal human cells. *Science* **279**, 349–352 (1998).
334. Vaziri, H. & Benchimol, S. Reconstitution of telomerase activity in normal human cells leads to elongation of telomeres and extended replicative life span. *Curr. Biol.* **8**, 279–282 (1998).
335. Potapova, T. A., Zhu, J. & Li, R. Aneuploidy and chromosomal instability: a vicious cycle driving cellular evolution and cancer genome chaos. *Cancer Metastasis Rev.* **32**, 377–389 (2013).
336. Dürrbaum, M. & Storchová, Z. Effects of aneuploidy on gene expression: implications for cancer. *FEBS J.* **283**, 791–802 (2016).
337. Warner, J. P., Barron, L. H. & Brock, D. J. A new polymerase chain reaction (PCR) assay for the trinucleotide repeat that is unstable and expanded on Huntington's disease chromosomes. *Mol. Cell. Probes* **7**, 235–239 (1993).
338. Walen, K. H. Human diploid fibroblast cells in senescence; cycling through polyploidy to mitotic cells. *In Vitro Cell. Dev. Biol. Anim.* **42**, 216–224 (2006).
339. Debacq-Chainiaux, F., Erusalimsky, J. D., Campisi, J. & Toussaint, O. Protocols to detect senescence-associated beta-galactosidase (SA- β gal) activity, a biomarker of senescent cells in culture and in vivo. *Nat. Protoc.* **4**, 1798 (2009).
340. Lemons, J. M. S. *et al.* Quiescent fibroblasts exhibit high metabolic activity. *PLoS Biol.* **8**, e1000514 (2010).
341. Küppers, M., Ittrich, C., Faust, D. & Dietrich, C. The transcriptional programme of contact-inhibition. *J. Cell. Biochem.* **110**, 1234–1243 (2010).
342. Goldstein, S. & Singal, D. P. Senescence of cultured human fibroblasts: mitotic versus

- metabolic time. *Exp. Cell Res.* **88**, 359–364 (1974).
343. Schwarzacher, H. G. & Schnedl, W. ENDOREDUPPLICATION IN HUMAN FIBROBLAST CULTURES. *Cytogenetics* **4**, 1–18 (1965).
344. Noble, J. R. *et al.* Alterations in the p16(INK4a) and p53 tumor suppressor genes of hTERT-immortalized human fibroblasts. *Oncogene* **23**, 3116–3121 (2004).
345. van Waarde-Verhagen, M. A. W. H., Kampinga, H. H. & Linskens, M. H. K. Continuous growth of telomerase-immortalised fibroblasts: how long do cells remain normal? *Mech. Ageing Dev.* **127**, 85–87 (2006).
346. Munsie, L. N., Desmond, C. R. & Truant, R. Cofilin nuclear–cytoplasmic shuttling affects cofilin–actin rod formation during stress. *J. Cell Sci.* (2012).
347. Muchowski, P. J., Ning, K., D’Souza-Schorey, C. & Fields, S. Requirement of an intact microtubule cytoskeleton for aggregation and inclusion body formation by a mutant huntingtin fragment. *Proc. Natl. Acad. Sci. U. S. A.* **99**, 727–732 (2002).
348. Hoffner, G., Kahlem, P. & Djian, P. Perinuclear localization of huntingtin as a consequence of its binding to microtubules through an interaction with beta-tubulin: relevance to Huntington’s disease. *J. Cell Sci.* **115**, 941–948 (2002).
349. Folch, J. *et al.* Role of cell cycle re-entry in neurons: a common apoptotic mechanism of neuronal cell death. *Neurotox. Res.* **22**, 195–207 (2012).
350. Lu, M., Boschetti, C. & Tunnacliffe, A. Long Term Aggresome Accumulation Leads to DNA Damage, p53-dependent Cell Cycle Arrest, and Steric Interference in Mitosis. *J. Biol. Chem.* **290**, 27986–28000 (2015).
351. Nath, S., Munsie, L. N. & Truant, R. A huntingtin-mediated fast stress response halting endosomal trafficking is defective in Huntington’s disease. *Hum. Mol. Genet.* **24**, 450–462 (2015).
352. Landles, C., Weiss, A., Franklin, S., Howland, D. & Bates, G. Caspase-6 does not contribute to the proteolysis of mutant huntingtin in the HdhQ150 knock-in mouse model of Huntington’s disease. *PLoS Curr.* **4**, e4fd085bfc9973 (2012).
353. Sapp, E. *et al.* Native mutant huntingtin in human brain: evidence for prevalence of full-length monomer. *J. Biol. Chem.* **287**, 13487–13499 (2012).
354. Atwal, R. S. & Truant, R. A stress sensitive ER membrane-association domain in Huntingtin protein defines a potential role for Huntingtin in the regulation of autophagy. *Autophagy* **4**, 91–93 (2008).
355. Vidal, R. L. *et al.* Targeting the UPR transcription factor XBP1 protects against Huntington’s disease through the regulation of FoxO1 and autophagy. *Hum. Mol. Genet.* **21**, 2245–2262 (2012).
356. Hall, L. L., Smith, K. P., Byron, M. & Lawrence, J. B. Molecular anatomy of a speckle. *Anat. Rec. A Discov. Mol. Cell. Evol. Biol.* **288**, 664–675 (2006).
357. Campalans, A., Amouroux, R., Bravard, A., Epe, B. & Radicella, J. P. UVA irradiation induces relocalisation of the DNA repair protein hOGG1 to nuclear speckles. *J. Cell Sci.* **120**, 23–32 (2007).
358. Lin, S., Coutinho-Mansfield, G., Wang, D., Pandit, S. & Fu, X.-D. The splicing factor SC35 has an active role in transcriptional elongation. *Nat. Struct. Mol. Biol.* **15**, 819–826 (2008).

359. Munsie, L. *et al.* Mutant huntingtin causes defective actin remodeling during stress: defining a new role for transglutaminase 2 in neurodegenerative disease. *Hum. Mol. Genet.* **20**, 1937–1951 (2011).
360. Wang, S. & El-Deiry, W. S. p53, cell cycle arrest and apoptosis. in *25 Years of p53 Research* 141–163 (Springer, 2007).
361. Shaw, P. H. The role of p53 in cell cycle regulation. *Pathol. Res. Pract.* **192**, 669–675 (1996).
362. Reinhardt, H. C. & Schumacher, B. The p53 network: cellular and systemic DNA damage responses in aging and cancer. *Trends Genet.* **28**, 128–136 (2012).
363. Collado, M., Blasco, M. A. & Serrano, M. Cellular senescence in cancer and aging. *Cell* **130**, 223–233 (2007).
364. Ratovitski, T. *et al.* Huntingtin protein interactions altered by polyglutamine expansion as determined by quantitative proteomic analysis. *Cell Cycle* **11**, 2006–2021 (2012).
365. Liu, K.-Y. *et al.* Disruption of the nuclear membrane by perinuclear inclusions of mutant huntingtin causes cell-cycle re-entry and striatal cell death in mouse and cell models of Huntington's disease. *Hum. Mol. Genet.* **24**, 1602–1616 (2015).
366. Medvedev, S. P., Shevchenko, A. I. & Zakian, S. M. Induced Pluripotent Stem Cells: Problems and Advantages when Applying them in Regenerative Medicine. *Acta Naturae* **2**, 18–28 (2010).
367. Hewitt, K. J. & Garlick, J. A. Cellular reprogramming to reset epigenetic signatures. *Mol. Aspects Med.* **34**, 841–848 (2013).
368. Pereira, M. *et al.* Highly efficient generation of induced neurons from human fibroblasts that survive transplantation into the adult rat brain. *Sci. Rep.* **4**, 6330 (2014).
369. Dietrich, P., Johnson, I. M., Alli, S. & Dragatsis, I. Elimination of huntingtin in the adult mouse leads to progressive behavioral deficits, bilateral thalamic calcification, and altered brain iron homeostasis. *PLoS Genet.* **13**, e1006846 (2017).
370. Reiner, A., Dragatsis, I., Zeitlin, S. & Goldowitz, D. Wild-type huntingtin plays a role in brain development and neuronal survival. *Mol. Neurobiol.* **28**, 259–276 (2003).
371. Caron, N. S. Using Förster Resonance Energy Transfer (FRET) To Define the Conformational Changes of Huntingtin at the Clinical Threshold for Huntington's Disease. (2014).
372. Woloshansky, B. T. Primary Cilia Dynamics, Morphology and Acetylation are Abnormal in Huntingtin Disease Cell Models.
373. Patel, S. & Sc, B. PHOSPHORYLATION OF HUNTINGTIN N17 DOMAIN IS CELL CYCLE REGULATED AND BECOMES DYSREGULATED IN HUNTINGTON'S DISEASE.
374. Lu, A. L., Li, X., Gu, Y., Wright, P. M. & Chang, D. Y. Repair of oxidative DNA damage: mechanisms and functions. *Cell Biochem. Biophys.* **35**, 141–170 (2001).
375. Graser, S. *et al.* Cep164, a novel centriole appendage protein required for primary cilium formation. *J. Cell Biol.* **179**, 321–330 (2007).
376. Kaliszewski, M., Knott, A. B. & Bossy-Wetzel, E. Primary cilia and autophagic dysfunction in Huntington's disease. *Cell Death Differ.* **22**, 1413–1424 (2015).
377. Liu, J.-P. & Zeitlin, S. O. The long and the short of aberrant ciliogenesis in Huntington

- disease. *J. Clin. Invest.* **121**, 4237–4241 (2011).
378. Barnum, K. J. & O’Connell, M. J. Cell Cycle Regulation by Checkpoints. in *Cell Cycle Control: Mechanisms and Protocols* (eds. Noguchi, E. & Gadaleta, M. C.) 29–40 (Springer New York, 2014).
379. Martz, E. & Steinberg, M. S. The role of cell-cell contact in ‘contact’ inhibition of cell division: A review and new evidence. *J. Cell. Physiol.* **79**, 189–210 (1972).
380. Herrup, K. & Yang, Y. Cell cycle regulation in the postmitotic neuron: oxymoron or new biology? *Nat. Rev. Neurosci.* **8**, 368–378 (2007).
381. Lee, H.-G. *et al.* Cell cycle re-entry mediated neurodegeneration and its treatment role in the pathogenesis of Alzheimer’s disease. *Neurochem. Int.* **54**, 84–88 (2009).
382. Liu, D. X. & Greene, L. A. Neuronal apoptosis at the G1/S cell cycle checkpoint. *Cell Tissue Res.* **305**, 217–228 (2001).
383. Kruman, I. I. *et al.* Cell cycle activation linked to neuronal cell death initiated by DNA damage. *Neuron* **41**, 549–561 (2004).
384. Kruman, I. I. Why do neurons enter the cell cycle? *Cell Cycle* **3**, 769–773 (2004).
385. Schwartz, E. I. *et al.* Cell cycle activation in postmitotic neurons is essential for DNA repair. *Cell Cycle* **6**, 318–329 (2007).
386. Folch, J. *et al.* Role of cell cycle re-entry in neurons: a common apoptotic mechanism of neuronal cell death. *Neurotox. Res.* **22**, 195–207 (2012).
387. Premo FUCCI Cell Cycle Sensor (BacMam 2.0) - Thermo Fisher Scientific. Available at: <https://www.thermofisher.com/order/catalog/product/P36237>. (Accessed: 24th May 2018)
388. Segev, H., Zenvirth, D., Simpson-Lavy, K. J., Melamed-Book, N. & Brandeis, M. Imaging Cell Cycle Phases and Transitions of Living Cells from Yeast to Woman. *Methods Mol. Biol.* **1342**, 321–336 (2016).
389. Stukenberg, P. T. *et al.* Systematic identification of mitotic phosphoproteins. *Curr. Biol.* **7**, 338–348 (1997).
390. Dephoure, N. *et al.* A quantitative atlas of mitotic phosphorylation. *Proc. Natl. Acad. Sci. U. S. A.* **105**, 10762–10767 (2008).
391. Karam, A. *et al.* A novel function of Huntingtin in the cilium and retinal ciliopathy in Huntington’s disease mice. *Neurobiol. Dis.* **80**, 15–28 (2015).
392. Keryer, G. *et al.* Ciliogenesis is regulated by a huntingtin-HAP1-PCM1 pathway and is altered in Huntington disease. *J. Clin. Invest.* **121**, 4372–4382 (2011).
393. Haremaki, T., Deglincerti, A. & Brivanlou, A. H. Huntingtin is required for ciliogenesis and neurogenesis during early *Xenopus* development. *Dev. Biol.* **408**, 305–315 (2015).
394. Kim, S. & Tsiokas, L. Cilia and cell cycle re-entry: more than a coincidence. *Cell Cycle* **10**, 2683–2690 (2011).
395. Goto, H., Inoko, A. & Inagaki, M. Cell cycle progression by the repression of primary cilia formation in proliferating cells. *Cell. Mol. Life Sci.* **70**, 3893–3905 (2013).
396. Izawa, I., Goto, H., Kasahara, K. & Inagaki, M. Current topics of functional links between primary cilia and cell cycle. *Cilia* **4**, 12 (2015).
397. Johnson, C. A. & Collis, S. J. Ciliogenesis and the DNA damage response: a stressful relationship. *Cilia* **5**, 19 (2016).

398. Walz, G. Role of primary cilia in non-dividing and post-mitotic cells. *Cell Tissue Res.* **369**, 11–25 (2017).
399. Attanasio, M. Ciliopathies and DNA damage: an emerging nexus. *Curr. Opin. Nephrol. Hypertens.* **24**, 366–370 (2015).
400. McClure-Begley, T. D. & Klymkowsky, M. W. Nuclear roles for cilia-associated proteins. *Cilia* **6**, 8 (2017).
401. Mielcarek, M. & Isalan, M. A shared mechanism of muscle wasting in cancer and Huntington's disease. *Clin. Transl. Med.* **4**, 34 (2015).
402. Fulda, S., Gorman, A. M., Hori, O. & Samali, A. Cellular stress responses: cell survival and cell death. *Int. J. Cell Biol.* **2010**, 214074 (2010).
403. Bonora, M. *et al.* ATP synthesis and storage. *Purinergic Signal.* **8**, 343–357 (2012).
404. Fasullo, M. & Endres, L. Nucleotide salvage deficiencies, DNA damage and neurodegeneration. *Int. J. Mol. Sci.* **16**, 9431–9449 (2015).
405. Kalathur, R. K. R., Ayasolla, K. & Futschik, M. E. The Unfolded Protein Response and its potential role in Huntington's disease. [precedings.nature.com/documents/7145/version/1](https://www.nature.com/documents/7145/version/1) (2012). doi:10.1038/npre.2012.7145.1
406. Goyal, M. S. *et al.* Loss of Brain Aerobic Glycolysis in Normal Human Aging. *Cell Metab.* **26**, 353–360.e3 (2017).
407. Micheli, V. *et al.* Neurological disorders of purine and pyrimidine metabolism. *Curr. Top. Med. Chem.* **11**, 923–947 (2011).
408. Hertz, N. T. *et al.* A neo-substrate that amplifies catalytic activity of parkinson's-disease-related kinase PINK1. *Cell* **154**, 737–747 (2013).
409. Pinna, L. A. Protein kinase CK2: a challenge to canons. *J. Cell Sci.* **115**, 3873–3878 (2002).
410. Weber, J. J., Sowa, A. S., Binder, T. & Hübener, J. From pathways to targets: understanding the mechanisms behind polyglutamine disease. *Biomed Res. Int.* **2014**, 701758 (2014).
411. Matilla-Dueñas, A. *et al.* Consensus paper: pathological mechanisms underlying neurodegeneration in spinocerebellar ataxias. *Cerebellum* **13**, 269–302 (2014).
412. Pérez Ortiz, J. M. & Orr, H. T. Spinocerebellar Ataxia Type 1: Molecular Mechanisms of Neurodegeneration and Preclinical Studies. in *Polyglutamine Disorders* (eds. Nóbrega, C. & Pereira de Almeida, L.) 135–145 (Springer International Publishing, 2018).
413. Bettencourt, C. *et al.* DNA repair pathways underlie a common genetic mechanism modulating onset in polyglutamine diseases. *Ann. Neurol.* **79**, 983–990 (2016).
414. Zannini, L., Delia, D. & Buscemi, G. CHK2 kinase in the DNA damage response and beyond. *J. Mol. Cell Biol.* **6**, 442–457 (2014).
415. Folch, J. *et al.* Role of cell cycle re-entry in neurons: a common apoptotic mechanism of neuronal cell death. *Neurotox. Res.* **22**, 195–207 (2012).
416. Ko, H. L. & Ren, E. C. Functional Aspects of PARP1 in DNA Repair and Transcription. *Biomolecules* **2**, 524–548 (2012).
417. Verdin, E. NAD⁺ in aging, metabolism, and neurodegeneration. *Science* **350**, 1208–1213 (2015).
418. Gregory, R. P. F. The Production of ATP. in *Photosynthesis* (ed. Gregory, R. P. F.)

95–110 (Springer Netherlands, 1989).